UNIVERSIDAD AUTÓNOMA DE MADRID
&
INSTITUTO DE FÍSICA TEÓRICA UAM/CSIC

DOCTORAL THESIS

Determination of Fundamental Parameters in the Hadronic Sector of the Standard Model

---

Author:
Mr. David PRETI

Supervisor:
Prof. Carlos PENA

A thesis submitted in fulfillment of the requirements for the degree of Doctor of Philosophy

in

Theoretical Physics

The superior man perseveres long
in his course, adapts to the times,
but remains firm in his direction
and correct in his goals.

I Ching

Determination of Fundamental Parameters in the Hadronic Sector of the Standard Model

by Mr. David PRETI

Abstract

Renormalization Group (RG) is an essential tool which allow to study how physical quantities change respect to the physical scale at which are measured. In asymptotic free theories QCD-like, the perturbative computation of RG evolution is limited to a short range scales at high energies. This strong theoretical limitation cannot be overcame, making impossible to connect low-energy non-perturbative quantities with high energy ones entering in phenomenological computations. In this thesis we present a non-perturbative first-principle computation of the scaling of several composite operators relevant for phenomenology, and of quark masses. We take advantage of numerical simulation of the theory discretised on a space-time hyper cubic lattice to compute renormalization constants. Thanks to recursive finite-size scaling techniques developed by the ALPHA collaboration, we are able to provide the non-perturbative running over two order of magnitude in scales, from low energies $\mathcal{O}(\Lambda_{\rm QCD})$ to high energies $\mathcal{O}(M_{\rm W})$. The latter, allow as to connect with perturbative calculations and compute the Renormalization Group Invariant (RGI) quantity for all the operators investigated in the thesis. In particular, we provide both perturbative and non-perturbative calculation in the Schrödinger Functional renormalization scheme for tensor currents in $N_{\rm f} = 0, 2$ QCD. The procedure is also extended to account for the BSM four-fermion operators with a net flavour exchange which exhibit mixing under renormalization group. In this case the non-perturbative computation has been performed for $N_{\rm f} = 2$ QCD. As a final results, we also employ a slightly innovative procedure involving two renormalization schemes defined in high and low energy regions to carry out the non-perturbative running of quark masses with $N_{\rm f} = 2+1$ flavours. The latter is an essential step required for the ongoing computation of the value of quark masses, in particular the strange quark mass m_s.

Determination of Fundamental Parameters in the Hadronic Sector of the Standard Model

by Mr. David PRETI

Abstract

El Grupo de Renormalización (RG) es una herramienta esencial que permite estudiar cómo cambian las cantidades físicas respecto a la escala física a la que son medidas.

En teorías asintóticamente libres como QCD, el cálculo perturbativo de la evolución RG está limitado al rango de escalas de altas energías. Esta fuerte limitación teórica no puede ser superada, haciendo imposible el contacto entre las cantidades no perturbativas a baja energía con las de alta energía que aparecen en cálculos fenomenológicos.

En esta tesis presentamos un cálculo no perturbativo desde primeros principios del scaling de varios operadores compuestos relevantes para la fenomenología, así como de las masas de quark. Utilizamos simulaciones numéricas de la teoría discretizada en una red espaciotemporal hipercúbica para calcular constantes de renormalización. Gracias a las técnicas recursivas de scaling en volumen finito desarrolladas por la Colaboración ALPHA podemos obtener el running no perturbativo sobre dos órdenes de magnitud en escalas, desde bajas energías $\mathcal{O}(\Lambda_{\rm QCD})$ hasta altas energías $\mathcal{O}(M_{\rm W})$. Estas últimas permiten hacer contacto con cálculos perturbativos y calcular la cantidad Invariante bajo Grupo de Renormalización (RGI) para todos los operadores investigados en esta tesis.

En particular, describimos un cálculo tanto perturbativo como no perturbativo de la renormalización en esquemas Schrödinger Functional para corrientes tensoriales en $N_{\rm f} = 0, 2$ QCD. El procedimiento se extiende a operadores de cuatro fermiones BSM con cambio neto de sabor, que exhiben mezcla bajo RG. En este caso el cálculo no perturbativo ha sido realizado para $N_{\rm f} = 2$ QCD. Por último, utilizamos un procedimiento innovador, que emplea dos esquemas de renormalización diferentes a altas y bajas energías, para calcular el running no perturbative de las masas de quark con $N_{\rm f} = 2 + 1$ sabores. Este es un paso esencial en el cálculo en curso de la masa de los quarks en particular para el quark extraño m_s.

Acknowledgements

The support, knowledge and help of many people contributed to the completion of this thesis. Firstly, I would like to thank my supervisor Carlos for the huge amount of time he spent with me. His continuous support and encouragement throughout all my time in Madrid has been fundamental for the conclusion of this work.
Secondly I would like to thank Alberto, Isabel, Mauro, Gregorio and Patrick for all the fruitful collaborations and discussions. I would like to thank also Francesco Capponi for all the support and very interesting scientific discussions. A special thanks also to my Parents and Ilaria who allowed me to achieve this important step in my life. An extra thanks also to Manuel from CPA centre at UAM for a fundamental support, without which I will not be here.

Contents

Dedicated to Ilaria

Introduction

Quantum Field theory (QFT) is recognised as the natural theoretical framework for describing the dynamics of fundamental particles and their interactions. Since its inception [1], it has been subjected to a continuous evolution process, characterized by several signicant phases. Among these, one could recollect the formulation of Fermi theory of beta decay, the adoption of Feynman path integral formalism in perturbation theory, or, last but not less important, the establishment of the Standard Model.

Along this evolution path, one of the most important landmarks is surely represented by the emergence of the renormalization group (RG). This is a fundamental tool which allow to understand how the scale dependence of all fundamental parameters of the theory is enforced in order not to have infinities once the high energy modes are included in the theory. The RG machinery has been successfully applied to Quantum Chromodynamics (QCD). In this theory, the β-function, governing the behaviour of the renormalized gauge coupling, shows that it tends to zero at short distances, i.e. large energies (UV). This phenomenon takes the name of asymptotic freedom [2]. As opposite, the coupling increases toward the low energy scales (IR). This interesting behaviour of the theory, limits the applicability of perturbative methods, which are defined only in the high energy region. This points out that non-perturbative strategies had to be employed to probe low energy dynamics of the theory.

In this context, a natural way to regularise the theory is elegantly provided by the formulation on the lattice. The theory is defined on a discretised lattice space-time with lattice spacing a, which acts as a momentum cutoff. In this framework, it is possible to carry out numerical computation starting from first principles, without relying on perturbative expansions.

In this work, the lattice regularisation has been the technical tool for studying a well known, hot topic of quantum field theory: the renormalization of composite operators. The main goal of this procedure is to render on-shell correlation functions containing the insertion of some local operators, which are not in the action, finite as the cut-off is removed. These operators play a central role in the phenomenological study of particle physics interactions. In fact, a standard approach to describe such interactions is the Operator Product Expansion (OPE) [3]. The latter allow to express physical amplitudes as a sum over matrix elements of local operators. The coefficient of this expansion, usually called Wilson coefficients, encode the high energy short distance physical effects, while the matrix elements contain the low energy dynamics, which is completely dominated by non-perturbative phenomena. The latter, is computed on the lattice on large volume simulations and constitute a challenging theoretical and computational task. A fundamental ingredient in this procedure is the renormalization the bare matrix elements.

In this thesis we focus on the non-perturbative renormalization for composite operators. We employ a finite volume renormalization scheme with Dirichlet boundary conditions in time direction, and periodic conditions in space which takes the name of "Schrödinger Functional". Taking advantage of recursive techniques developed along the years by the ALPHA collaboration, we are not only able to extract the renormalization constants, but also to compute the non-perturbative running over two order of magnitude in energy scales, from an hadronic region $\mathcal{O}(\Lambda_{\mathrm{QCD}})$ to a perturbative one $\mathcal{O}(M_{\mathrm{W}})$. Once the latter is reached non-perturbatively it is safe to make contact with perturbation

theory and access to another fundamental quantity called the Renormalization Group Invariants (RGI). These, as the name suggests, are independent on the scale, and (except for the coupling) do not carry any dependence on the renormalization scheme (provided the scheme is massless).

In particularly, in this work we consider the full set of (non flavour-singlet) Lorentz invariant bilinears (in quark fields). Through Ward Identities (WI) we observe that the only two operators which transform independently under RG are the pseudoscalar density and the tensor currents. The first one plays a very special role, since it can be shown, that its renormalization properties are the inverse of the one of quark masses. The high precision knowledge of the running of the latter, together with ongoing large volume simulations allows for an unprecedented accuracy in the determination of some of the fundamental parameters of QCD. We provide non-perturbative study of the scaling of the renormalized mass in $N_{\rm f} = 2 + 1$ QCD with a novel approach, involving two different renormalization schemes respectively at low and high energy regions, which allow to compute directly for the first time the non-perturbative anomalous dimension of quark masses.

Hadronic matrix elements of tensor currents also play an important rôle in several relevant problems in particle physics. Some prominent examples are rare heavy meson decays that allow to probe the consistency of the SM flavour sector (see, e.g., [4, 5, 6] for an overview), or precision measurements of β-decay and limits on the neutron electric dipole moment (see, e.g., [7, 8, 9] for an up-to-date lattice-QCD perspective). Also in this case, a non-perturbative high precision renormalization is required. In this case we provide a complete 1-loop perturbative analysis and the non-perturbative calculation with $N_{\rm f} = 0$ and $N_{\rm f} = 2$ QCD.

Moreover, we provide an explorative extension of the well established renormalization procedure cited above to the case of operators which does not renormalise multiplicatively. In particular we focused on the full set of Beyond Standard Model (BSM) four-fermion operators with a net flavour exchange. Hadronic matrix elements involving those operators play an important rôle in the study of flavour physics within the SM, as well as in searches for new physics. In particular, they are essential to the study of CP-violation in the hadron sector in both the SM and BSM models, where they parametrise the effect of new interactions.

The material presented in this thesis can be summarised as follow:

- Chapter 1-2. After a brief introduction about Wilsonian Renormalization group and generalities about RG function, we move to the renormalization of composite operators. The definition of the RGI is discussed for both multiplicative and non-multiplicative renormalizable operators. Basic concepts, like the step scaling functions are introduced at this very first stage.

- Chapter 3. We introduce the Lattice regularisation, fixing the notation and presenting the discretisation for both gauge and fermion actions, where the latter, induces an explicit chiral symmetry breaking by the Wilson term. We then summarise renormalization pattern for currents and densities, with particular attention to the renormalization of the mass.

- Chapter 4. We define the Schrödinger Functional, first in the continuum then its realisation on the lattice. The definition of the renormalized gauge coupling which naturally provided by the SF is discussed as well as the recursive finite-volume techniques. In the same chapter, in parallel with the SF coupling we provide another independent coupling definition taking advantage of the Gradient Flow, as discussed in [10, 11].

- Chapter 5. Symanzik's Improvement theory is presented, and its application to a variety of quantities is provided. In particular the improvement of the action (both gauge and fermion part), of the flow equations and fermionic currents and densities are discussed.

- Chapter 6. We present our results for a perturbative 1-loop study in the Schrödinger Functional of the tensor currents, analysing cutoff effects and, through a scheme-matching procedure, quoting the results for the 2-loop tensor anomalous dimension in this scheme. Then, a full non-perturbative computation of the running over two orders of magnitude in scales is provided for both $N_{\mathrm{f}} = 0$ and $N_{\mathrm{f}} = 2$ QCD.

- Chapter 7. We present our results for the non-perturbative running of quark masses in $N_{\mathrm{f}} = 2 + 1$ QCD. In this case we adopt a different renormalization scheme, given by a different definition of the renormalized coupling, in the high energy region and the low energy region. The non-perturbative running is scheme-matched at an intermediate scale.

- Chapter 8. We present our 1-loop perturbative study about the parity violating four-fermion operators with a net flavour exchange. The computation of the 2-loop (matrix) anomalous dimension is presented, as well as the computation of cutoff effects in the Step Scaling Functions (SSFs). Non-perturbative results for the running are provided for $N_{\mathrm{f}} = 2$ QCD.

Introducción

La Teoría Cuántica de Campos (QFT) es el marco teórico natural para describir la dinámica de las partículas funamentales y sus interacciones. Desde su desarrollo [1], ha estado sometida a un proceso continuo de evolución, caracterizado por varias fases significativas. Entre ellas, es necesario mencionar la formulación de la teoría de Fermi para las desintegraciones beta, la adopción del formalismo de integral de caminos de Feynman en teoría de perturbaciones, o, por último, pero no por ello menos importante, la construcción del Modelo Estándar.

A lo largo de esta evolución, una de las piedras miliares más importantes es seguramente la aparición del Grupo de Renormalización (RG), una herramienta fundamental que permite comprender cómo imponer la correcta dependencia de la escala de todos los parámetros fundamentales de la teoría para evitar la aparición de divergencias asociadas a los modos de alta energía. La maquinaria de RG ha sido aplicada con éxito a la Cromodinámica Cuántica (QCD). En esta teoría la función β, que gobierna el comportamiento del acoplamiento renormalizado, tiende a cero a cortas distancias, i.e. altas energías (UV). Este fenómeno se denomina libertad asintótica [2]. Por el contrario, el valor del acoplamiento aumenta a baja energía (IR). Este interesante comportamiento limita la aplicabilidad de los métodos perturbativos, que están definidos sólo en la región de alta energía. Por ello, es necesario el uso de estrategias no perturbativas para estudiar la dinámica de la teoría a baja energía.

En este contexto, una manera natural y elegante de regularizar la teoría es formularla en una red. La teoría se define en un retículo espaciotemporal discreto con espaciado a, que actúa como un cutoff en momentos. En este formalismo es posible llevar a cabo un cálculo numérico desde primeros principios, sin depender de expansiones perturbativas.

En este trabajo se usa la regularización en una red como herramienta para estudiar un tema crucial en QFT: la renormalización de operadores compuestos. El objetivo principal es hacer que las funciones de correlación en capa de masas de operadores locales, que no aparecen en la acción, sean finitas en el límite en que se elimina el cutoff. Los operadores compuestos tienen un papel esencial en el estudio fenomenológico de las interacciones en física de partículas. De hecho, la descripción habitual de las mismas puede ser realizada a través de la Expansión en Producto de Operadores (OPE) [3]. Este último permite expresar las amplitudes físicas en términos de sumas sobre elementos de matriz de operadores locales. Los coeficientes de esta expansión, normalmente llamados coeficientes de Wilson, contienen la información sobre los efectos físicos de alta energía (corta distancia), mientras que los elementos de matriz contienen la dinámica de baja energía, completamente dominada por fenómenos no perturbativos. Estos últimos son calculados en la red en simulaciones en grandes volúmenes, que constituyen un desafío tanto a nivel teórico como computacional. Un ingrediente esencial del cálculo es la renormalización de los elementos de matriz.

En esta tesis nos concentramos en la renormalización no perturbativa de operadores compuestos. Utilizamos un esquema de renormalización de volumen finito con condiciones de contorno de tipo Dirichlet en la dirección temporal, y condiciones de contorno periódicas en el espacio. Esta técnica recibe el nombre “Schrödinger Functional”. A través de las técnicas recursivas desarrolladas por la colaboración ALPHA, podemos no

sólo extraer las constantes de renormalización, sino también calcular el running no perturbativo a lo largo de dos órdenes de magnitud en escalas de energía, desde la región hadrónica $\mathcal{O}(\Lambda_{\rm QCD})$ hasta una perturbativa $\mathcal{O}(M_{\rm W})$. Una vez alcanzada esta última, es posible establecer el contacto con la teoría de perturbaciones, y acceder a otra cantidad fundamental llamada Invariante bajo Grupo de Renormalización (RGI). Este último, como su nombre sugiere, es independiente de la escala, y (salvo en el caso del RGI asociado al acoplamiento) es independiente del esquema de renormalización (si este último es un esquema sin masa).

En particular, en este trabajo consideramos el conjunto completo de bilineales (en campos de quark) invariantes Lorentz en los canales de no singlete. A través de las identidades de Ward (WI) es posible demostrar que sólo dos operadores se transforman de manera independiente bajo RG: la densidad pseudoescalar (o, equivalentemente, la escalar), y las corrientes tensoriales. La primera tiene un papel muy especial, porque es posible demostrar que su renormalización es la misma que la de las masas de quark, con un cambio de signo en la dimensión anómala. Un cálculo de alta precisión de la renormalización de la densidad pseudoescalar, por lo tanto, permite una precisión sin precedentes para la determinación de algunos de los parámetros fundamentales de QCD. Llevamos a cabo un estudio no perturbativo del escaleo de la masa renormalizada en QCD $N_{\rm f} = 2+1$ con una nueva técnica, que implica el uso de dos esquemas diferentes a alta y baja energías, lo que permite calcular por primera vez de manera directa la dimensión anómala no perturbativa.

Los elementos de matriz de corrientes tensoriales también tienen un papel importante en numerosos problemas relevantes en física de partículas. Algunos ejemplos prominentes son la desintegraciones raras de mesones pesados, que permiten poner a prueba la consistencia del sector de sabor del SM (ver, e.g., [4, 5, 6] para una visión global), o las medidas de precisión de la desintegración beta y los límites sobre el momento dipolar eléctrico del neutrón (ver, e.g., [7, 8, 9] para obtener una perspectiva del estado del arte en QCD en la red). También en este caso es necesario una renormalización no perturbativa de alta precisión. En este trabajo hemos realizado un estudio completo a un loop y la renormalización no perturbativa para $N_{\rm f} = 0$ y $N_{\rm f} = 2$.

Por último, proporcionamos una extensión exploratoria de los procedimientos de renormalización para operadores que no renormalizan multiplicativamente. En particular, nos concentramos en el conjunto completo de operadores de cuatro fermiones más allá del SM (BSM) con cambio de sabor. Los elementos de matriz hadrónicos de estos operadores tienen un importante papel en el estudio de la física del sabor en el SM y en la búsqueda de nueva física. En particular, son esenciales para el estudio de la violación de CP en el sector hadrónico en SM y BSM, ya que parametrizan los efectos de nuevas interacciones.

El material presentado en esta tesis se resume así:

- Capítulo 1-2. Tras una breve introducción al RG wilsoniano y generalidades sobre funciones RG, se discute la renormalización de operadores compuestos. Se discute la definición del RGI para operadores renormalizables tanto multiplicativa como no multiplicativamente. A este nivel se introducen conceptos básicos, como las step-scaling functions.

- Capítulo 3. Se introduce la regularización reticular, fijando la notación y discutiendo la discretización tanto de campos gauge como de campos fermiónicos, incluyendo la rotura de simetría quiral en este último sector debido a la presencia del término de Wilson. A continuación discutimos el patrón de renormalización de corrientes y densidades, prestando particular atención a las masas de quark.

- Capítulo 4. Se define el Schrödinger Functional, primero en el continuo y a continuación en la red. Se discute la definición del acoplamiento renormalizado proporcionado de manera natural por el SF, así como las técnicas recursivas de volumen finito. En paralelo a la definición SF del acoplamiento, se discute una definición independiente que usa el Gradient Flow (GF) introducida en [10, 11].

- Capítulo 5. Se presentan la teoría efectiva de Symanzik para la mejora de la regularización en la red, y su aplicación a varias cantidades. En particular, se discuten la mejora de la acción (tanto de su parte gauge como de su parte fermiónica), de las ecuaciones de GF, y de las corrientes y densidades fermiónicas.

- Capítulo 6. Presentamos nuestros resultados para un estudio perturbativo a un loop en el SF de las corrientes tensoriales, analizando los efectos de cutoff y, a través de un procedimiento de matching de esquemas, el resultado del cálculo de las dimensiones anómalas a dos loops de las corrientes tensoriales en este esquema. A continuación presentamos un cálculo completamente no perturbativo del running en dos órdenes de magnitud en escalas de energía tanto para QCD con $N_{\mathrm{f}} = 0$ como para $N_{\mathrm{f}} = 2$.

- Capítulo 7. Presentamos nuestros resultados para el running no perturbativo de masas de quark en QCD $N_{\mathrm{f}} = 2 + 1$. En este caso adoptamos un esquema de renormalización distinto, que usa una definición diferente del acoplamiento renormalizado, en las regiones de alta y baja energía. El matching de los dos running se realiza de manera no perturbativa a una escala intermedia.

- Capítulo 8. Presentamos un estudio perturbativo a un loop de los operadores de cuatro fermiones que violan paridad, así como los efectos de cutoff de sus SSF en esquemas SF. Se proporcionan resultados no perturbativos para QCD $N_{\mathrm{f}} = 2$.

Part I

Theoretical Background

1 Renormalization

In this section we give the basic concepts of the renormalization approach in QFT. Before starting it is worth to observe that the terminology *The Renormalization Group* is unfortunate [12], while the mathematical structure of the procedure somewhat reminds the one of a group this comparison cannot be stressed too much. The word *Renormalization* which arises historically from perturbative calculation in QFT is also misleading as well as the article *The* which gives the impression of a very general tool which might be applied blindly to any physical problem. In practice, renormalization group, is a powerful tool to study a statistical system close to criticality.
All renormalization group studies have in common the idea of re-expressing the fundamental parameters of the theory in terms of some others, while keeping unchanged those physical aspects of the problems which are of interest.
In the next section we define the Renormalization Group (RG) approach à la Wilson introducing the concept of *effective actions* as a consequence of a *coarse graining* RG transformation. This allows to delineate the concept of RG flows and finally the meaning of the continuum limit in terms of RG fixed points. Later on, we move to the well known continuum RG notation, where the scale dependence of operators or couplings is made explicit by the introduction of the energy scale μ which defines the *subtraction point* at which the renormalization conditions are imposed and the cutoff is safely removed. While both approaches lead exactly to the same procedure, they are both summarised in this thesis in order to present a complete picture.

1.1 Scaling and Wilsonian Renormalization Group

The intimate connection of renormalizability in QFT and critical phenomena in statistical physics has been presented by K. Wilson [13, 14, 15], via the formulation of *renormalization group transformations* in terms of effective actions. Following [16] we can assume a QFT in d dimensions governed by the action

$$S_{\Lambda_0}[\varphi] = \int d^d x \left\{ \sum_i \Lambda_0^{d-d_i} g_{0i} \mathbf{O}_i(x) + \mathcal{K}[\varphi] \right\} . \tag{1.1.1}$$

Here we allowed arbitrary local operators $\mathbf{O}_i(x)$ of dimension $d_i > 0$ to appear in the action. Each $\mathbf{O}_i$ can be a Lorentz-Invariant combination of fields and derivatives. In order to keep the formulation as general as possible, we introduce a generic kinetic term $\mathcal{K}[\varphi]$ quadratic in the (generic) fields $\varphi(x)$, accounting for all kind of actions. For later convenience we consider the couplings g_{0i} dimensionless by the introduction of the *energy scale* Λ_0 which carries all the dimensions and plays the rôle of a *momentum cutoff*. For such a *regularized* theory, the partition function reads

$$\mathcal{Z}_{\Lambda_0}(g_{0i}) = \int_{C^\infty(M)_{\leq \Lambda_0}} D\varphi e^{-S_{\Lambda_0}[\varphi]} \tag{1.1.2}$$

Where the integral have to be taken over the space $C^\infty(M)_{\leq\Lambda_0}$ of smooth functions (fields) on the manyfold M whose momentum is at most Λ_0.[1] In this way we allow only momentum modes up to the cutoff scale Λ_0, preventing eventual UV divergencies[2], since the infinite energy region is absent. However, the inclusion of the UV region is crucial and will be discussed in detail Section 1.2.1. It is natural at this stage to separate the field components integrating those modes between Λ_0 and $\Lambda < \Lambda_0$. Therefore

$$\varphi(x) = \left(\int_{|p|\leq\Lambda} + \int_{\Lambda<|p|\leq\Lambda_0} \right) e^{ip\cdot x} \frac{d^d p}{(2\pi)^d} \tilde{\varphi}(p) = \phi(x) + \chi(x)\,, \tag{1.1.3}$$

where $\phi \in C^\infty_{\leq\Lambda}$ is the low-energy part of the field while $\chi \in C^\infty_{(\Lambda,\Lambda_0]}$ contains the high energy modes, and the integral measure in the path integral can be consequently factorised as $D\varphi = D\phi D\chi$. Performing an integral over the high-energy modes χ defines an *effective action* at the new scale Λ

$$S^{\text{eff}}_\Lambda[\phi] = -\log\left[\int_{C^\infty_{(\Lambda,\Lambda_0]}} D\chi e^{-S_{\Lambda_0}[\phi+\chi]} \right], \tag{1.1.4}$$

involving the low-energy modes only. This process is usually called "integrating-out" high energy modes, consequently changing the scale of the theory. The process can be iterated, integrating out further modes, and obtaining again a new effective action

$$S^{\text{eff}}_{\Lambda'}[\phi] = -\log\left[\int_{C^\infty_{(\Lambda',\Lambda]}} D\chi e^{-S_{\Lambda}[\phi+\chi]} \right], \tag{1.1.5}$$

at a still lower scale $\Lambda' < \Lambda$.

What is crucial in the above iterative construction is that the partition function

$$\mathcal{Z}_\Lambda(g_i(\Lambda)) = \int_{C^\infty(M)_{\leq\Lambda}} D\phi e^{-S^{\text{eff}}_\Lambda[\varphi]} \tag{1.1.6}$$

is exactly the same as the one defined at Λ_0 if we re-absorb the change of the cutoff into the couplings, viz

$$\mathcal{Z}_\Lambda(g_i(\Lambda)) = \mathcal{Z}_{\Lambda_0}(g_{0i})\,. \tag{1.1.7}$$

In particular, if the scale is lowered infinitesimally, the above equation reads

$$\Lambda \frac{d\mathcal{Z}(g_i(\Lambda)}{d\Lambda} = \left(\Lambda \frac{\partial}{\partial\Lambda}\bigg|_{g_i} + \Lambda \frac{\partial g_i(\Lambda)}{\partial\Lambda} \frac{\partial}{\partial g_i}\bigg|_{\Lambda} \right) \mathcal{Z}_\Lambda(g_i(\Lambda)) = 0\,. \tag{1.1.8}$$

Eq. (1.1.8) is a particular case for partition function of *Callan-Symanzik equation*, which in general are differential equations which, once integrated, give the dependence of a given quantity respect to the energy scale. On the other hand, Eq. (1.1.8) simply tells how the couplings of the effective action S^{eff}_Λ vary to account for the change in the degrees of freedom over which we take the path integral, so that the partition function is in fact independent on the scale at which we define our theory, provided this scale is below our initial cutoff Λ_0.

[1] In general in a quantum theory it is not always possible to describe the theory in terms of smooth fields, but in order to make this construction easier we work under this assumption.

[2] In this work we do not consider IR divergencies

With a generic initial action, the effective action can be written as

$$S_\Lambda^{\text{eff}}[\phi] = \int d^d x \left\{ \sum_i \Lambda^{d-d_i} Z_\phi(\Lambda)^{n_i/2} g_i(\Lambda) \mathbf{O}_i(x) + Z_\phi(\Lambda) \mathcal{K}[\phi] \right\} \tag{1.1.9}$$

where n_i is the dimension of the operator $\mathbf{O}_i$ and $Z_\phi(\Lambda)$ defines the *renormalized* field

$$\varphi(x) = Z_\phi^{1/2}(\Lambda)\phi(x)\,. \tag{1.1.10}$$

In this case we talk about wave function renormalization, but the same can be done for the composite operators and parameters as we will see in the following. It is crucial at this stage to already introduce the β-functions for the couplings as

$$\beta_i(g_i) = \Lambda \frac{\partial g_i(\Lambda)}{\partial \Lambda}\,. \tag{1.1.11}$$

For a dimensionless coupling we can then write

$$\beta_i(g_j(\Lambda)) = (d_i - d) g_i(\Lambda) + \beta_i^{\text{quant}}(g_j)\,, \tag{1.1.12}$$

where the first term is the "naive" scaling of the coupling and the latter β_i^{quant} represents the quantum effect of integrating out the high-energy modes. Similarly to the β-function we can define another fundamental quantity called *anomalous dimension* of the field as

$$\gamma_\phi(\Lambda) = -\frac{1}{2}\Lambda \frac{\partial \log Z_\phi(\Lambda)}{\partial \Lambda}\,, \tag{1.1.13}$$

where the factor $1/2$ comes from the power in Eq. (1.1.10). The meaning of the name *anomalous* will be clear in the following. Like the β-functions γ_ϕ depends on the value of all the couplings in the theory[3].

Suppose an n-point correlation function in the regularised theory, given by

$$\langle \phi(x_1) \dots \phi(x_n) \rangle = \frac{1}{\mathcal{Z}} \int_{C^\infty(M)_{\leq \Lambda}} D\phi\, e^{-S_\Lambda^{\text{eff}}[Z^{1/2}(\Lambda)\phi; g_i(\Lambda_0)]} \phi(x_1) \dots \phi(x_n)\,, \tag{1.1.14}$$

with field insertions at $x_1, \dots, x_n \in M$ and for $i \neq j$, $x_i \neq x_j$, using the scale Λ . Renormalizing the fields with Eq. (1.1.10) we have

$$\langle \phi(x_1) \dots \phi(x_n) \rangle = Z_\phi^{-n/2}(\Lambda) \langle \varphi(x_1) \dots \varphi(x_n) \rangle\,. \tag{1.1.15}$$

Since the change in the measure $D\phi \to D\varphi$ cancels as we have normalised by the partition function. Upon performing the φ path integral we will (in principle) evaluate the remaining φ correlator as some function $\Gamma_\Lambda^{(n)}(x_1, \dots, x_n; g_i(\Lambda))$ that depends on the scale Λ, couplings and positions x_i. If the modes just involve momenta $\ll \Lambda$ then the same correlation function can be computed using just an effective lower scale theory. In other words, the operator insertions will be unaffected as we integrate out modes in range $(s\Lambda, \Lambda]$ for $s < 1$. The correlator $\Gamma_\Lambda^{(n)}(x_1, \dots, x_n; g_i(\Lambda))$ is than given by

$$Z_\phi^{-n/2}(s\Lambda)\Gamma_{s\Lambda}^{(n)}(x_1, \dots, x_n; g_i(s\Lambda)) = Z_\phi^{-n/2}(\Lambda)\Gamma_\Lambda^{(n)}(x_1, \dots, x_n; g_i(\Lambda))\,, \tag{1.1.16}$$

[3] As we will show in the following, this is one of the main reasons for using a massless renormalization scheme.

or in the differential form we have the usual Callan-Symanzik equation for correlators

$$\Lambda\frac{d}{d\Lambda}\Gamma^{(n)}_{\Lambda}(x_1,\ldots,x_n;g_i(\Lambda)) = \left(\Lambda\frac{\partial}{\partial\Lambda}+\beta_i(g)\frac{\partial}{\partial g_i}+n\gamma_\phi\right)\Gamma^{(n)}_{\Lambda}(x_1,\ldots,x_n,g_i(\Lambda)) = 0\,. \tag{1.1.17}$$

Let us now define better the rôle of the anomalous dimension. We integrate out modes in the range $(s\Lambda,\Lambda]$ as above, but we also change coordinates introducing a spacial dilatation by $x^\mu \to sx^\mu = x'^\mu$. The scaling of a field with dimension d_ϕ in d space-time dimensions is [4]

$$\phi(sx) = s^{(d_\phi-d)/2}\phi(x)\,. \tag{1.1.18}$$

Since for the kinetic term $\int d^dx'\,\mathcal{K}[\phi(x')] = \int d^dx\,\mathcal{K}[\phi(x)]$, the remaining terms in the action are likewise unchanged by the rescaling provided by $\Lambda \to \Lambda/s$ in the opposite direction of x. The energy scale $s\Lambda$ is then restored to its original value Λ. In this operation the scaling is not induced by a RG transformation, is simply a change of coordinate. We find then for a correlation function

$$\begin{aligned}\Gamma^{(n)}_{\Lambda}(x_1,\ldots,x_n;g_i(\Lambda)) &= \left(\frac{Z_\phi(\Lambda)}{Z_\phi(s\Lambda)}\right)^{-n/2}\Gamma^{(n)}_{s\Lambda}(x_1,\ldots,x_n;g_i(s\Lambda))\\ &= \left(s^{(d_\phi-d)}\frac{Z_\phi(\Lambda)}{Z_\phi(s\Lambda)}\right)^{n/2}\Gamma^{(n)}_{\Lambda}(sx_1,\ldots,sx_n;g_i(s\Lambda))\,.\end{aligned} \tag{1.1.19}$$

From the r.h.s. of the above equation we see the classical "naive" scaling of an object with mass dimension as $n(d-d_\phi)/2$, but the effect of integrating out high modes modifies the naive scaling. If we consider $s = 1+\delta s$ with $\delta s \ll 1$ from Eq. (1.1.19) we have

$$\left(s^{(d_\phi-d)}\frac{Z_\phi(\Lambda)}{Z_\phi(s\Lambda)}\right)^{1/2} = 1+\left(\frac{d-d_\phi}{2}+\gamma_\phi\right)\delta s+\mathcal{O}(\delta s^2)\,, \tag{1.1.20}$$

with the anomalous dimension γ_ϕ given by Eq. (1.1.13). The *scaling dimension* of the field is then given by

$$\gamma_\phi^{\text{classical}}+\gamma_\phi \quad \text{with} \quad \gamma_\phi^{\text{classical}} = \frac{d-d_\phi}{2}\,. \tag{1.1.21}$$

1.2 Renormalization Group flow

In order to present the flow induced in the theory parameters by the RG transformation, let us change the formalism in order to make contact with the one practically used in this work. Consider a QFT regularized on a space-time lattice with $a = \Lambda_0^{-1}$ as the regulator. In this section we are interested in the identification of the continuum limit. In that respect, instead of lowering the cutoff as in the previous section, let us send $a \to 0$ (or $\Lambda_0 \to \infty$), removing the cutoff and including high-energy modes into the theory.

The existence of a continuum limit is given by

$$m_{\text{phys}}a \to 0 \tag{1.2.1}$$

for $a \to 0$. The above equation implies than that inverse of the "physical" mass, interpreted as the correlation length $\xi \sim m_{\text{phys}}^{-1}$ of a two point correlation function has to

[4] I.e. for a scalar field $[\phi] = (2-d)/2$ while for a spinor $[\psi] = (1-d)/2$.

diverge as it would happen in a second order phase transition in a statistical system at the *critical point*. Let us suppose that we have a lattice theory with $m \ll 1/a$. As showed in the previous section, if the theory is local and consequently the action (with an explicit dependence on the regulator $\Lambda = 1/a$) is given by Eq. (1.1.1), the long-distance behaviour of the system may be decoupled from the short-distance (high-momentum) dynamics, which can be reabsorbed into a change of the theory parameters $g_i(a)$ as a function of the cutoff.

In order to approach the continuum limit we proceed here with the so called "Coarse Graining" approach[5]. We consider a series of lattice spacings (corresponding to the scales Λ) inducing a series of effective actions as

$$a > a_1 > a_2 > \cdots > a_n = (1-\epsilon)^n a\,, \quad \text{with} \quad \epsilon \ll 1\,, \tag{1.2.2}$$

$$S^{(0)}(a) \to S^{(1)}(a) \to S^{(2)}(a) \to \cdots \to S^{(n)}(a)\,, \tag{1.2.3}$$

where $S^{(n)}(a)$ is simply obtained by the n-th action at a_n after integrating out recursively the extra high-momentum (between $1/a_{n-1}$ and $1/a_n$) degrees of freedom appearing at each iteration. It is natural to consider the RG transformation as the action of an RG evolution operator R_i acting on the coupling space as

$$R_i : g_i^{(n)} \to g_i^{(n+1)}\,. \tag{1.2.4}$$

A crucial point in this formulation is the existence of *fixed points* of R_i

$$R_i(g^*) = g^* \tag{1.2.5}$$

where the parameters are unchanged by the application of the RG transformation[6]. In other words, the action remains unchanged as we move toward continuum limit. The fixed points are therefore critical points, since Eq. (1.2.1) can be recast as

$$\lim_{n\to\infty} m_{\text{phys}}(g^*) a_n \to 0\,, \tag{1.2.6}$$

unless the physical critical mass diverges, which would be uninteresting for a QFT. It turns out, that such fixed points, if they exist, are rather universal, because they can be approached by tuning just a few parameters, called relevant couplings. Let us be more qualitative.

In order to understand the critical dynamics of the theory close to the critical point we can linear expand the RG evolution as

$$g_i^{(n+1)} - g_i^* = \sum_j \left.\frac{\partial R_i}{\partial g_j}\right|_{g^*} (g_j^{(n)} - g_j^*)\,, \tag{1.2.7}$$

the distance from the critical point $\Delta g_i^{(n)}$ change then accordingly to

$$\Delta g_i^{(n+1)} = \sum_j M_{ij} \Delta g_j^{(n)} \quad \text{with} \quad M_{ij} = \left.\frac{\partial R_i}{\partial g_j}\right|_{g^*}\,. \tag{1.2.8}$$

Looking at the eigenvalues λ_i of M_{ij} we can identify the three situations sketched in Fig. 1.1 :

[5]Not the usual coarse graining, since we are going towards the continuum, and not towards the IR, as in the original formulation by Wilson [14]. This implies that the RG flow has its direction reversed

[6]Sometimes in the literature authors refer to *Renormalization Group Flow* or *Renormalization Group Transformation* whether it is a continuous transformation or it is a discrete one. In the present thesis we will use both nomenclatures without making any distinction

- $\lambda_i > 1$ define a *relevant direction* in RG space, increasing as $n \to \infty$
- $\lambda_i = 1$ define a *marginal direction* which stays the same as $n \to \infty$
- $\lambda_i < 1$ define an *irrelevant direction* which decreases as $n \to \infty$.

In the first case, since the RG transformation is repulsive respect to the fixed point those couplings, called *relevant couplings* need to be tuned along the iterations. The third case is also interesting because irrelevant directions play an important rôle in terms of improving the RG scaling of the theory. The remaining possibility of marginal operators is a situation where Lyapunov theorem of stability cannot be applied. In this situation, the stability of the fixed point is given by the non-linear part of the equation, and can be attractive or repulsive.

A key feature in this framework is given by the *universality* of critical phenomena, which translates to our context to the *universality of the continuum limit*. This concept has fundamental implication and is discussed more in detail in Section 5.

1.2.1 Continuum Limit and Asymptotic Freedom

The continuum limit is approached removing the cutoff $a \to 0$ whilst keeping the same physics at any momentum $p < a^{-1}$. This concept of "keeping the physics constant" plays a fundamental rôle in this work, and we will often refer to the renormalized trajectory as a *line of constant physics* (LCP) since some interesting physical quantity is kept unchanged while scaling towards the continuum limit (e.g. see [17]). As discussed more in detail in following chapters, this thesis the LCP is defined by requiring the renormalized coupling is constant while approaching to the continuum.

The existence of such a limit is highly non-trivial and encodes the renormalizability of the theory of interest. It is important to say that taking the continuum limit involves the inverse RG flow, which is going toward the UV.

From now on we consider only one coupling in our theory calling it g_0 (e.g. we will think of it as the bare coupling of a 4-dimensional gauge theory). This means that when we send $a \to 0$ we are interested in $g_0(a) \to g_0(0)$ which is a fixed point of RG.

In case of QCD with $N_\mathrm{f} < 33/2$ the theory is said to be *asymptotically free* [18], meaning $g_0(a = 0) = g^* = 0$. In this case since the theory is not interacting at g^*, this is called *Gaussian Fixed Point*. The resulting trajectory $g_0(a)$ is known as a "renormalized trajectory" since it defines the theory at all scales (not depending on the cutoff). Clearly a renormalized trajectory has to have the infinite set of irrelevant couplings at the UV fixed-point vanishing. As mentioned in the last section, thanks to universality, the continuum theory is not reached only by the renormalized trajectory. We can think about a class of theories defined with cut-off $a' \neq a$ and with coupling $\tilde{g}(a')$ (which is not necessary the one on the RG trajectory) for which $\tilde{g}(a = 0)$ lies on the critical surface in the domain of attraction of the UV fixed point. In this sense the limit $a' \to 0$ is defined in such a way that the IR physics at the original cut-off a is fixed.

There are then many ways of taking the continuum limit of the theory which differ by irrelevant operators, leading to the same continuum theory. This opens the possibility of modifying the theory with the inclusion of some irrelevant operators (respecting the symmetry of the action) which may improve the scaling toward the continuum. This simple idea is actually very interesting topic, described in more detail in section 5 under the name of "Symanzik Improvement".

More in general, if we suppose an initial coupling $g(a)$ to be on the critical surface, within the domain of attraction of the fixed point g^*, by lowering the cutoff, the theory

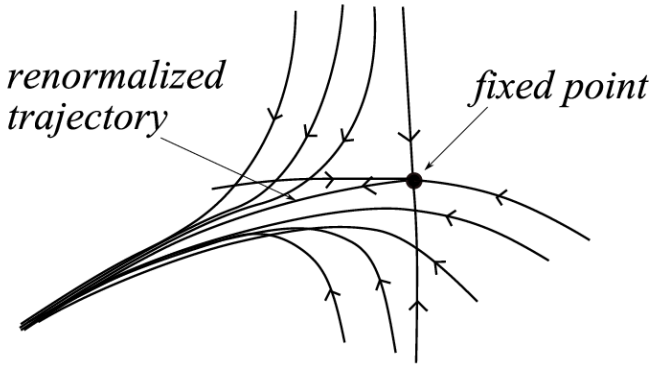

FIGURE 1.1: A sketch of the RG flow (from [20]), where the renormalized trajectory flows out from the UV fixed point when moving toward the IR energy region.

we obtain at any fixed scale $< 1/a$ will be driven to the critical point, as all the irrelevant operators become suppressed by the cutoff itself. The critical point is a fixed point of the RG flow and so, by definition, is scale invariant, so we can remove the cutoff without affecting the theory. The resulting (massless) theory at the critical point will be a Conformal Field Theory (CFT), independent on the scale.

In general QCD as well as Yang-Mills theories are not CFT, and several relevant or marginally relevant operators are turned on by the interactions. The crucial observation is that due to the asymptotic freedom the theory becomes free (i.e. scale independent) at the gaussian fixed point. However, the scale independence is only in the "bare" coupling, since the renormalized one survives in the continuum (assuming a non trivial theory), making the (renormalized) theory not conformal.

The existence of other attractive IR fixed point $g'^* \neq 0$ is still an open problem. Models engineered in order to exhibit a conformal or *quasi*-conformal behaviour (meaning the β-function is very small) in the non-perturbative low-energy region are vastly discussed in literature (among many others we can cite [19] as a review on the topic) and may offer an intriguing extension of the SM.

2 Renormalization of composite operators

Let us now focus on the renormalization of composite operators, which is the central topic of this thesis. The notation is slightly changed with respect to the previous chapter in order to match the one more commonly used in the context of particle physics.

Theory parameters and operators are renormalised at the renormalisation scale μ. The scale dependence of renormalised quantities is then governed by renormalisation group evolution. We will consider QCD with $N_{\rm f}$ quark flavours and N colours. The Callan-Symanzik equations satisfied by the gauge coupling and quark masses are of the form

$$q\frac{\partial}{\partial q}\bar{g}(q) = \beta(\bar{g}(q))\,, \tag{2.0.1}$$

$$q\frac{\partial}{\partial q}\overline{m}_{\rm f}(q) = \tau(\bar{g}(q))\,\overline{m}_{\rm f}(q)\,, \tag{2.0.2}$$

respectively, and satisfy the initial conditions

$$\bar{g}(\mu) = g_{\rm R}\,, \tag{2.0.3}$$

$$\overline{m}_{\rm f}(\mu) = m_{\rm R,f}\,, \tag{2.0.4}$$

where f is a flavour label. In a mass-independent scheme, like the one we use here, the β-function and mass anomalous dimension τ depend on the coupling and the number of flavours, but not on quark masses. Asymptotic perturbative expansions read

$$\beta(g) \underset{g\sim 0}{\approx} -g^3(b_0 + b_1 g^2 + \ldots)\,, \tag{2.0.5}$$

$$\tau(g) \underset{g\sim 0}{\approx} -g^2(d_0 + d_1 g^2 + \ldots)\,. \tag{2.0.6}$$

The universal coefficients of the perturbative beta function and mass anomalous dimension are

$$\begin{aligned} b_0 &= \frac{1}{(4\pi)^2}\left[\frac{11}{3}N - \frac{2}{3}N_{\rm f}\right]\,,\\ b_1 &= \frac{1}{(4\pi)^4}\left[\frac{34}{3}N^2 - \left(\frac{13}{3}N - \frac{1}{N}\right)N_{\rm f}\right]\,,\\ d_0 &= \frac{1}{(4\pi)^2}\,\frac{3(N^2-1)}{N}\,. \end{aligned} \tag{2.0.7}$$

We collect here to simplify the presentation, the first non-universal perturbative coefficient of the β function and τ for the SF scheme (which will be introduced in Chapter 4)

as

$$b_2 = \frac{1}{(4\pi)^3}\left(0.483 - 0.275N_{\rm f} + 0.0361N_{\rm f}^2 - 0.00175N_{\rm f}^3\right)\,, \tag{2.0.8}$$

$$d_1 = \frac{1}{(4\pi)^2}\left(0.2168 + 0.084N_{\rm f}\right)\,. \tag{2.0.9}$$

We will deal with Euclidean correlation functions of gauge-invariant composite operators. Without loss of generality, let us consider correlation functions of the form

$$G_k(x; y_1, \ldots, y_n) = \langle O_k(x)\mathcal{O}_1(y_1)\cdots\mathcal{O}_n(y_n))\rangle\,, \tag{2.0.10}$$

with $x \neq y_j\ \forall j,\ y_j \neq y_k\ \forall j \neq k$, where $\{O_k\}$ is a set of operators that mix under renormalisation, and where $\mathcal{O}_k$ are multiplicatively renormalisable operators.[1] Renormalised correlation functions satisfy a system of Callan-Symanzik equations obtained by imposing that G_k is independent of the renormalisation scale μ, viz.

$$\mu\frac{\mathrm{d}}{\mathrm{d}\mu}\bar{G}_j = \sum_k\left[\gamma_{jk}(g_{\rm R}) - \sum_{l=1}^{n}\tilde{\gamma}_l(g_{\rm R})\right]\bar{G}_k\,, \tag{2.0.11}$$

which, expanding the total derivative, leads to

$$\left\{\mu\frac{\partial}{\partial\mu} + \beta(g_{\rm R})\frac{\partial}{\partial g_{\rm R}} + \beta_\lambda(g_{\rm R})\lambda\,\frac{\partial}{\partial\lambda} + \sum_{\rm f=1}^{N_{\rm f}}\tau(g_{\rm R})m_{\rm R,f}\frac{\partial}{\partial m_{\rm R,f}} + \sum_{l=1}^{n}\tilde{\gamma}_l(g_{\rm R})\right\}\bar{G}_j = \sum_k\gamma_{jk}(g_{\rm R})\,\bar{G}_k\,, \tag{2.0.12}$$

where γ is a matrix of anomalous dimensions describing the mixing of $\{O_k\}$, and $\tilde{\gamma}_l$ is the anomalous dimension of $\mathcal{O}_l$. For completeness, we have included a term which takes into account the dependence on the gauge parameter λ in covariant gauges; this term is absent in schemes like $\overline{\rm MS}$ (irrespective of the regularisation prescription) or the SF schemes we will introduce, but is present in the RI schemes we will also be concerned with later. The RG function β_λ is given by

$$q\frac{\partial}{\partial q}\lambda(q) = \beta_\lambda(\bar{g}(q))\lambda(q)\,, \tag{2.0.13}$$

and its perturbative expansion has the form

$$\beta_\lambda(g) = -g^2(b_0^\lambda + b_1^\lambda g^2 + \ldots)\,, \tag{2.0.14}$$

where the universal coefficient is given by

$$b_0^\lambda = \frac{1}{(4\pi)^2}\left[\left(\lambda - \frac{13}{3}\right)N + \frac{4}{3}N_{\rm f}\right]\,. \tag{2.0.15}$$

In the Landau gauge ($\lambda = 0$) the term with β_λ always vanishes. From now on, in order to avoid unnecessary complications, we will assume that whenever RI anomalous dimensions are employed they will be in Landau gauge, and consequently drop terms with β_λ in all equations.

[1] To avoid burdening the notation, we have omitted the dependence of G_k on coupling and masses, as well as on the renormalisation scale.

From now on, in order to simplify the notation we will use the shorthand notation

$$q\frac{\partial}{\partial q}\,\overline{O}_j(q) = \sum_k \gamma_{jk}(\bar{g}(q))\,\overline{O}_k(q) \tag{2.0.16}$$

for the Callan-Symanzik equation satisfied by the insertion of a composite operator in a renormalised, on-shell correlation function (i.e. Eq. (8.1.8) is to be interpreted in the sense provided by Eq. (2.0.12)). The corresponding initial condition can be written as

$$\overline{O}_k(\mu) = O_{\mathrm{R},k}\,, \tag{2.0.17}$$

and the perturbative expansion of the anomalous dimension matrix γ as

$$\gamma(g) \underset{g\sim 0}{\approx} -g^2(\gamma_0 + \gamma_1 g^2 + \ldots)\,. \tag{2.0.18}$$

The connection between the bare operator and its renormalized counterpart is given by the renormalization constants, defined by the limit equation

$$\overline{O}_k(\mu) = \lim_{a\to 0} Z_{kj}(a\mu) O_j^{\mathrm{bare}}(a)\,, \tag{2.0.19}$$

where a is the usual cutoff. Both Z and O^{bare} are divergent at $a = 0$ in a way that $\overline{O}$ is finite. An explicit definition of the renormalization constants will be discussed when the renormalization conditions are introduced for every operator of interest in this work.

2.1 Formal solution of the RG equation

Let us now consider the solution to Eq. (8.1.8). To that purpose we start by introducing the (matrix) renormalisation group evolution operator $U(\mu_2, \mu_1)$ that evolves renormalised operators between the scales[2] μ_1 and $\mu_2 < \mu_1$.

$$\overline{O}_i(\mu_2) = U_{ij}(\mu_2, \mu_1)\,\overline{O}_j(\mu_1)\,. \tag{2.1.1}$$

By substituting into Eq. (8.1.8) one has the equation for $U(\mu_2, \mu_1)$

$$\mu_2\,\frac{\partial}{\partial \mu_2}\,U(\mu_2, \mu_1) = \gamma[\bar{g}(\mu_2)]U(\mu_2, \mu_1)\,, \tag{2.1.2}$$

(n.b. the matrix product on the r.h.s.) with initial condition $U(\mu_1, \mu_1) = \mathbf{1}$. Following a standard procedure, this differential equation for U can be converted into a Volterra-type integral equation and solved iteratively, viz.

$$U(\mu_2, \mu_1) = T\exp\left\{\int_{\bar{g}(\mu_1)}^{\bar{g}(\mu_2)} \mathrm{d}g\,\frac{1}{\beta(g)}\,\gamma(g)\right\}\,, \tag{2.1.3}$$

where as usual the notation Texp refers to a definition in terms of the Taylor expansion of the exponential function with "powers" of the integral involving argument-ordered

[2] Restricting the evolution operator to run towards the IR avoids unessential algebraic technicalities below. The running towards the UV can be trivially obtained by taking $[U(\mu_2, \mu_1)]^{-1}$.

integrands — explicitly, for a generic matrix function M, one has

$$\begin{aligned} T\exp\left\{\int_{x_-}^{x_+}\mathrm{d}x\,M(x)\right\} \equiv \mathbf{1} &+ \int_{x_-}^{x_+}\mathrm{d}x\,M(x) \\ &+ \int_{x_-}^{x_+}\mathrm{d}x_1\,M(x_1)\int_{x_-}^{x_1}\mathrm{d}x_2\,M(x_2) \\ &+ \int_{x_-}^{x_+}\mathrm{d}x_1\,M(x_1)\int_{x_-}^{x_1}\mathrm{d}x_2\,M(x_2)\int_{x_-}^{x_2}\mathrm{d}x_3\,M(x_3) \\ &+ \dots \\ = \mathbf{1} &+ \int_{x_-}^{x_+}\mathrm{d}x\,M(x) \\ &+ \frac{1}{2!}\int_{x_-}^{x_+}\mathrm{d}x_1\int_{x_-}^{x_+}\mathrm{d}x_2\left\{\theta(x_1-x_2)M(x_1)M(x_2)+\right. \\ &\qquad\left.\theta(x_2-x_1)M(x_2)M(x_1)\right\} \\ &+ \dots \end{aligned} \tag{2.1.4}$$

2.1.1 RGI in the absence of mixing

The RG equations, for coupling, mass or a generic composite operator multiplicatively renormalizable can be formally solved in terms of the renormalization group invariants (RGIs).

Let us derive the RGIs for composite operators, the one for the coupling can be obtained analogously.

We assume here γ (or τ equivalently) and U are scalar objects (in the next section we generalise to the matrix case), therefore Eq. (2.1.1) can be manipulated as

$$\begin{aligned} \overline{O}(\mu_2) &= \exp\left\{\int_{\bar g(\mu_1)}^{\bar g(\mu_2)}\mathrm{d}g\,\frac{\gamma(g)}{\beta(g)}\right\}\overline{O}(\mu_1) \\ &= \exp\left\{\int_{\bar g(\mu_1)}^{\bar g(\mu_2)}\mathrm{d}g\,\frac{\gamma_0}{b_0 g}\right\}\exp\left\{\int_{\bar g(\mu_1)}^{\bar g(\mu_2)}\mathrm{d}g\,\left[\frac{\gamma(g)}{\beta(g)}-\frac{\gamma_0}{b_0 g}\right]\right\}\overline{O}(\mu_1) \\ &= \left[\frac{\bar g^2(\mu_2)}{\bar g^2(\mu_1)}\right]^{\frac{\gamma_0}{2b_0}}\exp\left\{\int_{\bar g(\mu_1)}^{\bar g(\mu_2)}\mathrm{d}g\,\left[\frac{\gamma(g)}{\beta(g)}-\frac{\gamma_0}{b_0 g}\right]\right\}\overline{O}(\mu_1)\,, \end{aligned} \tag{2.1.5}$$

yielding the identity

$$\left[\frac{\bar g^2(\mu_2)}{\mathcal{N}}\right]^{-\frac{\gamma_0}{2b_0}}\overline{O}(\mu_2) = \left[\frac{\bar g^2(\mu_1)}{\mathcal{N}}\right]^{-\frac{\gamma_0}{2b_0}}\exp\left\{\int_{\bar g(\mu_1)}^{\bar g(\mu_2)}\mathrm{d}g\,\left[\frac{\gamma(g)}{\beta(g)}-\frac{\gamma_0}{b_0 g}\right]\right\}\overline{O}(\mu_1)\,, \tag{2.1.6}$$

where we introduce an arbitrary normalisation $\mathcal{N}$. Common choices[3] are

$$\mathcal{N} = \begin{cases} 4\pi & \text{for generic composite operator} \\ 1/(2b_0) & \text{for the mass}\,. \end{cases} \tag{2.1.7}$$

The advantage of having rewritten Eq. (2.1.1) in this way is that now the integral in the exponential is finite as either integration limit is taken to zero; in particular, the r.h.s. is

[3] Overall normalizations are a matter of convention, apart from that of Λ_{QCD}, which is universal. Our choice for M_i follows Gasser and Leutwyler [21, 22, 23], whereas for Eq. (2.1.12) we have chosen the most usual normalization with a power of α_s.

well-defined when $\mu_2 \to \infty \;\Leftrightarrow\; \bar{g}(\mu_2) \to 0$, and therefore so is the l.h.s. Thus, we define the RGI operator insertion as

$$\hat{O} \equiv \lim_{\mu\to\infty} \left[\frac{\bar{g}^2(\mu)}{\mathcal{N}}\right]^{-\frac{\gamma_0}{2b_0}} \overline{O}(\mu)\,, \tag{2.1.8}$$

upon which we have an explicit expression to retrieve the RGI operator from the renormalised one at any value of the renormalisation scale μ, provided the anomalous dimension and the β-function are known for scales $\geq \mu$,

$$\hat{O} = \left[\frac{\bar{g}^2(\mu)}{\mathcal{N}}\right]^{-\frac{\gamma_0}{2b_0}} \exp\left\{-\int_0^{\bar{g}(\mu)} \mathrm{d}g\, \left[\frac{\gamma(g)}{\beta(g)} - \frac{\gamma_0}{b_0 g}\right]\right\} \overline{O}(\mu)\,. \tag{2.1.9}$$

Starting from the latter equation, it is easy to check explicitly that $\hat{O}$ is invariant under a change of renormalisation scheme.

Explicitly, for Λ_{QCD}, M and a generic composite operator $\hat{O}$ we have:

$$\Lambda_{\mathrm{QCD}} \;=\; \mu\, \frac{[b_0\bar{g}^2(\mu)]^{-b_1/2b_0^2}}{e^{1/2b_0\bar{g}^2(\mu)}}\, \exp\left\{-\int_0^{\bar{g}(\mu)} \mathrm{d}g\, \left[\frac{1}{\beta(g)} + \frac{1}{b_0 g^3} - \frac{b_1}{b_0^2 g}\right]\right\}. \tag{2.1.10}$$

$$M_i \;=\; \overline{m}_i(\mu)\,[2b_0\bar{g}^2(\mu)]^{-d_0/2b_0}\, \exp\left\{-\int_0^{\bar{g}(\mu)} \mathrm{d}g\, \left[\frac{\tau(g)}{\beta(g)} - \frac{d_0}{b_0 g}\right]\right\}, \tag{2.1.11}$$

$$\hat{O} \;=\; \overline{O}(\mu)\, \left[\frac{\bar{g}^2(\mu)}{4\pi}\right]^{-\gamma_0/2b_0}\, \exp\left\{-\int_0^{\bar{g}(\mu)} \mathrm{d}g\, \left[\frac{\gamma(g)}{\beta(g)} - \frac{\gamma_0}{b_0 g}\right]\right\}. \tag{2.1.12}$$

We introduce here the "running", denoted by $\hat{c}(\mu)$ as the ratio between the l.h.s. of the above equations and μ in Eq. (2.1.10), $\overline{m}_i(\mu)$ in Eq. (2.1.11) and finally $\overline{O}(\mu)$ in Eq. (2.1.12).

It is important to observe that while the value of the Λ_{QCD} parameter depends on the renormalization scheme chosen, M_i and $\hat{O}$ are the same for all schemes. In this sense, they can be regarded as meaningful physical quantities, as opposed to their scale-dependent counterparts. The aim of the non-perturbative determination of the RG running of parameters and operators is to connect the RGIs — or, equivalently, the quantity renormalized at a very high energy scale, where perturbation theory applies — to the bare parameters or operator insertions, computed in the hadronic energy regime. In this way the three-orders-of-magnitude leap between the hadronic and weak scales can be bridged without significant uncertainties related to the use of perturbation theory.

Note that the crucial step in the manipulation has been to add and subtract the term $\frac{\gamma_0}{b_0 g}$ in the integral that defines the RG evolution operator, which allows to obtain a quantity that is UV-finite by removing the logarithmic divergence induced at small g by the perturbative behaviour $\gamma(g)/\beta(g) \sim 1/g$. When γ is a matrix of anomalous dimensions this step becomes non-trivial, since in general $[\gamma(g), \gamma_0] \neq 0$; the derivation has thus to be performed somewhat more carefully.

2.1.2 RGI in the presence of mixing

Let us start by studying the UV behaviour of the matrix RG evolution operator in Eq. (2.1.1), using its actual definition in Eq. (2.1.4). To that purpose, we first observe that by taking the leading-order approximation for $\gamma(g)/\beta(g)$ the T-exponential becomes a standard exponential, since $[\gamma_0 g_1^2, \gamma_0 g_2^2] = 0\ \forall g_1, g_2$. One can then perform the integral trivially and

write

$$U(\mu_2,\mu_1) \underset{\rm LO}{=} \left[\frac{\bar g^2(\mu_2)}{\bar g^2(\mu_1)}\right]^{\frac{\gamma_0}{2b_0}} \equiv U_{\rm LO}(\mu_2,\mu_1)\,. \tag{2.1.13}$$

When next-to-leading order corrections are included the T-exponential becomes non-trivial. In order to make contact with the literature (see e.g. [24, 25]), we write[4]

$$U(\mu_2,\mu_1) \equiv [W(\mu_2)]^{-1}\; U_{\rm LO}(\mu_2,\mu_1) W(\mu_1)\,. \tag{2.1.15}$$

Upon inserting Eq. (2.1.15) in Eq. (2.1.2) we obtain for W the RG equation

$$\begin{aligned}\mu\frac{\partial}{\partial\mu}W(\mu) &= -W(\mu)\gamma(\bar g(\mu)) + \beta(\bar g(\mu))\frac{\gamma_0}{b_0\bar g(\mu)}W(\mu)\\ &= [\gamma(\bar g(\mu)), W(\mu)] - \beta(\bar g(\mu))\left(\frac{\gamma(\bar g(\mu))}{\beta(\bar g(\mu))} - \frac{\gamma_0}{b_0\bar g(\mu)}\right)W(\mu)\,.\end{aligned} \tag{2.1.16}$$

The matrix W can be interpreted as the piece of the evolution operator containing contributions beyond the leading perturbative order. It is easy to check by expanding perturbatively (see below) that W is regular in the UV, and that all the logarithmic divergences in the evolution operator are contained in $U_{\rm LO}$; in particular,

$$W(\mu) \underset{\mu\to\infty}{=} \mathbf{1}\,. \tag{2.1.17}$$

Note also that in the absence of mixing Eq. (2.1.16) can be solved explicitly to get

$$W(\mu) \underset{\text{no mixing}}{=} \exp\left\{-\int_0^{\bar g(\mu)} {\rm d}g\,\left[\frac{\gamma(g)}{\beta(g)} - \frac{\gamma_0}{b_0 g}\right]\right\}\,. \tag{2.1.18}$$

Now it is easy, by analogy with the non-mixing case, to define RGI operators. We rewrite Eq. (2.1.1) as

$$\left[\frac{\bar g^2(\mu_2)}{4\pi}\right]^{-\frac{\gamma_0}{2b_0}} W(\mu_2)\overline{O}(\mu_2) = \left[\frac{\bar g^2(\mu_1)}{4\pi}\right]^{-\frac{\gamma_0}{2b_0}} W(\mu_1)\overline{O}(\mu_1)\,, \tag{2.1.19}$$

where $\overline{O}$ is a vector of renormalised operators on which the RG evolution matrix acts, cf. Eq. (2.1.1). The l.h.s. (resp. r.h.s.) is obviously finite for $\mu_1\to\infty$ (resp. $\mu_2\to\infty$), which implies that the vector of RGI operators can be obtained as

$$\hat O = \left[\frac{\bar g^2(\mu)}{4\pi}\right]^{-\frac{\gamma_0}{2b_0}} W(\mu)\overline{O}(\mu) \equiv \tilde U(\mu)\overline{O}(\mu)\,. \tag{2.1.20}$$

When there is no mixing, the use of Eq. (2.1.18) immediately brings back Eq. (2.1.9).

[4]The property underlying this equation is that the evolution operator can actually be factorised, in full generality, as

$$U(\mu_2,\mu_1) = \left[\tilde U(\mu_2)\right]^{-1}\tilde U(\mu_1)\,,\qquad \tilde U(\mu) = \left[\frac{\bar g^2(\mu)}{4\pi}\right]^{-\frac{\gamma_0}{2b_0}} W(\mu) \tag{2.1.14}$$

with a $W(\mu)$ that satisfies Eq. (2.1.16) below.

2.2 Step-Scaling Functions

In order to describe non-perturbatively the scale dependence of the gauge coupling and composite operators, we will use the step-scaling functions (SSFs) σ and σ_O, respectively, defined as

$$-\log(s) = \int_{\sqrt{u}}^{\sqrt{\sigma(u)}} \frac{dg'}{\beta(g')}\,, \tag{2.2.1}$$

$$\sigma_O(s,u) = \exp\left\{\int_{\sqrt{u}}^{\sqrt{\sigma(u)}} \frac{\gamma(g')}{\beta(g')}dg'\right\}\,, \tag{2.2.2}$$

or, equivalently,

$$\sigma(s,u) = \bar{g}^2(\mu/s)\big|_{u=\bar{g}^2(\mu)}\,, \tag{2.2.3}$$

$$\sigma_O(s,u) = U(\mu/s,\mu)\,, \tag{2.2.4}$$

where

$$U(\mu_2,\mu_1) = \exp\left\{\int_{\sqrt{\bar{g}^2(\mu_1)}}^{\sqrt{\bar{g}^2(\mu_2)}} \frac{\gamma(g')}{\beta(g')}dg'\right\} \tag{2.2.5}$$

is the RG evolution operator for the operator at hand, which connects renormalized operators at different scales as $\overline{O}(\mu_2) = U(\mu_2,\mu_1)\overline{O}(\mu_1)$. The SSFs are thus completely determined by, and contain the same information as, the RG functions γ and β. In particular, $\sigma_O(s,u)$ corresponds to the RG evolution operator of $\overline{O}$ between the scales μ/s and μ; from now on, we will set $s=2$, and drop the parameter s in the dependence. The SSF can be related to renormalization constants via the identity

$$\sigma_O(u) = \lim_{a\to 0}\Sigma_O(u,a\mu)\,, \qquad \Sigma_O(u,a\mu) = \left.\frac{Z_O(g_0^2,a\mu/2)}{Z_O(g_0^2,a\mu)}\right|_{u=\bar{g}^2(\mu)}\,. \tag{2.2.6}$$

This will be the expression we will employ in practice to determine σ_O, and hence operator anomalous dimensions, for a broad range of values of the renormalized coupling u. In the case with mixing the definition of the SSF is essentially the same but it involves the ordered exponential respect to the multiplicative renormalizable case. This topic is extensively discussed in Chapter 8.

3 Lattice Formulation and Symmetries

3.1 Lattice QCD

In this Chapter we describe the lattice formulation of QCD [26]. The first step consists in introducing the lattice spacing a thus discretising the Euclidean space-time. By a Fourier transformation it can be showed that the lattice spacing translates into a momentum cut-off π/a. However, if we consider a finite volume $V = L^d$ in d-dimensional space-time, momenta became discrete as well $p_\mu = 2\pi n/L$. Hence, QFT with infinite degrees of freedom can be recovered sending $a \to 0$ after the thermodynamic limit $V \to \infty$.

The gauge potential $A_\mu(x) = A^a_\mu T^a \in \mathfrak{su}(\mathfrak{n})$ is represented on the lattice by the *link* $U_\mu(x) \in SU(N)$ as

$$U_\mu(x) = e^{g_0 a A_\mu(x)} \,. \tag{3.1.1}$$

Parallel transporters $U_\mu(x)$ sits on the link connecting the sites x and $x + a\hat{\mu}$ ($\hat{\mu}$ denotes the unit vector in μ-direction). It is easy to see that each closed loop made up of links is a gauge invariant observable.
Quark and antiquark fields $\psi(x)$ and $\bar{\psi}(x)$ are defined on the lattice sites and live in Dirac, colour and flavour space. The lattice action has the form of

$$S[U, \bar{\psi}, \psi] = S_{\mathrm{G}}[U] + S_{\mathrm{F}}[U, \bar{\psi}, \psi] \,, \tag{3.1.2}$$

where S_{G} and S_{F} denote respectively the gauge and the fermion action. Since the continuum theory have to be reproduced only when $a \to 0$, the way to discretize the theory is not unique. In general we can think about lattice theories as a class whose elements differ each others by cutoff effects (which, by definition, vanish in the continuum). This idea is better formalised under the name of Symanzik's Improvement Program, which is discussed in Section 5. At this stage, we introduce the actions without any improvement.

Explicitly, gauge action is given by the so-called Plaquette Wilson action as

$$S_{\mathrm{G}}[U] = \frac{1}{g_0^2} \sum_p \mathrm{Tr}\{1 - U(p)\} \tag{3.1.3}$$

with the bare gauge coupling constant $g_0^2 = 2N/\beta$ (which has nothing to do with the RG β-function) and the parallel transporter around a closed loop $U(p)$. The index p in the sum in Eq. (3.1.3) runs over the *oriented* plaquettes p on the lattice. It is interesting to notice that this action approaches to the continuum quadratically in a. In fact, thanks to the presence of translation and gauge invariance all $\mathcal{O}(a)$-terms are forbidden. [1]

Before introducing a discretisation of fermions on the lattice, we replace derivatives with finite differences. This can be done in several ways, e.g. we can have the "forward"

[1] We are implicitly assuming boundary conditions (BC) which preserve translations, e.g. periodic BC.

derivative

$$a\partial_\mu f(x) = f(x + a\hat{\mu}) - f(x)\,, \tag{3.1.4}$$

"backward" derivative

$$a\partial^*_\mu f(x) = f(x) - f(x - a\hat{\mu})\,, \tag{3.1.5}$$

or the "symmetric" combination [2] of the two above

$$2a\tilde{\partial}_\mu f(x) = f(x + a\hat{\mu}) - f(x - a\hat{\mu})\,. \tag{3.1.6}$$

It is interesting to notice already at this point that while backward and forward derivative approaches the continuum derivative linearly in a, the symmetric one approaches quadratically in the lattice spacing. This is a first naive example of $\mathcal{O}(a)$-improvement. The covariant version of the discrete derivative can be interpreted as a "covariant shift" by plugging a link into the derivative, as

$$a\nabla_\mu \psi(x) = U_\mu(x)\psi(x + a\hat{\mu}) - \psi(x)\,, \tag{3.1.7}$$

and the analogous for the backward and symmetric derivatives.

Starting from a free theory the usual Dirac Lagrangian (in euclidean space), reads

$$\mathcal{L}_F = (\gamma_\mu \partial_\mu + m_0)\psi(x)\,. \tag{3.1.8}$$

If we substitute naively the derivative with a finite difference, the free fermionic propagator in momentum space becomes

$$S_{\alpha\beta}(p) = [m_0 + \sum_\mu i\gamma_\mu \tilde{p}_\mu]_{\alpha\beta}\,, \quad \tilde{p}_\mu = \frac{1}{a}\sin(p_\mu a)\,, \quad p_\mu \in [0, \frac{2\pi}{a}]\,, \tag{3.1.9}$$

with α, β spin indices. Eq. (3.1.9) in the continuum for $d = 4$ describes 2^3 "spatial" copies of the same particle with energy

$$E^2 = m^2 + \frac{1}{a^2}\sum_k \sin^2(ap_k) \overset{a\to 0}{\to} m^2 + \vec{P}^2\,, \quad a\vec{p} = (n_1, n_2, n_3)\pi + a\vec{P}\,. \tag{3.1.10}$$

In addition to this, the time-slice propagator $S(x_0, \mathbf{p})$ has other 2 poles. To summarise, starting with one particle on the lattice, we end up with 2^d degenerate fermions in the continuum limit. The extra poles in the propagator are called "doublers". The same can be seen also in the interacting theory.

The presence of doublers is an important feature of the theory. Their existence can be interpreted as a manifestation of the chiral anomaly, which is reabsorbed by doublers, leaving the theory anomaly-free. This effect is absent for scalar theories which might be discretised naively on the lattice.

Several interesting solutions have been introduced to overcome this "doublers problem". Wilson's solution for this is to add an irrelevant operator to the Lagrangian which enhance the derivative order of the Dirac operator. We introduce the so-called Wilson

[2] It can be showed that symmetric derivative is invariant under an hermitian conjugation. This is not true for the other discretizations, which are transformed one into another.

fermion action as

$$S_{\rm W} = a^a \sum_x \bar{\psi}(x) \frac{1}{2} [\gamma_\mu (\nabla_\mu + \nabla^*_\mu) + 2m_0 - ar \nabla_\mu \nabla^*_\mu] \psi(x) = a^4 \sum_x \bar{\psi}(x) D_{\rm W} \psi(x) \,. \tag{3.1.11}$$

It can be noted immediately that the effect of the extra term, called "Wilson Term" in momentum space

$$-\frac{ar}{2} \nabla_\mu \nabla^*_\mu \to \frac{ar}{2} \hat{p}^2 = \frac{2r}{a} \sum_\mu \sin^2(\frac{p_\mu a}{2}) = \frac{r}{a} \sum_\mu (1 - \cos(p_\mu a)) \,, \tag{3.1.12}$$

is to add a term $\mathcal{O}(a^{-1})$ to the dispersion relation, such that states which before had the same energy at $ap_\mu = \pi$ now decouples in the continuum limit and only the "physical" pole at $ap_\mu = (0,0,0,0)$ in the Brillouin zone survives.

Wilson action is invariant under parity (P), charge conjugation (C) and time reversal (T). Moreover it has the additional symmetry called γ_5-hermiticity $\gamma_5 D_{\rm W} \gamma_5 = D^\dagger_{\rm W}$ which implies important relations on the eigenvalues spectrum [27]. However, the payback of this extra term is that it explicitly breaks chiral symmetry, which is restored only in the continuum limit. At finite lattice spacing chiral symmetry can be also reached, but instead of requiring the bare masses to vanish, the latter have to be tuned along a critical line which depends on cutoff.

With all those elements we can write the complete QCD action with $N_{\rm f}$ Wilson's fermions as

$$S = S_{\rm G} + \sum_{f=1}^{N_{\rm f}} [a^4 \sum_x \bar{\psi}_f(x) D_{\rm W}(m_{0,f}) \psi_f(x)] \,. \tag{3.1.13}$$

For convenience instead of writing explicitly the bare mass in the Lagrangian, it is common to replace it with the *hopping parameter* $\kappa_f = (2m_{0,f}+8)^{-1}$. In terms of this parametrisation, and for $r = 1$ (the parameter entering in the Wilson term), for a flavour f the action reads

$$S^f_{\rm W} = \sum_x \bar{\psi}^f(x) \{1 - \kappa_f \sum_{\mu=0}^{3} [(1-\gamma_\mu) U_\mu(x) \delta_{x,x+a\hat{\mu}} + \delta_{x,x-a\hat{\mu}} (1+\gamma_\mu) U^\dagger_\mu(x)]\} \psi^f(x) \,. \tag{3.1.14}$$

Renormalization properties of operators and currents with Wilson fermions can be formulated in terms of symmetries, which are briefly presented in the following section.

3.2 Ward Identities

At the classical level Noether's theorem relates the presence of conserved currents and charges to continuous symmetries of the Lagrangian. At a quantum level, once the theory is quantized, Ward Identities (WI) tell us how those symmetries are expressed in terms of Green functions. As we will explain in this chapter, the renormalization pattern of composite operators is constrained by symmetries underlying the WI. After a very brief "textbook" discussion about continuum WI, we summarise the WI on the lattice with a discretisation which breaks explicitly the chiral symmetry, in particular the Wilson fermions formulation introduced in the previous section.

3.2.1 Quark bilinear operators

In this thesis we make use extensively of local quark bilinear operators. The general form is

$$\mathbf{O}^f_\Gamma(x) = \bar{\psi}(x)\Gamma\frac{\lambda^f}{2}\psi(x)\,, \tag{3.2.1}$$

where Γ stands for a generic Dirac matrix and $f = 1, \ldots, N_F^2 - 1$ (for the flavour non-singlet case). The specific bilinear operator is denote according to their Lorentz group transformations: the scalar, pseudoscalar and tensor densities are:

$$S^f(x) = \bar{\psi}(x)\frac{\lambda^f}{2}\psi(x)\,, \tag{3.2.2}$$

$$P^f_\mu(x) = \bar{\psi}(x)\gamma_5\frac{\lambda^f}{2}\psi(x)\,, \tag{3.2.3}$$

$$T^f_{\mu\nu}(x) = i\bar{\psi}(x)\sigma_{\mu\nu}\frac{\lambda^f}{2}\psi(x) \tag{3.2.4}$$

respectively. In the tensor $\sigma_{\mu\nu} = \frac{i}{2}[\gamma_\mu, \gamma_\nu]$. Whereas for the vector and axial currents

$$V^f_\mu(x) = \bar{\psi}(x)\gamma_\mu\frac{\lambda^f}{2}\psi(x)\,, \tag{3.2.5}$$

$$A^f_\mu(x) = \bar{\psi}(x)\gamma_\mu\gamma_5\frac{\lambda^f}{2}\psi(x)\,. \tag{3.2.6}$$

In the above, implicit colour and spin indices are contracted.

3.2.2 Continuum WI

The formal continuum theory with N_f mass-less fermions is invariant under $U(N_f)_L \times U(N_f)_R$ chiral transformations. The introduction of a positive mass matrix $M_0 = \mathrm{diag}(m_{0,1}, \ldots, m_{0,N_f})$ breaks it to a smaller subgroup. From the variation of fermion fields deriving from a generic $SU(N_f)_L \times SU(N_f)_R$ transformation (which we rewrite in the usual infinitesimal vector-axial form) we have

$$\delta\psi = i\left[\alpha^a_V\frac{\lambda^a}{2} + \alpha^a_A\gamma_5\frac{\lambda^a}{2}\right]\psi\,, \tag{3.2.7}$$

$$\delta\bar{\psi} = -i\bar{\psi}\left[\alpha^a_V\frac{\lambda^a}{2} - \alpha^a_A\gamma_5\frac{\lambda^a}{2}\right]\,, \tag{3.2.8}$$

with $\lambda^a \in \mathfrak{su}(N_f)$ and $a = 1, \ldots, N_f^2 - 1$. The conservation of currents associated to *global* vector and axial transformation read

$$\mathrm{PCVC}: \quad \partial_\mu V^a_\mu(x) + \bar{\psi}(x)\left[\frac{\lambda^a}{2}, M_0\right]\psi(x) = 0 \tag{3.2.9}$$

$$\mathrm{PCAC}: \quad \partial_\mu A^a_\mu(x) - \bar{\psi}(x)\left\{\frac{\lambda^a}{2}, M_0\right\}\psi(x) = 0\,. \tag{3.2.10}$$

From the above equations it is clear that PCVC relation is satisfied with degenerate quark masses $m_{0,1} = m_{0,2} = \cdots = m_{0,N_f}$, while the axial current is conserved only for massless quarks[3].

[3]Even if not specified in the text we will always refer to the non-anomalous (i.e. flavour non-singlet) PCAC relation

Beyond classical level WI are to be understood as relations among operators. More precisely they are insertions in expectation values of operators $\mathbf{O}(x_1,\dots,x_n)$ consisting in products of quark and gluon fields at different points of space-time $x_i \neq x_j$ for $i,j=1,\dots,N$, viz

$$\langle \mathbf{O}(x_1,\dots,x_n)\rangle = \frac{1}{\mathcal{Z}}\int [DU][D\psi][D\bar{\psi}]\mathbf{O}(x_1,\dots,x_n)e^{-[S_G(U)+S_F(U,\psi,\bar{\psi})]}\,. \tag{3.2.11}$$

WI are obtained by requiring that

$$\delta_{\alpha^a(x)}\langle \mathbf{O}(x_1,\dots,x_n)\rangle = 0\,, \tag{3.2.12}$$

where $\delta_{\alpha^a(x)}$ is the local variation respect to a vector or axial transformation, depending on the symmetry considered once promoted to be a *local* symmetry. Eq. (3.2.12) is trivially satisfied since the infinitesimal transformation acts as a local change of variable in the fermionic fields, which are integration variables. This variation in the functional integral then leads to

$$\left\langle \frac{\delta \mathbf{O}(x_1,\dots,x_n)}{\delta\alpha^a(x)}\right\rangle = \left\langle \mathbf{O}(x_1,\dots,x_n)\frac{\delta S_F}{\delta\alpha^a(x)}\right\rangle\,, \tag{3.2.13}$$

for which explicitly

$$\mathbf{O}(x_1,\dots,x_n) = \bar{\psi}(x)\gamma_\mu\frac{\lambda^a}{2}\psi(x)\mathbf{O}'(y) = V^a_\mu(x)\mathbf{O}'(y) \tag{3.2.14}$$

$$\mathbf{O}(x_1,\dots,x_n) = \bar{\psi}(x)\gamma_\mu\gamma_5\frac{\lambda^a}{2}\psi(x)\mathbf{O}'(y) = A^a_\mu(x)\mathbf{O}'(y)\,, \tag{3.2.15}$$

lead to the integrated version of PCVC and PCAC relations respectively. Let us now move to the lattice, where due to the explicit loss of chiral symmetry even for $m_0 = 0$ caused by the Wilson term, the situation is slightly more complicated.

3.2.3 Mass renormalization with Wilson Fermions

We focus here in Wilson discretisation for fermion fields. Even in the absence of mass matrix M_0 the presence of the Wilson term $a\bar{\psi}\nabla^*_\mu\nabla_\mu\psi$ in the action breaks explicitly chiral symmetry. Consequently $SU(N_f)_L \times SU(N_f)_R$ is not anymore a symmetry. In order to present what is the consequence of this loss of chiral symmetry, let us focus on the renormalization on the quark mass. We can rewrite the bare mass matrix M_0 separately for the singlet and non-singlet part as

$$M_0 = \sum_d \tilde{m}^d\lambda^d + m^{\rm av}\mathbb{1}\,, \tag{3.2.16}$$

where the sum runs only over diagonal generators $\lambda^a \in \mathfrak{su}(N_f)$ and $\tilde{m}^a$, $m^{\rm av}$ are given by

$$\tilde{m}^a = \frac{1}{2}{\rm Tr}[M_0\lambda^a]\,,\quad m^{\rm av} = \frac{{\rm Tr}[M_0]}{N_f}\,. \tag{3.2.17}$$

For a given flavour f Eq. (3.2.16) reads

$$m_{0,f} = \sum_d \tilde{m}^d\lambda^a_{ff} + m^{\rm av}\,, \tag{3.2.18}$$

with λ^a_{ff} is the diagonal fth-element of the generator λ^a. The reason why we stressed to separate singlet and non-singlet components of M_0 is because, since they have different

symmetries, they show a different renormalization pattern[4]. In fact while $\tilde{m}^a$ transform in the adjoint representation of $SU(N_f)$ with a *multiplicative renormalization*, the singlet $m^{\rm av}$ due to the lack of chiral symmetry is allowed to mix with the identity, introducing then an *additive renormalization*, viz

$$[\tilde{m}^a(\bar{g}(\mu))]_R = \lim_{a\to 0} Z_m(g_0, a\mu)\tilde{m}^a(g_0)\,, \tag{3.2.19}$$

$$[m^{\rm av}(\bar{g}(\mu))]_R = \lim_{a\to 0} Z_{m^0}(g_0, a\mu)[m^{\rm av}(g_0) - m_{\rm cr}]\,. \tag{3.2.20}$$

In Eq. (3.2.20) Z_m and Z_{m^0} represent the renormalization constants of the non-singlet and singlet mass terms respectively. It is very important to stress here that the additive subtraction $m_{\rm cr}$ is flavour independent and define what is usually called *critical line*. This extra term is also a power divergence (effect that can be appreciated already at tree level where $m_{\rm cr} = -4/a$). This extra counter term is one of the most important features of Wilson fermions, a discussion about the tuning of the critical line is present in Section 7. Finally, combining Eq. (3.2.20) together we have

$$[m_f(\bar{g}(\mu)]_R = \lim_{a\to 0} Z_m(g_0, a\mu)\left[m_{0,f} - m_{\rm cr} + \left(\frac{Z_{m^0}(g_0, a\mu)}{Z_m(g_0, a\mu)} - 1\right)(m^{\rm av} - m_{\rm cr})\right]\,. \tag{3.2.21}$$

Focusing on the most relevant case for the present thesis, of degenerate masses and defining the *subtracted* bare quark mass $m_f = m_{0,f} - m_{\rm cr}$

$$[m_f(\bar{g}(\mu)]_R = \lim_{a\to 0}[Z_{m^0}(g_0, a\mu)m_f(g_0, m_{0,f})]\,. \tag{3.2.22}$$

In order to have a massless theory with Wilson fermions, all the bare quark masses have to be set to the critical value $m_{0,f} = m_{\rm cr}$.

3.2.4 Lattice WI

Let us define the *point-split* axial and vector currents as

$$\tilde{V}^a_\mu(x) = \frac{1}{2}[\bar{\psi}(x)(\gamma_\mu - 1)U_\mu(x)\frac{\lambda^a}{2}\psi(x + a\hat{\mu}) + \bar{\psi}(x + a\hat{\mu})(\gamma_\mu + 1)U^\dagger_\mu\frac{\lambda^a}{2}\psi(x)]\,, \tag{3.2.23}$$

$$\tilde{A}^a_\mu(x) = \frac{1}{2}[\bar{\psi}(x)\gamma_\mu\gamma_5 U_\mu(x)\frac{\lambda^a}{2}\psi(x + a\hat{\mu}) + \bar{\psi}(x + a\hat{\mu})\gamma_\mu\gamma_5 U^\dagger_\mu\frac{\lambda^a}{2}\psi(x)]\,. \tag{3.2.24}$$

The vector WI can be derived [28] for the point-split current. It is easy to show that $\nabla_\mu\tilde{V}^a_\mu(x) = 0$. As showed in [29], $\tilde{V}_\mu$ can be inserted into an expectation value with two extra quarks ψ_1 and ψ_2 with corresponding bare masses $m_{0,1}$ and $m_{0,2}$, viz

$$\begin{aligned}\nabla_\mu\langle\psi_1(x_1)\tilde{V}_\mu(x)\bar{\psi}_2(x_2)\rangle &= [m_{0,1} - m_{0,2}]\langle\psi_1(x_1)S(x)\bar{\psi}_2(x_2)\rangle \\ &\quad - \delta(x_2 - x)\langle\psi_1(x_1)\bar{\psi}_1(x_2)\rangle - \delta(x_1 - x)\langle\psi_2(x_1)\bar{\psi}_2(x_2)\rangle\end{aligned} \tag{3.2.25}$$

In principle since the above relation is among bare quantities, it is expected to diverge in the continuum limit. In order to simplify the notation we can take the mass degenerate case $m_{0,1} = m_{0,2}$ for which the first term at r.h.s vanish. Furthermore, it is easy to see that the l.h.s is finite, once we renormalise the wave functions with $Z_\psi^{1/2}$. Consequently the r.h.s. is finite and $Z_{\tilde{V}} = 1$ [30]. Extracting the WI for the "standard" vector current is less intuitive and have to be carried out more carefully. The same no-renormalization

[4]It can be shown that there is a spurionic symmetry which relates singlet and non-singlet masses, enforcing the same renormalization for both terms. However, unlike in regularisation which preserve chiral symmetry, it is broken by Wilson term.

theorem holds but now even tough Z_V is a finite renormalization constant it deviates from unity due to the lattice discretisation $Z_V(g_0) = 1 - c(g_0) \neq 0$. A consequence of this results is a relation between the mass renormalization and the scalar density

$$Z_S(g_0, a\mu) = Z_m^{-1}(g_0, a\mu)\,, \tag{3.2.26}$$

and than

$$\gamma_S = -\gamma_m\,. \tag{3.2.27}$$

The lattice axial WI is less intuitive. In fact even at vanishing quark masses $M_0 = 0$ the lattice action is not invariant under global axial transformation. Analogously to what have been done for the vector current, we have

$$\begin{aligned} i\left\langle \frac{\partial \mathbf{O}(x_1,\ldots,x_n)}{\partial \alpha_A^a(x)} \right\rangle &= a^4 \sum_\mu \nabla_\mu \langle \tilde{A}_\mu^a(x)\mathbf{O}(x_1,\ldots,x_n)\rangle \\ &- a^4\langle \bar{\psi}(x)\{\frac{\lambda^a}{2}, M_0\}\gamma_5\gamma_\mu\psi(x)\mathbf{O}(x_1,\ldots,x_n)\rangle - a^4\langle X^a(x)\mathbf{O}(x_1,\ldots,x_n)\rangle \end{aligned} \tag{3.2.28}$$

where X^a is the variation of the Wilson term, reading

$$X^a(x) = -\frac{a}{2}[\bar{\psi}(x)\frac{\lambda^a}{2}\gamma_5 \overrightarrow{\nabla^2}\,\psi(x) + \bar{\psi}(x)\,\overleftarrow{\nabla^2}\,\frac{\lambda^a}{2}\gamma_5\psi(x)]\,, \tag{3.2.29}$$

with the discrete second (covariant) derivative ∇^2 acting on quark fields as

$$a^2\,\overrightarrow{\nabla^2}\,\psi(x) = \sum_\mu [U_\mu(x)\psi(x+a\hat{\mu}) + U_\mu^\dagger(x-a\hat{\mu})\psi(a-a\hat{\mu}) - 2\psi(x)]\,, \tag{3.2.30}$$

$$a^2\bar{\psi}(x)\,\overleftarrow{\nabla^2} = \sum_\mu [\bar{\psi}(x+a\hat{\mu})U_\mu^\dagger(x) + \bar{\psi}(x-a\hat{\mu})U_\mu(x-a\hat{\mu}) - 2\psi(x)]\,. \tag{3.2.31}$$

We can write the Wilson term contribution to the above expression as a 5-dimensional operator proportional to the lattice spacing a as

$$X^a(x) = a\mathbf{O}_5^a(x)\,, \tag{3.2.32}$$

whose renormalized counterpart (including all the mixing) reads

$$[\mathbf{O}_5^a(x)]_R = Z_5\left[\mathbf{O}_5^a(x) + \bar{\psi}(x)\left\{\frac{\lambda^a}{2}, \frac{\bar{M}}{a}\right\}\gamma_5\psi(x) + \frac{(Z_{\tilde{A}}-1)}{a}\nabla_\mu\tilde{A}_\mu^a(x)\right]\,. \tag{3.2.33}$$

Combining together Eq. (3.2.28), and Eq. (3.2.33), the renormalized WI reads

$$\begin{aligned} i\left\langle \frac{\partial \mathbf{O}(x_1,\ldots,x_n)}{\partial \alpha_A^a(x)} \right\rangle &= a^4 \sum_\mu \nabla_\mu \langle Z_{\tilde{A}}\tilde{A}_\mu^a(x)\mathbf{O}(x_1,\ldots,x_n)\rangle \\ - a^4\langle \bar{\psi}(x)\{\frac{\lambda^a}{2}, [M_0-\bar{M}]\}\gamma_5\gamma_\mu\psi(x)\mathbf{O}(x_1,\ldots,x_n)\rangle &- a^4\langle \frac{X_R^a(x)}{Z_5}\mathbf{O}(x_1,\ldots,x_n)\rangle\,. \end{aligned} \tag{3.2.34}$$

without loss of generality in order understand Eq. (3.2.34), as in the vector case we can consider $\mathbf{O}(x_1, x_2) = \psi_1(x_1)\bar{\psi}_2(x_2)$ and a given combination of λ^a it becomes

$$\begin{aligned}\nabla_\mu \langle \psi_1(x_1) Z_{\tilde{A}} \tilde{A}_\mu(x) \bar{\psi}_2(x_2)\rangle = [m_{0,1} - \bar{m}_1 + m_{0,2} - \bar{m}_2]\langle \psi_1(x_1) P(x) \bar{\psi}_2(x_2)\rangle \\ - \delta(x - x_2)\langle \psi_1(x_1)\bar{\psi}_1(x_2)\gamma_5\rangle - \delta(x - x_1)\langle \gamma_5\psi_2(x_1)\bar{\psi}_2(x_2)\rangle \\ + \frac{a}{Z_5}\langle \psi_1(x_1)[\mathbf{O}_5(x)]_R \bar{\psi}_2(x_2)\rangle \,, \quad (3.2.35)\end{aligned}$$

with $\bar{m}_i$ the diagonal entry of $\bar{M}$. In Eq. (3.2.35) the last term on the r.h.s. simply vanish in the continuum, we can then rewrite it in terms of $m_{f,\mathrm{PCAC}} = m_{0,f} - \bar{m}_{0,f}(g_0, m_{0,1}, \ldots, m_{0,N_f})$ for $f = 1, 2, \ldots, N_f$, as

$$\begin{aligned}\nabla_\mu \langle \psi_1(x_1) Z_{\tilde{A}} \tilde{A}_\mu(x_2) \bar{\psi}_2(x)\rangle = [m_{1,\mathrm{PCAC}} + m_{2,\mathrm{PCAC}}]\langle \psi_1(x_1) P(x) \bar{\psi}_2(x_2)\rangle \\ - \delta(x - x_2)\langle \psi_1(x_1)\bar{\psi}_1(x_2)\gamma_5\rangle - \delta(x - x_1)\langle \gamma_5\psi_2(x_1)\bar{\psi}_2(x_2)\rangle \,. \quad (3.2.36)\end{aligned}$$

Here a similar argument as in the vector case can be applied. It has been shown that the point-split and "standard" axial renormalization constant are finite and $Z_{\tilde{A}}, Z_A \neq 1$ due to discretisation effects being

$$[A^a_\mu(x)]_R = \lim_{a\to 0}[Z_{\tilde{A}} \tilde{A}^a_\mu(x)] = \lim_{a\to 0}[Z_A A^a_\mu(x)] \,. \quad (3.2.37)$$

As in the vector case, after eliminating the surface term with the divergence of the axial current on the l.h.s. in Eq. (3.2.36), once we renormalise the wave functions with Z_ψ everything is finite. Given that pseudoscalar operator P is renormalized multiplicatively, the renormalization pattern for the PCAC mass reads

$$[m_f(\bar{g}(\mu), \mu)]_R = Z_P^{-1}(g_0, a\mu) m_{f,\mathrm{PCAC}}(g_0, m_{0,1}, \ldots, m_{0,N_f}) \,, \quad (3.2.38)$$

and consequently for the anomalous dimensions

$$\gamma_P = -\gamma_m \,. \quad (3.2.39)$$

Summarising, the scale dependence of scalar, pseudoscalar and mass is enforced to be the same by WI, while axial and vector currents do not depend on the scale but their renormalization constants deviate from the identity due to discretisation effect. Since there are no relation involving the tensor current, it is the only other bilinear with an independent anomalous dimension (and consequently RG running).

4 Finite Volume Renormalization Scheme - Schrödinger Functional

In asymptotic free theories, like QCD, perturbative approaches to RG are only applicable to a class of high-energy processes. However, QCD is a candidate theory for the hadronic interactions at all energies. In particular in numerical QCD computations it is possible to determine low-energy observables. In such studies the bare quark masses can be fixed by ratios of hadronic quantities, e.g. m_π/f_π, m_K/f_K to their physical values and then $af_\pi(g_0)$ gives the lattice spacing $a(g_0)$ for the pion decay constant f_π fixed. This procedure is usually called *hadronic renormalization scheme*.

In order to connect a hadronic scheme to a perturbative one, it is necessary to compute the non-perturbative running between the two scales $\mathcal{O}(\Lambda_{\rm QCD}) \to \mathcal{O}(M_W)$. For this purpose, we present the most common non-perturbative renormalization schemes, and then focus on the one adopted in this thesis.

4.1 Lattice Renormalization schemes

There exist many methods to implement (non-perturbative) renormalization. We easily can classify schemes into two types: *infinite-volume* schemes and *finite-volume* ones. Let us proceed in order. Infinite-volume schemes like the "RI-MOM" (Renormalization Invariant Momentum Subtraction) have been suggested for the first time in [31]. The proposed procedure mimics what is often done in perturbation theory. The renormalization constants are determined by requiring that vertex functions (amputated Green functions between off-shell quark states with momentum) assume their three-level value when the scale of external momenta is equal to the renormalization scale. For example if we consider the generic bilinear operators $O_\Gamma = \bar{\psi}\Gamma\psi$, we may impose the condition

$$Z_{O_\Gamma}\langle p|O_\Gamma|p\rangle|_{p^2=-\mu^2} = \langle p|O_\Gamma|p\rangle_{\rm tree-level}\,, \tag{4.1.1}$$

where Γ is a generic Dirac structure and $\langle p|O_\Gamma|p\rangle_{\rm tree-level}$ is the tree-level matrix element. Since one works with non gauge-invariant correlation functions, a gauge must be fixed, usually the Landau gauge is chosen. Moreover the renormalization condition is intended to be imposed at zero quark masses in order to have a mass-independent renormalization scheme. In practice this is done by extrapolating to the chiral limit the numerical results obtained for non-zero values of the quark masses. In principle, this procedure completely solves the problem of large corrections in lattice perturbation theory and yields the exact renormalization constant at the scale μ up to lattice artifacts which are of order $\mathcal{O}(\mu a, \Lambda a)$. In order to keep lattice artifacts and finite-size effect under control, the range of validity of this kind of approach is given by

$$\frac{L}{a} \gg \frac{1}{\mu a} \gg 1\,, \tag{4.1.2}$$

and bare couplings such that

$$\frac{L}{a} \gg \frac{1}{\Lambda a} \gg 1\,, \tag{4.1.3}$$

where L is the linear lattice size in physical units. In principle such a procedure, largely employed in literature (see e.g. [31]), allows to compute the renormalization constants with high precision respecting Eq. (4.1.2), Eq. (4.1.3). Moreover, the accuracy of the procedure is limited by the needing of chiral extrapolations and the subtraction of the *Goldstone pole* which may contaminates the states [32], in addition to some tecnical complications like gauge fixing procedure to avoid Gribov ambiguities.
In order to overcome the above limitations a possibility is to consider *Finite-Volume schemes*. These schemes are the practical application of the important observation due to Symanzik [33] which states that renormalizability is not spoiled when a field theory is put on a finite space-time manifold. We can then define a finite volume renormalization scheme naturally identifying the linear size L of this space-time manifold as the renormalization scale μ without the need of injecting external momenta. The first big advantage of this approach with respect to the infinite-volume one, is that Eq. (4.1.2), Eq. (4.1.3) reduce to the much weaker:

$$\frac{L}{a} \gg 1, \quad \Lambda a \ll 1\,, \tag{4.1.4}$$

thanks to the recursiveness of the finite volume approach, removing the need of accommodating all the physical scales on the same lattice. The second advantage is that a proper choice of the boundary conditions (as we will see in the following) naturally produces a gap of order $1/L$ in the spectrum of the Dirac-Wilson operator [34] which survives in the chiral limit $m \to 0$. It is then possible to work *safely* with massless fermions avoiding chiral extrapolations. Finally, a careful examination shows that nontrivial results can be obtained without fixing a particular gauge [17].
Let us then focus in the following section on a particular finite-volume renormalization scheme, which is the one used in this thesis. The aim of this section is to give a very brief overview to one of these schemes called the Schrödinger Functional (SF). We proceed with the formulation in the continuum and then on the lattice to establish basic formalism and highlight the most important features, crucial for the work carried out in this thesis. As explained in [17], the SF will be used to explore the scaling properties of the theory exploiting the finite volume, taken as a "hyper-cylinder" with periodic space directions of length L and finite time extent T. The formalism and approach is taken from [17, 35].

4.2 Schrödinger Functional

Let us present the SF by a quantum-mechanical interpretation and then move to QFT for the pure gauge theory and its extension including fermions.

4.2.1 Quantum-Mechanical Interpretation

Let us assume SU(N) gauge fields are represented by a space-periodic vector potential $A_k(\mathbf{x})$ on $\mathbb{R}^3$ with values in $\mathfrak{su}(n)$, the algebra of SU(N). The gauge transformation of the vector potential reads

$$A_k(\mathbf{x}) \to A_k^\Lambda(\mathbf{x}) = \Lambda(\mathbf{x}) A_k(\mathbf{x}) \Lambda(\mathbf{x})^{-1} + \Lambda(\mathbf{x}) \partial_k \Lambda(\mathbf{x})^{-1}, \tag{4.2.1}$$

where, in order to preserve periodicity, only periodic gauge functions $\Lambda(\mathbf{x})$ are admitted. The choice of the name "Schrödinger" has to be traced back to the Schödinger representation in classical quantum mechanics. In fact, defining the wave functional state as $\psi(A)$, with A running over all the gauge fields as described above. A scalar product among wave functions can be defined as

$$\langle\psi|\chi\rangle = \int D[A]\,\psi[A]^*\chi[A], \quad D[A] = \prod_{\mathbf{x},k,a} dA_k^a(\mathbf{x}). \tag{4.2.2}$$

Focusing only on the gauge invariant wave functions $\psi(A) = \psi(A^\Lambda)$ we can define a projector $\mathbb{P}$ on (physical) gauge-invariant states as

$$\psi(A) \to \mathbb{P}\psi(A) = \int D[\Lambda]\psi(A^\Lambda), \quad D[\Lambda] = \prod_{\mathbf{x}} d\Lambda(\mathbf{x}), \tag{4.2.3}$$

The canonical "Chromo-Electric" field can be defined as

$$F_{0k}^a(\mathbf{x}) = \frac{1}{i}\frac{\delta}{\delta A_k^a(\mathbf{x})}, \tag{4.2.4}$$

while the "Chromo-Magnetic" components are the usual

$$F_{kl}^a(\mathbf{x}) = \partial_k A_l^a(\mathbf{x}) - \partial_l A_k^a(\mathbf{x}) + f^{abc}A_k^b(\mathbf{b})A_l^c(\mathbf{x}), \tag{4.2.5}$$

both entering the definition of the Hamilton operator $\mathbb{H}$, reading

$$\mathbb{H} = \int_0^L d^3x \left\{ \frac{g_0^2}{2}F_{0k}^a(\mathbf{x})F_{0k}^a(\mathbf{x}) + \frac{1}{4g_0^2}F_{kl}^a(\mathbf{x})F_{kl}^a(\mathbf{x}) \right\}, \tag{4.2.6}$$

with g_0 the bare gauge coupling. Analogously any smooth classical gauge field $C_k(\mathbf{x})$ a state $|C\rangle$ can be introduced as

$$\langle C|\psi\rangle = \psi[C]. \tag{4.2.7}$$

This state can be projected on a gauge invariant subspace, and the (euclidean) SF partition function is defined as

$$\mathcal{Z}[C', C] = \langle C'|e^{-\mathbb{H}T}\mathbb{P}|C\rangle. \tag{4.2.8}$$

In the above formula $T > 0$ represent the "physical" time-extent of the volume. The dependence on T is implicit in the $\mathcal{Z}$, since it is encoded into the two "boundary" states C and C'. In this formalism the spectral representation of the SF is obtained by inserting a gauge invariant orthonormal basis $|\psi_n\rangle$ with $n = 1, 2, \ldots, \infty$,

$$\mathcal{Z}[C, C'] = \sum_{n=0}^{\infty} e^{-E_n T}\psi_n[C']\psi_n[C]^*, \tag{4.2.9}$$

where E_n are the (discrete) energy eigenvalues.
It is important to stress that since this formulation is defined in terms of gauge invariant states, the whole $\mathcal{Z}[C', C]$ is gauge invariant under arbitrary gauge transformations of boundary fields C and C'.

4.2.2 Pure Gauge

In QFT functional integral representation on a finite four-dimensional volume with $0 \leq x^0 \leq T$ and periodic boundary condition in the spacial direction we can assign explicitly an initial and final "Dirichlet" boundary condition in time for the gauge field as

$$A_k(x) = \begin{cases} C_k^{\Lambda}(\mathbf{x}) & \text{at} \quad x^0 = 0\,, \\ C'_k(\mathbf{x}) & \text{at} \quad x^0 = T\,. \end{cases} \tag{4.2.10}$$

The functional integral representation of the Schrödinger Functional thus reads

$$\mathcal{Z}[C, C'] = \int D[\Lambda] \int D[A]\, e^{-S[A]}\,, \tag{4.2.11}$$

where the measure $D[A]$ is intended as an integration over all the components of the Euclidean gauge field. The gauge action is given by

$$S[A] = \frac{1}{2g_0^2} \int d^4x\, \mathrm{Tr}\{F_{\mu\nu}F_{\mu\nu}\} \tag{4.2.12}$$

with

$$F_{\mu\nu} = \partial_\mu A_\nu - \partial_\nu A_\mu + [A_\mu, A_\nu]\,. \tag{4.2.13}$$

It is important to notice that the dependence on the time component of the gauge field appearing in the functional integral can be reabsorbed into a specific gauge transformation. In fact, since Eq. (4.2.11) and boundaries in Eq. (4.2.17) are invariant under a gauge transformation of the form

$$A_\mu(x) \to \Omega(x) A_\mu(x) \Omega(x)^{-1} + \Omega(x)\partial_\mu \Omega(x)^{-1}\,, \tag{4.2.14}$$

$$\Lambda(\mathbf{x}) \to \Omega(x)|_{x_0=0} \Lambda(\mathbf{x})\,, \tag{4.2.15}$$

provided that $\Omega(x)|_{x_0=T} = \mathbf{1}$. A straightforward choice which satisfies the above conditions is the *temporal gauge* $A_0 = 0$. In this way the contact with the Hamiltonian formalism in Eq. (4.2.6) is clear.

4.2.3 Topology

If we take into account the existence of different disconnected topological sectors labeled by the integer n called *winding number*, the SF partition function reads

$$\mathcal{Z}[C', C] = \sum_{n=-\infty}^{\infty} \int D[A]\, e^{-S[A]}\,, \tag{4.2.16}$$

where now the boundaries satisfy

$$A_k(x) = \begin{cases} C_k^{\Lambda_n}(\mathbf{x}) & \text{at} \quad x^0 = 0\,, \\ C'_k(\mathbf{x}) & \text{at} \quad x^0 = T\,, \end{cases} \tag{4.2.17}$$

where Λ_n is some representative gauge transformation in the class of gauge functions with winding number n. A convenient choice can be to set $\Lambda_0 = 1$ [17]. An interesting

semiclassical inequivalence [36] called *instanton bound* states

$$S[A] \geq \frac{8\pi^2}{g_0^2}|Q[A]|\,, \tag{4.2.18}$$

where the topological charge for a given configuration A is given by

$$Q[A] = -\frac{1}{32\pi^2}\int d^4x\,\mathrm{Tr}\{\epsilon_{\mu\nu\rho\sigma}F_{\mu\nu}F_{\rho\sigma}\}\,. \tag{4.2.19}$$

It can be shown [17] that the quantity $Q[A]$ takes an extra contribution coming from the time-boundaries surface terms. In fact, using the equality

$$\frac{1}{4}\mathrm{Tr}\{\epsilon_{\mu\nu\rho\sigma}F_{\mu\nu}F_{\rho\sigma}\} = \epsilon_{\mu\nu\rho\sigma}\partial_\mu\mathrm{Tr}\{A_\nu\partial_\rho A_\sigma + \frac{2}{3}A_\nu A_\rho A_\sigma\} \tag{4.2.20}$$

we have that

$$Q[A] = S_{\mathrm{CS}}[C'] - S_{\mathrm{CS}}[C] - n\,, \tag{4.2.21}$$

with

$$S_{\mathrm{CS}}[C] = -\frac{1}{8\pi^2}\int d^3x\,\epsilon_{klj}\mathrm{Tr}\{C_k\partial_l C_j + \frac{2}{3}C_kC_lC_j\} \tag{4.2.22}$$

the *Chern-Simons* term of the boundary C.
The topological properties of gauge theories offer a rich environment for the study of non-perturbative effects. On the other hand, the presence of topological fluctuations makes numerical simulation challenging for the standard local sampling algorithms commonly used. In this work, we do not explore algorithmic solutions, but include the topological charge within the definition of our fermionic correlation functions. More details about this discussion are given in Section 7.

4.2.4 Induced Background Field and SF Coupling

The SF allows for a natural non-perturbative definition of the renormalized coupling as a "response coefficient" given by the change of a background (BG) field induced by the choice of the boundary fields C and C'.
In the perturbative energy region the functional integral is dominated by the fields close to the classical ones lying in the minima of the action. In general the non-perturbative dynamics is driven by the presence of several gauge inequivalent minimal action configurations occurring in different winding number sectors. We assume that the minimal action configuration $B_\mu(x)$ is unique up to a gauge transformation and occurs in the $n = 0$ sector [1]. For an arbitrary choice of C and C' it is usually difficult (or even impossible) to obtain an analytic form for the induced BG field. However proceeding in reverse we can first *define* the boundary fields and than compute the BG field. A common choice can be simply

$$C_k(\mathbf{x}) = B_k(x) \quad \text{at} \quad x^0 = 0\,, \tag{4.2.23}$$
$$C'_k(\mathbf{x}) = B_k(x) \quad \text{at} \quad x^0 = T\,. \tag{4.2.24}$$

which trivially correspond to a constant BG field $B_k(x)$. As mentioned above, it can be proved [17] taking advantage of Eq. (4.2.21) that this solution B is the unique minimal

[1] Both statements are proven for an abelian gauge field in the appendix of [17]

action configuration with these boundary values. In practice other choices for the boundaries are made.
In the weak coupling domain, the SF can be computed by a saddle-point expansion around the classical solution B of the functional integral. The effective (one particle irreducible generating functional) reads

$$\Gamma[B] = -\ln \mathcal{Z}[\mathrm{C}', \mathrm{C}]\,, \tag{4.2.25}$$

and admits an asymptotic expansion in a power series in g_0^2

$$\Gamma[B] = \frac{\Gamma_0[B]}{g_0^2} + \Gamma_1[B] + g_0^2\Gamma_2[B] + \dots \tag{4.2.26}$$

Focusing on the leading term of the above series we have

$$\Gamma_0[B] = g_0^2 S[B]\,, \tag{4.2.27}$$

while the higher order terms contain increasing number of vacuum polarisation loops.
If we now consider a generic choice of boundary fields to be dependent on an extra dimensionless parameter η it can be inferred that

$$\Gamma'[B] = \frac{\partial}{\partial\eta}\Gamma[B]\,, \tag{4.2.28}$$

is a renormalization group invariant quantity [17], and an "operative" definition of the renormalized coupling follows naturally as

$$\bar{g}^2_{\mathrm{SF}} = \frac{\Gamma'_0[B]}{\Gamma'[B]}\,, \tag{4.2.29}$$

where $\Gamma_0[B]$ is just a normalisation factor which forces the value of $\bar{g}^2_{\mathrm{SF}}$ to coincide with the g_0^2 at one-loop. The renormalization properties for the SF have been analysed performing a one-loop [17] and two-loop [37] calculation for arbitrarily BG field. The most important result of this computation is that the SF is finite after eliminating the bare coupling in favour of the renormalized one. The presence of boundaries does not introduce any extra divergence. This result can be conjectured to hold at all orders in perturbation theory, because there are no local gauge invariant operators with $d \leq 3$ living on the boundaries in the pure gauge theory. However, there is no formal proof to all orders in perturbation theory.

4.2.5 Fermion fields

In this section we follow the elegant approach presented in [35] and [38].
We consider a massless free fermion on $\mathbb{S}^1 \times \mathbb{T}^3$ with Lagrangian density

$$\mathcal{L} = \bar{\psi}(x)\gamma_\mu\partial_\mu\psi(x)\,, \tag{4.2.30}$$

where we define $\mathcal{D} = \gamma_\mu\partial_\mu$ and we impose anti-periodic boundary condition in temporal direction with extent $2T$

$$\psi(\mathbf{x}, x_0 + 2T) = -\psi(\mathbf{x}, x_0)\,, \quad \bar{\psi}(\mathbf{x}, x_0 + 2T) = -\bar{\psi}(\mathbf{x}, x_0)\,. \tag{4.2.31}$$

An orbifolding $\mathbb{S}^1/\mathbb{Z}_2$ in the temporal direction is implemented by the identification $-x_0 \leftrightarrow x_0$, which translates into a generic transformation that includes time reflection

R of the fermion fields

$$\psi(x) \to \Sigma\psi(-x_0, \mathbf{x}) \,, \quad \bar{\psi}(x) \to \bar{\psi}(-x_0, \mathbf{x})\Sigma \,, \quad \Sigma = i\gamma_5\gamma_0 R \,. \tag{4.2.32}$$

It is easy to identify the fixed points of R, located in $x_0 = 0, T$; they are, respectively, symmetric and antisymmetric fixed points (because of anti-periodicity), viz

$$R\psi(\mathbf{x}, 0) = \psi(\mathbf{x}, 0) \,, \quad R\psi(\mathbf{x}, T) = -\psi(\mathbf{x}, T) \,. \tag{4.2.33}$$

At this stage it is possible to add another symmetry, like e.g. chiral symmetry

$$\psi(x) \to -i\gamma_5\psi(x) \,, \quad \bar{\psi}(x) \to -\bar{\psi}(x)i\gamma_5 \,, \tag{4.2.34}$$

and combine them together into $\Gamma = -i\gamma_5 R = \gamma_0 R$ acting as

$$\psi(x) \to -\Gamma\psi(x) \,, \quad \bar{\psi}(x) \to \bar{\psi}(x)\Gamma \,. \tag{4.2.35}$$

The orbifolding of the fermion field is given by selecting the symmetric subspace for which

$$\Pi_+\psi(x) = 0 \,, \tag{4.2.36}$$
$$\bar{\psi}(x)\Pi_- = 0 \,, \tag{4.2.37}$$

where $\Pi_\pm = \frac{1\pm\Gamma}{2}$. Starting from an anti-periodic fermion field living on a torus with time-length of $2T$, thanks to the orbifold we end up with fermion fields obeying SF Dirichlet boundary condition [35] imposed at times $x_0 = 0, T$, viz,

$$P_+\psi(x)|_{x_0=0} = 0 \quad P_-\psi(x)|_{x_0=T} = 0 \,, \tag{4.2.38}$$
$$\bar{\psi}(x)P_-|_{x_0=0} = 0 \quad \bar{\psi}(x)P_+|_{x_0=T} = 0 \,, \tag{4.2.39}$$

with the usual spin projectors $P_\pm = \frac{1\pm\gamma_0}{2}$. Applying this procedure with a non-vanishing mass term is not straightforward. Although Dirac operator does not have chiral symmetry, it is possible to introduce the mass as a function of x_0 which is compatible with the orbifolding transformation, i.e. $\{M, \Gamma\} = 0$. One of the possible time-dependent mass terms is $M = m\eta(x_0)$ with

$$\eta(-x_0) = -\eta(x_0) \,, \tag{4.2.40}$$
$$\eta(x_0) = 0 \quad \text{for} \quad 0 < x_0 < T \,, \tag{4.2.41}$$

with the requirement of being periodic $\eta(x_0 + 2T) = \eta(x_0)$. The Dirac operator, in the interacting theory, becomes

$$\mathcal{D}(m) = \gamma_\mu(\partial_\mu - iA_\mu(x)) + m\eta(x_0) \,, \tag{4.2.42}$$

which satisfies the anti-commutator with the orbifolding symmetry $\{\mathcal{D}(m), \Gamma\} = 0$. The "SF" Dirac operator D_{SF} is than related to the one before orbifolding by the projection

$$D_{\mathrm{SF}}(m) = \Pi_+\mathcal{D}(m)\Pi_- \,. \tag{4.2.43}$$

In the next section we translate this formulation into objects commonly used on the lattice. [2]

[2] Several complications arise when trying to apply orbifolding to Dirac operators field which explicitly break chiral symmetry. Such difficulties are avoided for the Chirally-rotated SF or for Ginsparg-Wilson fermions. which are not topics of this thesis.

4.3 Lattice Formulation

From the Euclidean point of view in the SF setup the time direction is distinguished from the others and there is no translation invariance in the time-direction. Therefore in this case we generalize the Plaquette action Eq. (3.1.3) to

$$S_{\mathrm{W_{sf}}} = \beta \sum_{\mathcal{C}\in\mathcal{S}_0} \omega(\mathcal{C}) Re\mathrm{Tr}[1 - U(\mathcal{C})]\,. \tag{4.3.1}$$

Here the novelty is the plaquette dependent weight ω for which the transfer matrix formalism suggests to take $\omega(\mathcal{C}) = 1$ for all plaquettes except the purely spatial ones on the boundary where $\omega(\mathcal{C}) = 1/2$. This is so because it is natural to symmetrically distribute these contributions to the two adjacent transfer matrix factors. The SF Dirichlet boundary condition in time are than imposed on the link fields at $t = 0$ and $t = T$ as follows [35]:

$$U(x,k)|_{x_0=0} = e^{aC_k} = W(\mathbf{x},k)\,, \tag{4.3.2}$$

$$U(x,k)|_{x_0=T} = e^{aC'_k} = W'(\mathbf{x},k)\,, \tag{4.3.3}$$

for $k = 1, 2, 3$. In general for SU(N) the choice of boundaries follows the same prescription as for the first exploratory study in SU(2) [17], where

$$C_k = \frac{i}{L}\begin{pmatrix} \phi_1 & 0 & \cdots & 0 \\ 0 & \phi_2 & \cdots & 0 \\ \vdots & \vdots & \ddots & \vdots \\ 0 & 0 & \cdots & \phi_N \end{pmatrix} \quad \text{and} \quad C'_k = \frac{i}{L}\begin{pmatrix} \phi'_1 & 0 & \cdots & 0 \\ 0 & \phi'_2 & \cdots & 0 \\ \vdots & \vdots & \ddots & \vdots \\ 0 & 0 & \cdots & \phi'_N \end{pmatrix} \tag{4.3.4}$$

with the constraint that $\sum_i \phi_i = 0$ and $\sum_i \phi'_i = 0$ in order to have $W \in$ SU(N). With the above prescription the minimum of the action [39] corresponds to the "classical link" $V(x,\mu) = exp(aB_\mu(x))$ with

$$B_0 = 0 \qquad B_k(x_0) = [x_0 C'_k + (L - x_0)C_k]/L\,, \tag{4.3.5}$$

which is a linear interpolation between the two boundaries. As showed in [39], this solution satisfies uniqueness and stability, provided

$$\phi_1 < \phi_2 < \cdots < \phi_N \quad \text{and} \quad \phi_N - \phi_1 < 2\pi\,. \tag{4.3.6}$$

Eq. (4.3.6) defines a fundamental domain which is an irregular $(N-1)$-simplex [40] with vertices at points

$$\mathbf{X}_1 = \frac{2\pi}{N}(-N+1, 1, 1, 1, \ldots, 1)\,, \tag{4.3.7}$$

$$\mathbf{X}_2 = \frac{2\pi}{N}(-N+2, -N+2, 2, \ldots, 2)\,, \tag{4.3.8}$$

$$\mathbf{X}_3 = \frac{2\pi}{N}(-N+3, -N+3, -N+3, 3, \ldots, 3)\,, \tag{4.3.9}$$

$$\vdots \tag{4.3.10}$$

$$\mathbf{X}_N = (0, 0, \ldots, 0)\,. \tag{4.3.11}$$

Restricting to QCD we can introduce an extra parameter usually called "curve parameter" η allowing to induce a small deformation of the boundary fields. The curve of angles

for $N = 3$, (ϕ_1, ϕ_2, ϕ_3) now reads

$$\phi_1 = \eta\omega_1 - \frac{\pi}{3}\,, \qquad w_1 = 1\,, \tag{4.3.12}$$

$$\phi_2 = \eta\omega_2\,, \qquad \omega_2 = -\frac{1}{2} + \nu \tag{4.3.13}$$

$$\phi_3 = \eta\omega_3 + \frac{\pi}{3}\,, \qquad \omega_3 = -\frac{1}{2} - \nu \tag{4.3.14}$$

and the "primed" angles are defined to be

$$\phi_1' = -\phi_1 - \frac{4\pi}{3}\,, \tag{4.3.15}$$

$$\phi_2' = -\phi_3 + \frac{2\pi}{3}\,, \tag{4.3.16}$$

$$\phi_3' = -\phi_3 + \frac{2\pi}{3}. \tag{4.3.17}$$

As in the continuum case, the SF coupling [17] in full generality is identified by the relation

$$\left.\frac{\partial\Gamma}{\partial\eta}\right|_{\eta=0} = k\left\{\frac{1}{\bar{g}^2_{\rm SF}} - \nu\bar{v}\right\} \tag{4.3.18}$$

where k is the Leading Order (LO) $\partial\Gamma_0/\partial\eta$ and $\bar{v}$ is another renormalized quantity. The parameter ν (introduced in [41]) allows for different renormalization schemes, which provides a good test of the universality of continuum limit. So far we have discussed a possible definition of the strong coupling constant in pure gauge theory (in particular for SU(3), but this approach is very general [39]). Let us now introduce fermions on the lattice.

For practical purposes the lattice implementation of boundary conditions on fermion fields is slightly different from the one presented in the previous section. We consider a generalisation of periodic boundary conditions in space up to an abelian phase θ_k in direction $k = 1, 2, 3$ for quark fields

$$\psi(x + L\hat{k}) = e^{i\theta_k}\psi(x)\,, \quad \bar{\psi}(x + L\hat{k}) = e^{-i\theta_k}\bar{\psi}(x)\,. \tag{4.3.19}$$

this leaves all gauge-invariant quantities (containing the couple $\bar{\psi}$ and ψ) to be periodic. The angle is usually taken to be the same in all directions $\theta_k = \theta$. The effect of this choice can be interpreted as an induced constant background abelian chromomagnetic field which enters into the finite size kinematics (and consequently the renormalization scheme [42]) in useful ways. Boundary conditions in time read

$$P_+\psi(x)|_{x_0=0} = \rho(\mathbf{x})\,, \quad P_-\psi(x)|_{x_0=T} = \rho'(\mathbf{x})\,, \tag{4.3.20}$$

and

$$\bar{\psi}(x)|_{x_0=0}P_- = \bar{\rho}(\mathbf{x})\,, \quad \bar{\psi}(x)|_{x_0=T}P_+ = \bar{\rho}'(\mathbf{x})\,, \tag{4.3.21}$$

with the usual $P_\pm = \frac{1\pm\gamma_0}{2}$. Boundary fermion fields $\rho, \rho', \bar{\rho}, \bar{\rho}'$ have to be taken as formal Grassmann variables like $\psi, \bar{\psi}$. The total SF partition function is now given by

$$\mathcal{Z}[C', \bar{\rho}', \rho'; C, \bar{\rho}, \rho] = \int D[U]D[\psi]D[\bar{\psi}]e^{-S(U,\psi,\bar{\psi})}\,. \tag{4.3.22}$$

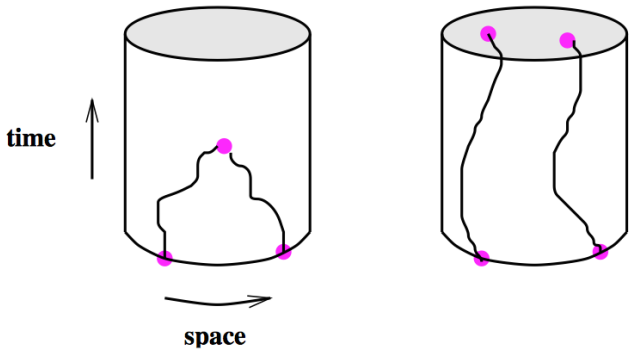

FIGURE 4.1: A sketch of the SF with two points correlation functions and boundary-to-boundary correlators (courtesy of [43])

The above equation is valid for any action. More elaborate actions respect to the ones introduced so far are introduced in Section 5.

4.3.1 Fermionic Correlation Functions in the SF

We introduce boundary sources by the usual functional differentiation,

$$\zeta(\mathbf{x}) = a^{-3}\frac{\partial}{\partial\bar{\rho}(\mathbf{x})}\,, \quad \bar{\zeta}(\mathbf{x}) = -a^{-3}\frac{\partial}{\partial\rho(\mathbf{x})}\,, \tag{4.3.23}$$

$$\zeta'(\mathbf{x}) = a^{-3}\frac{\partial}{\partial\bar{\rho}'(\mathbf{x})}\,, \quad \bar{\zeta}'(\mathbf{x}) = -a^{-3}\frac{\partial}{\partial\rho'(\mathbf{x})}\,. \tag{4.3.24}$$

A generic correlation function made up multi-local gauge invariant operators constructed out of fundamental links and fermion fields $\mathbf{O}(U,\psi,\bar{\psi})$, mediated with the partition function than reads

$$\langle\mathbf{O}\rangle = \left[\frac{1}{\mathcal{Z}}\int D[U]D[\psi]D[\bar{\psi}]\mathbf{O}(U,\psi,\bar{\psi})\exp -S(U,\psi,\bar{\psi})\right]_{\rho=\rho'=\bar{\rho}=\bar{\rho}'=0} \tag{4.3.25}$$

Taking advantage of Eq. (4.3.23) we can introduce "boundary operators" $\mathbf{O}^a$ with a as a generic flavour index as

$$\mathbf{O}^a = a^6\sum_{\mathbf{u},\mathbf{v}}\bar{\zeta}(\mathbf{u})\gamma_5\frac{\tau^a}{2}\zeta(\mathbf{v})\,, \tag{4.3.26}$$

and analogously at $x_0 = T$ for primed boundary fields Eq. (4.3.24) we have $\mathbf{O}'^a$.

We introduce the SF correlators [44], by contracting the bilinear operators Eq. 3.2.6,3.2.3, 3.2.5,3.2.4 (with an explicit colour index a) with boundary operators $\mathbf{O}$, viz

$$f_{\mathrm{A}}(x_0) = -a^6 \sum_{\mathbf{y},\mathbf{z}} \frac{1}{3} \langle A_0^a(x) \bar{\zeta}(\mathbf{y}) \gamma_5 \frac{\tau^a}{2} \zeta(\mathbf{z}) \rangle \,, \tag{4.3.27}$$

$$f_{\mathrm{P}}(x_0) = -a^6 \sum_{\mathbf{y},\mathbf{z}} \frac{1}{3} \langle P^a(x) \bar{\zeta}(\mathbf{y}) \gamma_5 \frac{\tau^a}{2} \zeta(\mathbf{z}) \rangle \,, \tag{4.3.28}$$

$$k_{\mathrm{V}}(x_0) = -a^6 \sum_{\mathbf{y},\mathbf{z}} \frac{1}{9} \langle V_k^a(x) \bar{\zeta}(\mathbf{y}) \gamma_k \frac{\tau^a}{2} \zeta(\mathbf{z}) \rangle \,, \tag{4.3.29}$$

$$k_{\mathrm{T}}(x_0) = -a^6 \sum_{\mathbf{y},\mathbf{z}} \frac{1}{9} \langle T_{k0}^a(x) \bar{\zeta}(\mathbf{y}) \gamma_k \frac{\tau^a}{2} \zeta(\mathbf{z}) \rangle \,, \tag{4.3.30}$$

and boundary-to-boundary correlators

$$f_1 = -\frac{a^{12}}{L^6} \sum_{\mathbf{u},\mathbf{v},\mathbf{y},\mathbf{z}} \frac{1}{3} \langle \bar{\zeta}'(\mathbf{u}) \gamma_5 \frac{\tau^a}{2} \zeta'(\mathbf{v}) \bar{\zeta}(\mathbf{y}) \gamma_5 \frac{\tau^a}{2} \zeta(\mathbf{z}) \rangle \tag{4.3.31}$$

$$k_1 = -\frac{a^{12}}{L^6} \sum_{\mathbf{u},\mathbf{v},\mathbf{y},\mathbf{z}} \frac{1}{3} \langle \bar{\zeta}'(\mathbf{u}) \gamma_k \frac{\tau^a}{2} \zeta'(\mathbf{v}) \bar{\zeta}(\mathbf{y}) \gamma_k \frac{\tau^a}{2} \zeta(\mathbf{z}) \rangle \,. \tag{4.3.32}$$

Their renormalized counterparts (with the b_X improvement coefficients discussed in Section 5) read

$$\begin{aligned}
[f_{\mathrm{A}}(x_0)]_R &= Z_A(1 + b_A a m_q) Z_\zeta^2 (1 + b_\zeta a m_q)^2 \\
&\quad \times \{ f_{\mathrm{A}}(x_0) + a c_A \frac{1}{2} (\partial_0^* + \partial_0) f_{\mathrm{P}}(x_0) \} \,, && (4.3.33) \\
[f_{\mathrm{P}}(x_0)]_R &= Z_P(1 + b_P a m_q) Z_\zeta^2 (1 + b_\zeta a m_q)^2 f_{\mathrm{P}}(x_0) \,, && (4.3.34) \\
[k_{\mathrm{V}}(x_0)]_R &= Z_V(1 + b_V a m_q) Z_\zeta^2 (1 + b_\zeta a m_q)^2 \\
&\quad \times \{ k_{\mathrm{V}}(x_0) + a c_V \frac{1}{2} (\partial_0^* + \partial_0) k_{\mathrm{T}}(x_0) \} \,, && (4.3.35) \\
[k_{\mathrm{T}}(x_0)]_R &= Z_T(1 + b_T a m_q) Z_\zeta^2 (1 + b_\zeta a m_q)^2 \\
&\quad \times \{ k_{\mathrm{T}}(x_0) + a c_T \frac{1}{2} (\partial_0^* + \partial_0) k_{\mathrm{V}}(x_0) \} \,, && (4.3.36) \\
[f_1]_R &= Z_\zeta^4 (1 + b_\zeta a m_q)^4 f_1 \,, && (4.3.37) \\
[k_1]_R &= Z_\zeta^4 (1 + b_\zeta a m_q)^4 k_1 \,. && (4.3.38)
\end{aligned}$$

In this work we are only interested in studying the renormalization properties of the above operators, therefore since all the components of the currents share the same renormalization constant we do not consider all the possible Lorentz contractions.

4.4 Gradient Flow

In this section we introduce the Gradient Flow in the continuum, and its discretisation on the lattice. This is an important ingredient for the work since it gives an independent determination of the strong coupling which, together with the SF coupling, gives another approach to the non-perturbative determination of the running.
Let us first introduce an "extra dimension" parametrised by the commonly called "flow time" $t \geq 0$ with dimension $[E]^{-2}$. We can define $B_\mu(x,t)$ as the 5-dimensional extension of the gauge potential reproducing the 4-dimensional one at $t = 0$, i.e. $B_\mu(x, t = 0) =$

$A_\mu(x)$, the field strength at $t > 0$ is given by

$$G_{\nu\mu}(x,t) = \partial_\nu B_\mu(x,t) - \partial_\mu B_\nu(x,t) + [B_\nu(x,t), B_\mu(x,t)]\,. \tag{4.4.1}$$

The way how the gauge fields are evolving at $t > 0$ is given by the *Gradient Flow* equation [45] as

$$\frac{dB_\mu(x,t)}{dt} = D_\nu G_{\nu\mu}(x,t)\,. \tag{4.4.2}$$

An analogous equation can be written for fermion fields [46], opening the possibility to take advantage of this powerful tool to renormalize composite operators, however, this application it is not discussed in this thesis.
Eq. (4.4.2) can be interpreted as a gauge-invariant smearing procedure controlled by the continuous parameter t. At very large flow time, in fact, quantum fluctuation are smoothed down and the gauge field tends to the minimum[3] of the action $A^{\min}$

$$\lim_{t\to\infty} B_\mu(x,t) = A^{\min}_\mu(x)\,. \tag{4.4.3}$$

In particular it can be showed that the shape of the smearing is Gaussian (as a classical heat equation) where the typical smearing radius is given by $\sqrt{8t}$. At leading order in perturbation theory it is easy to observe that

$$B^{(1)}_\mu(x,t) = \int d^4y \mathcal{K}(x,y,t) A_\mu(y) \tag{4.4.4}$$

where the *heat kernel* $\mathcal{K}$ is given by a Gaussian

$$\mathcal{K}(x,y,t) = \frac{1}{(4\pi t)^2} e^{-\frac{(x-y)^2}{4t}} \tag{4.4.5}$$

which squeezes to a delta function when $\lim_{t\to 0}\mathcal{K}(x,y,t) = \delta^4(x-y)$. Without entering into the details of the formulation of flow which are discussed at length in literature (e.g. see [47]), since we are interested in the flow as a tool for a definition of the gauge coupling constant, can be defined the *action density* [48] in terms of fields at $t > 0$ as[4]

$$\langle E(t)\rangle = -\frac{1}{2}\langle \mathrm{Tr}[G_{\mu\nu}(x,t)G_{\mu\nu}(x,t)]\rangle\,, \tag{4.4.6}$$

which leads to a finite and well-defined continuum limit [49]. The above quantity given by Eq. (4.4.6) is an ideal candidate for an accurate scale setting. In fact we can define the reference flow time t_0 through

$$t^2\langle E(t)\rangle|_{t=t_0} = 0.3\,, \tag{4.4.7}$$

as discussed in [48]. Most importantly for this work, it gives a non-perturbative definition the renormalized coupling (alternative respect to the SF) through

$$g^2_{\mathrm{GF}}(\mu) = \frac{16\pi^2}{3} t^2\ \langle E(t)\rangle|_{\mu=\frac{1}{\sqrt{8t}}}\ . \tag{4.4.8}$$

For the purpose of this thesis, avoiding further complication we point to [49] for all the technical details. A very interesting possibility is given by the combination of the flow equation with a finite volume with linear extent L [50, 51], fixing the ratio between the

[3] this also include the possibility to end up in some secondary minimum of the action.
[4] note that at $t = 0$ the energy density would diverge when approaching the continuum limit $\propto 1/a^4$

smoothing radius and L as

$$\sqrt{8t}/L = c\,, \tag{4.4.9}$$

with c as a fixed proportionality constant enters into the definition of the renormalization scheme. Usually it is taken to be $c = 0.3$. We report here that the first application of the above renormalization scheme with SF boundary condition is discussed in [11].
The lattice version of Eq. (4.4.2) reads

$$a^2 \frac{\partial V_\mu(x,t)}{\partial t} V_\mu(x,t)^{-1} = -g_0 \partial_{x,\mu} S[V]\,, \tag{4.4.10}$$

with $V_\mu(x, t = 0) = U_\mu(x)$ and $S[V]$ any lattice gluon action. In practice, in this thesis we refer to the GF coupling obtained only from the space component of the energy density and projected at $Q = 0$ sector

$$\bar{g}^2_{\rm GF}(L) = \mathcal{N}^{-1}(c) \frac{t^2}{4} \left. \frac{\langle G^a_{ij}(x,t) G^a_{ij}(x,t) \delta_{Q,0} \rangle}{\langle \delta_{Q,0} \rangle} \right|_{\sqrt{8t}=cL, x_0=T/2}\,, \tag{4.4.11}$$

while the normalisation is discussed in [11]. An improved version of the coupling is the one given by a modified version of the flow, called "Zeuthen Flow" [52] is discussed in Chapter 5.

4.5 Running of the Strong Coupling

The non-perturbative computation of the running coupling is a remarkable application of the SF formalism summarised in this thesis. The recursive procedure allowed to bypass the usual limitation of infinite-volume renormalization schemes, making possible to cover several orders of magnitude in energy scales. Even though the computation of the scale dependence of the strong coupling is not the topic of this thesis, the renormalization of composite operators is a shared effort with the coupling projects. Let us then summarise briefly the strategy employed in $N_{\rm f} = 0, 2$ and $N_{\rm f} = 2 + 1$ projects, as we will see the latter differ from the first two.

4.5.1 Recursive finite-size technique in the SF

As stressed in the previous sections, SF is a well defined tool which allows for a very natural definition of the gauge coupling, and make possible the computation of correlation functions in *finite volume*. The volume, denoted by its extension along space directions L is a free scale in our quantities which can be naturally interpreted as the inverse of the physical energy scale $\mu = 1/L$.[5] Here we summarise the main feature of the recursive procedure, without entering into details of any specific renormalization project, whose details will be given along with the renormalization of composite operators in Chapters 6, 7, 8. The goal of any renormalization project is to calculate the scale evolution of the strong coupling, or in general renormalization constants from a low energy scales denoted by $\mu_{\rm had}$ where it is possible to match with typical bare coupling β used in large volume simulations to high energy region $\mu_{\rm pt}$ where perturbation theory is (supposed to be) safe and match with perturbation theory.
The first step, before studying the finite size scaling, is to fix the *Line of Constant Physics*

[5] It is here chosen the notation where the renormalized coupling at the scale $\mu = 1/L$ is written as $\bar{g}(L)$ instead of the usual $\bar{g}(1/L)$.

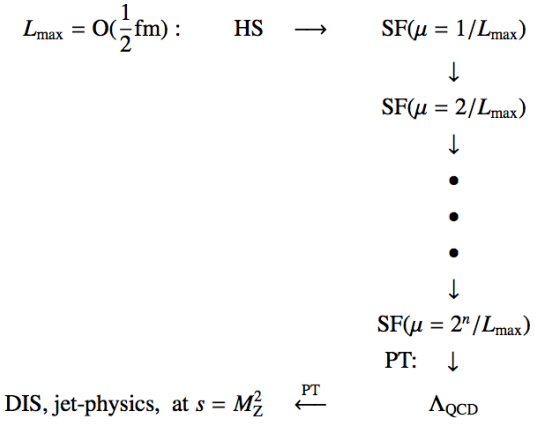

FIGURE 4.2: A sketch of the iterative procedure allowing to match a low energy HS (Hadronic Scheme) with perturbation theory at high energy (from [53])

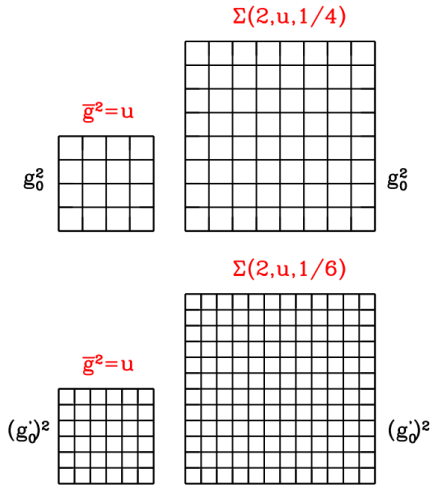

FIGURE 4.3: A sketch the step scaling function of the coupling for the volumes $L/a = 4, 6$. Both lattices on the lhs of the picture lies on the same LCP defined by $u = g^2(L)$ but at different βs. (from [53])

(LCP), given by the tuning of bare parameters (β, κ) such that

$$\bar{g}^2(L) = u \quad \text{and} \quad m_0 = m_c\,. \tag{4.5.1}$$

This work, of tuning the bare parameters in order to be on the critical line with vanishing masses usually requires a lot of effort but is a fundamental step in our renormalization procedure, since it ensures that the renormalization scheme given by this lattice setup is *mass independent*. The value of the critical line $\kappa_c(\beta, L)$ is obtained by requiring the bare $\mathcal{O}(a)$-improved PCAC mass (which will be introduced in the following chapter) to be equal to zero for each lattice size L and β. As expected being the PCAC mass a very local observable, the volume dependence of the critical line is small and only appreciated at small betas where the theory is fully dominated by non-perturbative dynamics.
Once the couple $(\beta, \kappa_c(\beta, L))$ is provided, it is possible to compute $u = \bar{g}^2(L)$ and repeat

the computation with *twice*[6] the volume size while keeping fixed the bare parameters. This defines another renormalized coupling $u' = \bar{g}^2(2L)$ [7]. We remind here the definition of the lattice SSF for the coupling as

$$\Sigma(u, a/L) = \bar{g}^2(2L)|_{\bar{g}^2(L)=u;m=0}\,. \tag{4.5.2}$$

In the real calculation, $\Sigma(u, a/L)$ is commonly replaced with its 2-loop improved version

$$\tilde{\Sigma}(u, a/L) = \frac{\Sigma(u, a/L)}{1 + \delta_1(a/L)u + \delta_2(a/L)u^2} \tag{4.5.3}$$

with the relative cutoff effects at 1-loop and 2-loop, respectively δ_1 and δ_2 are given by

$$\delta(u, a/L) = \frac{\Sigma(u, a/L) - \sigma(u)}{\sigma(u)} = \delta_1(a/L)u + \delta_2(a/L)u^2 + \mathcal{O}(u^3)\,, \tag{4.5.4}$$

whose numerical values are provided in [54]. Finally this quantity can be extrapolated to the continuum by iterating this procedure for several (usually 3 or 4) lattices as

$$\sigma(u) = \lim_{a\to 0} \tilde{\Sigma}(u, a/L)\,. \tag{4.5.5}$$

Typical values of L/a are $6, 8, 12, 16$ and respective double size (more details are given later). From now on, all the procedure deals only with continuum quantities. In order to compute the running over several orders of magnitudes it is necessary to interpolate (usually with some polynomial ansatz) the continuum SSF, viz

$$\sigma(u) = u(1 + s_0 u + s_1 u^2 + \dots)\,, \tag{4.5.6}$$

where the coefficients can be estimated from Eq. (2.2.1) (for $s = 2$) in perturbation theory (and may be kept fixed or not in the fitting procedure) as

$$s_0 = 2b_0 \log(2)\,, \tag{4.5.7}$$
$$s_1 = (2b_0 \log(2))^2 + 2b_1 \log(2)\,, \tag{4.5.8}$$
$$s_2 = (2b_0 \log(2))^3 + 10 b_0 b_1 (\log(2))^2 + 2b_2 \log(2)\,. \tag{4.5.9}$$

As stressed in Chapter 2, the SSF is simply an integrated and discretized version of the β-function for a given step scale s. Once an analytical form of $\sigma(u)$ is obtained, it is possible to build the recursion

$$u_i = \bar{g}^2(2^{-i} L_{\rm had}) \quad \text{for} \quad i = 0, \dots, n\,. \tag{4.5.10}$$

The starting point of the recursion $u_0 = u_{\rm had} = \bar{g}^2(L_{\rm had})$ is chosen in a way to match the large volume βs. The number of steps n of the coupling chain it is usually chosen to be $n = 7, 8$ in order to reach a factor of 2^7 or 2^8 in scales. This means that, if for instance the starting scale corresponds to $\mu_{\rm had} = 1/L_{\rm had} \sim \Lambda_{\rm QCD}$ the final scale $\mu_{\rm pt} \sim M_W$ where perturbation theory is guaranteed to describe well the theory. The RGI of the coupling defined by Eq. (2.1.10) can be than reached through the trivial iteration

$$\frac{\Lambda_{\rm QCD}}{\mu_{\rm had}} = \frac{\Lambda_{\rm QCD}}{2^n \mu_{\rm had}} \frac{2^n \mu_{\rm had}}{2^{n-1} \mu_{\rm had}} \cdots \frac{2\mu_{\rm had}}{\mu_{\rm had}}\,. \tag{4.5.11}$$

[6] actually, it is not mandatory to double the size. In principle it is possible to define the scale step s to be an arbitrary *non*-integer number. But for historical reasons it is chosen to be $s = 2$.

[7] Since the chiral tuning is performed on L lattices, the simulation at $2L$ will have a mass different from zero by lattice arctifacts, vanishing in the continuum limit

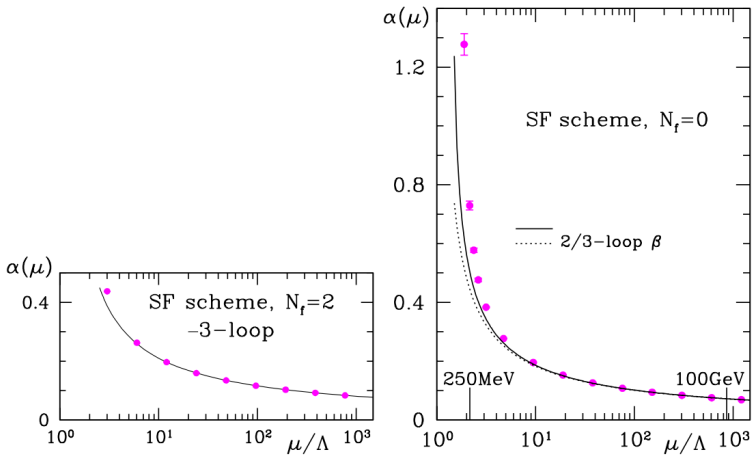

FIGURE 4.4: Running of $\alpha_s = \bar{g}^2(\mu/\Lambda)/(4\pi)$ for $N_f = 2$ on the left [39] and $N_f = 0$ on the right [53] .

The first term on the r.h.s. is computed perturbatively, while the rest of terms are computed through the non-perturbative recursion.

The value of $L_{\rm had}$ is determined in terms of physical units like the Sommer's parameter r_0 [55], the flow time t_0 [56], or combination of hadron masses and decay constants (e.g. [57]).

Numerical details, and references are provided in the context of the renormalization of the tensor current in Section 6.

4.5.2 Scheme Switching

The iterative procedure summarised in the last section has been successfully used for computing the running coupling in $N_f = 0, 2, 4$ and in the SU(2) pure gauge theory in

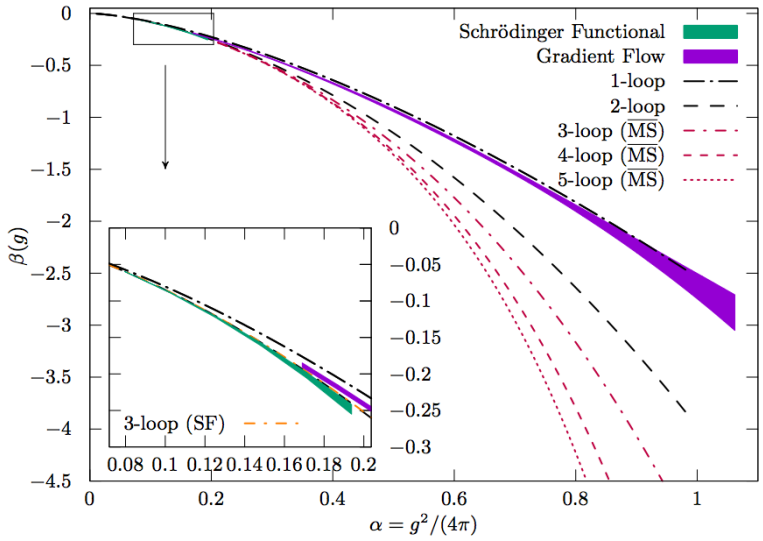

FIGURE 4.5: β-function for $N_f = 3$ QCD as a function of α_s [10]. The Scheme switch SF-GF at $\bar{g}^2_{\rm SF}(L_0) = 2.012$ or equivalentely $\bar{g}^2_{\rm GF}(2L_0) = 2.6723(64)$ is displayed in the zoom.

[39, 58, 59, 60]. However, in order to go beyond that precision and access to new levels of accuracy it has been necessary to introduce a different renormalization scheme, and perform a non-perturbative matching.

As discussed in the above sections, the SF coupling definition relies on the presence of the BG field induced by the non trivial Dirichlet boundary condition in time. The correlators, entering the definition of the SF coupling are expensive to measure, and it has been observed that the relative error increase fast at large couplings, i.e. in the "deep" non-perturbative regime. On the other hand, perturbative calculation up to 2-loops have been performed [37], and a NLO perturbative matching can be performed.

The novel GF coupling, seems to be computationally cheaper than the SF, and much more accurate while moving toward hadronic energy region. Moreover, since this definition is not based on the presence of BG field, this can be turned off improving noticeably the accuracy of results. As we will see in the Chapter 7, the absence of BG field, allowed us to use the same gauge ensembles[8] which have been produced to analyse the running coupling in [10].

Despite the observation that the GF coupling seems much more suited at low energy scales, it has to be mentioned that it is affected by larger cutoff effects compared to its SF counterpart, requiring then the simulation of larger volumes. Moreover, currently there are no perturbative calculation beyond the leading order[9] , and, therefore that is the highest order entering in the perturbative matching.

This general picture suggest to use different couplings definition in different energy regions, namely GF at low energy to make contact with CLS large volume simulations [62] and SF at high energy to make contact with perturbation theory. The two schemes are non-perturbatively matched at an intermediate scale, called the "Switching Scale" $\mu_0 = 1/L_0 \sim 4, \mathrm{GeV}$. This procedure has been successfully applied for $N_\mathrm{f} = 2 + 1$ QCD, yielding to the final determination of $\Lambda^{(3)}_{\overline{\mathrm{MS}}}$ is provided in [63].

[8] it has been observed that the presence of a non trivial BG field deteriorate the signal of fermionic correlators.

[9] preliminary results in this direction can be found in [61].

5 Symanzik Improvement

In this section we summarise briefly the main ideas, originally from Symanzik [64, 65, 66], to interpret and identify the sources of cutoff effects. Once presented the general features we restrict to the formulation in finite volume with SF boundary conditions, which is the interesting case for this thesis.

5.1 Local Effective Action

Close to the continuum limit, the lattice theory can be defined in terms of local effective actions

$$S_{\text{eff}} = S_0 + aS_1 + a^2 S_2 + \dots \,, \tag{5.1.1}$$

where the non-vanishing term when $a \to 0$ is just the continuum theory and the other terms can be interpreted as operator insertions in the continuum theory.
While in the original formulation [64, 65, 66] the continuum is defined in dimensional regularisation, here, following [44] we can employ a discretised theory with lattice spacing much smaller than a.

In general the cutoff effects proportional to a can be written as

$$S_k = \int d^4x \mathcal{L}_k(x) \,, \tag{5.1.2}$$

where $\mathcal{L}_k(x)$ is a combination of local composite fields of dimension $4+k$, in particular for $\mathcal{L}_1(x)$ we have

$$\mathbf{O}_1 = \bar{\psi}\sigma_{\mu\nu}F_{\mu\nu}\psi \,, \tag{5.1.3}$$

$$\mathbf{O}_2 = \bar{\psi}D_\mu D_\mu \psi + \bar{\psi}\overleftarrow{D}_\mu\overleftarrow{D}_\mu\,\psi \,, \tag{5.1.4}$$

$$\mathbf{O}_3 = m\mathrm{Tr}\{F_{\mu\nu}F_{\mu\nu}\} \,, \tag{5.1.5}$$

$$\mathbf{O}_4 = m\{\bar{\psi}\gamma_\mu D_\mu\psi - \bar{\psi}\overleftarrow{D}_\mu\,\gamma_\mu\psi\} \tag{5.1.6}$$

$$\mathbf{O}_5 = m^2\bar{\psi}\psi \,. \tag{5.1.7}$$

It can be seen [44] that on-shell the only independent term is given by $\mathbf{O}_1$. We can than write the on-shell $\mathcal{O}(a)$-improved fermion action as

$$S_F^I[U,\bar{\psi},\psi] = S_F[U,\bar{\psi},\psi] + \delta S_F[U,\bar{\psi},\psi] \,, \tag{5.1.8}$$

with

$$\delta S_F[U,\bar{\psi},\psi] = a^5 \sum_x c_{\text{sw}}\bar{\psi}(x)\frac{i}{4}\sigma_{\mu\nu}\hat{F}_{\mu\nu}(x)\psi(x) \,. \tag{5.1.9}$$

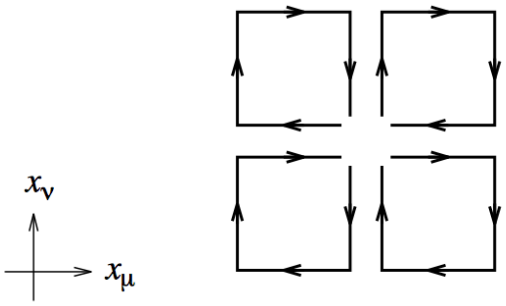

FIGURE 5.1: A sketch (from [68]) of the Clover plaquette term, providing the $\mathcal{O}(a)$-improvement of the Wilson fermion action once the coefficient $c_{\rm sw}$ is opportunely tuned.

The term proportional to $c_{\rm sw}$ originally written down in [67] is sometime called "Clover Term" because of the plaquette shape of $\hat{F}_{\mu\nu}$, given by

$$\hat{F}_{\mu\nu}(x) = \frac{1}{8a^2}[Q_{\mu\nu}(x) - Q_{\nu\mu}]\,, \tag{5.1.10}$$

where the clover Q can be written as [67][1]

$$\begin{aligned} Q_{\mu\nu}(x) = & \\ & U_\mu(x)U_\nu(x+a\hat{\mu})[U_\mu(x+a\hat{\nu})]^{-1}[U_\nu(x)]^{-1} \\ & + U_\nu(x)[U_\mu(x-a\hat{\mu}+a\hat{\nu})]^{-1}[U_\nu(x-a\hat{\mu})]^{-1}U_\mu(x-a\hat{\nu}) \\ & + [U_\mu(x-a\hat{\mu})]^{-1}[U_\nu(x-a\hat{\mu}-a\hat{\nu})]^{-1}U_\mu(x-a\hat{\mu}-a\hat{\nu})U_\nu(x-a\hat{\nu}) \\ & + [U_\nu(x-a\hat{\nu})]^{-1}U_\mu(x-a\hat{\nu})U_\nu(x+a\hat{\mu}-a\hat{\nu})[U_\mu(x)]^{-1}\,. \end{aligned} \tag{5.1.11}$$

A sketch of the above link structure is shown in Fig. 5.1. It has been showed that at the lowest order in perturbation theory $c_{\rm sw} = 1$.

As usual, when studying a QFT discretised on the lattice the quantity of interests are the (renormalized and connected) correlation functions

$$(Z_\phi)^{n/2}\langle\phi(x_1)\dots\phi(x_n)\rangle_{\rm con} \tag{5.1.12}$$

which have a well defined continuum limit, providing the appropriate renormalization for the fields $Z_\phi^{1/2}\phi(x)$ and the absence of contact terms. In the local effective theory we can also power expand in a the field around the continuum as

$$\phi_{\rm eff}(x) = \phi_0(x) + a\phi_1(x) + a^2\phi_2(x)\dots\,, \tag{5.1.13}$$

where the fields $\phi_k(x)$ are linear combinations of local fields with appropriate dimension and symmetry properties. At order a the lattice correlation function get a contribution

[1] note that it is not the only way to orient the "leafs".

from both the action and the correlator itself as

$$\langle\phi_0(x_1)\dots\phi_0(x_n)\rangle_{\rm conn} - a\int d^4y\langle\phi_0(x_1)\dots\phi_0(x_n)\mathcal{L}_1(y)\rangle_{\rm con} + a\sum_{k=1}^{n}\langle\phi_0(x_1)\dots\phi_1(x_k)\dots\phi_0(x_n)\rangle_{\rm con} + \mathcal{O}(a^2)\,, \quad (5.1.14)$$

where the expectation value with subscript "con" is meant to be taken in the continuum theory with action S_0. It is clear from Eq. (5.1.14) that in order to have a *full* $\mathcal{O}(a)$-improved correlation function [2] it is necessary to improve both the action and the operator with appropriate counter'terms.

5.2 On-shell improved gauge action

On the same line with the fermionic improvement[3], the same can be done for the gauge plaquette action Eq. (3.1.3). In this case the list of independent dimension-6 gauge invariant operators respecting the symmetry of the action contributing at $\mathcal{O}(a^2)$, accordingly to [69] are given by

$$\mathbf{O}_1 = \sum_{\mu,\nu}\mathrm{Tr}D_\mu F_{\mu\nu}D_\nu F_{\mu\nu}\,, \quad (5.2.1)$$

$$\mathbf{O}_2 = \sum_{\mu,\nu,\rho}\mathrm{Tr}D_\mu F_{\nu\rho}D_\mu F_{\nu\rho} \quad (5.2.2)$$

$$\mathbf{O}_3 = \sum_{\mu,\nu,\rho}\mathrm{Tr}D_\mu F_{\mu\rho}D_\nu F_{\nu\rho} \quad (5.2.3)$$

where $D_\mu F_{\mu\rho} = \partial_\mu F_{\mu\rho} + g_0[A_\mu, F_{\nu\rho}]$. The general form of the improved gauge action (for $N = 3$) is given by

$$S_{\rm imp} = \frac{2}{g_0^2}\sum_i c_i(g_0)\sum_{\mathcal{C}_i\in\mathcal{S}_i}\mathcal{L}(\mathcal{C}_i) \qquad \text{with} \qquad \mathcal{L}(\mathcal{C}_i) = Re\mathrm{Tr}[1 - U(\mathcal{C})]\,, \quad (5.2.4)$$

where $U(\mathcal{C})$ is the ordered product of link variables around the closed curves $\mathcal{C}$, and $\mathcal{S}_i$ are sets with a given "link"-topology, i.e.

- $\mathcal{S}_0$ is the standard wilson plaquette.
- $\mathcal{S}_1$ is the set of 2×1 rectangles,
- $\mathcal{S}_2$ the set of "twisted chairs",
- $\mathcal{S}_3$ the set of "chairs".

All the shapes are summarised in Fig. 5.2. It is conventional [69] to normalise the action by requiring

$$c_0 + 8c_1 + 8c_2 + 16c_3 = 1\,, \quad (5.2.5)$$

[2] with vanishing masses

[3] note that while for fermions the improvement is done $\mathcal{O}(a)$, for the gauge action the improvement is done at $\mathcal{O}(a^2)$. As mentioned in the text, there are no linear cutoff contribution for the gauge action in infinite volume. The case in finite volume is discussed later on.

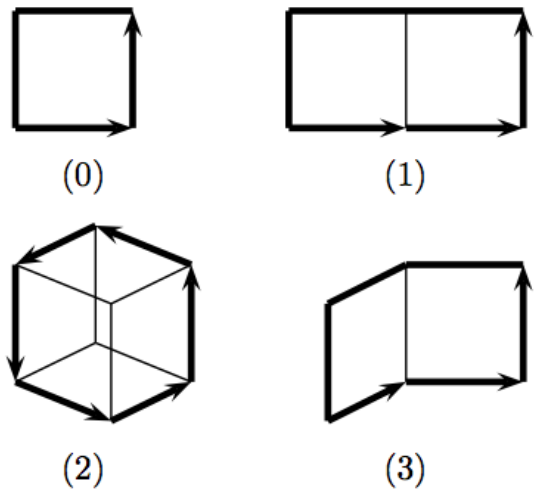

FIGURE 5.2: 4 and 6 links closed loops on the lattice (from [68])

such that the standard continuum gluon action is obtained in the classical continuum limit, with any choice of the 3 free parameters[4]. With the choice of $c_0 = 1$, $c_{i\geq 1} = 0$ we reproduce the standard Wilson plaquette action, while for $c_0 = 5/3$, $c_1 = -1/12$, $c_{i\geq 2} = 0$ we have the tree-level improved Lüscher-Weisz (LW) action.

5.3 Improved currents and density

As we showed in Eq. (5.1.14) in order to subtract all the cutoff effect $\propto a$ it is necessary to isolate (and than remove) the a dependence in correlation functions. A very important example is given by the axial current, since leads to the definition of the PCAC mass. All the possible contributions $\mathcal{O}(a)$ to $A^a_\mu(x)$ are

$$(\mathbf{O}_6)^a_\mu = \bar{\psi}\gamma_5\frac{\tau^a}{2}\sigma_{\mu\nu}D_\nu\psi - \bar{\psi}\overleftarrow{D}_\nu\,\sigma_{\mu\nu}\gamma_5\frac{\tau^a}{2}\psi\,, \tag{5.3.1}$$

$$(\mathbf{O}_7)^a_\mu = \bar{\psi}\frac{\tau^a}{2}\gamma_5 D_\mu\psi + \bar{\psi}\overleftarrow{D}_\mu\,\gamma_5\frac{\tau^a}{2}\psi\,, \tag{5.3.2}$$

$$(\mathbf{O}_8)^a_\mu = m\bar{\psi}\gamma_\mu\gamma_5\frac{\tau^a}{2}\psi\,. \tag{5.3.3}$$

Following the same strategy applied for the improvement of the Wilson action, it can be showed [44] that the only relevant operator is given by $\mathbf{O}_7$. We can then define an $\mathcal{O}(a)$-improved axial current as

$$(A_I)^a_\mu(x) = A^a_\mu(x) + ac_{\rm A}(g_0^2)\frac{1}{2}(\partial^*_\mu + \partial_\mu)P^a(x)\,, \tag{5.3.4}$$

[4]Taking into account a constraint arising from positivity [69].

where $c_{\rm A}$ have to be tuned appropriately.
Analogously, improvement pattern can be worked out [70] for all the currents and densities, viz

$$(V_I)^a_\mu(x) = V^a_\mu(x) + ac_{\rm V}(g_0^2)\frac{1}{2}(\partial^*_\nu + \partial_\nu)T^a_{\mu\nu}\,, \tag{5.3.5}$$

$$(T_I)^a_{\mu\nu}(x) = T^a_{\mu\nu} + ac_{\rm T}(g_0^2)\frac{1}{2}[(\partial^*_\mu + \partial_\mu)V^a_\nu - (\partial^*_\nu + \partial_\nu)V^a_\mu]\,. \tag{5.3.6}$$

Interestingly, there are no $\mathcal{O}(a)$ counter terms for pseudoscalar and scalar correlators.

It can be observed that if we are in a non-vanishing mass setup, $\mathcal{O}(a)$ terms proportional to the subtracted mass affect the theory and have to be subtracted from all the other quantities. More in general, the improvement of the theory requires a renormalization of the bare parameters of the form $1 + ab_X(g_0^2)m_q$, where m_q is the bare subtracted mass introduced in Section 3, and X denotes a specific parameter.

We can consider *modified* bare parameters, in particular coupling and mass as

$$\tilde{g}_0^2 = g_0^2(1 + b_g a m_q)\,, \tag{5.3.7}$$

$$\tilde{m}_q = m_q(1 + b_m a m_q)\,. \tag{5.3.8}$$

So that the renormalized counterparts read

$$\bar{g}^2 = Z_g(g_0, a\mu)(1 + b_g a m_q)g_0^2\,, \tag{5.3.9}$$

$$\bar{m} = Z_m(g_0, a\mu)(1 + b_m a m_q)m_q\,, \tag{5.3.10}$$

as for the fields

$$\phi_{\rm R} = Z_\phi(\tilde{g}_0^2, a\mu)(1 + b_\phi a m_q)\phi_I(x)\,. \tag{5.3.11}$$

Exactly the same have to be considered for all renormalized correlation functions, even those who does not shown an explicit $\mathcal{O}(a)$ dependence like the pseudoscalar density. We do not go deeper on this topic, fully investigated in [44], since all our renormalization procedure is imposed at vanishing quark masses (i.e. $m_q = 0$), simplifying considerably the scaling toward the continuum of all the interesting quantities.
More details on the renormalization procedure are provided in last chapters.

5.4 Improvement of the gradient flow and flow observables

Since this topic is very technical and out of the scope of this thesis, we will only mention the most important features to give a general idea, avoiding technicalities. For a full detailed analysis see [52].
In order to formulate a theory satisfying the flow equation Eq. (4.4.10), it is necessary to modify the original $4-$dimensional action incorporating the flow equation itself as a constraint by the introduction of Lagrange multiplier fields [45]. We call the latter $L_\mu(t,x)$ which are hermitian.
The $4+1$ dimensional action of this theory, restricting to the gauge part, takes the general form of

$$S[V,L] = S_G[U] - 2a^4\int_0^\infty dt\sum_{x,\mu}\mathrm{Tr}\{L_\mu(t,x)F_\mu(t,x)\} \tag{5.4.1}$$

where we are assuming

$$V_\mu(0,x) = U_\mu(x)\,, \tag{5.4.2}$$

and

$$F_\mu(t,x) = a^{-1}(\partial_t V_\mu(t,x))V_\mu(t,x)^\dagger - a^{-3}g_0^2\partial_{x;\mu}S_{\rm G}[V]\,. \tag{5.4.3}$$

Given the above action it is possible to define expectation values of composite fields $\mathbf{O}[V,L]$ at $t \geq 0$ as

$$\langle \mathbf{O}[V,L]\rangle_t = \mathcal{Z}^{-1}\int D[V]D[L]\mathbf{O}[V,L]\exp\left(-S[V,L]\right), \tag{5.4.4}$$

where with $\langle\cdot\rangle_t$ we denote the average taken at flow time t. Accordingly to Symanzik's effective action for the $4+1$ theory

$$S_{\rm eff}[B,L] = S_0^{\rm cont}[B,L] + a^2 S_2[B,L] + \mathcal{O}(a^4)\,, \tag{5.4.5}$$

it is possible to identify two contribution at $\mathcal{O}(a^2)$. [5] In particular

$$S_2[B,L] = S_{2,\rm fl}[B,L] + S_{2,\rm b}[B,L]\,, \tag{5.4.6}$$

were the first term at the r.h.s. is the "flow" contribution at $t>0$ and the second term is the "boundary" contribution at $t=0$. These two objects have the general form of

$$S_{2,\rm fl}[B,L] = \int_0^\infty \int d\,t\,d^4\,x \sum_{i=1}^{n_{fl}} Q_i(t,x)\,, \tag{5.4.7}$$

$$S_{2,\rm b}[B,L] = \int d^4\,x \sum_{i=1}^{n_b} O_i(x)\,, \tag{5.4.8}$$

where Q_i are gauge-invariant polynomials in the fundamental fields $B(t,x)$, $L(t,x)$ and derivatives, while O_i are the analogous at $t=0$. It can be observed that the dimension of the two kind of counter terms is different at $t=0$ and $t>0$. In fact Q_i is dimension-8 while O_i is dimension-6. It is observed with a perturbative analysis in [47] that there are not loop diagrams in the bulk, which imply that a classical improvement of the flow action yields exactly the $\mathcal{O}(a^2)$ effects. By the same argument, $\mathcal{O}(a^2)$ improvement is achieved for composite operators at $t>0$ by choosing a discretisation which does not generate $\mathcal{O}(a^2)$ effects when expanded classically. In other words, once the flow equation is improved it does not generate any $\mathcal{O}(a^2)$ effects in the observables. The only source of cutoff effects $\mathcal{O}(a^2)$ which receive quantum corrections are the one living at the boundary $t=0$ time-slice (i.e. the standard 4-dimensional formulation).
Applying those general considerations, $S_{2,\rm fl}$ is computed in [52] by a classical expansion in a, yielding to

$$S_{2,\rm fl}|_{\rm LW} = -2\int_0^\infty dt \int d^4\,x \sum_{\mu,\nu} {\rm Tr}\{L_\mu(t,x)\frac{1}{12}D_\mu^2 D_\nu G_{\nu\mu}(t,x)\}\,. \tag{5.4.9}$$

[5] only odd powers of a appear in the expansion because of extra symmetries of the $5-$dimensional formulation [52].

Eq. (5.4.9) vanishes with the Lüscher-Weisz choice of coefficients in the discretisation of gauge action, if the gradient entering in the flow equation is modified by the term

$$1 + \frac{1}{12} a^2 \nabla^*_\mu \nabla_\mu \,, \tag{5.4.10}$$

This leads to an "improved" flow equation where all the $\mathcal{O}(a^2)$ effects are removed, commonly referred in the literature by *Zeuthen Flow* [71, 52] as

$$a^2 \frac{\partial V_\mu(x,t)}{\partial t} V_\mu^{-1}(x,t) = -g_0^2 (1 + \frac{a^2}{12} D^*_\mu D_\mu) \partial_{x,\mu} S_{\rm LW}[V] \,. \tag{5.4.11}$$

Concerning flow observables, we have

$$\langle \mathbf{O} \rangle^{\rm lat} = \langle \mathbf{O}_0 \rangle + a^2 (\langle \mathbf{O}_2 \rangle - \langle \mathbf{O}_0 S_{2,\rm fl} \rangle - \langle \mathbf{O}_0 S_{2,\rm b} \rangle) + \mathcal{O}(a^4) \,. \tag{5.4.12}$$

Also in this case the last ingredient in order to remove $\mathcal{O}(a^2)$ contribution is the knowledge of $S_{2,\rm b}$, which, as shown in [52] can be realized as a change of initial condition of the flow equation. The corresponding coefficient $c_b(g_0^2)$ is a function of the bare coupling which happens to vanish at tree level for plaquette and LW action. Skipping all the technicalities, one of the most important results of the afore-mentioned paper, for the scope of this thesis, is that with LW discretisation of gauge action, and with the modified version of the flow given by Eq. (5.4.11), the tree level $\mathcal{O}(a^2)$ improvement is achieved for flow observables. This is particularly important for the energy density, which, as we have showed in the previous chapter gives a non-perturbative definition of the strong coupling constant.

5.5 Improvement in the SF

As in the previous sections, also the approach of the SF to the continuum limit can be described by a local effective theory. The difference here, respect to the infinite volume case where the only independent $\mathcal{O}(a)$-term is the one appearing with coefficient $c_{\rm sw}$ Eq. (5.1.9), is given by the finiteness of the volume. In fact, as extensively discussed in [44], the cutoff contribution coming from the boundary can isolated as

$$S_k = \int d^4x \, \mathcal{L}_k(x) + \lim_{\epsilon \to 0} \int d^3x \, \left\{ \mathbf{L}_k(x)|_{x_0=\epsilon} + \mathbf{L}'_k(x)|_{x_0=T-\epsilon} \right\} \tag{5.5.1}$$

where $\mathbf{L}_k(x)$ and $\mathbf{L}'_k(x)$ are local operators of dimension $3+k$. Since we are interested in removing the linear a contribution, restricting to $\mathcal{L}_1$, we find

$$S_{\rm imp}[U, \bar\psi, \psi] = S[U, \bar\psi, \psi] + \delta S_{\rm bulk}[U, \bar\psi, \psi] + \delta S_{G,b}[U] + \delta S_{F,b}[U, \bar\psi, \psi] \,, \tag{5.5.2}$$

where the bulk contribution is the one given by Eq. (5.1.9) but without including the first and last time-slice [44], viz

$$\delta S_{\rm bulk}[U, \bar\psi, \psi] = a^5 \sum_{x_0=a}^{T-a} \sum_{\mathbf{x}} c_{\rm sw}(g_0) \bar\psi(x) \frac{i}{4} \sigma_{\mu\nu} \hat{F}_{\mu\nu}(x) \psi(x) \,. \tag{5.5.3}$$

Let us now focus separately on the boundary improvements $\delta S_{G,b}$ and $\delta S_{F,b}$, respectively for gauge and fermion actions. In pure gauge formulations the only possible operators

with $d \geq 4$ are given by [44]

$$\mathbf{O}_9 = \mathrm{Tr}\{F_{kl}, F_{kl}\}\,, \tag{5.5.4}$$
$$\mathbf{O}_{10} = \mathrm{Tr}\{F_{0k}, F_{0k}\}\,. \tag{5.5.5}$$

For the associated $\mathcal{O}(a)$ counter term is taken [17]

$$\delta S_{G,b}[U] = \frac{1}{2g_0^2}\left\{(c_s(g_0)-1)\sum_{p_s}\mathrm{Tr}[1-U(p_s)] + (c_t(g_0)-1)\sum_{p_t}\mathrm{Tr}[1-U(p_t)]\right\} \tag{5.5.6}$$

where the sums run over all the oriented space-like and time-like plaquettes p_s and p_t living at the boundaries. The presence of quark fields allow to create more composite operators $d = 4$ which can combine into $\delta S_{F,b}$. A basis is given by [44]

$$\mathbf{O}_{11} = \bar{\psi}P_+ D_0\psi + \bar{\psi}\overleftarrow{D}_0 P_-\psi\,, \tag{5.5.7}$$
$$\mathbf{O}_{12} = \bar{\psi}P_- D_0\psi + \bar{\psi}\overleftarrow{D}_0 P_+\psi\,, \tag{5.5.8}$$
$$\mathbf{O}_{13} = \bar{\psi}P_+\gamma_k D_k\psi - \bar{\psi}\overleftarrow{D}_k \gamma_k P_-\psi\,, \tag{5.5.9}$$
$$\mathbf{O}_{14} = \bar{\psi}P_-\gamma_k D_k\psi - \bar{\psi}\overleftarrow{D}_k \gamma_k P_+\psi\,, \tag{5.5.10}$$
$$\mathbf{O}_{15} = m\bar{\psi}\psi\,. \tag{5.5.11}$$

With similar consideration to the ones used for the bulk improvement and taking advantage of the equation of motions we reduce to

$$\delta S_{F,b}[U,\bar{\psi},\psi] = a^4\sum_{\mathbf{x}}\left\{(\tilde{c}_s(g_0)-1)[\hat{\mathbf{O}}_s(\mathbf{x}) + \hat{\mathbf{O}}'_s(\mathbf{x})] + (\tilde{c}_t(g_0)-1)[\hat{\mathbf{O}}_t(\mathbf{x}) + \hat{\mathbf{O}}'_t(\mathbf{x})]\right\} \tag{5.5.12}$$

where [44]

$$\hat{\mathbf{O}}_s(\mathbf{x}) = \frac{1}{2}\bar{\rho}(\mathbf{x})\gamma_k(\nabla_k^* + \nabla_k)\rho(\mathbf{x}) \tag{5.5.13}$$
$$\hat{\mathbf{O}}'_s(\mathbf{x}) = \frac{1}{2}\bar{\rho}'(\mathbf{x})\gamma_k(\nabla_k^* + \nabla_k)\rho'(\mathbf{x}) \tag{5.5.14}$$
$$\hat{\mathbf{O}}_t(\mathbf{x}) = [\bar{\psi}(y)P_+\nabla_0^*\psi(y) + \bar{\psi}(y)\overleftarrow{\nabla}_0^* P_-\psi(y)]|_{y=(a,\mathbf{x})}\,, \tag{5.5.15}$$
$$\hat{\mathbf{O}}'_t(\mathbf{x}) = [\bar{\psi}(y)P_-\nabla_0\psi(y) + \bar{\psi}(y)\overleftarrow{\nabla}_0 P_+\psi(y)]|_{y=(T-a,\mathbf{x})}\,. \tag{5.5.16}$$

It is observed that "spatial" improvement are never entering in relevant boundary-to-bulk correlators. We are left with three improvement parameters to be tuned, $c_{\mathrm{t}}, \tilde{c}_{\mathrm{t}}, c_{\mathrm{sw}}$.

In general it is possible to compute the improvement coefficients non-perturbatively or expanding in g_0^2 to some given order. While in the first case the removal of the leading a effect is completely achieved, in the latter there is a remainder $\mathcal{O}(g_0^{2(n+1)}a)$ cutoff effect still present in the interesting quantities, where n denotes the number of loops at which the computation is carried out.

Part II

Renormalization of Tensor Currents

6 Tensor currents

6.1 Motivation

Hadronic matrix elements of tensor currents play an important rôle in several relevant problems in particle physics. Some prominent examples are rare heavy meson decays that allow to probe the consistency of the Standard Model (SM) flavour sector (see, e.g., [4, 5, 6] for an overview), or precision measurements of β-decay and limits on the neutron electric dipole moment (see, e.g., [7, 8, 9] for an up-to-date lattice-QCD perspective).

One of the key ingredients in these computations is the renormalization of the current. Indeed, partial current conservation ensures that non-singlet vector and axial currents require at worst finite normalizations, and fixes the anomalous dimension of scalar and pseudoscalar densities to be minus the quark mass anomalous dimension. They however do not constrain the tensor current, which runs with the only other independent anomalous dimension among quark bilinears. Controlling the current renormalization and running at the non-perturbative level, in the same fashion achieved for quark masses [72, 43, 73, 74], is therefore necessary in order to control systematic uncertainties, and allow for solid conclusions in new physics searches.

The anomalous dimension of tensor currents is known to three-loop order in continuum schemes [75, 76], while on the lattice perturbative studies have been carried out to two-loop order [77]. Non-perturbative determinations of renormalization constants in RI/MOM schemes, for the typical few-GeV values of the renormalization scale accessible to the latter, have been obtained for various numbers of dynamical flavours and lattice actions [78, 79, 80, 81, 82, 83, 84]. The purpose of this work is to set up the strategy for the application of finite-size scaling techniques based on the Schrödinger Functional (SF) [17], in order to obtain a fully non-perturbative determination of both current renormalization constants at hadronic energy scales, and the running of renormalized currents to the electroweak scale. This completes the ALPHA Collaboration non-perturbative renormalization programme for non-singlet quark field bilinears [72, 43, 73, 74, 85, 86, 87] and four-quark operators [88, 89, 90, 91, 92, 93, 94].

As part of the strategy, we will set up a family of SF renormalization schemes, and perform a perturbative study with the main purpose of computing the perturbative anomalous dimension up to two loops, in order to make safe contact with perturbative physics at the electroweak scale. Preliminary results of this work have already appeared as proceedings contributions [95].[1] We will then apply our formalism to the fully non-perturbative renormalization of non-singlet tensor currents in $N_{\mathrm{f}} = 0$ and $N_{\mathrm{f}} = 2$ QCD. Our results for $N_{\mathrm{f}} = 3$ QCD, that build on the non-perturbative determination of the running coupling [97, 10, 98] and the renormalization of quark masses [73, 74, 85], will be provided in a separate publication [99].

The layout of this part of the thesis is as follows. In section 2 we will introduce our notation and discuss the relevant renormalization group equations. In section 3 we

[1] During the development of this work, Dalla Brida, Sint and Vilaseca have performed a related perturbative study as part of the setup of the chirally rotated Schrödinger Functional [96]. Their results for the one-loop matching factor required to compute the NLO tensor anomalous dimensions in SF schemes coincide with ours (cf. section 6.3), previously published in [95]. This constitutes a strong crosscheck of the computation.

will introduce our SF schemes, generalizing the ones employed for quark mass renormalization. In section 4 we will study these schemes in one-loop perturbation theory, and compute the matching factors that allow to determine the NLO values of anomalous dimensions. In section 5 we will discuss our non-perturbative computations, and provide results for the running of the currents between hadronic and high-energy scales and for the renormalization constants needed to match bare hadronic observables at low energies. Section 6 contains our conclusions. Some technical material, as well as several tables and figures, are gathered in appendices.

6.2 Renormalization conditions

RG evolution of multiplicative renormalizable operators have been introduced in Chapter 2. We then, refer to the formulae presented in that general context. We remind, the (flavour non-singlet) tensor bilinear is defined as

$$T_{\mu\nu}(x) = i\,\bar{\psi}_{s_1}(x)\sigma_{\mu\nu}\psi_{s_2}(x)\,, \tag{6.2.1}$$

where $\sigma_{\mu\nu} = \frac{i}{2}[\gamma_\mu, \gamma_\nu]$, and $s_1 \neq s_2$ are flavour indices. Since all the Lorentz components have the same anomalous dimension, as far as renormalization is concerned it is enough to consider the "electric" operator T_{0k}. As already discussed in the introduction, it is important to observe that the tensor current is the only bilinear operator that evolves under RG transformation in a different way respect to the quark mass — partial conservation of the vector and axial currents protect them from renormalization, and fixes the anomalous dimension of both scalar and pseudoscalar densities to be $-\tau$. We report here, the one-loop (universal) coefficient of the tensor anomalous dimension is

$$\gamma_{\rm T}^{(0)} = \frac{2C_{\rm F}}{(4\pi)^2} \quad \text{with} \quad C_{\rm F} = \frac{N^2-1}{2N}, \tag{6.2.2}$$

which will enter in several relations.

The renormalization schemes we will consider are based on the Schrödinger Functional [17, 42, 35]. A detailed discussion of the implementation and notation is provided in Chapter 4. We will always consider $L = T$ and trivial gauge boundary fields (i.e. there is no background field induced by the latter) and identify the renormalization scale with the inverse box size, i.e. $\mu = 1/L$.

To define suitable SF renormalization conditions we can follow the same strategy as in [100, 101, 43, 102], which has been applied successfully also to several other composite operators both in QCD [103, 104, 105, 88, 89, 90, 91, 92, 86, 87] and other theories.[2] We remind here[3] the two-point function in the SF entering in our computation given by

$$k_{\rm T}(x_0) = -\frac{1}{6}\sum_{k=1}^{3}\langle T_{0k}(x)\,\mathcal{O}[\gamma_k]\rangle\,, \tag{6.2.3}$$

$$f_1 = -\frac{1}{2L^6}\langle \mathcal{O}'_{s_2s_1}[\gamma_5]\mathcal{O}_{s_1s_2}[\gamma_5]\rangle\,, \tag{6.2.4}$$

and

$$k_1 = -\frac{1}{6L^6}\langle \mathcal{O}'_{s_2s_1}[\gamma_k]\mathcal{O}_{s_1s_2}[\gamma_k]\rangle\,. \tag{6.2.5}$$

[2] See, e.g., [106] for a recent review.

[3] all the correlators in the SF are discussed in Chapter 4)

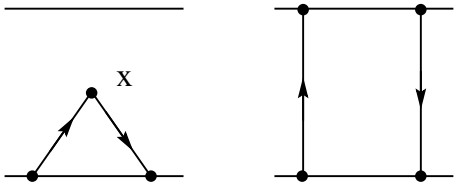

(a) (b)

FIGURE 6.1: Sketch of correlation function in the SF: bilinear insertion on the left and boundary-to-boundary on the right.

where

$$\mathcal{O}[\Gamma] = a^6 \sum_{\mathbf{x},\mathbf{y}} \bar{\zeta}_{s_2}(\mathbf{x})\, \Gamma\, \zeta_{s_1}(\mathbf{y}) \tag{6.2.6}$$

is a source operator built with the $x_0 = 0$ boundary fields $\zeta, \bar{\zeta}$. A sketch of the correlation function in the SF is provided in Fig.6.1. The renormalization constant $Z_{\rm T}$ is then defined by

$$Z_{\rm T}(g_0, a/L)\frac{k_{\rm T}(L/2)}{f_1^{1/2-\alpha}k_1^{\alpha}} = \left.\frac{k_{\rm T}(L/2)}{f_1^{1/2-\alpha}k_1^{\alpha}}\right|_{m_0=m_{\rm cr},\, g_0^2=0}, \tag{6.2.7}$$

where m_0 is the bare quark mass, and $m_{\rm cr}$ is the critical mass, needed if Wilson fermions are used in the computation — as will be our case. The factor $f_1^{1/2-\alpha}k_1^{\alpha}$ cancels the renormalization of the boundary fields contained in $\mathcal{O}[\Gamma]$, which holds for any value of the parameter α; we will restrict ourselves to the choices $\alpha = 0, 1/2$. The only remaining parameter in Eq. (6.2.7) is the kinematical variable θ entering spatial boundary conditions; once its value is specified alongside the one of α, the scheme is completely fixed. We will consider the values $\theta = 0, 0.5, 1.0$ in the perturbative study discussed in the next section, and in the non-perturbative computation we will set $\theta = 0.5$.

The condition in Eq. (6.2.7) involves the correlation function $k_{\rm T}$, which is not O(a) improved. Therefore, the scaling of the renormalized current towards the continuum limit,

$$\overline{T}(\mu) = \lim_{a\to 0} Z_{\rm T}(g_0^2, a\mu)T(g_0^2) \tag{6.2.8}$$

will be affected by O(a) effects. The latter can be removed by subtracting suitable counterterms, following the standard on-shell O(a) improvement strategy for SF correlation functions [107]. On the lattice, and in the chiral limit, the O(a) improvement pattern of the tensor currents is given by Eq. (5.3.6), viz

$$T^{\rm I}_{\mu\nu} = T_{\mu\nu} + a c_{\rm T}(g_0^2)(\tilde{\partial}_\mu V_\nu - \tilde{\partial}_\nu V_\mu)\,, \tag{6.2.9}$$

where, as usual in this thesis, $\tilde{\partial}$ is the symmetrized lattice derivative and $V_\mu = \bar{\psi}_{s_1}\gamma_\mu\psi_{s_2}$ is the vector current. Focusing again only on the electric part, the above formula reduces to

$$T^{\rm I}_{0k} = T_{0k} + a c_{\rm T}(g_0^2)(\tilde{\partial}_0 V_k - \tilde{\partial}_k V_0)\,, \tag{6.2.10}$$

which results in an O(a) improved version of the two-point function $k_{\rm T}$ of the form

$$k^{\rm I}_{\rm T}(x_0) = k_{\rm T}(x_0) + c_{\rm T}(g_0^2)\tilde{\partial}_0 k_{\rm V}(x_0)\,, \tag{6.2.11}$$

with

$$k_{\mathrm{V}}(x_0) = -\frac{1}{6}\sum_{k=1}^{3}\langle V_k(x)\,\mathcal{O}[\gamma_k]\rangle\,. \tag{6.2.12}$$

Note that the contribution involving the spatial derivative vanishes. Inserting $k_{\mathrm{T}}^{\mathrm{I}}$ in Eq. (6.2.7), and the resulting Z_{T} in Eq. (6.2.7) alongside the O(a) improved current, will result in O(a^2) residual cutoff effects in the value of the SSF Σ_{T} defined in Eq. (2.2.6), provided the action and m_{cr} are also O(a) improved.

6.3 Perturbative study

We will now study our renormalization conditions in one-loop perturbation theory. The aim is to obtain the next-to-leading (NLO) anomalous dimension of the tensor current in our SF schemes, necessary for a precise connection to RGI currents, or continuum schemes, at high energies; and compute the leading perturbative contribution to cutoff effects, useful to better control continuum limit extrapolations.

We will expand the relevant quantities in powers of the bare coupling g_0^2 as

$$X = \sum_{n=0}^{\infty} g_0^2 X^{(n)} \tag{6.3.1}$$

where X can be any of Z_{T}, k_{T}, k_{V}, f_1, or k_1. To $\mathcal{O}(g_0^2)$, Eq. (6.2.10) can be written as

$$k_{\mathrm{T}}^{\mathrm{I}}(x_0) = k_{\mathrm{T}}^{(0)}(x_0) + g_0^2\left[k_{\mathrm{T}}^{(1)}(x_0) + ac_{\mathrm{T}}^{(1)}\tilde{\partial}_0 k_{\mathrm{V}}^{(0)}(x_0)\right] + \mathcal{O}(ag_0^4)\,, \tag{6.3.2}$$

with $c_{\mathrm{T}}(g_0^2) = c_{\mathrm{T}}^{(1)}g_0^2 + \mathcal{O}(g_0^4)$. The renormalization constant for the improved tensor correlator $k_{\mathrm{T}}^{\mathrm{I}}$ at one-loop is then given by

$$\begin{aligned}
&Z_{\mathrm{T}}^{(1)}(a/L) = \\
&-\left\{\frac{1}{k_{\mathrm{T}}^{(0)}(T/2)}\left[k_{\mathrm{T}}^{(1)}(T/2) + \tilde{c}_{\mathrm{t}}^{(1)}k_{\mathrm{T;bi}}^{(0)}(T/2) + m_{\mathrm{cr}}^{(1)}\frac{\partial k_{\mathrm{T}}^{(0)}(T/2)}{\partial m_0} + c_{\mathrm{T}}^{(1)}\tilde{\partial}_0 k_{\mathrm{V}}^{(0)}(T/2)\right]\right. \\
&-\left(\frac{1}{2}-\alpha\right)\frac{1}{f_1^{(0)}}\left[f_1^{(1)} + \tilde{c}_{\mathrm{t}}^{(1)}f_{1;\mathrm{bi}}^{(0)} + m_{\mathrm{cr}}^{(1)}\frac{\partial f_1^{(0)}}{\partial m_0}\right] \\
&\left.-\alpha\frac{1}{k_1^{(0)}}\left[k_1^{(1)} + \tilde{c}_{\mathrm{t}}^{(1)}k_{1;\mathrm{bi}}^{(0)} + m_{\mathrm{cr}}^{(1)}\frac{\partial k_1^{(0)}}{\partial m_0}\right]\right\}
\end{aligned} \tag{6.3.3}$$

where $\tilde{c}_{\mathrm{t}}$ is the coefficient of the counterterm that subtracts the O(a) contribution coming from the fermionic action at the boundaries, and $am_{\mathrm{cr}}^{(1)}$ is the one-loop value of the critical mass, for which we employ the continuum values of $am_{\mathrm{cr}}^{(1)}$ from [89, 107]. The one-loop value of the improvement coefficient c_{T} has been obtained using SF techniques in [70]. We have repeated the computation of this latter quantity as a crosscheck of our perturbative setup as discussed in section 6.3.2.

6.3.1 Perturbative scheme matching

Any two mass-independent renormalization schemes (indicated by primed and unprimed quantites, respectively) can be related by a finite parameter and operator renormalization

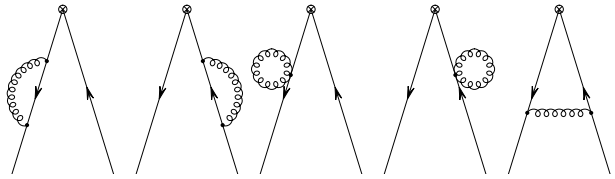

FIGURE 6.2: One-loop diagrams for boundary-to-bulk correlators.

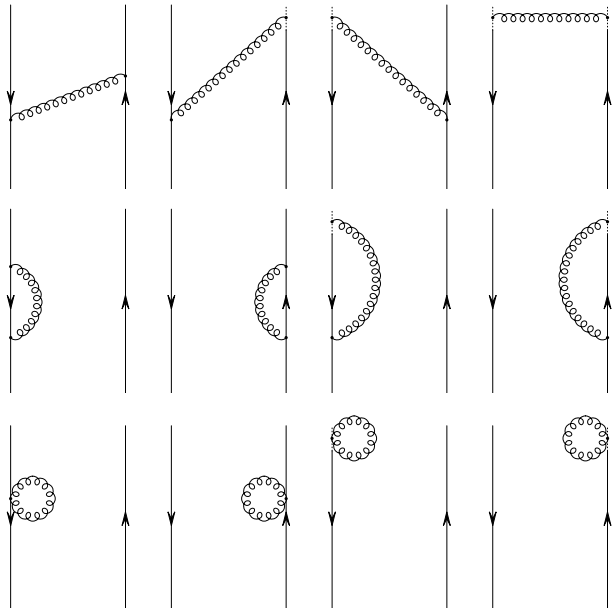

FIGURE 6.3: One-loop diagrams for boundary-to-boundary correlators.

of the form

$$\bar{g}'^2 = \chi_g(\bar{g})\bar{g}^2, \tag{6.3.4}$$

$$\overline{m}'_f = \chi_m(\bar{g})\,\overline{m}_f, \quad f = 1, \ldots, N_{\mathrm{f}}, \tag{6.3.5}$$

$$\overline{O}'_j = (\chi_O)_{jk}(\bar{g})\,\overline{O}_k\,, \tag{6.3.6}$$

where, in general, we have assumed O to present mixing. The scheme change factors χ can be expanded perturbatively as

$$\chi(g) \overset{g\sim 0}{\approx} 1 + \chi^{(1)} g^2 + \mathcal{O}(g^4)\,. \tag{6.3.7}$$

Plugging Eqs. (6.3.4, 6.3.5, 6.3.6) into the Callan-Symanzik equations allows to relate a change in a renormalized quantity to the change in the corresponding RG function, viz.

$$\beta'(g') = \left[\beta(g)\frac{\partial g'}{\partial g}\right]_{g=g(g')}, \tag{6.3.8}$$

$$\tau'(g') = \left[\tau(g) + \beta(g)\frac{\partial}{\partial g}\log(\chi_m(g))\right]_{g=g(g')}, \tag{6.3.9}$$

$$\gamma'(g') = \left[\gamma(g) + \beta(g)\frac{\partial}{\partial g}\log(\chi_O(g))\right]_{g=g(g')}. \tag{6.3.10}$$

In particular, expanding Eq. (6.3.10) to order g^2 provides a useful relation between the 2-loop coefficient of the anomalous dimension in the two schemes. For the quark masses

and composite operators with mixing it respectively reads,

$$d_1' = d_1 + 2b_0\mathcal{X}_{\rm m}^{(1)} - d_0\mathcal{X}_{\rm g}^{(1)}\,, \tag{6.3.11}$$

$$\gamma'^{(1)} = \gamma^{(1)} + [\mathcal{X}_O^{(1)}, \gamma^{(0)}] + 2b_0\mathcal{X}_O^{(1)} + b_0^\lambda \frac{\partial}{\partial\lambda}\mathcal{X}_O^{(1)} - \gamma^{(0)}\mathcal{X}_{\rm g}^{(1)}\,. \tag{6.3.12}$$

It is easy to observe that if the operator is multiplicatively renormalizable the commutator in Eq. (6.3.12) vanishes, and we obtain the same structure of Eq. (6.3.11) (where we assume Landau gauge). The one-loop matching coefficient $\chi_g^{(1)}$ for the SF coupling was computed in [39, 54],

$$\chi_g^{(1)} = 2b_0\log(L\mu) - \frac{1}{4\pi}(c_{1,0} + c_{1,1}N_{\rm f})\,, \tag{6.3.13}$$

where the logarithm vanishes with our choice $\mu = 1/L$, and for the standard definition of the SF coupling one has

$$c_{1,0} = 1.25563(4) \qquad c_{1,1} = 0.039863(2)\,. \tag{6.3.14}$$

The other finite term χ_O in Eq. (6.3.10) will provide the operator matching between the lattice-regulated SF scheme and some reference scheme where the NLO anomalous dimension is known, such as $\overline{\rm MS}$ or RI, that we will label as "cont". The latter usually are based on variants of the dimensional regularization procedure; our SF schemes will be, on the other hand, regulated by a lattice. The practical application of Eq. (6.3.12) thus involves a two-step procedure, in which the lattice-regulated SF scheme is first matched to a lattice-regulated continuum scheme, that is in turned matched to the dimensionally-regulated continuum scheme. This yields

$$[\chi_O^{(1)}]_{\rm SF;cont} = [\chi_O^{(1)}]_{\rm SF;lat} - [\chi_O^{(1)}]_{\rm cont;lat}\,. \tag{6.3.15}$$

The one-loop matching coefficients $[\chi_O^{(1)}]_{\rm cont;lat}$ that we need can be extracted from the literature [108, 77, 109], while the term $[\chi_O^{(1)}]_{\rm SF;lat}$ is obtained from our one-loop calculation of renormalization constants. Indeed, the asymptotic expansion for the one-loop coefficient of a renormalization constant in powers and logarithms of the lattice spacing a has the form

$$Z^{(1)}(L/a) = \sum_{n\geq 0}\left(\frac{a}{L}\right)^n \{r_n + s_n\log(L/a)\}\,, \tag{6.3.16}$$

where $s_0 = \gamma_{\rm T}^{(0)}$ and the finite part surviving the continuum limit is the matching factor we need,

$$[\chi_0^{(1)}]_{\rm SF;lat} = r_0\,. \tag{6.3.17}$$

Our results for $[\chi_0^{(1)}]_{\rm SF;lat}$ have been obtained by computing the one-loop renormalization constants on a series of lattices of sizes ranging from $L/a = 4$ to $L/a = 48$, and fitting the results to Eq. (6.3.16) to extract the expansion coefficients. The computation has been carried out with O(a) improved fermions for three values of θ for each scheme, and without O(a) improvement for $\theta = 0.5$, which allows for a crosscheck of our computation and of the robustness of the continuum limit (see below). The results for the matching factors are provided in Table 6.1; details about the fitting procedure and the assignment of uncertainties are discussed in Appendix F.

Inserting our results in Eq. (6.3.12), we computed for the first time the NLO anomalous dimension in our family of SF schemes for the tensor currents, which are given in

θ	α	$r^{\alpha;\theta}_{0;\mathrm{SF}}$ $(\mathrm{c_{sw}}=0)$	$r^{\alpha;\theta}_{0;\mathrm{SF}}$ $(\mathrm{c_{sw}}=1)$
0.0	0	n/a	$-0.0198519(3)\times C_\mathrm{F}$
	1/2	n/a	$-0.0198519(3)\times C_\mathrm{F}$
0.5	0	$-0.096821(5)\times C_\mathrm{F}$	$-0.05963(4)\times C_\mathrm{F}$
	1/2	$-0.099979(5)\times C_\mathrm{F}$	$-0.06279(4)\times C_\mathrm{F}$
1.0	0	n/a	$-0.0827(2)\times C_\mathrm{F}$
	1/2	n/a	$-0.0866(2)\times C_\mathrm{F}$

TABLE 6.1: Finite parts of one-loop renormalization constants in the scheme specified by the parameters θ and α for the unimproved and O(a)-improved fermion actions

.

θ	α	$\gamma^{(1)}_{\mathrm{T;SF}}$	$\gamma^{(1)}_{\mathrm{T;SF}}/\gamma^{(0)}_\mathrm{T}$
0.0	0	$0.0143209(6)-0.00067106(3)\times N_\mathrm{f}$	$0.84805(3)-0.0397383(2)\times N_\mathrm{f}$
	1/2	$0.0143209(6)-0.00067106(3)\times N_\mathrm{f}$	$0.84805(3)-0.0397383(2)\times N_\mathrm{f}$
0.5	0	$0.0069469(8)-0.00022415(5)\times N_\mathrm{f}$	$0.41138(5)-0.013273(6)\times N_\mathrm{f}$
	1/2	$0.0063609(8)-0.00018863(5)\times N_\mathrm{f}$	$0.37668(5)-0.011170(6)\times N_\mathrm{f}$
1.0	0	$0.00266(3)+0.000036(2)\times N_\mathrm{f}$	$0.157(2)+0.0021(1)\times N_\mathrm{f}$
	1/2	$0.00192(3)+0.000081(2)\times N_\mathrm{f}$	$0.114(2)+0.0048(1)\times N_\mathrm{f}$

TABLE 6.2: NLO anomalous dimensions for various SF schemes, labeled by the parameters θ and α. The ratio to the LO anomalous dimension is also provided, as an indicator of the behaviour of the perturbative expansion. For comparison, $\gamma^{(1)}_{\mathrm{T};\overline{\mathrm{MS}}}/\gamma^{(0)}_\mathrm{T}=0.1910-0.091\times N_\mathrm{f}$

.

Table 6.2. We have crosschecked the computation by performing the matching with and without O(a) improvement, and proceeding through both $\overline{\mathrm{MS}}$ and RI as reference continuum schemes, obtaining the same results in all cases. In this context we observe that the NLO correction to the running is in general fairly large. It is also worth mentioning that the choice of $\theta=0.5$, which leads to a close-to-minimal value of the NLO mass anomalous dimension in SF schemes analogous to the ones considered here [101], is not the optimal choice for the tensor current[4]. We will still use $\theta=0.5$ in the non-perturbative computation, since our simulations take advantage of the one used for quark mass renormalization projects.

Finally, as already mentioned in the introduction, parallel to our work Dalla Brida, Sint and Vilaseca have performed a related, fully independent perturbative study as part of the setup of the chirally rotated Schrödinger Functional [96]. Their results for the one-loop matching factors $[\chi^{(1)}_O]_{\mathrm{SF;lat}}$ are perfectly consistent with ours, providing a very strong crosscheck.

6.3.2 Perturbative improvement

The improvement coefficient c_T for the tensor current can, by definition, be determined by requiring an O(a) improved approach to the continuum of the renormalized correlation function at any given order in perturbation theory. As discussed previously, the

[4]We considered three values of $\theta=0,1,0.5$. we notice that the choice $\theta=0.5$ does not correspond to the smallest anomalous dimension (among the three), as it happen for the quark masses. Moreover, it should be noticed that cutoff effects gets larger when increasing θ.

computation of $c_{\rm T}$ to one loop has been carried out in [70]; here we reproduce it, mainly as a crosscheck of our perturbative setup.

We introduce the following notation for the *renormalized* tensor correlator $k_{\rm T;R}$ in the chiral limit evaluated with SF boundary conditions at $x_0 = T/2$,

$$h_{\rm T}(\theta, a/L) \equiv k_{\rm T;R}(T/2)\,. \tag{6.3.18}$$

where the θ as well as the a/L dependence have been made explicit. The one-loop expansion reads

$$h_{\rm T} = k_{\rm T}^{(0)}(T/2) + \bar{g}^2\{k_{\rm T}^{(1)}(T/2) + \tilde{c}_{\rm t}^{(1)} k_{\rm T;bi}^{(0)}(T/2) + am_0^{(1)}\frac{\partial k_{\rm T}^{(0)}(T/2)}{\partial m_0} + \left(Z_{\rm T}^{(1)} + 2Z_\xi^{(1)}\right) k_{\rm T}^{(0)}(T/2) + c_{\rm T}^{(1)}\tilde{\partial}_0 k_{\rm V}^{(0)}(T/2)\} + \mathcal{O}(\bar{g}^4)\,, \tag{6.3.19}$$

where Z_ξ is the renormalization constant of the boundary fermionic fields, and $c_{\rm T}$ is the coefficient we are interested in, providing the $\mathrm{O}(a)$ improvement of the operator. In order to determine $c_{\rm T}^{(1)}$ we have adopted two different strategies.

The first one proceeds by imposing the condition

$$\frac{h_{\rm T}(\theta, a/L)}{h_{\rm T}(0, a/L)} = \text{const} + \mathcal{O}(a^2)\,. \tag{6.3.20}$$

With some trivial algebra, and observing that $\tilde{\partial}_0 k_{\rm V}^{(0)}(\theta = 0) = 0$, we end up with the relation

$$\frac{\bar{k}_{\rm T}^{(1)}(\theta, a/L)}{k_{\rm T}^{(0)}(\theta, a/L)} - \frac{\bar{k}_{\rm T}^{(1)}(0, a/L)}{k_{\rm T}^{(0)}(0, a/L)} = -c_{\rm T}^{(1)}\frac{\tilde{\partial}_0 k_{\rm V}^{(0)}(\theta, a/L)|_{x_0=T/2}}{k_{\rm T}^{(0)}(\theta, a/L)}\,, \tag{6.3.21}$$

where $\bar{k}_{\rm T}$ is a shorthand notation for the correlator including the subtraction of the boundary and mass $\mathrm{O}(a)$ terms. The divergent part of $Z_{\rm T}^{(1)}$, as well as of Z_ξ, cancel out in the ratio, since they are independent of θ at one loop. Following [110], in order to remove the constant term on the r.h.s. of Eq. (6.3.20) — which is indeed proportional to the difference of the finite parts at two different values of θ — we take a symmetric derivative in L, defined as

$$\tilde{\partial}_L f(L) = \frac{1}{2a}\left[f(L+a) - f(L-a)\right]\,, \tag{6.3.22}$$

and apply it to both sides of Eq. (6.3.21), obtaining

$$R(\theta, a/L) = -\frac{\tilde{\partial}_L C(L)}{\tilde{\partial}_L A(L)} = c_{\rm T}^{(1)} + \mathrm{O}(a)\,, \tag{6.3.23}$$

with $C(L)$ as the l.h.s of Eq. (6.3.21), and $A(L)$ the r.h.s. without the term with $c_{\rm T}^{(1)}$.

As a second strategy to determine $c_{\rm T}$ to one loop, one can exploit the tree-level identities obtained in [110], which relate $k_{\rm V}^{(0)}, k_{\rm T}^{(0)}, f_{\rm A}^{(0)}$ and $f_{\rm P}^{(0)}$, and impose

$$-\bar{k}_{\rm T}^{(1)} + \frac{1}{3}\bar{f}_{\rm P}^{(1)} - \frac{2}{3}\bar{f}_{\rm A}^{(1)} - Z_{\rm T}^{(1)}k_{\rm T}^{(0)} + \frac{1}{3}Z_{\rm P}^{(1)}f_{\rm P}^{(0)} - c_{\rm T}^{(1)}\tilde{\partial}_0 k_{\rm V}^{(0)}|_{x_0=T/2} - \frac{2}{3}c_A^{(1)}\tilde{\partial}_0 f_{\rm P}^{(0)}|_{x_0=T/2}) = \text{const} + \mathcal{O}(a^2). \tag{6.3.24}$$

After some simple algebra we find

$$F(\theta, a/L) \equiv \frac{\tilde{\partial}_L C(L)}{\tilde{\partial}_L A(L)} - c_A^{(1)} = c_{\rm T}^{(1)} + {\rm O}(a)\,, \tag{6.3.25}$$

where now

$$C(L) = -\bar{k}_{\rm T}^{(1)}(L/a) + \frac{1}{3}\bar{f}_{\rm P}^{(1)}(L/a) - \frac{2}{3}\bar{f}_{\rm A}^{(1)}(L/a) + \frac{8}{3(4\pi^2)}\log(L/a)[-k_{\rm T}^{(0)}(L/a) - f_{\rm P}^{(0)}(L/a)]\,, \tag{6.3.26}$$

$$A(L) = \tilde{\partial}_0 k_{\rm V}^{(0)}(T/2)\,. \tag{6.3.27}$$

Using the results for $c_{\rm A}^{(1)}$ quoted in [110], we reproduce with similar size errors the value quoted in [70], which reads

$$c_{\rm T}^{(1)} = 0.00896(1) C_{\rm F}\,. \tag{6.3.28}$$

The comparison between our determination and the one in [70] is displayed in Fig. 6.4. In all cases, the continuum extrapolation has been performed using similar techniques to the one employed for the finite part of renormalization constants (see Appendix F).

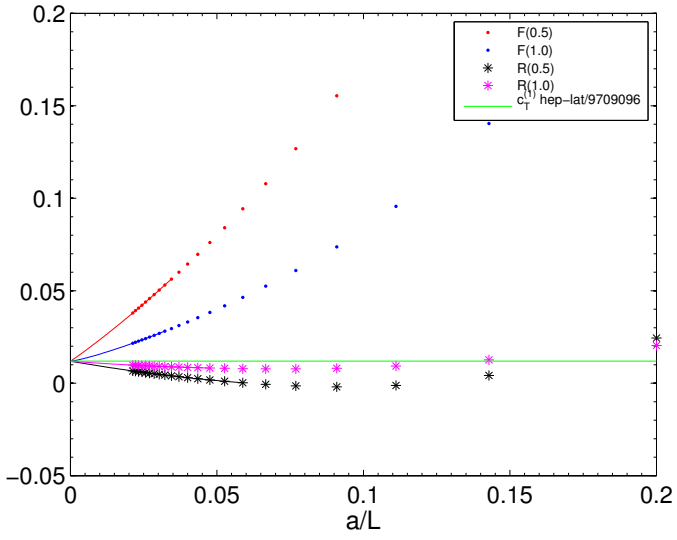

FIGURE 6.4: Extraction of $c_{\rm T}^{(1)}$, compared with the result in [70].

6.3.3 One-loop cutoff effects in the step scaling function

As mentioned above, the RG running is accessed via SSFs, defined in Eq. (2.2.6). It is thus both interesting and useful to study the scaling of $\Sigma_{\rm T}$ within perturbation theory. Plugging the one-loop expansion of the renormalization constant in Eq. (2.2.6), we obtain an expression of the form

$$\Sigma_{\rm T}(u, L/a) = 1 + k(L/a)\bar{g}^2 + \mathcal{O}(\bar{g}^4)\,, \tag{6.3.29}$$

where

$$k(L/a) = Z_{\rm T}^{(1)}(2L/a) - Z_{\rm T}^{(1)}(L/a)\,. \tag{6.3.30}$$

In order to extract the cutoff effect which quantifies how fast the continuum limit σ_{T} is approached, we define

$$k(\infty) = \gamma_{\mathrm{T}}^{(0)} \log(2)\,, \tag{6.3.31}$$

and the relative cutoff effect δ_k

$$\delta_k(L/a) = \frac{k(L/a)}{k(\infty)} - 1\,. \tag{6.3.32}$$

The one-loop values of δ_k for both the improved and unimproved renormalization conditions are listed in Table 6.3. The behaviour of δ_k as a function of the lattice size is shown in Fig. 6.5. The figure shows that the bulk of the linear cutoff effect is removed by the improvement of the action, and that the improvement of the current has a comparatively small impact. Note also that $\theta = 0.5$ leads to the smaller perturbative cutoff effects among the values explored, cf. Table 6.3.

6.4 Non-perturbative computations

We will now present non-perturbative results for both $N_{\mathrm{f}} = 0$ and $N_{\mathrm{f}} = 2$ QCD. The simulations underlying each of the two cases are those in [88] (which in turn reproduced and extended the simulations in [72]) and [43], respectively. For $N_{\mathrm{f}} = 2$ simulations are performed with non-perturbatively O(a) improved Wilson fermions, whereas in the quenched case the computation was performed both with and without O(a) improvement, which, along with the finer lattices used, allows for a better control of the continuum limit (cf. below). A gauge plaquette action is always used. In both cases, we rely on the computation of the SF coupling and its non-perturbative running, given in [39, 72] for $N_{\mathrm{f}} = 0$ and [58] for $N_{\mathrm{f}} = 2$.

6.4.1 $N_{\mathrm{f}} = 0$

Simulation details for the quenched computation are given in [88]. Simulation parameters have been determined by tuning β such that the value of the renormalized SF coupling is kept constant with changing L/a, and fixing the bare quark mass to the corresponding non-perturbatively tuned value of κ_{c}. A total of fourteen values of the renormalized coupling have been considered, namely, $u = \{0.8873,\ 0.9944,\ 1.0989,\ 1.2430,\ 1.3293,\ 1.4300,\ 1.5553,\ 1.6950,\ 1.8811,\ 2.1000,\ 2.4484,\ 2.7700,\ 3.1110,\ 3.4800\}$, corresponding to fourteen different physical lattice lengths L. In all cases the renormalization constants Z_{T} are determined, in the two schemes given by $\alpha = 0, 1/2$, on lattices of sizes $L/a = \{6, 8, 12, 16\}$ and $2L/a = \{12, 16, 24, 32\}$, which allows for the determination of $\Sigma_{\mathrm{T}}(u, a/L)$ at four values of the lattice spacing.

As mentioned above, two separate computations have been performed, with and without an O(a) improved fermion action with a non-perturbatively determined c_{sw} coefficient.[5] This allows to improve our control over the continuum limit extrapolation for σ_{T}, by imposing a common result for both computations based on universality. It is important to note that the gauge ensembles for the improved and unimproved computations are different, and therefore the corresponding results are fully uncorrelated. Another important observation is that the c_{T} coefficient for the O(a) improvement counterterm of the tensor current is not known non-perturbatively, but only to leading order

[5] The SF boundary improvement counterterms proportional to c_{t} and $\tilde{c}_{\mathrm{t}}$ are taken into account at two- and one-loop order in perturbation theory, respectively.

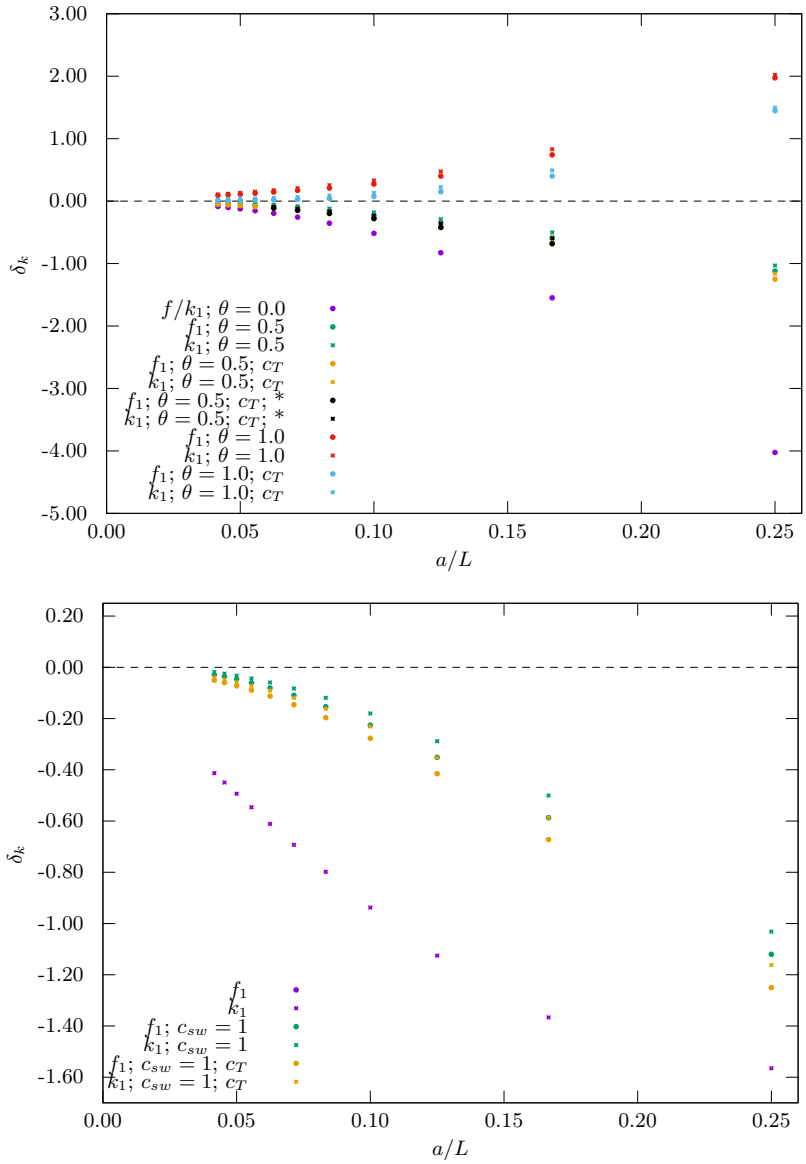

FIGURE 6.5: Upper panel: cutoff effects as a function of a/L for the various schemes considered and the O(a) improved fermion action. Results with and without operator improvement are provided. Lower panel: zoom-in displaying only results for the schemes with $\theta = 0.5$ (which will be the one employed in the non-perturbative computation), also including those with an unimproved fermion action.

in perturbation theory. In our computation of $Z_{\rm T}$ for $N_{\rm f} = 0$ we have thus never included the improvement counterterm in the renormalization condition, even when the action is improved, and profit only from the above universality constraint to control the continuum limit, as we will discuss in detail below. The resulting numerical values of the renormalization constants and SSFs are reported in Tables 6.4 and 6.5.

Continuum extrapolation of SSFs

As discussed above, the continuum limit for $\Sigma_{\rm T}$ is controlled by studying the scaling of the results obtained with and without an O(a) improved actions. To that respect, we first check that universality holds within our precision, by performing independent continuum extrapolations of both datasets. Given the absence of the $c_{\rm T}$ counterterm, we always

assume that the continuum limit is approached linearly in a/L, and parametrize

$$\Sigma_{\rm T}^{c_{\rm sw}=0}(u,a/L) = \sigma_{\rm T}^{c_{\rm sw}=0}(u) + \rho_{\rm T}^{c_{\rm sw}=0}(u)\frac{a}{L}\,, \tag{6.4.1}$$

$$\Sigma_{\rm T}^{c_{\rm sw}={\rm NP}}(u,a/L) = \sigma_{\rm T}^{c_{\rm sw}={\rm NP}}(u) + \rho_{\rm T}^{c_{\rm sw}={\rm NP}}(u)\frac{a}{L}\,. \tag{6.4.2}$$

We observe that, in general, fits that drop the coarsest lattice, corresponding to the step $L/a = 6 \to 12$, are of better quality; when the $\Sigma_{\rm T}(L/a = 6)$ datum is dropped, $\sigma_{\rm T}^{c_{\rm sw}=0}(u)$ and $\sigma_{\rm T}^{c_{\rm sw}={\rm NP}}(u)$ always agree within $\sim 1\sigma$. The slopes $\rho_{\rm T}^{c_{\rm sw}={\rm NP}}(u)$ are systematically smaller than $\rho_{\rm T}^{c_{\rm sw}=0}(u)$, showing that the bulk of the leading cutoff effects in the tensor current is subtracted by including the Sheikholeslami-Wohlert (SW) term in the action.

We thus proceed to obtain our best estimate for $\sigma_{\rm T}(u)$ from a constrained extrapolation, where we set $\sigma_{\rm T}^{c_{\rm sw}=0}(u) = \sigma_{\rm T}^{c_{\rm sw}={\rm NP}}(u) = \sigma_{\rm T}(u)$ in Eq. (6.4.1), and drop the $L/a = 6 \to 12$ step from the fit. The results for both schemes are provided in Table 6.6, and illustrated in Figs. 6.10, 6.11.

Fits to continuum step-scaling functions

In order to compute the RG running of the operator in the continuum limit, we fit the continuum-extrapolated SSFs to a functional form in u. The simplest choice, motivated by the perturbative expression for $\gamma_{\rm T}$ and β, and assuming that $\sigma_{\rm T}$ is a smooth function of the renormalized coupling within the covered range of values of the latter, is a polynomial of the form

$$\sigma_{\rm T}(u) = 1 + p_1 u + p_2 u^2 + p_3 u^3 + p_4 u^4 + \dots\,. \tag{6.4.3}$$

The perturbative prediction for the first two coefficients of Eq. (6.4.3) reads

$$p_1^{\rm pert} = \gamma_{\rm T}^{(0)}\log(2)\,, \tag{6.4.4}$$

$$p_2^{\rm pert} = \gamma_{\rm T}^{(1)}\log(2) + \left[\frac{(\gamma_{\rm T}^{(0)})^2}{2} + b_0\gamma_{\rm T}^{(0)}\right](\log(2))^2\,. \tag{6.4.5}$$

Note, in particular, that perturbation theory predicts a dependence on $N_{\rm f}$ only at $\mathcal{O}(u^2)$.

We have considered various fit ansätze, exploring combinations of the order of the polynomial and possible perturbative constraints, imposed by fixing either p_1 or both p_1 and p_2 to the values in Eqs. (6.4.4,6.4.5). We always take as input the results from the joint $c_{\rm sw} = 0$ and $c_{\rm sw} = {\rm NP}$ extrapolation, discussed above. The results for the various fits are shown in Table 6.7. All the fits result in a good description of the non-perturbative data, with values of $\chi^2/{\rm d.o.f.}$ close to unity and little dependence on the ansatz. The coefficients of powers larger than u^3 are consistently compatible with zero within one standard deviation. We quote as our preferred fit the one that fixes p_1 to its perturbative value, and reaches $\mathcal{O}(u^3)$ (fit B in Table 6.7). This provides an adequate description of the non-perturbative data, without artificially decreasing the goodness-of-fit by including several coefficients with large relative errors (cf., e.g., fit E). The result for $\sigma_{\rm T}$ from fit B in our two schemes is illustrated in Fig. 6.6. It is also worth pointing out that the value for p_2 obtained from fits A and B is compatible with the perturbative prediction within 1 and 1.5 standard deviations, respectively, for the two schemes; this reflects the small observed departure of $\sigma_{\rm T}$ from its two-loop value until the region $u \gtrsim 2$ is reached, cf. Fig. 6.6.

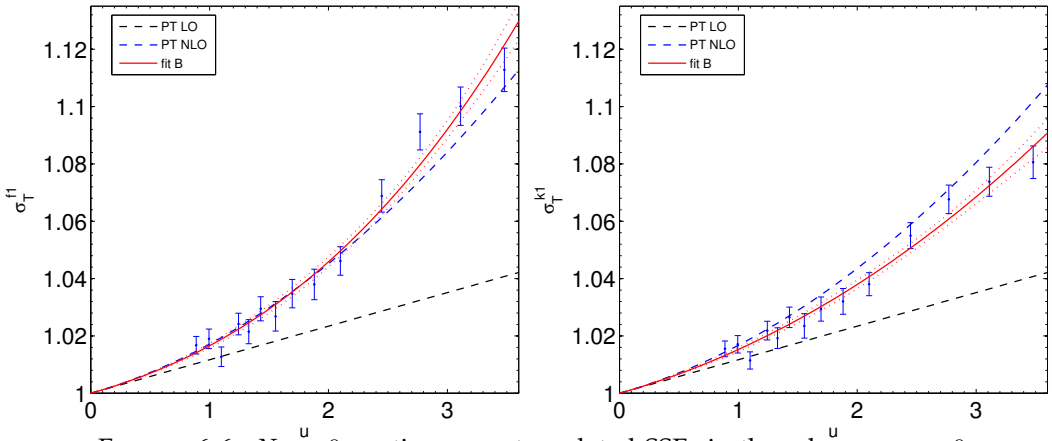

FIGURE 6.6: $N_f = 0$ continuum-extrapolated SSFs in the schemes $\alpha = 0$ (left) and $\alpha = 1/2$ (right), and their fitted functional forms following fit B in Table 6.7. The one- and two-loop perturbative predictions are also shown for comparison.

Determination of the non-perturbative running factor

Once a given fit for σ_T is chosen, it is possible to compute the running between two well-separated scales through a finite-size recursion. The latter is started from the smallest value of the energy scale $\mu_{had} = L_{had}^{-1}$, given by the largest value of the coupling for which σ_T has been computed, viz.

$$\bar{g}^2(2\mu_{had}) = 3.48\,. \tag{6.4.6}$$

Using as input the coupling SSF $\sigma(u)$ determined in [72], we construct recursively the series of coupling values

$$u_{k+1} = \bar{g}^2(2^{k+2}\mu_{had}) = \sigma^{-1}(u_k)\,, \quad u_0 = 3.48\,. \tag{6.4.7}$$

This in turn allows to compute the product

$$U(\mu_{had}, \mu_{pt}) = \prod_{k=0}^{n} \sigma_T(u_k)\,, \quad \mu_{pt} = 2^{n+1}\mu_{had}\,, \tag{6.4.8}$$

where U is the RG evolution operator in Eq. (2.2.5), here connecting the renormalised operators at scales μ_{had} and $2^{n+1}\mu_{had}$. The number of iterations n is dictated by the smallest value of u at which σ_T is computed non-perturbatively, i.e. $u = 0.8873$. We find $u_7 = 0.950(11)$ and $u_8 = 0.865(10)$, corresponding respectively to 8 and 9 steps of recursion. The latter involves a short extrapolation from the interval in u covered by data, in a region where the SSF is strongly constrained by its perturbative asymptotics. This point is used only to test the robustness of the recursion, but is not considered in the final analysis. The values of u_k and the corresponding running factors are given in Tables 6.8 and 6.9.

Once $\mu_{pt} = 2^8\mu_{had}$ has been reached, perturbation theory can be used to make contact with the RGI operator. We thus compute the total running factor $\hat{c}(\mu)$ in Eq. (2.1.12) at $\mu = \mu_{had}$ as

$$\hat{c}(\mu_{had}) = \frac{\hat{c}(\mu_{pt})}{U(\mu_{had}, \mu_{pt})}\,, \tag{6.4.9}$$

where $\hat{c}(\mu_{pt})$ is computed using the highest available orders for γ and β in our schemes (NLO and NNLO, respectively). In order to assess the systematic uncertainty arising

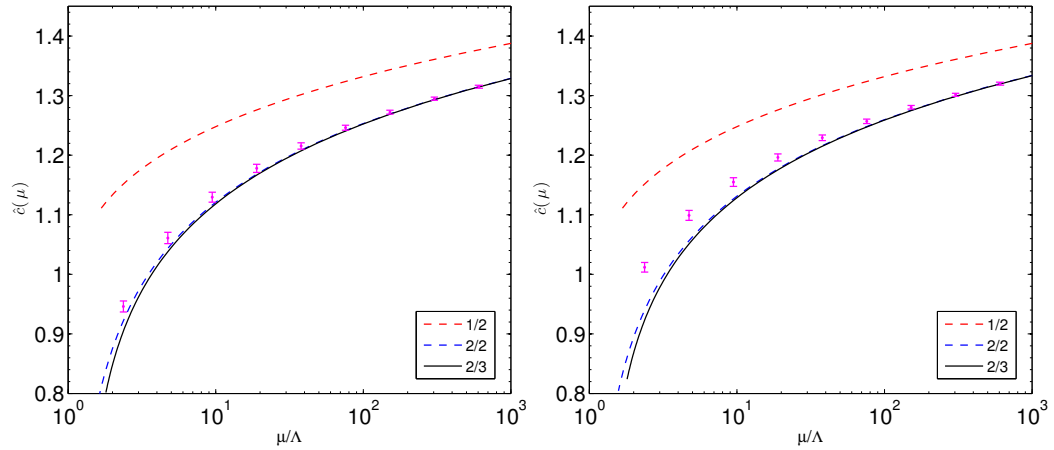

FIGURE 6.7: Running of the tensor current for $N_{\rm f} = 0$ in the schemes $\alpha = 0$ (left) and $\alpha = 1/2$ (right), compared to perturbative predictions using the $1/2$-, $2/2$-, and $2/3$-loop values for $\gamma_{\rm T}/\beta$.

from the use of perturbation theory, we have performed two crosschecks:

(i) Perform the matching to perturbation theory at all the points in the recursion, and check that the result changes within a small fraction of the error.

(ii) Match to perturbation theory using different combinations of perturbative orders in γ and β: other than our NLO/NNLO preferred choice, labeled "$2/3$" — after the numbers of loops — in Tables 6.8 and 6.9, we have used matchings at $1/2$-, $2/2$-, and $3/3$-loop order, where in the latter case we have employed a mock value of the NNLO anomalous dimension given by $\gamma^{(2)} \equiv (\gamma^{(1)})^2/\gamma^{(0)}$ as a means to have a guesstimate of higher-order truncation uncertainties.

We thus quote as our final numbers

$$\begin{aligned} \hat{c}(\mu_{\rm had})|_{N_{\rm f}=0} &= 0.9461(95)\,, \quad \text{scheme } \alpha = 0\,; \\ \hat{c}(\mu_{\rm had})|_{N_{\rm f}=0} &= 1.0119(83)\,, \quad \text{scheme } \alpha = 1/2\,. \end{aligned} \tag{6.4.10}$$

In Fig. 6.7 we plot the non-perturbative running of the operator in our two schemes, obtained by running backwards from the perturbative matching point corresponding to the renormalized coupling $u_7 = 0.950(11)$. with our non-perturbative $\sigma_{\rm T}$, and compare it with perturbation theory. In order to set the physical scale corresponding to each value of the coupling, we have used $\Lambda_{\rm SF}/\mu_{\rm had} = 0.422(32)$, from [72]. The latter work also provides the value of $\mu_{\rm had}$ in units of the Sommer scale r_0 [55], viz. $(2r_0\mu_{\rm had})^{-1} = 0.718(16)$ — which, using $r_0 = 0.5$ fm, translates into $\mu_{\rm had} = 274(6)$ MeV. It is important to stress that the results in Eq. (6.4.10) are given in the continuum, and therefore do not contain any dependence on the regularization procedures employed to obtain them.

Hadronic matching

The final piece required for a full non-perturbative renormalization is to compute renormalization constants at the hadronic scale $\mu_{\rm had}$ within the interval of values of the bare gauge coupling covered by non-perturbative simulations in large, hadronic volumes. We have thus proceeded to obtain $Z_{\rm T}$ at four values of the bare coupling, $\beta = \{6.0129, 6.1628, 6.2885, 6.4956\}$, tuned to ensure that L — and hence the renormalized SF coupling — stays constant when $L/a = \{8, 10, 12, 16\}$, respectively. The results, both with and without O(a) improvement,

are provided in Tables 6.10 and 6.11. These numbers can be multiplied by the corresponding value of the running factor in Eq. (6.4.10) to obtain the quantity

$$\hat{Z}_{\rm T}(g_0^2) = \hat{c}(\mu_{\rm had}) Z_{\rm T}(g_0^2, a\mu_{\rm had})\,, \tag{6.4.11}$$

which relates bare and RGI operators for a given value of g_0^2. They are quoted in Table 6.12; it is important to stress that the results are independent of the scheme within the $\sim 1\%$ precision of our computation — as they should, since the scheme dependence is lost at the level of RGI operators, save for the residual cutoff effects which in this case are not visible within errors. A second-order polynomial fit to the dependence of the results in β

$$\hat{Z}_{\rm T}(g_0^2) = z_0 + z_1(\beta - 6) + z_2(\beta - 6)^2 \tag{6.4.12}$$

for the numbers obtained from the scheme $\alpha = 1/2$, which turns out to be slightly more precise, yields

$$\begin{aligned} c_{\rm sw} = {\rm NP}: \quad & z_0 = 0.9814(9)\,, \quad z_1 = 0.138(8)\,, \quad z_2 = -0.06(2)\,; \\ c_{\rm sw} = 0: \quad & z_0 = 0.8943(4)\,, \quad z_1 = 0.127(3)\,, \quad z_2 = -0.024(6)\,, \end{aligned} \tag{6.4.13}$$

with correlation matrices among the fit coefficients

$$\begin{aligned} C[c_{\rm sw} = {\rm NP}] &= \begin{pmatrix} 1.000 & -0.766 & 0.605 \\ -0.766 & 1.000 & -0.955 \\ 0.605 & -0.955 & 1.000 \end{pmatrix}\,, \\ C[c_{\rm sw} = 0] &= \begin{pmatrix} 1.000 & -0.768 & 0.615 \\ -0.768 & 1.000 & -0.960 \\ 0.615 & -0.960 & 1.000 \end{pmatrix}\,. \end{aligned} \tag{6.4.14}$$

These continuous form can be obtained to renormalize bare matrix elements, computed with the appropriate action, at any convenient value of β.

6.4.2 $N_{\rm f} = 2$

In this case all our simulations were performed using an O(a) improved Wilson action, with the SW coefficient $c_{\rm sw}$ determined in[111]. Renormalization constants have been computed at six different values of the SF renormalized coupling $u = \{0.9703, 1.1814, 1.5078, 2.0142, 2.4792, 3.3340\}$, corresponding to six different physical lattice lengths L. For each physical volume, three different values of the lattice spacing have been simulated, corresponding to lattices with $L/a = 6, 8, 12$ and the double steps $2L/a = 12, 16, 24$, for the computation of the renormalization constant $Z_{\rm T}(g_0, a/L)$. All simulational details, including those referring to the tuning of β and κ, are provided in [43].

Concerning O(a) improvement, the configurations at the three weaker values of the coupling were produced using the one-loop perturbative estimate of $c_{\rm t}$ [17], while for the three stronger couplings the two-loop value [37] was used. In addition, for $L/a = 6$, $\beta = 7.5420$ and $L/a = 8$, $\beta = 7.7206$ separate simulations were performed with the one- and two-loop value of $c_{\rm t}$, which results in two different, uncorrelated ensembles, with either value of $c_{\rm t}$, being available for $u = 1.5078$. For $\tilde{c}_{\rm t}$ the one-loop value is used throughout. Finally, since, contrary to the quenched case, we do not have two separate (improved and unimproved) sets of simulations to control the continuum limit, we have included in our analysis the improvement counterterm to the tensor current, with the one-loop value of $c_{\rm T}$ [70].

The resulting values for the renormalization constants $Z_{\rm T}$ and the SSF $\Sigma_{\rm T}$ are listed in Table 6.13. The estimate of autocorrelation times has been computed using the "Gamma Method" of [112].

Continuum extrapolation of SSFs

In this case, our continuum limit extrapolations will assume an $\mathrm{O}(a^2)$ scaling of $\Sigma_{\rm T}$. This is based on the fact that we implement $\mathrm{O}(a)$ improvement of the action (up to small $\mathcal{O}(ag_0^4)$ effects in $\tilde{c}_{\rm t}$ and $\mathcal{O}(ag_0^4)$ or $\mathcal{O}(ag_0^6)$ in $c_{\rm t}$, cf. above); and that the residual $\mathcal{O}(ag_0^4)$ effects associated to the use of the one-loop perturbative value for $c_{\rm T}$ can be expected to be small, based on the findings discussed above for $N_{\rm f} = 0$. Our ansatz for a linear extrapolation in a^2 is thus of the form

$$\Sigma_{\rm T}(u, a/L) = \sigma_{\rm T}(u) + \rho_{\rm T}(u) \left(\frac{a}{L}\right)^2 . \tag{6.4.15}$$

Furthermore, in order to ameliorate the scaling we subtract the leading perturbative cutoff effects that have been obtained in Sec. 6.3, by rescaling our data for $\Sigma_{\rm T}$ as

$$\Sigma'_{\rm T}(u, a/L) = \frac{\Sigma_{\rm T}(u, a/L)}{1 + u\delta_k(a/L)\gamma_{\rm T}^{(0)}\log(2)} , \tag{6.4.16}$$

where the values of the relative cutoff effects $\delta_k(a/L)$ are taken from the last column of Table 6.3. Continuum extrapolations are performed both taking $\Sigma_{\rm T}$ and the one-loop improved $\Sigma'_{\rm T}$ as input; the two resulting continuum limits are provided in Tables 6.14 and 6.15, respectively. As showed in Fig. 6.5, the effect of including the perturbative improvement is in general non-negligible only for our coarsest $L/a = 6$ lattices. The slope of the continuum extrapolation is decreased by subtracting the perturbative cutoff effects at weak coupling, but for $u \gtrsim 2$ the quality of the extrapolation does not change significantly, and the slope actually flips sign. The $u = 1.5078$ case is treated separately, and a combined extrapolation to the continuum value is performed using the independent simulations carried out with the two different values of $c_{\rm t}$. We quote as our best results the extrapolations obtained from $\Sigma'_{\rm T}$.

Fits to continuum step-scaling functions

Here we follow exactly the same strategy described above for $N_{\rm f} = 0$, again considering several fit ansätze by varying the combination of the order of the polynomial and the number of coefficients fixed to their perturbative values. The results are listed in Table 6.16. As in the quenched case, we quote as our preferred result the fit obtained by fixing the first coefficient to its perturbative value and fitting through $\mathcal{O}(u^3)$ (fit B). The resulting fit, as well as its comparison to perturbative predictions, is illustrated in Fig. 6.8.

Non-perturbative running

Using as input the continuum SSFs, we follow the same strategy as in the quenched case to recursively compute the running between low and high energy scales. In this case the lowest scale reached in the recursion, following [43], is given by $\bar{g}^2_{\rm SF}(\mu_{\rm had}) = 4.61$. Using the coupling SSF from [58], the smallest value of the coupling that can be reached via the recursion without leaving the interval covered by data is $\bar{g}^2_{\rm SF}(\mu_{\rm pt}) = 1.017(10)$, corresponding to $n = 7$ (i.e. a total factor scale of 2^8 in energy, like in the $N_{\rm f} = 0$ case). The matching to the RGI at $\mu_{\rm pt}$ is again performed using the 2/3-loop values of the γ/β functions, and the same checks to assess the systematics are carried out

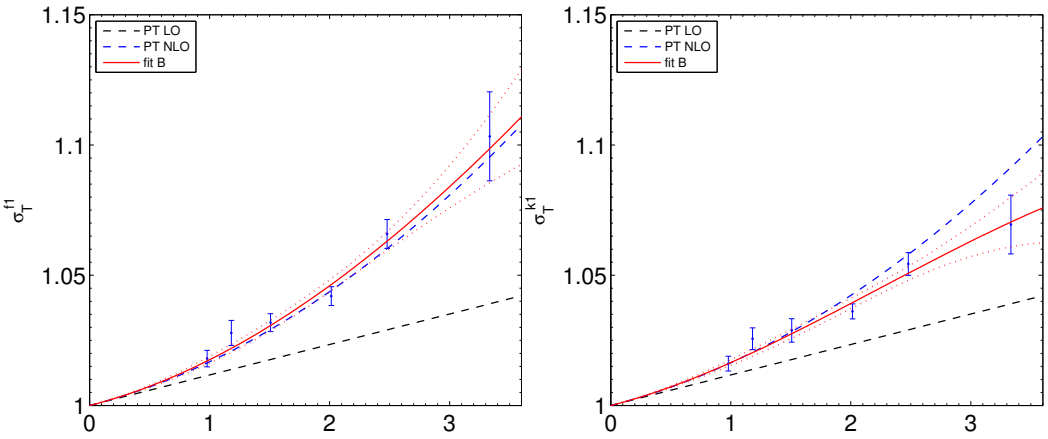

FIGURE 6.8: SSF for $N_f = 2$ in the scheme $\alpha = 0$ (left) and $\alpha = 1/2$ (right), compared with the LO and NLO perturbative predictions.

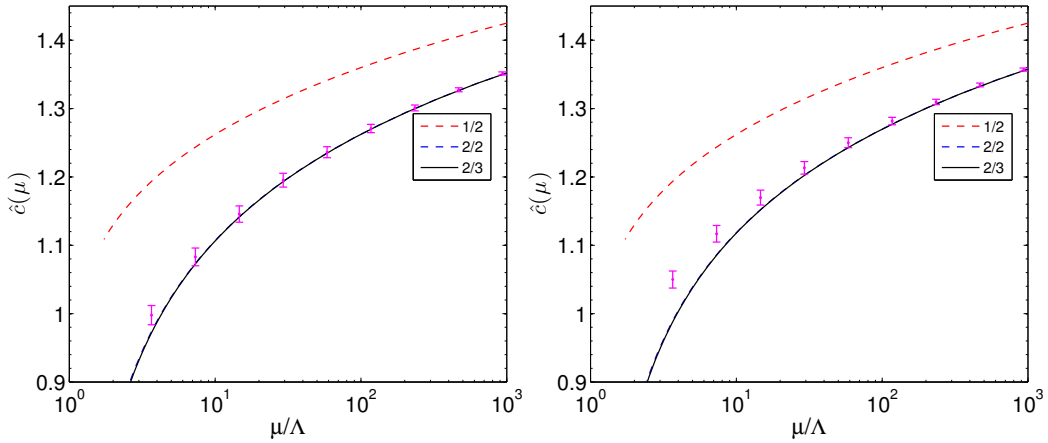

FIGURE 6.9: Running of the tensor current for $N_f = 2$ in the schemes $\alpha = 0$ (left) and $\alpha = 1/2$ (right), compared to perturbative predictions using the 1/2-, 2/2-, and 2/3-loop values for γ_T/β.

as in the quenched case. Now the value obtained for $\hat{c}(\mu_{\rm had})$ remains within the quoted error for all $n \geq 3$. Detailed results for the recursion in either scheme are provided in Tables 6.17 and 6.18. We quote as our final results for the running factor

$$\begin{aligned} \hat{c}(\mu_{\rm had})|_{N_f=2} &= 0.998(14)\,, \quad \text{scheme } \alpha = 0\,; \\ \hat{c}(\mu_{\rm had})|_{N_f=2} &= 1.050(13)\,, \quad \text{scheme } \alpha = 1/2\,. \end{aligned} \tag{6.4.17}$$

The running is illustrated, and compared with the perturbative prediction, in Fig. 6.9, where the value of $\log(\Lambda_{\rm SF}/\mu_{\rm had}) = -1.298(58)$ from [43] has been used. Using $r_0\Lambda_{\rm SF} = 0.30(3)$ from [58] and $r_0 = 0.50$ fm, this would correspond to a value of the hadronic matching energy scale $\mu_{\rm had} \approx 432(50)$ MeV.

Hadronic Matching

The computation of the renormalization constants at $\mu_{\rm had}$ needed to match bare hadronic quantities proceeds in a somewhat different way to the quenched case. The value of Z_T in either scheme has been computed at three values of β, namely $\beta = \{5.20, 5.29, 5.40\}$, again within the typical interval covered by large-volume simulations with non-perturbatively O(a) improved fermions and a plaquette gauge action. For each of the values of β two or three values of the lattice size L/a have been simulated, corresponding to different

values of L and therefore to different values of the renormalized coupling. The resulting values of $Z_{\rm T}$ are given in Table 6.19.

The lattice size $L/a = 6$ used at $\beta = 5.20$ corresponds within errors to $L = 1/\mu_{\rm had}$; for the other two values of β linear interpolations can be performed to obtain $Z_{\rm T}$ at the correct value $u = 4.610$; examples of such interpolations are illustrated in Fig. 6.13. The resulting values of $Z_{\rm T}$ can then be multiplied times the running factors in Eq. (6.4.17) to obtain the RGI renormalization factors for each β. The result is provided in Table 6.20. In this case the g_0^2 dependence is barely visible within the quoted errors, and the expected scheme independence holds only up to $\sim 3\sigma$.

6.5 Summary

In this part of the thesis ([113]) we have set up the strategy for a non-perturbative determination of the renormalization constants and anomalous dimension of tensor currents in QCD using SF techniques, and obtained results for $N_{\rm f} = 0$ and $N_{\rm f} = 2$. In the former case we employed both O(a) improved and unimproved Wilson fermions, and simulations were performed at four values of the lattice spacing for each of the fourteen different values of the renormalization scale, resulting in an excellent control of the continuum limit. For $N_{\rm f} = 2$ our simulations were carried out with O(a) improved fermions, at only three values of the lattice for each of the six renormalization scales. The precision of the running factors up to the electroweak scale in the schemes that allow for higher precision is 0.9% and 1.1%, respectively. The somewhat limited quality of our $N_{\rm f} = 2$ dataset, however, could result in the quoted uncertainty for that case not being fully free of unquantified systematics. We have also provided values of renormalization constants at the lowest energy scales reached by the non-perturbative running, which allows to match bare matrix elements computed with non-perturbatively O(a) improved Wilson fermions and the Wilson plaquette gauge action.

As part of the ALPHA programme, we are currently completing a similar study in $N_{\rm f} = 3$ QCD [99], that builds upon a high-precision determination of the strong coupling [97, 10, 98] and mass anomalous dimension [73, 74, 85]. Preliminary results indicate that a precision $\sim 1\%$ for the running to low-energy scales is possible even for values of the hadronic matching scale well below the one reached for $N_{\rm f} = 2$. This is an essential ingredient in order to obtain matrix elements of phenomenological interest with fully controlled uncertainties and target precisions in the few percent ballpark.

L/a	[0.0,0,1,1l,*]	[0.0,1/2,1,1l,*]	[1.0,0,1,1l,0]	[1.0,1/2,1,1l,0]	[1.0,0,1,1l,1l]	[1.0,1/2,1,1l,1l]
4	-4.024919	-4.024919	1.973892	2.021956	1.447601	1.495665
6	-1.548675	-1.548675	0.740155	0.831017	0.400972	0.491835
8	-0.826327	-0.826327	0.400756	0.475909	0.149798	0.224952
10	-0.516240	-0.516240	0.273405	0.331519	0.073971	0.132086
12	-0.353534	-0.353534	0.209692	0.254876	0.044116	0.089300
14	-0.257339	-0.257339	0.171319	0.207105	0.029721	0.065507
16	-0.195713	-0.195713	0.145443	0.174349	0.021731	0.050637
18	-0.153857	-0.153857	0.126680	0.150454	0.016828	0.040602
20	-0.124131	-0.124131	0.112377	0.132244	0.013584	0.033451
22	-0.102261	-0.102261	0.101072	0.117905	0.011310	0.028142
24	-0.085702	-0.085702	0.091888	0.106322	0.009641	0.024075

L/a	[0.5,0,0,0,0]	[0.5,1/2,0,0,0]	[0.5,0,1,1l,0]	[0.5,1/2,1,1l,0]	[0.5,0,1,1l,1l]	[0.5,1/2,1,1l,1l]	[0.5,0,1,1l,1l]*	[0.5,1/2,1,1l,1l]*
4	-1.467173	-1.564753	-1.120302	-1.031861	-1.250274	-1.161833	–	–
6	-1.318718	-1.366570	-0.587012	-0.500733	-0.672604	-0.586326	-0.682022	-0.595744
8	-1.097265	-1.125110	-0.351334	-0.288400	-0.415264	-0.352330	-0.421206	-0.358272
10	-0.919572	-0.937671	-0.225979	-0.179971	-0.277027	-0.231020	-0.279265	-0.233257
12	-0.785609	-0.798283	-0.153873	-0.119221	-0.196371	-0.161719	-0.197267	-0.162616
14	-0.683546	-0.692903	-0.109513	-0.082621	-0.145918	-0.119027	-0.146297	-0.119405
16	-0.603968	-0.611155	-0.080628	-0.059210	-0.112470	-0.091052	-0.112620	-0.091202
18	-0.540470	-0.546161	-0.060930	-0.043495	-0.089227	-0.071792	–	–
20	-0.488753	-0.493370	-0.046987	-0.032532	-0.072450	-0.057995	–	–
22	-0.445879	-0.449699	-0.036813	-0.024641	-0.059958	-0.047786	–	–
24	-0.409794	-0.413007	-0.029200	-0.018813	-0.050413	-0.040027	–	–

TABLE 6.3: Cutoff effects δ_k in tensor SSFs (see Eq. (6.3.32)) for various schemes and amounts of O(a) improvement. The headers of the columns correspond to the values of the parameters $[\theta, \alpha, c_{\rm sw}, \tilde{c}_{\rm t}, c_{\rm T}]$ ("1l" refers to the one-loop value of the coefficient). For $\theta = 0.0$ results at one loop are independent of the value of α, and the contribution from $c_{\rm T}$ vanishes. For $\theta = 0.5$ columns labeled with "$[]^*$" refer to results obtained with $m_{\rm c}^{(1)}(a/L)$, while for all the others $m_{\rm c}^{(1)}(\infty)$ has been used.

			Improved action				Unimproved action			
β	L/a	$\bar{g}^2(L)$	κ_c	$Z_T\left(g_0^2, L/a\right)$	$Z_T\left(g_0^2, 2L/a\right)$	$\Sigma_T\left(u, L/a\right)$	κ_c	$Z_T\left(g_0^2, L/a\right)$	$Z_T\left(g_0^2, 2L/a\right)$	$\Sigma_T\left(u, L/a\right)$
10.7503	6	0.8873(5)	0.130591(4)	0.9781(7)	0.9857(12)	1.0078(14)	0.134696(7)	0.9571(8)	0.9464(11)	0.9888(14)
11.0000	8	0.8873(10)	0.130439(3)	0.9812(7)	0.9923(12)	1.0113(14)	0.134548(6)	0.9569(7)	0.9522(12)	0.9951(15)
11.3384	12	0.8873(30)	0.130251(2)	0.9878(11)	1.0022(16)	1.0146(20)	0.134277(5)	0.9605(11)	0.9618(18)	1.0014(22)
11.5736	16	0.8873(25)	0.130125(2)	0.9918(10)	1.0061(23)	1.0144(25)	0.134068(6)	0.9637(11)	0.9686(20)	1.0051(24)
10.0500	6	0.9944(7)	0.131073(5)	0.9771(7)	0.9868(14)	1.0099(16)	0.135659(8)	0.9532(10)	0.9428(12)	0.9891(16)
10.3000	8	0.9944(13)	0.130889(3)	0.9820(11)	0.9927(12)	1.0109(17)	0.135457(5)	0.9535(8)	0.9472(13)	0.9934(16)
10.6086	12	0.9944(30)	0.130692(2)	0.9896(12)	1.0047(18)	1.0153(22)	0.135160(4)	0.9590(11)	0.9624(20)	1.0035(24)
10.8910	16	0.9944(28)	0.130515(2)	0.9936(11)	1.0073(20)	1.0138(23)	0.134849(6)	0.9641(13)	0.9686(33)	1.0047(37)
9.5030	6	1.0989(8)	0.131514(5)	0.9766(9)	0.9880(15)	1.0117(18)	0.136520(5)	0.9516(10)	0.9389(14)	0.9867(18)
9.7500	8	1.0989(13)	0.131312(3)	0.9798(9)	0.9964(16)	1.0169(19)	0.136310(3)	0.9515(9)	0.9475(13)	0.9958(17)
10.0577	12	1.0989(40)	0.131079(3)	0.9874(12)	1.0048(18)	1.0176(22)	0.135949(4)	0.9574(13)	0.9581(22)	1.0007(27)
10.3419	16	1.0989(44)	0.130876(2)	0.9963(14)	1.0090(19)	1.0127(24)	0.135572(4)	0.9619(18)	0.9676(22)	1.0059(30)
8.8997	6	1.2430(13)	0.132072(9)	0.9742(6)	0.9908(12)	1.0170(14)	0.137706(5)	0.9463(11)	0.9363(14)	0.9894(19)
9.1544	8	1.2430(14)	0.131838(4)	0.9806(8)	0.9988(17)	1.0186(19)	0.137400(4)	0.9487(10)	0.9426(17)	0.9936(21)
9.5202	12	1.2430(35)	0.131503(3)	0.9885(11)	1.0062(23)	1.0179(26)	0.136855(2)	0.9537(14)	0.9558(16)	1.0022(22)
9.7350	16	1.2430(34)	0.131335(3)	0.9971(21)	1.0201(22)	1.0231(31)	0.136523(4)	0.9564(14)	0.9661(23)	1.0101(28)
8.6129	6	1.3293(12)	0.132380(6)	0.9732(9)	0.9903(17)	1.0176(20)	0.138346(6)	0.9455(12)	0.9322(13)	0.9859(19)
8.8500	8	1.3293(21)	0.132140(5)	0.9797(10)	1.0036(18)	1.0244(21)	0.138057(4)	0.9475(10)	0.9397(18)	0.9918(22)
9.1859	12	1.3293(60)	0.131814(3)	0.9914(15)	1.0089(25)	1.0177(30)	0.137503(2)	0.9534(15)	0.9572(18)	1.0040(25)
9.4381	16	1.3293(40)	0.131589(2)	0.9962(14)	1.0207(30)	1.0246(33)	0.137061(4)	0.9578(22)	0.9645(23)	1.0070(33)
8.3124	6	1.4300(20)	0.132734(10)	0.9750(7)	0.9908(14)	1.0162(16)	0.139128(11)	0.9393(12)	0.9299(15)	0.9900(20)
8.5598	8	1.4300(21)	0.132453(5)	0.9800(9)	1.0011(16)	1.0215(19)	0.138742(7)	0.9445(11)	0.9381(20)	0.9932(24)
8.9003	12	1.4300(50)	0.132095(3)	0.9897(17)	1.0188(26)	1.0294(32)	0.138120(8)	0.9532(15)	0.9574(25)	1.0044(31)
9.1415	16	1.4300(58)	0.131855(3)	0.9976(12)	1.0248(28)	1.0273(31)	0.137655(5)	0.9592(16)	0.9655(26)	1.0066(32)
7.9993	6	1.5553(15)	0.133118(7)	0.9726(7)	0.9932(21)	1.0212(23)	0.140003(11)	0.9385(13)	0.9215(15)	0.9819(21)
8.2500	8	1.5553(24)	0.132821(5)	0.9785(11)	1.0073(22)	1.0294(25)	0.139588(8)	0.9422(11)	0.9359(20)	0.9933(24)
8.5985	12	1.5533(70)	0.132427(3)	0.9927(17)	1.0204(29)	1.0279(34)	0.138847(6)	0.9532(16)	0.9575(27)	1.0045(33)
8.8323	16	1.5533(70)	0.132169(3)	0.9999(19)	1.0305(35)	1.0306(40)	0.138339(7)	0.9594(22)	0.9671(34)	1.0080(42)

TABLE 6.4: $N_f = 0$ results for the renormalization constant Z_P and the step scaling function Σ_T for the scheme $\alpha = 0$.

			Improved action				Unimproved action		
β	L/a	$\bar{g}^2(L)$	κ_c	$Z_T\left(g_0^2, L/a\right)$	$Z_T\left(g_0^2, 2L/a\right)$	$\Sigma_T\left(u, L/a\right)$	κ_c	$Z_T\left(g_0^2, L/a\right)$	$Z_T\left(g_0^2, 2L/a\right)$	$\Sigma_T\left(u, L/a\right)$
7.7170	6	1.6950(26)	0.133517(8)	0.9729(10)	0.9977(7)	1.0255(13)	0.140954(12)	0.9380(13)	0.9199(18)	0.9807(24)
7.9741	8	1.6950(28)	0.133179(5)	0.9787(9)	1.0115(22)	1.0335(24)	0.140438(8)	0.9402(12)	0.9385(29)	0.9982(33)
8.3218	12	1.6950(79)	0.132756(4)	0.9953(7)	1.0268(23)	1.0316(24)	0.139589(6)	0.9505(18)	0.9616(28)	1.0117(35)
8.5479	16	1.6950(90)	0.132485(3)	1.0014(19)	1.0389(32)	1.0374(38)	0.139058(6)	0.9579(20)	0.9719(36)	1.0146(43)
7.4082	6	1.8811(22)	0.133961(8)	0.9702(10)	0.9992(8)	1.0299(13)	0.142145(11)	0.9346(14)	0.9122(18)	0.9760(24)
7.6547	8	1.8811(28)	0.133632(6)	0.9812(10)	1.0175(22)	1.0370(25)	0.141572(9)	0.9386(13)	0.9347(19)	0.9958(24)
7.9993	12	1.8811(38)	0.133159(4)	0.9980(7)	1.0317(32)	1.0338(33)	0.140597(6)	0.9498(18)	0.9559(32)	1.0064(39)
8.2415	16	1.8811(99)	0.132847(3)	1.0059(28)	1.0445(27)	1.0384(39)	0.139900(6)	0.9565(22)	0.9776(38)	1.0221(46)
7.1214	6	2.1000(39)	0.134423(9)	0.9720(12)	1.0039(9)	1.0328(16)	0.143416(11)	0.9243(16)	0.9067(21)	0.9810(28)
7.3632	8	2.1000(45)	0.134088(6)	0.9833(12)	1.0235(26)	1.0409(29)	0.142749(9)	0.9312(14)	0.9253(27)	0.9937(33)
7.6985	12	2.1000(80)	0.133599(4)	0.9995(8)	1.0427(25)	1.0432(26)	0.141657(6)	0.9480(14)	0.9564(22)	1.0089(28)
7.9560	16	2.100(11)	0.133229(3)	1.0090(21)	1.0564(27)	1.0470(35)	0.140817(7)	0.9594(22)	0.9749(35)	1.0162(43)
6.7807	6	2.4484(37)	0.134994(11)	0.9741(13)	1.0160(10)	1.0430(17)	0.145286(11)	0.9229(15)	0.9003(21)	0.9755(28)
7.0197	8	2.4484(45)	0.134639(7)	0.9866(13)	1.0301(29)	1.0441(32)	0.144454(7)	0.9318(15)	0.9256(23)	0.9933(29)
7.3551	12	2.4484(80)	0.134141(5)	1.0061(8)	1.0618(30)	1.0554(31)	0.143113(6)	0.9522(17)	0.9572(38)	1.0053(44)
7.6101	16	2.448(17)	0.133729(4)	1.0167(22)	1.0808(32)	1.0630(39)	0.142107(6)	0.9579(22)	0.9851(39)	1.0284(47)
6.5512	6	2.770(7)	0.135327(12)	0.9798(14)	1.0279(8)	1.0491(17)	0.146825(11)	0.9208(18)	0.8887(22)	0.9651(30)
6.7860	8	2.770(7)	0.135056(8)	0.9910(13)	1.0527(31)	1.0623(34)	0.145859(7)	0.9311(16)	0.9181(33)	0.9860(39)
7.1190	12	2.770(11)	0.134513(5)	1.0097(10)	1.0823(25)	1.0719(27)	0.144299(8)	0.9489(21)	0.9688(33)	1.0210(41)
7.3686	16	2.770(14)	0.134114(3)	1.0215(27)	1.1012(37)	1.0780(46)	0.143175(7)	0.9663(31)	1.0018(47)	1.0367(59)
6.3665	6	3.111(4)	0.135488(6)	0.9809(16)	1.0384(30)	1.0586(35)	0.148317(10)	0.9207(19)	0.8802(19)	0.9560(29)
6.6100	8	3.111(6)	0.135339(3)	0.9944(16)	1.0711(37)	1.0771(41)	0.147112(7)	0.9328(18)	0.9189(27)	0.9851(35)
6.9322	12	3.111(12)	0.134855(3)	1.0160(23)	1.1093(35)	1.0918(42)	0.145371(7)	0.9526(21)	0.9740(35)	1.0225(43)
7.1911	16	3.111(16)	0.134411(3)	1.0340(21)	1.1222(42)	1.0853(46)	0.144060(8)	0.9676(28)	1.0092(45)	1.0430(55)
6.2204	6	3.480(8)	0.135470(15)	0.9869(8)	1.0678(27)	1.0820(29)	0.149685(15)	0.9178(21)	0.8709(23)	0.9489(33)
6.4527	8	3.480(14)	0.135543(9)	1.0005(10)	1.0909(46)	1.0904(47)	0.148391(9)	0.9295(19)	0.9140(44)	0.9833(51)
6.7750	12	3.480(39)	0.135121(5)	1.0292(20)	1.1281(41)	1.0961(45)	0.146408(7)	0.9570(20)	0.9793(49)	1.0233(55)
7.0203	16	3.480(21)	0.134707(4)	1.0408(22)	1.1420(45)	1.0972(49)	0.145025(8)	0.9714(24)	1.0264(51)	1.0566(59)

TABLE 6.4: (continued)

			Improved action				Unimproved action			
β	L/a	$\bar{g}^2(L)$	κ_c	$Z_T\left(g_0^2, L/a\right)$	$Z_T\left(g_0^2, 2L/a\right)$	$\Sigma_T\left(u, L/a\right)$	κ_c	$Z_T\left(g_0^2, L/a\right)$	$Z_T\left(g_0^2, 2L/a\right)$	$\Sigma_T\left(u, L/a\right)$
10.7503	6	0.8873(5)	0.130591(4)	0.9687(6)	0.9769(11)	1.0085(13)	0.134696(7)	0.9497(8)	0.9388(10)	0.9885(13)
11.0000	8	0.8873(10)	0.130439(3)	0.9726(6)	0.9835(11)	1.0112(13)	0.134548(6)	0.9497(7)	0.9446(11)	0.9946(14)
11.3384	12	0.8873(30)	0.130251(2)	0.9795(10)	0.9930(14)	1.0138(18)	0.134277(5)	0.9529(10)	0.9536(16)	1.0007(20)
11.5736	16	0.8873(25)	0.130125(2)	0.9839(9)	0.9974(20)	1.0137(22)	0.134068(6)	0.9561(10)	0.9603(18)	1.0044(22)
10.0500	6	0.9944(7)	0.131073(5)	0.9661(7)	0.9761(11)	1.0104(14)	0.135659(8)	0.9448(9)	0.9339(11)	0.9885(15)
10.3000	8	0.9944(13)	0.130889(3)	0.9716(9)	0.9824(10)	1.0111(14)	0.135457(5)	0.9450(8)	0.9381(11)	0.9927(14)
10.6086	12	0.9944(30)	0.130692(2)	0.9800(11)	0.9942(16)	1.0145(20)	0.135160(4)	0.9500(10)	0.9521(18)	1.0022(22)
10.8910	16	0.9944(28)	0.130515(2)	0.9845(9)	0.9974(18)	1.0131(20)	0.134849(6)	0.9554(11)	0.9590(29)	1.0038(32)
9.5030	6	1.0989(8)	0.131514(5)	0.9642(8)	0.9761(13)	1.0123(16)	0.136520(5)	0.9419(9)	0.9290(12)	0.9863(16)
9.7500	8	1.0989(13)	0.131312(3)	0.9682(8)	0.9842(13)	1.0165(16)	0.136310(3)	0.9415(8)	0.9369(11)	0.9951(14)
10.0577	12	1.0989(40)	0.131079(3)	0.9766(10)	0.9934(15)	1.0172(19)	0.135949(4)	0.9471(12)	0.9466(18)	0.9995(23)
10.3419	16	1.0989(44)	0.130876(2)	0.9859(12)	0.9975(16)	1.0118(20)	0.135572(4)	0.9518(16)	0.9568(19)	1.0053(26)
8.8997	6	1.2430(13)	0.132072(9)	0.9598(6)	0.9759(10)	1.0168(12)	0.137706(5)	0.9351(10)	0.9243(12)	0.9885(17)
9.1544	8	1.2430(14)	0.131838(4)	0.9673(7)	0.9840(14)	1.0173(16)	0.137400(4)	0.9374(9)	0.9305(15)	0.9926(19)
9.5202	12	1.2430(35)	0.131503(3)	0.9762(9)	0.9926(19)	1.0168(22)	0.136855(2)	0.9421(12)	0.9433(13)	1.0013(19)
9.7350	16	1.2430(34)	0.131335(3)	0.9849(18)	1.0057(18)	1.0211(26)	0.136523(4)	0.9453(13)	0.9530(20)	1.0081(25)
8.6129	6	1.3293(12)	0.132380(6)	0.9577(8)	0.9742(15)	1.0172(18)	0.138346(6)	0.9332(11)	0.9191(12)	0.9849(17)
8.8500	8	1.3293(21)	0.132140(5)	0.9652(8)	0.9871(15)	1.0227(18)	0.138057(4)	0.9349(9)	0.9262(15)	0.9907(19)
9.1859	12	1.3293(60)	0.131814(3)	0.9776(13)	0.9934(20)	1.0162(25)	0.137503(2)	0.9403(13)	0.9428(15)	1.0027(21)
9.4381	16	1.3293(40)	0.131589(2)	0.9832(12)	1.0055(25)	1.0227(28)	0.137061(4)	0.9456(19)	0.9504(20)	1.0051(29)
8.3124	6	1.4300(20)	0.132734(10)	0.9579(6)	0.9731(11)	1.0159(13)	0.139128(11)	0.9263(11)	0.9153(13)	0.9881(18)
8.5598	8	1.4300(21)	0.132453(5)	0.9642(8)	0.9833(13)	1.0198(16)	0.138742(7)	0.9312(10)	0.9233(17)	0.9915(21)
8.9003	12	1.4300(50)	0.132095(3)	0.9748(14)	1.0001(21)	1.0260(26)	0.138120(8)	0.9396(13)	0.9411(20)	1.0016(25)
9.1415	16	1.4300(58)	0.131855(3)	0.9835(10)	1.0085(24)	1.0254(27)	0.137655(5)	0.9452(14)	0.9497(22)	1.0048(28)
7.9993	6	1.5553(15)	0.133118(7)	0.9537(6)	0.9725(17)	1.0197(19)	0.140003(11)	0.9239(11)	0.9066(13)	0.9813(18)
8.2500	8	1.5553(24)	0.132821(5)	0.9614(9)	0.9873(18)	1.0269(21)	0.139588(8)	0.9273(10)	0.9197(17)	0.9918(21)
8.5985	12	1.5533(70)	0.132427(3)	0.9765(14)	1.0006(24)	1.0247(29)	0.138847(6)	0.9376(14)	0.9403(24)	1.0029(30)
8.8323	16	1.5533(70)	0.132169(3)	0.9837(16)	1.0102(27)	1.0269(32)	0.138339(7)	0.9441(18)	0.9499(28)	1.0061(35)

TABLE 6.5: $N_f = 0$ results for the renormalization constant Z_P and the step scaling function Σ_T for the scheme $\alpha = 1/2$.

			Improved action				Unimproved action			
β	L/a	$\bar{g}^2(L)$	κ_c	$Z_T\left(g_0^2, L/a\right)$	$Z_T\left(g_0^2, 2L/a\right)$	$\Sigma_T\left(u, L/a\right)$	κ_c	$Z_T\left(g_0^2, L/a\right)$	$Z_T\left(g_0^2, 2L/a\right)$	$\Sigma_T\left(u, L/a\right)$
7.7170	6	1.6950(26)	0.133517(8)	0.9522(9)	0.9747(6)	1.0236(12)	0.140954(12)	0.9215(12)	0.9026(15)	0.9795(21)
7.9741	8	1.6950(28)	0.133179(5)	0.9599(7)	0.9887(18)	1.0300(20)	0.140438(8)	0.9234(11)	0.9204(24)	0.9968(29)
8.3218	12	1.6950(79)	0.132756(4)	0.9769(5)	1.0042(19)	1.0279(20)	0.139589(6)	0.9333(15)	0.9408(22)	1.0080(29)
8.5479	16	1.6950(90)	0.132485(3)	0.9839(16)	1.0160(26)	1.0326(31)	0.139058(6)	0.9412(17)	0.9522(31)	1.0117(38)
7.4082	6	1.8811(22)	0.133961(8)	0.9472(9)	0.9730(6)	1.0272(12)	0.142145(11)	0.9162(12)	0.8933(15)	0.9750(21)
7.6547	8	1.8811(28)	0.133632(6)	0.9597(8)	0.9912(18)	1.0328(21)	0.141572(9)	0.9197(11)	0.9129(16)	0.9926(21)
7.9993	12	1.8811(38)	0.133159(4)	0.9771(6)	1.0066(27)	1.0302(28)	0.140597(6)	0.9306(15)	0.9337(26)	1.0033(32)
8.2415	16	1.8811(99)	0.132847(3)	0.9865(24)	1.0178(22)	1.0317(34)	0.139900(6)	0.9380(18)	0.9547(32)	1.0178(39)
7.1214	6	2.1000(39)	0.134423(9)	0.9454(10)	0.9731(7)	1.0293(13)	0.143416(11)	0.9044(14)	0.8854(17)	0.9790(24)
7.3632	8	2.1000(45)	0.134088(6)	0.9585(9)	0.9914(19)	1.0343(22)	0.142749(9)	0.9104(12)	0.9021(22)	0.9909(27)
7.6985	12	2.1000(80)	0.133599(4)	0.9764(6)	1.0128(20)	1.0373(21)	0.141657(6)	0.9265(11)	0.9304(17)	1.0042(22)
7.9560	16	2.100(11)	0.133229(3)	0.9862(17)	1.0250(20)	1.0393(27)	0.140817(7)	0.9380(19)	0.9471(27)	1.0097(35)
6.7807	6	2.4484(37)	0.134994(11)	0.9431(11)	0.9768(8)	1.0357(15)	0.145286(11)	0.8989(13)	0.8745(17)	0.9729(24)
7.0197	8	2.4484(45)	0.134639(7)	0.9571(10)	0.9933(23)	1.0378(26)	0.144454(7)	0.9066(13)	0.8959(19)	0.9882(25)
7.3551	12	2.4484(80)	0.134141(5)	0.9777(7)	1.0229(23)	1.0462(25)	0.143113(6)	0.9260(14)	0.9250(29)	0.9989(35)
7.6101	16	2.448(17)	0.133729(4)	0.9905(18)	1.0406(25)	1.0506(32)	0.142107(6)	0.9325(18)	0.9520(29)	1.0209(37)
6.5512	6	2.770(7)	0.135327(12)	0.9431(11)	0.9807(6)	1.0399(14)	0.146825(11)	0.8932(16)	0.8591(17)	0.9618(26)
6.7860	8	2.770(7)	0.135056(8)	0.9572(10)	1.0057(24)	1.0507(27)	0.145859(7)	0.9026(13)	0.8859(26)	0.9815(32)
7.1190	12	2.770(11)	0.134513(5)	0.9782(8)	1.0326(18)	1.0556(20)	0.144299(8)	0.9195(17)	0.9287(25)	1.0100(33)
7.3686	16	2.770(14)	0.134114(3)	0.9910(21)	1.0505(28)	1.0600(36)	0.143175(7)	0.9365(24)	0.9595(36)	1.0246(47)
6.3665	6	3.111(4)	0.135488(6)	0.9399(13)	0.9825(21)	1.0453(27)	0.148317(10)	0.8889(16)	0.8452(15)	0.9508(24)
6.6100	8	3.111(6)	0.135339(3)	0.9572(13)	1.0133(28)	1.0586(33)	0.147112(7)	0.8999(15)	0.8802(20)	0.9781(28)
6.9322	12	3.111(12)	0.134855(3)	0.9803(18)	1.0474(25)	1.0684(32)	0.145371(7)	0.9189(16)	0.9258(26)	1.0075(33)
7.1911	16	3.111(16)	0.134411(3)	0.9988(16)	1.0633(30)	1.0646(35)	0.144060(8)	0.9349(22)	0.9601(31)	1.0270(41)
6.2204	6	3.480(8)	0.135470(15)	0.9405(6)	0.9952(19)	1.0582(21)	0.149685(15)	0.8833(17)	0.8316(19)	0.9415(28)
6.4527	8	3.480(14)	0.135543(9)	0.9575(8)	1.0198(31)	1.0651(34)	0.148391(9)	0.8933(15)	0.8701(34)	0.9740(41)
6.7750	12	3.480(39)	0.135121(5)	0.9871(15)	1.0568(29)	1.0706(34)	0.146408(7)	0.9199(16)	0.9247(35)	1.0052(42)
7.0203	16	3.480(21)	0.134707(4)	1.0003(16)	1.0705(32)	1.0702(36)	0.145025(8)	0.9349(19)	0.9657(36)	1.0329(44)

TABLE 6.5: (continued)

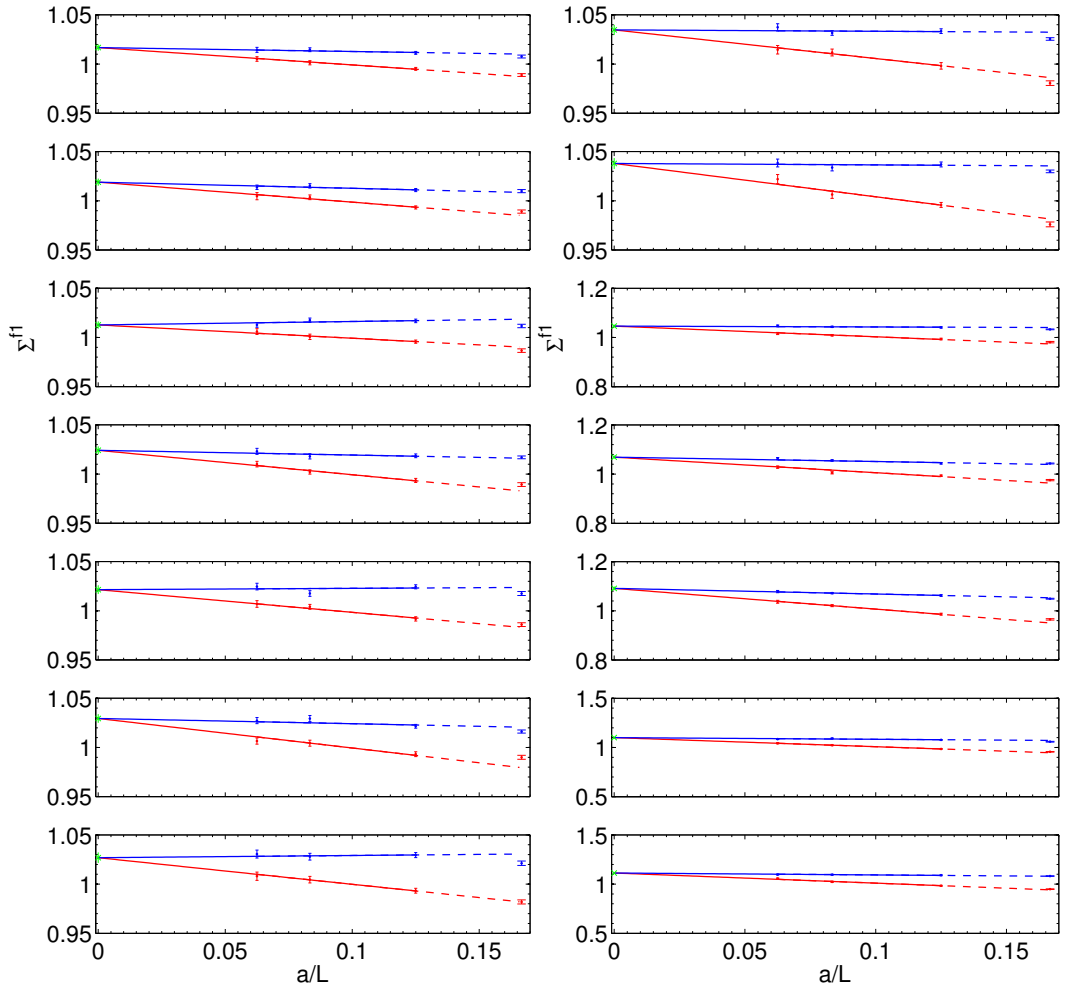

FIGURE 6.10: Continuum limit extrapolations of the $N_{\rm f} = 0$ SSF for the renormalization scheme $\alpha = 0$. Blue (red) points correspond to results with the O(a) improved (unimproved) action, respectively.

	$\alpha = 0$		$\alpha = 1/2$	
u	$\sigma_{\rm T}(u)$	$\chi^2/{\rm dof}$	$\sigma_{\rm T}(u)$	$\chi^2/{\rm dof}$
0.8873	1.0168(31)	0.23	1.0155(27)	0.20
0.9944	1.0190(34)	0.46	1.0171(30)	0.41
1.0989	1.0127(34)	0.69	1.0115(30)	1.18
1.2430	1.0242(38)	0.61	1.0219(33)	0.54
1.3293	1.0215(42)	1.49	1.0192(36)	1.83
1.4300	1.0295(42)	1.48	1.0265(36)	1.52
1.5553	1.0268(51)	0.20	1.0235(43)	0.20
1.6950	1.0347(50)	0.64	1.0294(42)	0.60
1.8811	1.0380(53)	1.01	1.0320(45)	1.03
2.1000	1.0461(50)	0.58	1.0381(40)	1.08
2.4484	1.0688(57)	3.41	1.0550(45)	3.65
2.7700	1.0912(63)	0.06	1.0677(50)	0.05
3.1110	1.1001(67)	1.00	1.0738(51)	0.86
3.4800	1.1128(76)	1.00	1.0806(57)	1.09

TABLE 6.6: Continuum-extrapolated values for the SSFs for $N_{\rm f} = 0$.

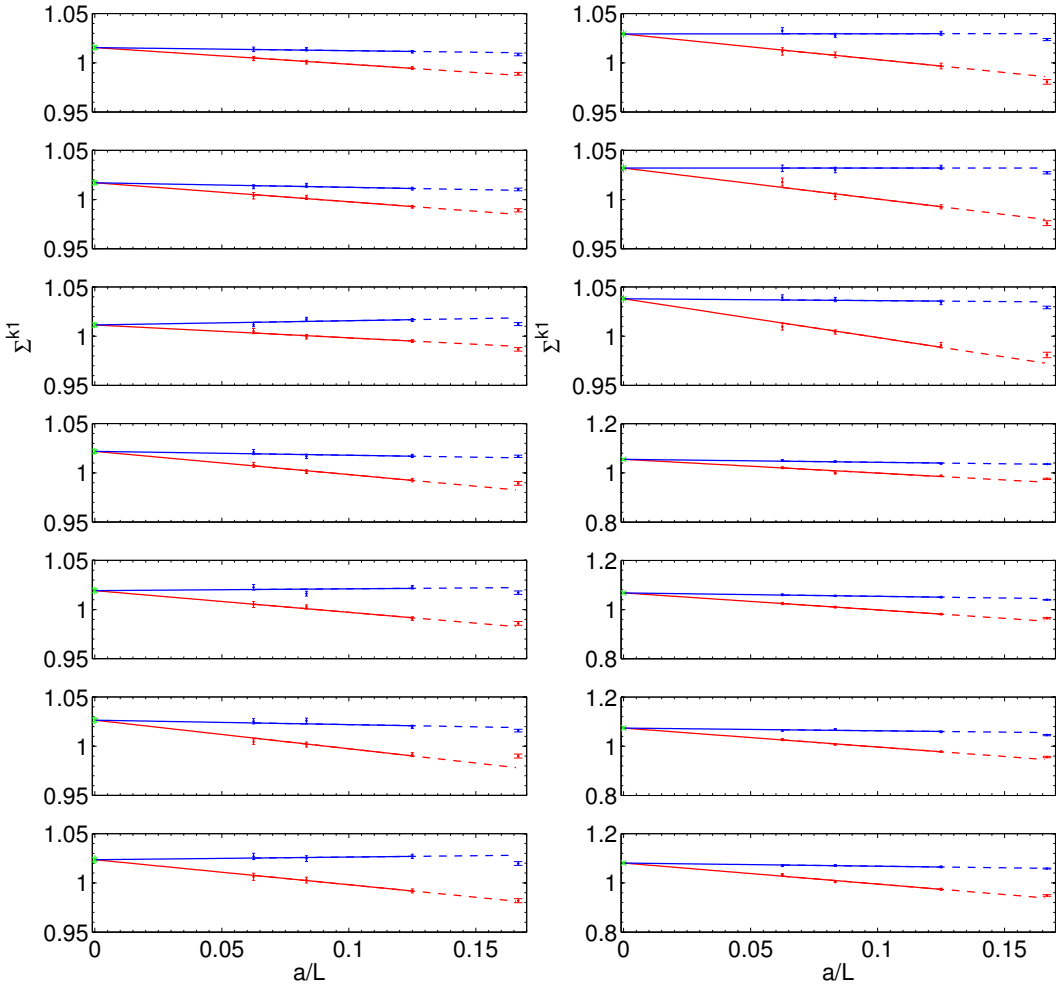

FIGURE 6.11: Continuum limit extrapolations of the $N_f = 0$ SSF for the renormalization scheme $\alpha = 1/2$. Blue (red) points correspond to results with the O(a) improved (unimproved) action, respectively.

	fit	p_1	p_2	p_3	p_4	χ^2/dof
$\alpha = 0$	A	0.011705	0.00611(32)	—	—	1.16
	B	0.011705	0.0042(12)	0.00072(45)	—	1.04
	C	0.011705	0.005449	0.00028(11)	—	1.04
	D	0.011705	0.005449	-0.00005(66)	0.00011(22)	1.11
	E	0.011705	-0.0006(37)	0.0051(32)	-0.00089(64)	0.96
$\alpha = 1/2$	A	0.011705	0.00370(25)	—	—	0.88
	B	0.011705	0.0035(10)	0.000072(36)	—	0.95
	C	0.011705	0.005043	-0.000455(88)	—	1.05
	D	0.011705	0.005043	-0.00098(54)	0.00017(17)	1.06
	E	0.011705	-0.0003(31)	0.0034(26)	-0.00068(52)	0.88

TABLE 6.7: Fits to the continuum $N_f = 0$ SSFs for various choices of polynomial ansatz, cf. Eq. (6.4.3).

k	u_k	$[U(\mu_{\rm had}, 2^{k+1}\mu_{\rm had})]^{-1}$	$\hat{c}^{1/2}(\mu_{\rm had})$	$\hat{c}^{2/2}(\mu_{\rm had})$	$\hat{\mathbf{c}}^{\mathbf{2/3}}(\boldsymbol{\mu}_{\mathbf{had}})$	$\hat{c}^{3/3}(\mu_{\rm had})$
0	3.480	0.8916(45)	1.0655(53)	0.9099(45)	0.9133(46)	0.8201(41)
1	2.455(18)	0.8376(51)	1.0377(64)	0.9256(59)	0.9272(59)	0.8768(59)
2	1.918(15)	0.8031(54)	1.0218(70)	0.9332(66)	0.9342(66)	0.9021(65)
3	1.584(13)	0.7783(57)	1.0113(76)	0.9378(72)	0.9384(72)	0.9160(72)
4	1.353(13)	0.7592(60)	1.0039(82)	0.9408(78)	0.9412(78)	0.9246(78)
5	1.184(12)	0.7436(63)	0.9983(87)	0.9429(84)	0.9433(84)	0.9304(84)
6	1.053(12)	0.7306(66)	0.9939(93)	0.9446(90)	0.9448(90)	0.9346(90)
7	0.950(11)	0.7195(68)	0.9905(98)	0.9459(95)	0.9461(95)	0.9377(95)
8	0.865(10)	0.7097(70)	0.9876(102)	0.9469(99)	0.9471(99)	0.9401(99)

TABLE 6.8: Non-perturbative $N_{\rm f} = 0$ running in the scheme $\alpha = 0$. (Our best result $\hat{c}^{2/3}(\mu_{\rm had})$ is stressed.)

k	u_k	$[U(\mu_{\rm had}, 2^{k+1}\mu_{\rm had})]^{-1}$	$\hat{c}^{1/2}(\mu_{\rm had})$	$\hat{c}^{2/2}(\mu_{\rm had})$	$\hat{\mathbf{c}}^{\mathbf{2/3}}(\boldsymbol{\mu}_{\mathbf{had}})$	$\hat{c}^{3/3}(\mu_{\rm had})$
0	3.480	0.9207(36)	1.1003(44)	0.9522(38)	0.9556(38)	0.8732(35)
1	2.455(18)	0.8762(41)	1.0855(52)	0.9776(49)	0.9792(49)	0.9344(49)
2	1.918(15)	0.8459(44)	1.0761(57)	0.9904(54)	0.9914(54)	0.9628(54)
3	1.584(13)	0.8231(47)	1.0695(63)	0.9981(60)	0.9987(60)	0.9787(60)
4	1.353(13)	0.8051(50)	1.0646(69)	1.0031(66)	1.0036(66)	0.9888(66)
5	1.184(12)	0.7902(54)	1.0608(74)	1.0068(72)	1.0071(72)	0.9956(72)
6	1.053(12)	0.7775(57)	1.0577(80)	1.0095(78)	1.0098(78)	1.0006(78)
7	0.950(11)	0.7665(59)	1.0552(85)	1.0116(83)	1.0119(83)	1.0043(83)
8	0.865(10)	0.7568(62)	1.0531(89)	1.0133(87)	1.0135(87)	1.0072(87)

TABLE 6.9: Non-perturbative $N_{\rm f} = 0$ running in the scheme $\alpha = 1/2$. (Our best result $\hat{c}^{2/3}(\mu_{\rm had})$ is stressed.)

		$c_{\rm sw} = \mathrm{NP}$		$c_{\rm sw} = 0$	
β	$\frac{L}{a}$	$\kappa_{\rm c}$	$Z_{\rm T}$	$\kappa_{\rm c}$	$Z_{\rm T}$
6.0219	8	0.135043(17)	1.0401(21)	0.153371(10)	0.9407(19)
6.1628	10	0.135643(11)	1.0606(13)	0.152012(7)	0.9617(16)
6.2885	12	0.135739(13)	1.0738(15)	0.150752(10)	0.9792(24)
6.4956	16	0.135577(7)	1.0950(35)	0.148876(13)	1.0022(35)

TABLE 6.10: Renormalization constants $Z_{\rm T}(g_0^2, L/a)$ at $L = 1/\mu_{\rm had}$ for $N_{\rm f} = 0$, scheme $\alpha = 0$.

		$c_{\rm sw} = \mathrm{NP}$		$c_{\rm sw} = 0$	
β	$\frac{L}{a}$	$\kappa_{\rm c}$	$Z_{\rm T}$	$\kappa_{\rm c}$	$Z_{\rm T}$
6.0219	8	0.135043(17)	0.9715(15)	0.153371(10)	0.8853(15)
6.1628	10	0.135643(11)	0.9909(9)	0.152012(7)	0.9033(13)
6.2885	12	0.135739(13)	1.0044(11)	0.150752(10)	0.9178(18)
6.4956	16	0.135577(7)	1.0236(24)	0.148876(13)	0.9399(27)

TABLE 6.11: Renormalization constants $Z_{\rm T}(g_0^2, L/a)$ at $L = 1/\mu_{\rm had}$ for $N_{\rm f} = 0$, scheme $\alpha = 1/2$.

	$c_{\rm sw} = \mathrm{NP}$		$c_{\rm sw} = 0$	
β	$\hat{Z}_{\rm T}^{\alpha=0}$	$\hat{Z}_{\rm T}^{\alpha=1/2}$	$\hat{Z}_{\rm T}^{\alpha=0}$	$\hat{Z}_{\rm T}^{\alpha=1/2}$
6.0129	0.984(10)	0.983(8)	0.890(9)	0.896(8)
6.1628	1.003(10)	1.003(8)	0.910(9)	0.914(8)
6.2885	1.016(10)	1.016(8)	0.926(10)	0.929(8)
6.4956	1.036(11)	1.036(9)	0.948(10)	0.951(8)

TABLE 6.12: RGI renormalization factors $\hat{Z}_{\rm T}$ for $N_{\rm f} = 0$.

				$\alpha = 0$			$\alpha = 1/2$		
$\bar{g}^2_{\rm SF}(L)$	β	$\kappa_{\rm c}$	L/a	$Z_{\rm T}(g_0^2, L/a)$	$Z_{\rm T}(g_0^2, 2L/a)$	$\Sigma_{\rm T}(g_0^2, L/a)$	$Z_{\rm T}(g_0^2, L/a)$	$Z_{\rm T}(g_0^2, 2L/a)$	$\Sigma_{\rm T}(g_0^2, L/a)$
0.9793	9.50000	0.131532	6	0.98153(89)	0.9912(14)	1.0098(17)	0.96914(76)	0.9795(12)	1.0107(14)
	9.73410	0.131305	8	0.98260(89)	0.9926(20)	1.0102(22)	0.97167(77)	0.9819(17)	1.0105(20)
	10.05755	0.131069	12	0.98950(93)	1.0070(26)	1.0177(28)	0.97945(80)	0.9955(23)	1.0163(25)
1.1814	8.50000	0.132509	6	0.97970(96)	0.9922(40)	1.0127(42)	0.96388(81)	0.9774(33)	1.0141(35)
	8.72230	0.132291	8	0.9847(18)	1.0046(15)	1.0202(24)	0.9702(15)	0.9895(13)	1.0199(21)
	8.99366	0.131975	12	0.9920(11)	1.0145(37)	1.0227(39)	0.97849(92)	0.9997(33)	1.0217(35)
1.5078	7.54200	0.133705	6	0.98204(96)	1.0045(30)	1.0229(32)	0.96022(81)	0.9818(24)	1.0224(27)
	7.72060	0.133497	8	0.9865(23)	1.0150(39)	1.0288(46)	0.9665(19)	0.9927(33)	1.0271(40)
1.5031	7.50000	0.133815	6	0.98189(86)	0.9955(36)	1.0138(37)	0.95991(73)	0.9744(29)	1.0151(32)
	8.02599	0.133063	12	0.9947(24)	1.02096(59)	1.0264(25)	0.9764(21)	0.9999(29)	1.0241(37)
2.0142	6.60850	0.135260	6	0.9871(13)	1.0193(22)	1.0326(26)	0.9544(11)	0.9841(17)	1.0311(21)
	6.82170	0.134891	8	0.9924(23)	1.0336(26)	1.0416(36)	0.9635(19)	0.9990(22)	1.0368(31)
	7.09300	0.134432	12	1.0070(23)	1.0449(13)	1.0376(27)	0.9797(18)	1.0127(11)	1.0337(22)
2.4792	6.13300	0.136110	6	0.9964(21)	1.0452(72)	1.0489(76)	0.9531(18)	0.9959(57)	1.0449(63)
	6.32290	0.135767	8	1.0006(14)	1.0467(85)	1.0461(87)	0.9620(12)	1.0011(68)	1.0406(71)
	6.63164	0.135227	12	1.0157(33)	1.0776(13)	1.0610(37)	0.9820(25)	1.03268(100)	1.0516(28)
3.3340	5.62150	0.136665	6	1.0118(40)	1.086(15)	1.073(16)	0.9494(30)	1.0050(95)	1.059(11)
	5.80970	0.136608	8	1.0237(40)	1.134(12)	1.108(13)	0.9671(28)	1.0447(98)	1.080(11)
	6.11816	0.136139	12	1.0377(57)	1.129(12)	1.088(13)	0.9885(42)	1.0505(68)	1.0627(83)

TABLE 6.13: $N_{\rm f} = 2$ results for the renormalization constant $Z_{\rm T}$ and the step scaling function $\Sigma_{\rm T}$.

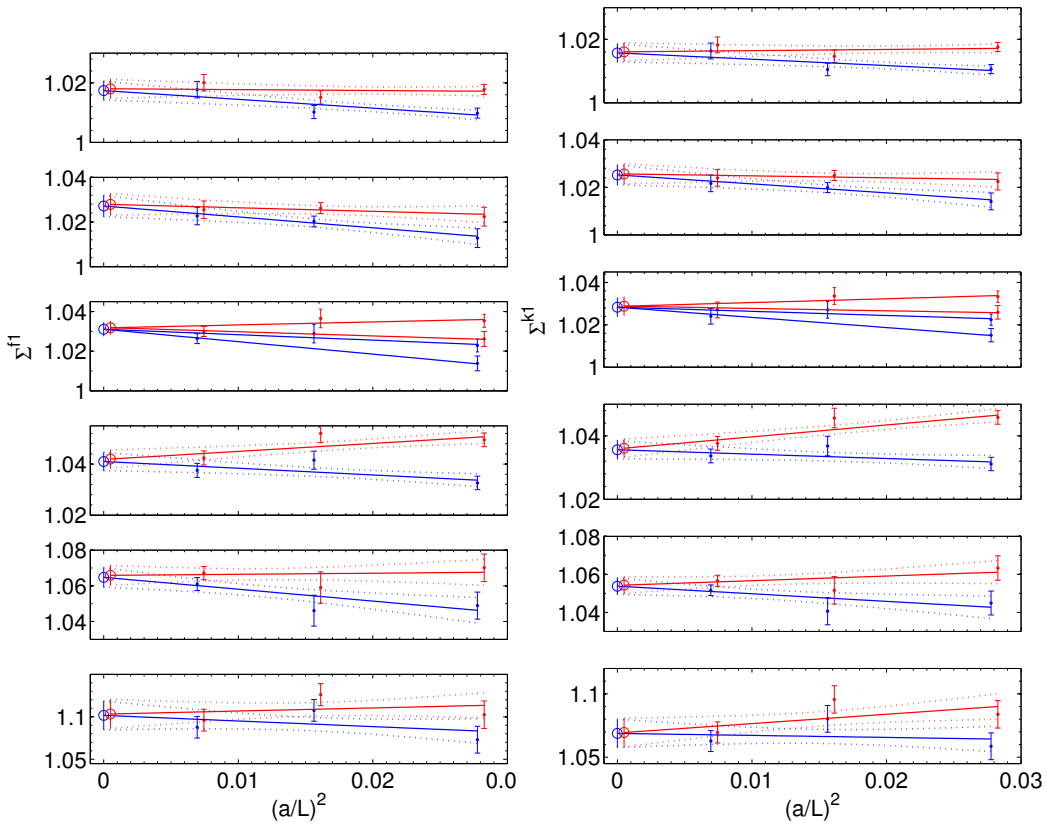

FIGURE 6.12: Continuum extrapolations of SSFs for $N_{\rm f} = 2$ in the schemes $\alpha = 0$ (left) and $\alpha = 1/2$ (right). Blue points are the data in Table 6.13; red points result from subtracting the one-loop value of cutoff effects.

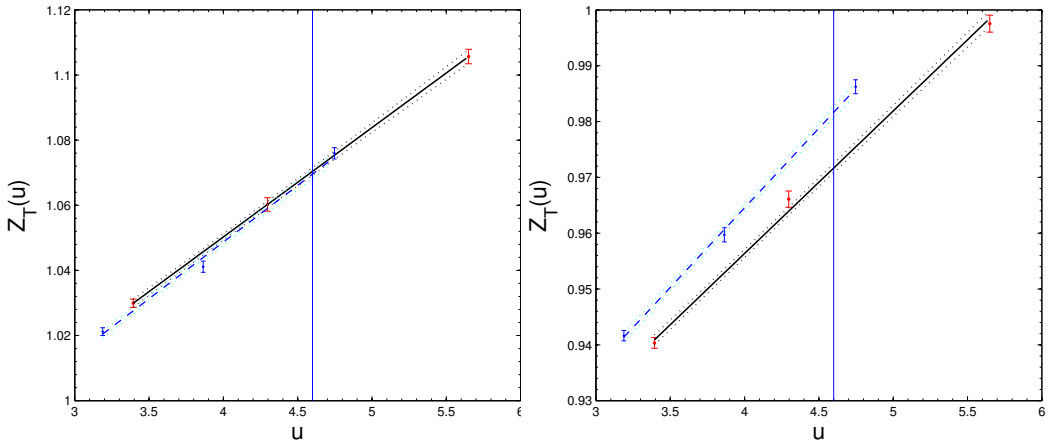

FIGURE 6.13: $N_{\rm f} = 2$, interpolation to $u_{\rm had}$.

	$\alpha = 0$			$\alpha = 1/2$		
u	σ_{T}	$\rho(u)$	χ^2/dof	σ_{T}	$\rho(u)$	χ^2/dof
0.9793	1.0174(32)	-0.30(14)	2.26	1.0157(28)	-0.20(13)	1.91
1.1814	1.0271(48)	-0.49(28)	0.20	1.0252(42)	-0.38(24)	0.19
1.5078	1.0311(34)	-0.28(12) -0.63(20)	0.25	1.0283(45)	-0.20(12) -0.48(0.20)	0.31
2.0142	1.0410(36)	-0.26(18)	2.24	1.0356(29)	-0.14(15)	1.49
2.4792	1.0647(55)	-0.66(40)	1.09	1.0538(43)	-0.40(32)	1.11
3.3340	1.102(17)	-0.66(97)	2.56	1.069(11)	-0.16(64)	2.38

TABLE 6.14: $N_{\mathrm{f}} = 2$ continuum-extrapolated values of σ_{T} without subtraction of perturbative cutoff effects. The two lines for $u = 1.5078$ correspond to the use of the one- and two-loop value of c_{t}, respectively.

	$\alpha = 0$			$\alpha = 1/2$		
u	$\sigma_{\mathrm{T}}(u)$	$\rho(u)$	χ^2/dof	$\sigma_{\mathrm{T}}(u)$	$\rho(u)$	χ^2/dof
0.9793	1.0180(32)	-0.03(15)	1.99	1.0161(28)	0.04(13)	1.73
1.1814	1.0279(48)	-0.16(28)	0.29	1.0256(42)	-0.08(24)	0.26
1.5078	1.0318(34)	0.15(12) -0.21(21)	0.32	1.0288(45)	0.18(12) -0.11(20)	0.37
2.0142	1.0420(36)	0.31(18)	2.64	1.0361(29)	0.38(15)	1.75
2.4792	1.0659(56)	0.06(40)	0.95	1.0543(44)	0.25(33)	0.99
3.3340	1.103(17)	0.37(99)	2.75	1.070(11)	0.74(65)	2.53

TABLE 6.15: $N_{\mathrm{f}} = 2$ continuum-extrapolated values of σ_{T} with subtraction of perturbative cutoff effects. The two lines for $u = 1.5078$ correspond to the use of the one- and two-loop value of c_{t}, respectively.

	fit	p_1	p_2	p_3	p_4	χ^2/dof
$\alpha = 0$	A	0.011705	0.00559(53)	-	-	0.72
	B	0.011705	0.0061(22)	-0.00021(95)	-	0.89
	C	0.011705	0.005070	0.00021(23)	-	0.76
	D	0.011705	0.005070	0.0003(11)	-0.00003(41)	0.94
	E	0.011705	0.0118(63)	-0.0056(55)	0.0012(12)	0.87
$\alpha = 1/2$	A	0.011705	0.00364(43)	-	-	1.00
	B	0.011705	0.0056(18)	-0.00083(76)	-	0.95
	C	0.011705	0.004713	-0.00048(18)	-	0.80
	D	0.011705	0.004713	-0.00022(85)	-0.00010(32)	0.98
	E	0.011705	0.0079(56)	-0.0028(47)	0.00041(96)	1.20

TABLE 6.16: Fits to the continuum $N_{\mathrm{f}} = 2$ SSFs for various choices of polynomial ansatz, cf. Eq. (6.4.3).

k	u_k	$[U(\mu_{\rm had}, 2^{k+1}\mu_{\rm had})]^{-1}$	$\hat{c}^{1/2}(\mu_{\rm had})$	$\hat{c}^{2/2}(\mu_{\rm had})$	$\hat{\mathbf{c}}^{\mathbf{2/3}}(\boldsymbol{\mu}_{\mathbf{had}})$	$\hat{c}^{3/3}(\mu_{\rm had})$
-1	4.610	1	1.1818	0.9483	0.9495	0.7871
0	3.032(16)	0.9214(71)	1.143(9)	0.984(8)	0.985(8)	0.904(7)
1	2.341(21)	0.8710(86)	1.115(11)	0.992(10)	0.992(10)	0.942(10)
2	1.918(20)	0.8348(90)	1.096(12)	0.994(11)	0.994(11)	0.960(11)
3	1.628(17)	0.8072(92)	1.082(13)	0.996(12)	0.996(12)	0.970(12)
4	1.414(14)	0.7852(94)	1.071(13)	0.996(13)	0.997(13)	0.977(12)
5	1.251(12)	0.7670(96)	1.063(14)	0.997(13)	0.997(13)	0.982(13)
6	1.121(11)	0.7516(99)	1.057(14)	0.997(14)	0.997(14)	0.985(14)
7	1.017(10)	0.7384(102)	1.052(15)	0.998(14)	0.998(14)	0.988(14)

TABLE 6.17: Non-perturbative $N_{\rm f} = 2$ running in the scheme $\alpha = 0$. (Our best result $\hat{c}^{2/3}(\mu_{\rm had})$ is stressed.)

k	u_k	$[U(\mu_{\rm had}, 2^{k+1}\mu_{\rm had})]^{-1}$	$\hat{c}^{1/2}(\mu_{\rm had})$	$\hat{c}^{2/2}(\mu_{\rm had})$	$\hat{\mathbf{c}}^{\mathbf{2/3}}(\boldsymbol{\mu}_{\mathbf{had}})$	$\hat{c}^{3/3}(\mu_{\rm had})$
-1	4.610	1	1.1818	0.965	0.9661	0.8241
0	3.032(16)	0.9401(55)	1.166(7)	1.016(6)	1.017(6)	0.946(6)
1	2.341(21)	0.8975(68)	1.149(9)	1.031(8)	1.032(8)	0.987(8)
2	1.918(20)	0.8654(71)	1.136(10)	1.039(9)	1.039(9)	1.008(9)
3	1.628(17)	0.8399(74)	1.126(10)	1.043(10)	1.043(10)	1.020(10)
4	1.414(14)	0.8191(78)	1.118(11)	1.045(11)	1.046(11)	1.028(11)
5	1.251(12)	0.8017(81)	1.111(12)	1.047(11)	1.047(11)	1.034(11)
6	1.121(11)	0.7867(85)	1.106(12)	1.049(12)	1.049(12)	1.038(12)
7	1.017(10)	0.7737(89)	1.102(13)	1.050(13)	1.050(13)	1.041(13)

TABLE 6.18: Non-perturbative $N_{\rm f} = 2$ running in the scheme $\alpha = 1/2$. (Our best result $\hat{c}^{2/3}(\mu_{\rm had})$ is stressed.)

β	κ_c	L/a	$\bar{g}^2_{\rm SF}(L)$	$Z_{\rm T}^{\alpha=0}$	$Z_{\rm T}^{\alpha=1/2}$
5.20	0.13600	4	3.65(3)	1.0433(14)	0.9423(11)
		6	4.61(4)	1.0797(17)	0.9715(12)
5.29	0.13641	4	3.394(17)	1.0299(13)	0.9403(10)
		6	4.297(37)	1.0602(21)	0.9661(14)
		8	5.65(9)	1.1057(22)	0.9975(15)
5.40	0.13669	4	3.188(24)	1.0212(12)	0.9416(9)
		6	3.864(34)	1.0411(17)	0.9597(13)
		8	4.747(63)	1.0760 (17)	0.9862(12)

TABLE 6.19: Renormalization constants $Z_{\rm T}(g_0^2, L/a)$ at $L = 1/\mu_{\rm had}$ for $N_{\rm f} = 2$.

β	$\hat{Z}_{\rm T}^{\alpha=0}$	$\hat{Z}_{\rm T}^{\alpha=1/2}$
5.20	1.077(15)	1.020(12)
5.29	1.068(15)	1.020(12)
5.40	1.068(15)	1.031(12)

TABLE 6.20: RGI renormalization factors $\hat{Z}_{\rm T}$ for $N_{\rm f} = 2$.

Part III

Renormalization of Quark Masses

7 Quark masses renormalization

7.1 Motivation

The masses of the light quarks are not directly accessible to experiment and have to be determined through non-perturbative calculations, taking as input low-energy hadronic data (e.g. m_K, f_K ...). Perturbative approaches, like Chiral perturbation theory [114, 115, 22] are able to estimate the value of quark masses [21] but they still relies on non-perturbative approaches like Lattice or QCD sum rules (for a review [116]).
In lattice QCD the extraction of quark masses is in principle straightforward, it is less easy to compute the running from a low-energy scale up to high energies. It is evident, that, in order to have a reliable determination the renormalization constant and its running have to be computed non-perturbatively. We follow here a similar strategy to the one presented in [72, 43], but as discussed in Chapter 4, following what has been done for the computation of the strong coupling [97, 10] we adopt two schemes, matched at an intermediate scale called "switching scale".

7.2 Strategy

7.2.1 Step-scaling functions

In our computation, as we did for the tensor currents, we will access the renormalisation group functions β and τ through the quantities σ and σ_{P}, repeated here as

$$\ln 2 = -\int_{\sqrt{u}}^{\sqrt{\sigma(u)}} \mathrm{d}g \, \frac{1}{\beta(g)} \,, \tag{7.2.1}$$

$$\sigma_{\mathrm{P}}(u) = \exp\left\{ -\int_{\sqrt{u}}^{\sqrt{\sigma(u)}} \mathrm{d}g \, \frac{\tau(g)}{\beta(g)} \right\} \,, \tag{7.2.2}$$

and to which we will refer as coupling and mass SSFs, respectively. Notice that σ_{P} is defined as the inverse of Eq. (2.2.2), because the anomalous dimension $\tau = -\gamma_P$. They correspond to the renormalisation group evolution operators for the coupling and quark mass between scales that differ by a factor of two, viz.

$$\sigma(u) = \bar{g}^2(\mu/2)\big|_{u=\bar{g}^2(\mu)} \,, \qquad \sigma_{\mathrm{P}}(u) = \frac{\overline{m}_i(\mu)}{\overline{m}_i(\mu/2)}\bigg|_{u=\bar{g}^2(\mu)} \,. \tag{7.2.3}$$

The main advantage of these quantities is that they can be computed accurately on the lattice, so that a well-controlled continuum limit is obtained, for a very wide range of scales. This allows to use a finite-size recursive procedure [72] to reconstruct the renormalisation group functions non-perturbatively between the hadronic regime and the electroweak scale, where contact with perturbation theory can safely be established.

In order to compute the SSF $\sigma_{\rm P}$, we remind that renormalised quark masses are defined thourgh the PCAC relation already introduced in the context of WI, as

$$\partial_\mu (A_{\rm R})^{ij}_\mu = (\overline{m}_i + \overline{m}_j) P^{ij}_{\rm R}\,, \tag{7.2.4}$$

where the renormalised, non-singlet ($i \neq j$) axial current and pseudoscalar density operators are given by

$$(A_{\rm R})^{ij}_\mu(x) = Z_{\rm A}\bar{\psi}_i(x)\gamma_\mu\gamma_5\psi_j(x)\,, \tag{7.2.5}$$

$$(P_{\rm R})^{ij}(x) = Z_{\rm P}\bar{\psi}_i(x)\gamma_5\psi_j(x)\,. \tag{7.2.6}$$

In these expressions $Z_{\rm P}$ is the renormalisation constant of the pseudoscalar density in the regularised theory, and $Z_{\rm A}$ is the finite axial current normalisation required when QCD is regularised on a lattice. Eq. (7.2.4) implies that current quark masses renormalise with $Z_{\rm P}^{-1}$. Therefore, the SSF $\sigma_{\rm P}$ of Eq. (7.2.2) can be obtained by computing $Z_{\rm P}$ at scales μ and $\mu/2$ for different values of the lattice spacing a, and taking the continuum limit of their ratio, viz.

$$\sigma_{\rm P}(u) = \lim_{a\to 0} \Sigma_{\rm P}(g_0^2, a\mu)\big|_{\bar{g}^2(\mu)=u}\,, \qquad \Sigma_{\rm P}(g_0^2, a\mu) \equiv \frac{Z_{\rm P}(g_0^2, a\mu/2)}{Z_{\rm P}(g_0^2, a\mu)}\,, \tag{7.2.7}$$

where g_0^2 is the bare coupling, univocally related to a in mass-independent schemes. The condition that the value of the renormalised coupling $u = \bar{g}^2(\mu)$ is kept fixed in the extrapolation ensures that the latter is taken along a line of constant physics.[1]

7.2.2 Renormalisation schemes

In order to control the connection between hadronic observables and RGI quantities, we will use intermediate finite-volume renormalisation schemes that allow to define fully non-perturbative renormalised gauge coupling and quark masses. To that purpose, as for $Z_{\rm T}$, $Z_{\rm P}$ will be defined by a renormalisation condition imposed using the SF.

The renormalisation of the pseudoscalar density, and hence of quark masses, is treated in the same way as in [72]. We remind here the SF correlation functions

$$f_{\rm P}(x_0) = -\frac{1}{3}\int {\rm d}^3x \langle P^{ij}(x)\,\mathcal{O}^{ji}\rangle\,, \tag{7.2.8}$$

$$f_1 = -\frac{1}{3}\langle \mathcal{O}'^{ij}\,\mathcal{O}^{ji}\rangle\,, \tag{7.2.9}$$

where P^{ij} is the un-renormalised pseudoscalar density, and $\mathcal{O}$, $\mathcal{O}'$ are operators with pseudoscalar quantum numbers made up with boundary quark fields,

$$\mathcal{O}^{ij} = \frac{1}{L^3}\int {\rm d}^3y \int {\rm d}^3z\, \bar{\zeta}_i(\mathbf{y})\gamma_5\zeta_j(\mathbf{z})\,, \quad \mathcal{O}'^{ij} = \frac{1}{L^3}\int {\rm d}^3y \int {\rm d}^3z\, \bar{\zeta}'_i(\mathbf{y})\gamma_5\zeta'_j(\mathbf{z})\,. \tag{7.2.10}$$

The pseudoscalar renormalisation constant is then defined as

$$Z_{\rm P}\,\frac{f_{\rm P}(L/2)}{\sqrt{3f_1}} = \left.\frac{f_{\rm P}(L/2)}{\sqrt{3f_1}}\right|_{\rm tree\ level}\,, \tag{7.2.11}$$

[1] Note that the assumption of a lattice regularisation in Eqs. (7.2.4,7.2.7) is inessential: the construction can be applied to any convenient regularisation, provided currents are correctly normalised, and $\sigma_{\rm P}$ is obtained by removing the regulator at constant physics.

L/a	β	κ	$N_{\mathrm{meas}}(L)$	$N_{\mathrm{meas}}(2L)$
6	8.54030	0.13233610	5000	5000
8	8.73250	0.13213380	5000	2683
12	8.99500	0.13186210	2769	1576
6	8.21700	0.13269030	5000	5000
8	8.40440	0.13247670	5000	2314
12	8.67690	0.13217153	2476	3759
6	7.90910	0.13305719	5000	5000
8	8.09290	0.13283120	5000	2273
12	8.37300	0.13249231	2729	3749
6	7.59090	0.13346930	5000	5000
8	7.77230	0.13322829	5000	2163
12	8.05780	0.13285364	2448	3762
6	7.26180	0.13393369	5000	5000
8	7.44240	0.13367450	5000	4500
12	7.72990	0.13326352	2710	6343
6	6.94330	0.13442200	5000	5000
8	7.12540	0.13414180	5000	2041
12	7.41070	0.13369922	2535	3412
6	6.60500	0.13498289	5000	5000
8	6.79150	0.13467650	5000	1807
12	7.06880	0.13420890	2339	2607
6	6.27350	0.13557130	5000	4435
8	6.46800	0.13523620	5000	4048
12	6.72995	0.13475972	3000	5094 + 512
16	6.93460	0.13441209	4604	2325

L/a	β	κ	$N_{\mathrm{meas}}(L)$	$N_{\mathrm{meas}}(2L)$
8	5.37150	0.13362120	5001	2001
12	5.54307	0.13331407	8000	2400
16	5.70000	0.13304840	7001	500
8	5.07100	0.13421678	5001	2001
12	5.24247	0.13387635	8000	2400
16	5.40000	0.13357851	6001	500
8	4.76490	0.13488555	5001	2001
12	4.93873	0.13450761	5001	2400
16	5.10000	0.13416889	6001	500
8	4.45760	0.13560675	5001	2001
12	4.63465	0.13519986	5001	2400
16	4.80000	0.13482139	5000	2000
8	4.15190	0.13632589	5001	2001
12	4.33166	0.13592664	5001	2400
16	4.50000	0.13552582	5000	2000
8	3.94790	0.13674684	5001	2001
12	4.12822	0.13640300	5001	2100
16	4.30000	0.13600821	5000	2500
8	3.75489	0.13701929	5001	2001
12	3.93682	0.13679805	5001	3682
16	4.10000	0.13647301	3200	2674

TABLE 7.1: Table with bare parameters used to produce gauge ensembles with $2 + 1$ dynamical flavours. High energy region simulation (top) are carried out using Plaquette gauge action and non-perturbatively $\mathcal{O}(a)$-improved Wilson fermions. We employed SF boundary conditions without BG field. With the same boundary conditions and wilson action but LW gauge action have been produced gauge ensembles for the coupling project.

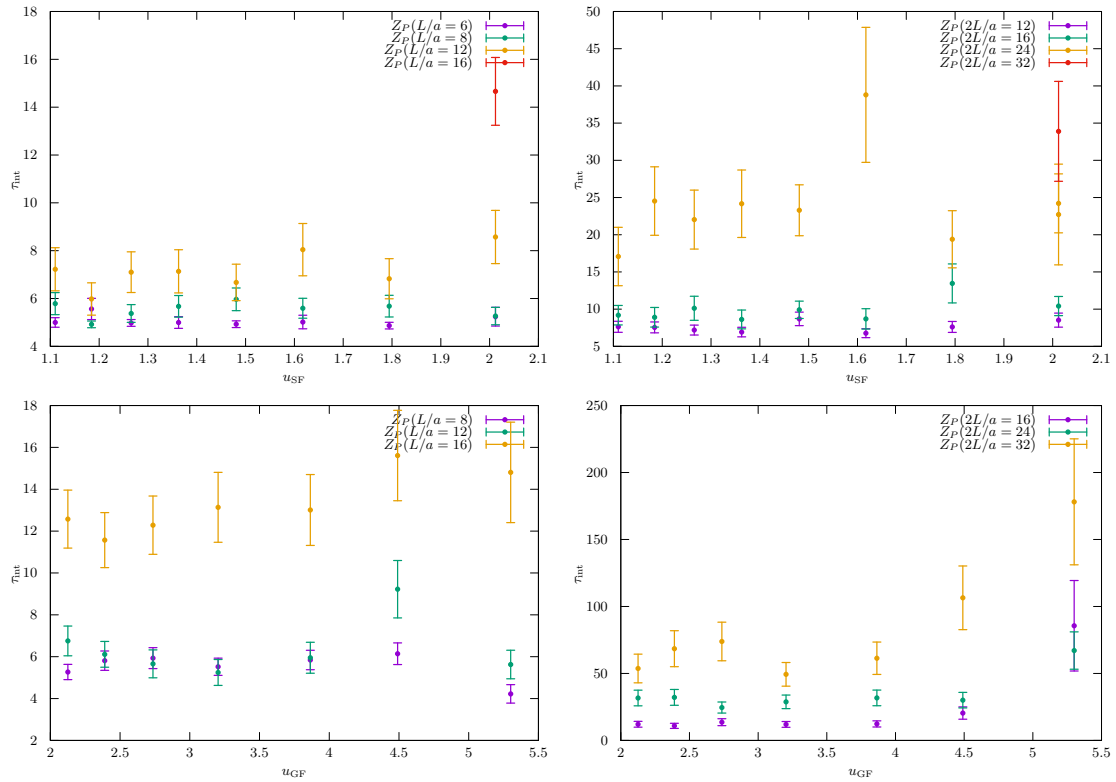

FIGURE 7.1: Integrated autocorrelation time for $Z_{\rm P}$ as a function of $\bar{g}_{\rm SF}(L)$, on the top two plots, and $\bar{g}_{\rm GF}(L)$ at the bottom. The left and right panel respectively contain information about L and $2L$ volume. Note that the coupling corresponding to a double volume is $\bar{g}^2(2L) = \sigma(\bar{g}^2(L))$, but for practical reasons we use the same scale for both volumes.

with all correlation functions computed at zero quark masses. The renormalisation condition is fully specified by fixing the boundary conditions and the box geometry, which we do as

$$T = L\,, \qquad C = C' = 0\,, \qquad \theta = \frac{1}{2}\,. \tag{7.2.12}$$

Furthermore, due to computational convenience (cf. below), all correlation functions will be computed in a fixed topological sector of the theory, which we choose to be the one with total topological charge $Q = 0$. This is just part of the scheme definition, and does not change the ultraviolet structure of the observables.

In order to completely fix the renormalisation scheme for quark masses, it is still needed to provide a definition of the renormalised coupling. This allows to relate the scale $\mu = 1/L$ to the bare coupling, and hence to the lattice spacing, in an unambiguous way, so that the continuum limit of $\Sigma_{\rm P}$ is precisely defined. Following [97, 10], we will introduce two different definitions, to be used in qualitatively different regimes. For renormalisation scales larger than some value $\mu_0 \equiv L_0^{-1}$, we will employ the non-perturbative SF coupling first introduced in [97]. Below that scale, we will use the gradient flow (GF) coupling defined in [10]. As explained in [11, 117], this allows to optimally exploit the variance properties of the couplings, so that a very precise computation of the β function, and ultimately of the Λ parameter, is achieved.[2] In our context, the main consequence of

[2] Also here, both couplings are computed from correlation functions projected to the $Q = 0$ sector of the theory.

this setup is that two different schemes for the mass result above and below μ_0; we will refer to them as SF $-$ SF and SF $-$ GF, respectively.

Note that the schemes differ only by the choice of renormalized coupling $\bar{g}^2$: the definition of $Z_{\rm P}$ is always given by Eq.(7.2.11).

The value of μ_0 is implicitly fixed by

$$\bar{g}^2_{\rm SF}(\mu_0) = 2.0120\,. \tag{7.2.13}$$

This leads to $\mu_0 \simeq 4.2$ GeV [10], i.e. the scheme switching takes place around the b quark mass scale. The running of the SF coupling is thus known accurately down to the scale $\mu_0/2$, reached by $\bar{g}^2_{\rm SF}(\mu_0/2) = \sigma(2.0120) = 2.452(11)$. The matching of the two schemes is completely specified by measuring the value of the GF coupling at $\mu_0/2$, for which one has [10]

$$\bar{g}^2_{\rm GF}(\mu_0/2) = 2.6723(64)\,. \tag{7.2.14}$$

It is important to stress that the scheme definition affects different quantities in distinct ways. In particular, the mass anomalous dimension τ — which is a function of the coupling — will be different in the two schemes, as will be β function. The values of renormalised masses, on the other hand, will be the same in both schemes, since they only depend on the scale μ, and the definition of $Z_{\rm P}$, which is fixed. This latter observation also provides the matching relation for the anomalous dimensions: for any fixed μ we have

$$\tau_{\rm SF-SF}(\bar{g}^2_{\rm SF}(\mu)) = \tau_{\rm SF-GF}(\bar{g}^2_{\rm GF}(\mu))\,. \tag{7.2.15}$$

Another important motivation for this strategy choice is the control over the perturbative expansion of the β function and mass anomalous dimension, which becomes relevant at very high energies. In the SF scheme (as reported at the beginning of this thesis) the first non-universal perturbative coefficient of the β function, b_2, and the next-to-leading order (NLO) mass anomalous dimension in the SF $-$ SF are known. A similar computation in the SF $-$ GF scheme is currently not possible, due to the absence of a full two-loop computation of the finite-volume GF coupling in QCD.

Results for the β-functions

Let us end this section sumarizing the results for the beta function in our choice of schemes. As discussed above, these results will be essential to determine the anomalous dimension $\tau(\bar{g})$ in the following sections. On the high energy side we have [97]

$$\beta_{\rm SF}(\bar{g}) = -\bar{g}^3 \sum_{n=0}^{3} b_n \bar{g}^{2n} \qquad \bar{g} \in [0, 2.45] \tag{7.2.16}$$

with $b_{0,1}$ given by eq. (2.0.7), b_2 given by eq. (2.0.8), and b_3 a fit parameter with value

$$(4\pi)^2 b_3 = 4(3)\,. \tag{7.2.17}$$

Note that the three leading coefficients are given by the perturbative predictions, which implies that a safe contact with the asymptotic perturbative behaviour has been made (this is the reason why eq. (7.2.16) is valid all the way up to $\bar{g} = 0$). On the other hand, on the low energy side, we have [10]

$$\beta_{\rm GF}(\bar{g}) = -\frac{\bar{g}^3}{\sum_{n=0}^{2} p_n \bar{g}^{2n}} \qquad \bar{g} \in [2.1, 11.3]\,, \tag{7.2.18a}$$

with fit parameters

$$p_0 = 16.07\,, \quad p_1 = 0.21\,, \quad p_2 = -0.013\,, \tag{7.2.18b}$$

with covariance matrix

$$\mathrm{cov}(p_i, p_j) = \begin{pmatrix} 5.12310 \times 10^{-1} & -1.77401 \times 10^{-1} & 1.32026 \times 10^{-2} \\ -1.77401 \times 10^{-1} & 6.60392 \times 10^{-2} & -5.10305 \times 10^{-3} \\ 1.32026 \times 10^{-2} & -5.10305 \times 10^{-3} & 4.06114 \times 10^{-4} \end{pmatrix} . \tag{7.2.18c}$$

These values are *not* exactly the same as those quoted as final results in [10]. There are two reasons for this. First we have added some statistics in some ensembles, where the uncertainty in $\Sigma_{\rm P}$ was too large. Second, a consistent treatment of the correlations and autocorrelations between Z_P and $\bar{g}^2_{\rm GF}$ requires to determine the joint autocorrelation function in a consistent way. This requirement results in a different covariance matrix between the fit parameters. In any case it is very important to point out that both results (eqs. (7.2.18b, 7.2.18c)) and those quoted in [10] are perfectly compatible. It can be easily checked that the differences in the β-function are hardly visible and, therefore, completely negligible within the quoted uncertainties.

7.3 Running in the high-energy region

7.3.1 Determination of Z_P and $\Sigma_{\rm P}$

Our simulations in the high-energy range above μ_0 have been performed at eight different values of the renormalised Schrödinger Functional coupling

$$u_{\rm SF} \in \{1.1100, 1.1844, 1.2656, 1.3627, 1.4808, 1.6173, 1.7943, 2.0120\}\,, \tag{7.3.1}$$

for which we have determined the step-scaling function $\Sigma_{\rm P}$ of Eq. (7.2.7) at three different values of the lattice spacing $L/a = 6, 8, 12$. At the strongest coupling $u_{\rm SF} = 2.012$ we have also simulated an extra finer lattice with $L/a = 16$, in order to have a strong crosscheck of our control over continuum limit extrapolations in the less favourable case. The value of the hopping parameter κ is tuned to its critical value $\kappa_{\rm c}$, so that the bare O(a)-improved PCAC mass

$$m(g_0^2, \kappa) = \left. \frac{\frac{1}{2}(\partial_0^* + \partial_0) f_{\rm A}(x_0) + c_{\rm A} a \partial_0^* \partial_0 f_{\rm P}(x_0)}{2 f_{\rm P}(x_0)} \right|_{x_0 = T/2}\,, \tag{7.3.2}$$

vanishes at the corresponding value of $\beta = 6/g_0^2$.[3]

The data for Σ_P is corrected by subtracting the cutoff effects to all orders in a and leading order in g_0^2, using the one-loop computation of [101]

$$\Sigma_P^{(I)}(u, a/L) = \frac{\Sigma_P(u, a/L)}{1 - u d_0 \log 2\, c(a/L)}\,, \tag{7.3.3}$$

where $c(a/L)$ is given in table 7.2. This correction affects mainly our coarser lattice with $L/a = 6$, and is well below our statistical uncertainties for $L/a > 6$.

The results of our simulations are summarised in Table 7.5. Alongside the results for $Z_{\rm P}$ at each simulation point, we quote the corresponding values of $\Sigma_{\rm P}^{(I)}$. The size of the one-loop correction (eq. (7.3.3)) is of the same order of our statistical uncertainties for our coarser lattices ($L/a = 6$), and negligible for the finer lattices. Given the non-monotonous

[3] Details can be found in [10, 97]; a discussion of the systematic impact of this procedure on our data is provided in Appendix 7.6.

behaviour of the 1-loop correction for our choices of lattice sizes, we suspect that our coarser data is contaminated by non $\mathcal{O}(a^2)$ effects. We cannot be sure that these are completely removed by our 1-loop correction, so we use the size of this 1-loop correction as an estimate of the remaining non-O(a^2) effects by adding in quadratures the 1-loop correction to our statistical uncertainty of $\Sigma_{\rm P}^{(I)}$. The uncertainties of $\Sigma_{\rm P}^{(I)}$, both statistical and systematical are quoted in table 7.5.

7.3.2 Determination of the anomalous dimension

Once the lattice step scaling function $\Sigma_{\rm P}(u, a/L)$ is known, our preferred analysis follows from a determination of the anomalous dimension $\tau(\bar{g})$ using eq. (7.2.2). A possibility consists in first extrapolating $\Sigma_P^{(\rm I)}(u, a/L)$ to the continuum at fixed u

$$\Sigma_P^{(\rm I)}(u, a/L) = \sigma_P(u) + \rho \left(\frac{a}{L}\right)^2 , \qquad (7.3.4)$$

and use the continuum values $\sigma(u)$ to determine $\tau(\bar{g})$ from the relation

$$\log\left(\sigma_P(u)\right) = -\int_{\sqrt{u}}^{\sqrt{\sigma(u)}} dx \left[\frac{\tau(x)}{\beta(x)}\right] . \qquad (7.3.5)$$

This analysis will be labelled "u-by-u". The advantage of this analysis in that one has full control over the continuum extrapolations, since they are performed independently from the determination of the anomalous dimension. In fact a detailed study of the continuum extrapolations shows that when extrapolating the data for $\Sigma_P^{(\rm I)}$ to the continuum linearly in $(a/L)^2$, the effect of the 1-loop correction to our data becomes noticeable (see Fig. 7.2.). The fits to the raw uncorrected data have a total $\chi^2/\text{dof} = 12.9/9$, while the fits to the corrected data have $\chi^2/\text{dof} = 8.6/9$. As we mentioned before, we add the 1-loop uncertainty to our data for $\Sigma_P^{(I)}$, and this procedure increases the size of the uncertainties of our continuum extrapolated values by about a 20-30%. Table (7.5) shows the continuum values $\sigma(u)$ at the eight values of the coupling determined following this conservative analysis.

L/a	c
4	0.213560
6	0.020787
8	-0.002626
10	-0.006178
12	-0.006368
14	-0.005848
16	-0.005210
18	-0.004605
20	-0.004073
22	-0.003615
24	-0.003224

TABLE 7.2: One-loop cutoff effects in $\Sigma_{\rm P}$ for the O(a) improved fermion action and $N = 3$. The values reported in the second column corresponding to $L/a = 6, \ldots, 16$ reproduce those in [101], where the notation δ_k is used for this quantity.

A alternative analysis consists in using the lattice data to extrapolate to the continuum at the same time that one determines the anomalous dimension. In this approach one uses the relation

$$\log\left(\Sigma_P^{(\rm I)}(u, a/L) - \rho(u)\left(\frac{a}{L}\right)^2\right) = -\int_{\sqrt{u}}^{\sqrt{\sigma(u)}} dx \left[\frac{\tau(x)}{\beta(x)}\right] , \qquad (7.3.6)$$

where the function $\rho(u)$ parametrizes the cutoff effects in the $\sigma_{\rm P}(u)$ (which we have already seen to be linear in $(a/L)^2$). We use a simple polynomial ansatze

$$\rho(u) = \sum_{n=2}^{n_\rho} \rho_n u^n . \qquad (7.3.7)$$

Note that since our data has been corrected for cutoff effects up to 1-loop, the functional form that describes the cutoff effects $\rho(u)$ cannot have any constant or linear term in u.

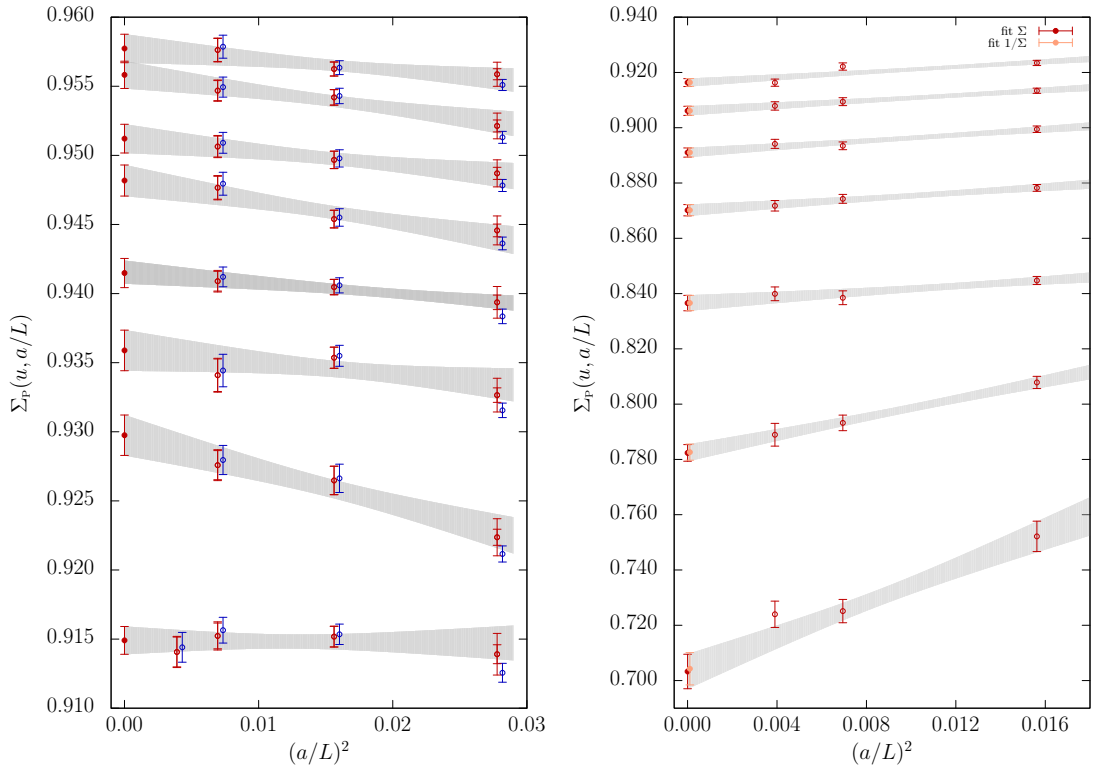

FIGURE 7.2: Results for the step-scaling function Σ_P and continuum-limit extrapolations at fixed value of u. (Right: high-energy region. Left: low-energy region. In both plots the value of the renormalised coupling increases from top to bottom.) In the left panel, blue points, slightly shifted for better visibility, denote the values of Σ_P quoted in Table 7.5; red points are obtained by subtracting cutoff effects to all orders in a at order g_0^2 in perturbation theory. The continuum-limit extrapolations shown correspond to these latter, perturbatively improved data.

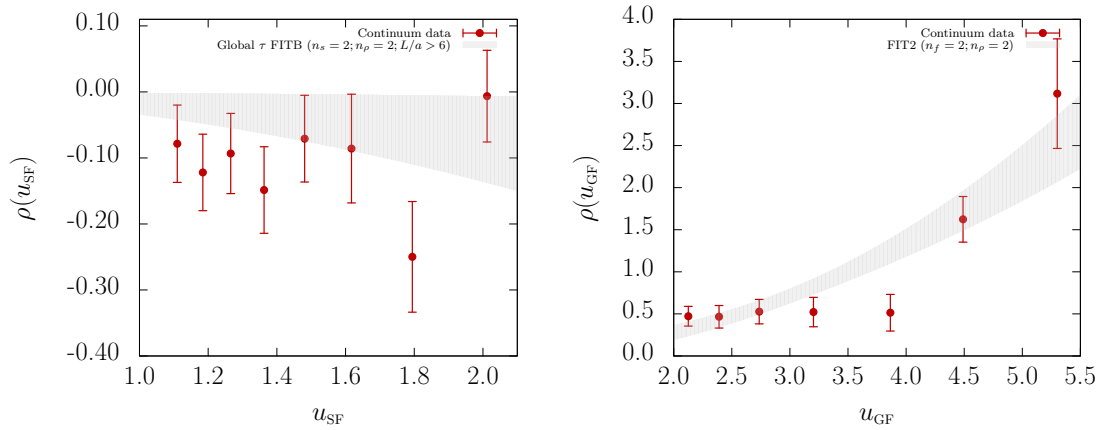

FIGURE 7.3: Slopes of the continuum-limit extrapolations $\Sigma_P(u, a/L) = \sigma_P(u) + \rho(u)(a/L)^2$, performed at fixed value of u. (Left: high-energy region. Right: low-energy region.)

In this approach we simultenously determine the $\tau(\bar{g})$ and perform a continuum extrapolation of our lattice data $\Sigma_P^{(I)}(u, a/L)$. This approach will be labelled "global", and has two advantages. First one can choose not to include the coarser lattice data points (i.e. one can use only the data with $L/a > 6$). Second the data does not need to be tuned to a constant value of the coupling u.

Type	n_s	n_ρ	$[L/a]_{\min}$	$M/m(\mu_0/2)$	χ^2/dof
FITA	2	2	6	1.758(11)	18 / 22
FITA	2	2	8	1.747(14)	11 / 14
FITB	2	2	6	1.7577(77)	18 / 23
FITB	2	2	8	1.7505(89)	12 / 15
FITB	3	2	6	1.7580(80)	18 / 22
FITB	3	2	8	1.7500(97)	12 / 14

TABLE 7.3: Different fits of the anomalous dimension and results for $M/\overline{m}(\mu_0/2)$ (see eq. (7.3.10) and text for more details).

All that is left is to parametrize the anomalous dimension $\tau(x)$ for which we use the polynomial ansatz

$$\tau(x) = -x^2 \sum_{n=0}^{n_s} t_n x^{2n} \,. \tag{7.3.8}$$

We always fix the leading universal coefficient with the perturturbative asymptotic prediction $t_0 = d_0 = 8/(4\pi)^2$, while we can choose to leave the rest of the coefficients to be determined by the fit (strategy FITA), or we can also fix the NLO coefficient to the perturbative prediction $t_1 = d_1 = 2.96871 \times 10^{-3}$ (labelled FITB).

This approach has the advantage that once the function $\tau(\bar{g})$ is obtained, one can directly determine the ratio of the RGI quark mass over the renormalized quark masses at any scale.

All in all, the global and the u-by-u approaches produce completely compatible results, as we will show in detail in the next section. Here we will just take the results of the global analysis for the quantity

$$\frac{M}{\bar{m}(\mu_0/2)} \;=\; [2b_0\bar{g}^2_{\rm SF}(\mu_0/2)]^{-d_0/2b_0} \exp\left\{ -\int_0^{\bar{g}_{\rm SF}(\mu_0/2)} dx \left[\frac{\tau(x)}{\beta(x)} - \frac{d_0}{b_0 x} \right] \right\} \,, \tag{7.3.9}$$

and compare the result for different fits. Table 7.3 shows the results for different fits. The agreement between different parametrizations of the anomalous dimension is very good. Fits that do not use the known value for t_1 tend to have larger errors, as expected, since the asymptotic perturbative behaviour is not constrained with the known analytic results. As final result, we quote

$$\frac{M}{\overline{m}(\mu_0/2)} = 1.7505(89) \,. \tag{7.3.10}$$

This result comes from a conservative approach: we discard our coarser lattices with $L/a = 6$, and the statistical error of the points is increased by the value of 1-loop correction. The result agrees nicely with all other fits. If one wants to be extra-conservative one can add the maximum spread (8×10^{-3}) by quadratures to the statistical error, resulting in

$$\frac{M}{\overline{m}(\mu_0/2)} = 1.751(12) \,. \tag{7.3.11}$$

We quote then the result for the anomalous dimension at high energies, given by

$$\tau(\bar{g}) = -\bar{g}^2 \sum_{n=0}^{2} t_n \bar{g}^{2n} \,, \tag{7.3.12}$$

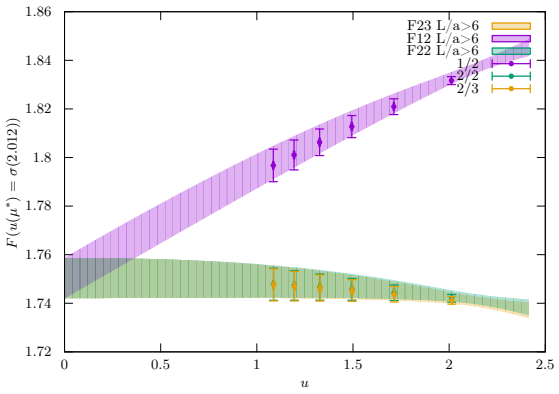

FIGURE 7.4: The plot shows the "functional approach" to $u = 0$ using SSF recursion (points) matched with perturbation theory at different orders and the one given by our anomalous dimension from the fit.

with

$$t_0 = 8/(4\pi)^2\,, \tag{7.3.13}$$
$$t_1 = 2.96871 \times 10^{-3}\,, \tag{7.3.14}$$
$$t_2 = -0.9(2.6) \times 10^{-4}\,. \tag{7.3.15}$$

The knowledge of the (non-perturbative) anomalous dimension offer the intriguing possibility to probe the systematics of perturbation theory. It is, then, instructive to fix $\mu_0/2$ as a reference scale and rephrase Eq. (7.3.10) as the function

$$F^{(k_1,k_2)}(\lambda) = \left[2b_0\bar{g}^2_{\rm SF}\left(\frac{\mu_0}{2}\right)\right]^{\frac{-d_0}{2b_0}} \exp\left\{-\int_0^\lambda dx\left[\frac{\tau^{(k_1)}(x)}{\beta^{(k_2)}(x)} - \frac{d_0}{b_0 x}\right]^{\rm PT}\right\} \times \exp\left\{-\int_\lambda^{\bar{g}\left(\frac{\mu_0}{2}\right)} dx\left[\frac{\tau(x)}{\beta(x)} - \frac{d_0}{b_0 x}\right]\right\}\,, \tag{7.3.16}$$

where $\tau^{(k_1)}$ and $\beta^{(k_2)}$ are the RG functions up to orders k_1 and k_2 respectively. The function $F^{(k_1,k_2)}(\lambda)$ measures the effect of using perturbation theory to determine the RGI mass at scales μ where $\bar{g}(\mu) < \lambda$. This observation is reported in Fig. 7.4, where the above quantity is computed using a standard SSF recursion (see next subsection) or by integrating the fitted anomalous dimensions.

7.3.3 Comparison between different analyses

In order to have a critical quantitative comparison between the different analysis techniques it is convenient to consider the quantity

$$R^{(k)} = \frac{\bar{m}(2^k\mu_0)}{\bar{m}(\mu_0/2)} = \prod_{n=0}^{k}\sigma_P(u_n)\,, \qquad \bar{g}^2_{\rm SF}(\mu_0) = 2.012 \text{ and } u_k = \bar{g}^2_{\rm SF}(2^k\mu_0)\,. \tag{7.3.17}$$

Note that the very same quantity can be computed as

$$R^{(k)} = \int_{\sqrt{u_k}}^{\sqrt{u_{-1}}} dx\,\frac{\tau(x)}{\beta(x)}\,, \tag{7.3.18}$$

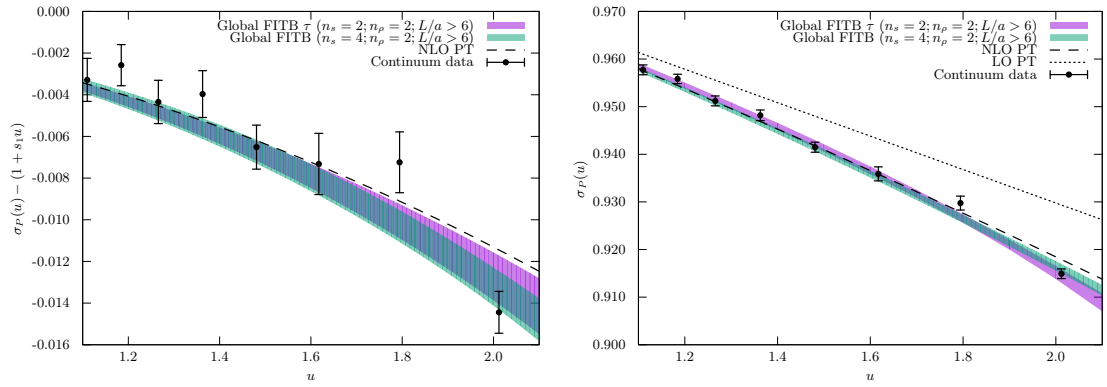

FIGURE 7.5: A comparison between two fits used to determine $\sigma_P(u)$ and our continuum extrapolated data.

providing an excellent way to check that different analysis strategies give the same results.

Figure 7.5 shows two different fits together with the continuum extrapolated points of $\sigma_P(u)$. As the reader can see, the agreement between the two fits, and our data is excellent.

In order to perform these checks we need to determine the continuum step scaling function $\sigma_P(u)$. As a first approach we can just parametrise the continuum values of table (7.5) as a polynomial functional form

$$\sigma_P(u) = 1 + s_1 u + \sum_{n=2}^{n_s} c_n u^n \,, \tag{7.3.19}$$

where the asymptotic universal behaviour for σ_P is imposed by fixing $s_1 = -d_0 \log 2$. The known NLO behaviour of the anomalous dimension can be used to fix the next to leading coefficient $c_2 = s_2 = -d_1 \log 2 + (\frac{1}{2} d_0^2 - b_0 d_0)(\log 2)^2$. As we did for the case of the anomalous dimension we will focus on two functional forms: `FITA`, where c_2 is determined by the data, or `FITB`, where c_2 is fixed to the perturbative prediction.

We can also use a "global" approach and fit the lattice data $\Sigma_P^{(I)}(u, a/L)$ to the functional form

$$\Sigma_P^{(I)}(u, a/L) = \sigma_P(u) + \rho(u) \left(\frac{a}{L}\right)^2 , \qquad \rho(u) = \sum_{n=2}^{n_\rho} \rho_n u^n \,. \tag{7.3.20}$$

Where the continuum $\sigma_P(u)$ is parametrized as in `FITA` or `FITB`. Note that since our data has been corrected for cutoff effects up to 1-loop, the functional form that describes the cutoff effects $\rho(u)$ cannot have any constant or linear term in u.[4]

Table 7.7 shows a comparison of the fit results for the quantity $R^{(k)}$ coming from different fit ansatze. In general the agreement is good, but one notice that the fit quality improves when the data with $L/a = 6$ is discarded.

In any case the most important point is that the agreement between the analysis coming from the recursion of the step scaling functions, and the analysis coming from the determination of the anomalous dimension explained in the previous section have a very good agreement.

[4] We have tried to fit the un-improved $\Sigma_P(u, a/L)$ with a similar global fit approach, obtaining compatible results.

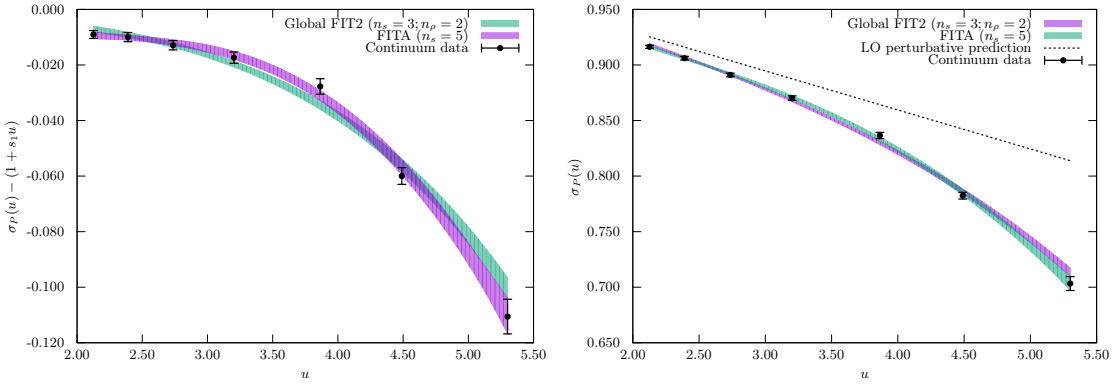

FIGURE 7.6: A comparison between two fits used to determine $\sigma_P(u)$ and our continuum extrapolated data (only as a reference!).

7.4 Running in the low-energy region

As already explained, at energies $\mu < \mu_0/2$ it turns out to be convenient to change to the GF scheme. The objective of the low energy running is to compute the ratio $\overline{m}(\mu_0/2)/\overline{m}(\mu_{\rm had})$, that together with the ratio $M/\overline{m}(\mu_0/2)$ of eq. (7.3.10) will provide the total running factor.

In the low-energy range below μ_0 we have carried out simulations at seven different values of the renormalised gradient flow coupling $u_{\rm GF}$ approximately fixed. For each value of $u_{\rm GF}$ we have again determined the step-scaling function $\Sigma_{\rm P}$ of Eq. (7.2.7) at three different values of the lattice spacing, now using lattices of size $T/a = L/a = 8, 12, 16$, and double lattices of size $L/a = 16, 24, 32$. This allows to better tackle cutoff effects, which are expected to be larger because of the stronger coupling, and the larger scaling violations exhibited by $u_{\rm GF}$ with respect to $u_{\rm SF}$ [11]. Simulations have been carried out using a tree-level improved Symanzik gauge action [69], and an O(a) fermion action [67] with the non-perturbative value of the improvement coefficient $c_{\rm sw}$ and one-loop values of the coefficients $c_{\rm t}, \tilde{c}_{\rm t}$ for boundary improvement counterterms. The chiral point is set using the same strategy as before [97, 10]. In contrast to the high energy region, here the coupling constant $\bar{g}^2_{\rm GF}$ and Z_P are measured on the same ensembles, and hereafter we take these correlations into account in our analysis.

As discussed in Section 7.2, computations are carried out at fixed topological charge $Q = 0$. The main motivation for this is the onset of topological freezing [117] within the range of bare coupling values covered by our simulations; setting $Q = 0$ allows to circumvent the large computational cost required to allow the charge to fluctuate in the ensembles involved. The projection is implemented as proposed in [10]. In practice, this is only an issue for the finest ensembles at the largest values of $u_{\rm GF}$ — for $u_{\rm GF} \lesssim 4$.

The results of our simulations are summarised in Table 7.6. Note that contrary to the high energy region, here the value of $u_{\rm GF}$ is not exactly tuned to a constant value for different L/a. In practice the slight mistuning is not visible when extrapolating our data to the continuum (Fig. 7.2, 7.3) , but in order to account for this effect, we decided to use the same global approach described in the previous section. This approach only requires to have pair of lattices of sizes L/a and $2L/a$ simulated at the same values of the bare parameters.

Moreover, there is no guarantee that when computing $\overline{m}(\mu_0/2)/\overline{m}(\mu_{\rm had})$ the scale factor $\mu_{\rm had}/\mu_0$ is an integer power (indeed, our SSF setup would require a step $\propto 2$). This speaks in favour of performing also this part of the analysis using the anomalous

dimension. As in the previous section, we will use the available information on the β-function eq. (7.2.18). We will parametrize the ratio of RG functions

$$f(x) = \frac{\tau(x)}{\beta(x)} = \frac{1}{x}\sum_{n=0}^{n_f} f_n x^{2n}\,, \tag{7.4.1}$$

and determine the fit parameters f_n via a fit to the usual relation

$$\log\left[\Sigma_{\rm P}(u,a/L) - \rho(u)(a/L)^2\right] = -\int_{\sqrt{u}}^{\sqrt{\sigma(u)}} dx\, f(x)\,. \tag{7.4.2}$$

Once more $\rho(u)$ describes the cutoff effects in $\sigma_{\rm P}(u)$.

When the fit parameters f_n are determined, we can reconstruct the anomalous dimension thanks to the relation

$$f(\bar g) = \frac{\tau(\bar g)}{\beta(\bar g)} \quad\Longrightarrow\quad \tau(\bar g) = -\bar g^2 \frac{\sum_{n=0}^{n_f} f_n \bar g^{2n}}{\sum_{k=0}^{k_t} p_k \bar g^{2k}}\,. \tag{7.4.3}$$

(Recall that the parameters p_n define our β-function in eq. (7.2.18)).

As for the high energy region, we also report our fit results in Tab 7.8 where a comparison with u-by-u analysis is provided only as a cross-check. In the table *FIT1* and *FIT2* differ by the definition of the cutoff effect. In the first case $\rho(u) = \sum_{n=0}^{n_\rho} r_n (a/L)^2 u^n$ while in the second case the lowest order in u is $\mathcal{O}(u)$. From our best fit labelled in Tab 7.8 as *FIT2* $n_f = 2$ $n_\rho = 2$, we quote the value of parameters f_n:

$$f_0 = 0.84(6)\,, \tag{7.4.4}$$
$$f_1 = -0.010(27)\,, \tag{7.4.5}$$
$$f_2 = 0.008(3)\,, \tag{7.4.6}$$

with covariance

$$C = \begin{pmatrix} 0.416511\times10^{-2} & -0.165838\times10^{-2} & 0.153855\times10^{-3} \\ -0.165838\times10^{-2} & 0.734154\times10^{-3} & -0.745845\times10^{-4} \\ 0.153855\times10^{-3} & -0.745845\times10^{-4} & 0.835009\times10^{-5} \end{pmatrix}, \tag{7.4.7}$$

It worth to notice, that f_0 is compatible within less than one standard deviation with the perturbative value $d_0/b_0 = 0.8889$.

7.5 Hadronic matching and total renormalisation factor

The last step in our strategy requires the computation of quark mass renormalisation factors of bare PCAC masses $Z_{\rm m}$ at hadronic scales, cf. Eq. (7.3.2). The latter can be written as

$$Z_{\rm m}(g_0^2, a\mu_{\rm had}) = \frac{Z_{\rm A}(g_0^2)}{Z_{\rm P}(g_0^2, a\mu_{\rm had})} \tag{7.5.1}$$

Since the values of the axial current normalisation $Z_{\rm A}$ are available from a separate computation [118, 96, 119], in order to obtain $Z_{\rm m}$ we just need to determine $Z_{\rm P}(g_0^2, a\mu_{\rm had})$ at a fixed value of $\mu_{\rm had}$ for changing bare coupling g_0^2. The values of g_0^2 have to be in the range used in large-volume simulations; for practical purposes, we will thus target the interval $\beta \in [3.40, 3.85]$ currently covered by CLS ensembles [56].

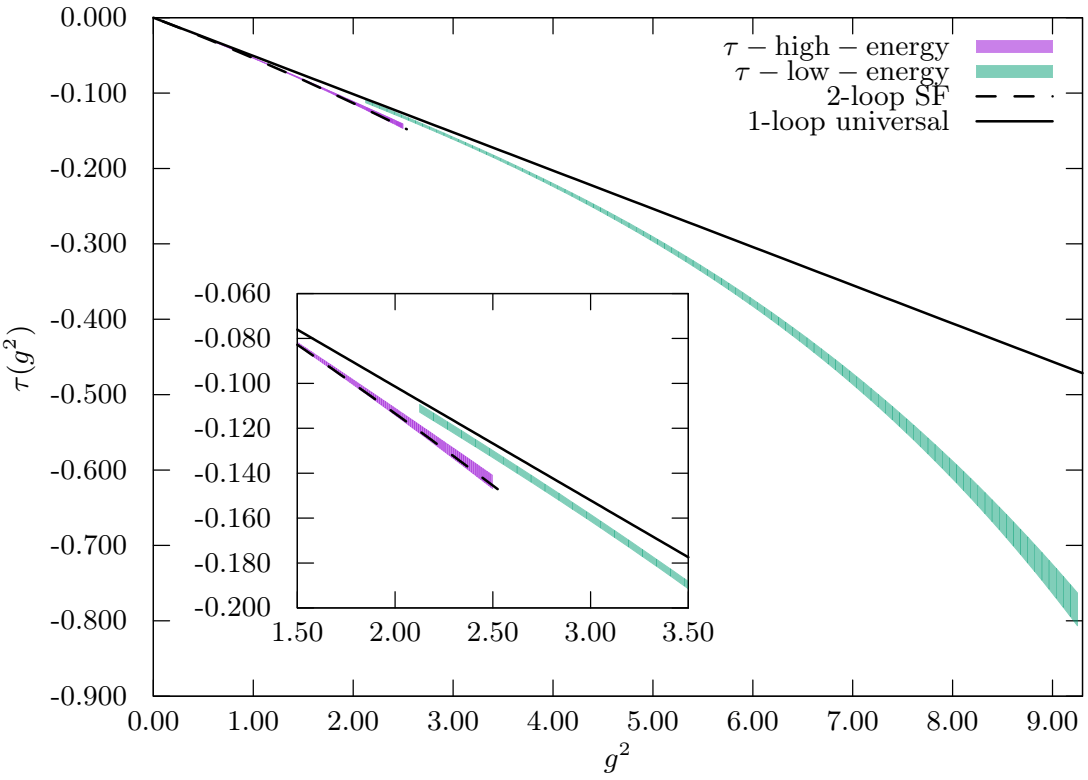

FIGURE 7.7: Non-perturbative mass anomalous dimension in the two energy regions. A comparison with universal 1-loop and SF 2-loop anomalous dimension is displayed.

Our strategy proceeds as follows. We first choose a value of $u_{\rm had} = \bar{g}^2_{\rm GF}(\mu_{\rm had})$ such that the relevant interval of values of g_0^2 is covered using accessible values of L/a. The precise value of $u_{\rm had}$ is fixed by simulating at one of the finest lattices. Finally, other lattice sizes are simulated, such that we can obtain an interpolating formula for $Z_{\rm P}(g_0^2, a\mu_{\rm had})$ as a function of g_0^2 along the line of constant physics fixed by $u_{\rm had}$. In order to have a crosscheck of the final result for renormalised masses, we have devised two different lines of constant physics, given by $u_{\rm had} = 8.63$ and $u_{\rm had} = 9.25$, respectively. In the first case (which does not cover the CLS finest ensembles) we have fixed the value of $u_{\rm had}$ by simulating on an $L/a = 16$ lattice at $\beta = 3.70$; lattice sizes $L/a = 12, 10, 8$ are then used at smaller β. In the second case, the value of $u_{\rm had}$ has been fixed by simulating on an $L/a = 20$ lattice at $\beta = 3.79$; lattice sizes $L/a = 16, 12, 10$ have then been used at smaller β, and two $L/a = 24$ lattices have been added so that the finest $\beta = 3.85$ point can be safely interpolated. Using the results in [98], the values of $u_{\rm had}$ we consider can be translated into hadronic matching energy scales as

$$\begin{aligned} u_{\rm had} = 9.25 \quad &\leftrightarrow \quad \mu_0/19.05(36) = \mu_{\rm had} \approx 221(4)\ \text{MeV}\,, \\ u_{\rm had} = 8.63 \quad &\leftrightarrow \quad \mu_0/17.77(34) = \mu_{\rm had} \approx 236(4)\ \text{MeV}\,, \end{aligned} \tag{7.5.2}$$

while our smallest SF coupling

$$min(u_{\rm SF}) = 1.1100 \quad \leftrightarrow \quad \mu_0 \times 27.04(60) = \mu_{\rm pt} \approx 114(3)\ \text{GeV}\,, \tag{7.5.3}$$

Our simulation results are summarised in Table 7.9. Deviations from the target values of $u_{\rm had}$ induce a small but visible effect on $Z_{\rm P}$, that can be safely described by a linear term in $(u_{\rm GF} - u_{\rm had})$ in the fit function. The measured values of the PCAC mass are often beyond our tolerance $|Lm| \lesssim 0.001$ (cf. App. 7.6), especially for the smaller lattice sizes.

This is a consequence of the fact that the interpolating formula for κ_c as a function of g_0^2 loses precision for $L/a = 10$, and of the small cutoff effect induced by computing at zero topological charge (which is part of our renormalisation condition). The dependence of Z_P on this effect is however very small, and again it can be safely fitted with a linear term in Lm. The $L/a = 8$ lattices employed for the matching at $u_{\rm had} = 8.63$ yield the target value of $u_{\rm GF}$ at a value of β significantly below 3.40. In this regime the GF coupling exhibits significant cutoff effects. Consequently, these lattices will be dropped from our fits. Note that, with this latter restriction, the values of Z_P that enter the fit functions at either value of $u_{\rm had}$ are never further away than 2.6 standard deviations from the value on the lattice that defines the line of constant physics. The fitted dependences on g_0^2, $u_{\rm GF}$, and Lm are thus very mild.

The measured values of Z_P are fitted to a function of the form

$$\begin{aligned} Z_P(g_0^2, u_{\rm GF}, Lm) &= Z_P^{\rm had}(g_0^2) + t_1\,(u_{\rm GF} - u_{\rm had}) + t_2\,Lm\,, \\ Z_P^{\rm had}(g_0^2) &= z_0 + z_1(\beta - \beta_0) + z_2(\beta - \beta_0)^2\,, \end{aligned} \tag{7.5.4}$$

where $u_{\rm had}$ is the target value and we fix $\beta_0 = 3.70$ and $\beta_0 = 3.79$ for $u_{\rm had} = 8.63$ and $u_{\rm had} = 9.25$, respectively. As discussed above, the terms with t_1 and t_2 parameterise the small deviations from the intended lines of constant physics, while $Z_P^{\rm had}$ is the interpolating function we are interested in. Note that the ensembles are fully uncorrelated among them, but within each ensemble the values of $u_{\rm GF}$, Lm, and Z_P are strongly correlated, which we take into account in the fit procedure. The results we obtain for $Z_P^{\rm had}$ are

$$z_0 = 0.3685\,, \quad z_1 = 0.0233\,, \quad z_2 = 0.1240\,, \qquad u_{\rm had} = 8.63\,; \tag{7.5.5}$$

$$z_0 = 0.3488\,, \quad z_1 = 0.0187\,, \quad z_2 = 0.0643\,, \qquad u_{\rm had} = 9.25\,, \tag{7.5.6}$$

with covariance matrices for fit parameters

$$C = \begin{pmatrix} 0.100327 \times 10^{-5} & 0.945168 \times 10^{-5} & 0.208942 \times 10^{-4} \\ 0.945168 \times 10^{-5} & 0.291366 \times 10^{-3} & 0.112858 \times 10^{-2} \\ 0.208942 \times 10^{-4} & 0.112858 \times 10^{-2} & 0.485953 \times 10^{-2} \end{pmatrix}, \qquad u_{\rm had} = 8.63\,; \tag{7.5.7}$$

$$C = \begin{pmatrix} 0.317679 \times 10^{-6} & 0.148966 \times 10^{-6} & -0.227555 \times 10^{-5} \\ 0.148966 \times 10^{-6} & 0.243264 \times 10^{-4} & 0.645229 \times 10^{-4} \\ -0.227555 \times 10^{-5} & 0.645229 \times 10^{-4} & 0.206467 \times 10^{-3} \end{pmatrix}, \quad u_{\rm had} = 9.25\,. \tag{7.5.8}$$

The respective values of the $\chi^2/\text{d.o.f.}$ are $0.26/2$ and $3.41/6$. The typical precision of the values of Z_P extracted from the interpolating function is thus at the few permille level.[5] The fits are illustrated in Fig. 7.8.

Now we can finally assemble the various factors entering (i.e. running factor and hadronic renormalization constants). Using the results from the previous section (low energy region) we can compute the running $\overline{m}(\mu_0/2)/\overline{m}(\mu_{\rm had})$ between the scheme-switching scale and hadronic matching scale, and multiply it times the value of $M/\overline{m}(\mu_0/2)$ given in Eq. (7.3.10). Combining the errors in quadrature, we obtain

$$\frac{M}{\overline{m}(\mu_{\rm had})} = \begin{cases} 0.966(9)\,, & u_{\rm had} = 8.63\,; \\ 0.919(10)\,, & u_{\rm had} = 9.25\,. \end{cases} \tag{7.5.9}$$

[5] In the case of $u_{\rm had} = 8.63$, the extrapolations to $\beta = 3.4$ and $\beta = 3.85$ yield errors of 0.5% and 1.2%, respectively, which shows that precision is rapidly lost outside the region covered by data. In the $u_{\rm had} = 9.25$ case the errors are 0.13% and 0.34%.

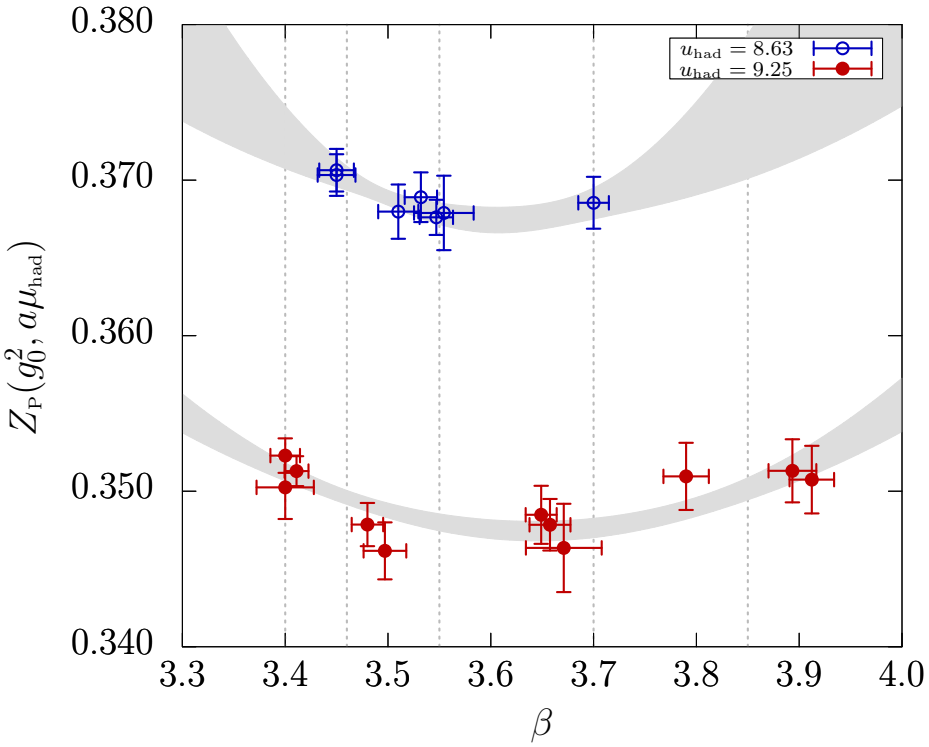

FIGURE 7.8: Projection on the $(\beta, Z_{\rm P})$ plane of the fits to $Z_{\rm P}$ (grey bands) at the two hadronic matching points, $u_{\rm had} = 8.63$ (open blue points) and $u_{\rm had} = 9.25$ (filled red points). The data points have been shifted to the target value of $u_{\rm GF}$ and $Lm = 0$ using the fit function. Horizontal error bars have been assigned to reflect the uncertainties coming from the value of $u_{\rm GF}$ for each point, by defining $\Delta g_0^2/g_0^2 = \Delta u_{\rm GF}/u_{\rm GF}$. Vertical dashed lines correspond to the β values of CLS ensembles.

The precision of these numbers is 1% and 1.1%, respectively. It is important to stress that the latter result is given in the SF − GF scheme and holds in the continuum, i.e. it is independent of any detail of the lattice computation. We can then take our interpolating formula for $Z_{\rm P}$ and the known results for $Z_{\rm A}$, and build the total factor $Z_{\rm M}$ that relates bare PCAC masses computed with a Wilson fermion action to RGI masses,

$$Z_{\rm M}(g_0^2) = \frac{M}{\overline{m}(\mu_{\rm had})} \frac{Z_{\rm A}(g_0^2)}{Z_{\rm P}(g_0^2, a\mu_{\rm had})} \,. \tag{7.5.10}$$

Recall that the dependence of $Z_{\rm M}$ on $\mu_{\rm had}$ has to cancel exactly, up to residual terms in the cutoff effects of $Z_{\rm M}(g_0^2)m(g_0^2)$. Using as input the very precise determination of $Z_{\rm A}$ in [96, 119],[6] and our results for $Z_{\rm P}$ at $u_{\rm had} = 9.25$, we finally obtain the interpolating formula

$$\begin{gathered} Z_{\rm M}(g_0^2) = Z_{\rm M}^{(0)} + Z_{\rm M}^{(1)}(\beta - 3.79) + Z_{\rm M}^{(2)}(\beta - 3.79)^2 \,; \\ Z_{\rm M}^{(0)} = 2.2799 \times \frac{M}{\overline{m}(\mu_{\rm had})} \,, \quad Z_{\rm M}^{(1)} = 0.0997 \times \frac{M}{\overline{m}(\mu_{\rm had})} \,, \quad Z_{\rm M}^{(2)} = -0.3059 \times \frac{M}{\overline{m}(\mu_{\rm had})} \,, \end{gathered} \tag{7.5.11}$$

[6] We thank the authors of [96, 119] for the private communication of the final results for $Z_{\rm A}$ prior to publication.

β	$Z_{\rm M}$	$Z_{\rm M}^{\rm tm}$
3.40	2.016(22)	2.615(29)
3.46	2.033(23)	2.627(29)
3.55	2.056(23)	2.639(30)
3.70	2.084(23)	2.642(30)
3.85	2.099(23)	2.623(30)

TABLE 7.4: Values of the renormalisation factors $Z_{\rm M}^{\rm w}$ and $Z_{\rm M}^{\rm tm}$ connecting RGI and bare PCAC masses in the standard Wilson and twisted-mass cases, respectively, at the values of β for CLS ensembles.

with covariance matrix

$$C = \begin{pmatrix} 0.135692 \times 10^{-4} & 0.953937 \times 10^{-5} & -0.868592 \times 10^{-4} \\ 0.953937 \times 10^{-5} & 0.130764 \times 10^{-2} & 0.342913 \times 10^{-2} \\ -0.868592 \times 10^{-4} & 0.342913 \times 10^{-2} & 0.107999 \times 10^{-1} \end{pmatrix} \times \left[\frac{M}{\overline{m}(\mu_{\rm had})}\right]^2 . \tag{7.5.12}$$

The quoted errors only contain the uncertainties from the determination of $Z_{\rm A}$ and $Z_{\rm P}$ at the hadronic scale. The error of the total running factor for $u_{\rm had} = 9.25$ in Eq. (7.5.9) has to be added in quadrature to the error in the final result for the RGI mass, since it only affects the continuum limit.

Finally, our results can be also used to obtain renormalised quark masses when a twisted-mass QCD Wilson fermion regularisation [120, 121] is employed in the computation. In that case the bare PCAC mass coincides with the bare twisted mass parameter, which can be renormalised with

$$Z_{\rm m}^{\rm tm}(g_0^2, a\mu_{\rm had}) = \frac{1}{Z_{\rm P}(g_0^2, a\mu_{\rm had})} . \tag{7.5.13}$$

The total renormalisation factor then acquires the form

$$Z_{\rm M}^{\rm tm}(g_0^2) = \frac{M}{\overline{m}(\mu_{\rm had})} \frac{1}{Z_{\rm P}(g_0^2, a\mu_{\rm had})} , \tag{7.5.14}$$

and values can be obtained by directly using our interpolating formula for $Z_{\rm P}^{\rm had}$.

The same comment about uncertainties as above applies.

Eqs. (7.5.9,7.5.11,7.5.14) are the final, and most important, results of this work. Recall that, contrary to the running factor, which depends only on the renormalisation scheme, the expressions for $Z_{\rm M}$ and $Z_{\rm M}^{\rm tm}$ depend on the action used in the computation, and hold for a non-perturbatively O(a) improved fermion action and a tree-level Symanzik improved gauge action. The values of $Z_{\rm M}$ and $Z_{\rm M}^{\rm tm}$ at the β values of CLS ensembles are given in Table 7.4.

7.6 Systematic uncertainties in the determination of step-scaling functions

7.6.1 Tuning of the critical mass

The tuning of the chiral point, as part of setting our lines of constant physics, is treated in detail in [97, 10]. Briefly, a set of tuning runs at various values of β and κ are used to compute the PCAC mass m in Eq. (7.2.4), and interpolate at fixed β values for $\kappa_{\rm c}$ such that $Lm \leq 0.001$, with an uncertainty of at most the same order. This implies that the values

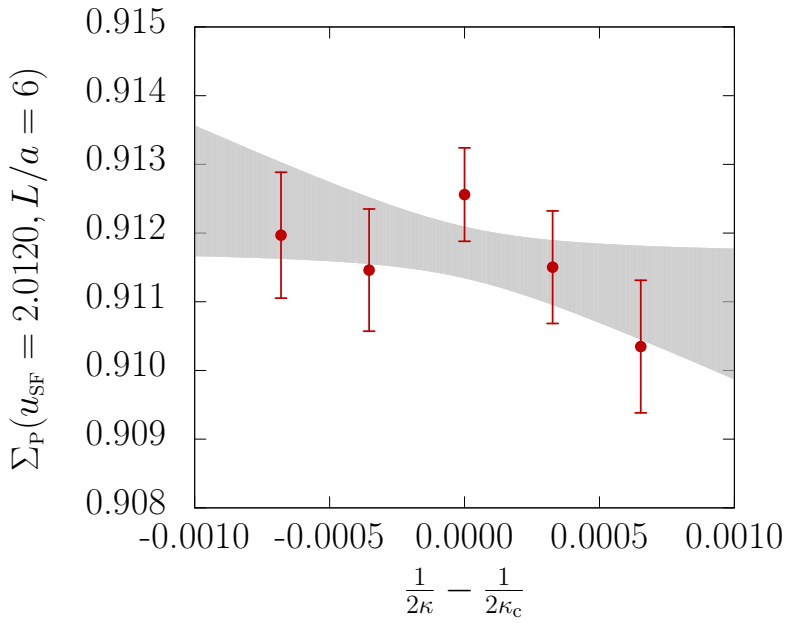

FIGURE 7.9: Variation of the ssf $\Sigma_{\rm P}(u_{\rm SF} = 2.0120, L/a = 6)$ with the value of the quark mass. The shadowed band is a linear fit of the data.

of the quark mass at which the renormalisation condition in Eq. (7.2.11) is imposed are not exactly zero.

In order to assess the relevant systematics, we have performed a dedicated set of simulations at strongest coupling covered in the SF − SF scheme, $u_{\rm SF} = 2.0120$, where the value of $\Sigma_{\rm P}(2.0120, L/a = 6)$ has been computed at the same value of $\beta = 6.2735$ indicated in Table 7.5, and four different values of κ, on top of the nominal one for $\kappa_{\rm c}$ given in Table 7.5. This is expected to be the simulation point within the high-energy regime where this systematics may have a stronger impact. The result of this exercise is shown in Fig. 7.9. A linear fit to the data allows to estimate the slope coefficient

$$\rho_{\kappa_{\rm c}} \equiv \frac{1}{L} \left. \frac{\partial \Sigma_{\rm P}}{\partial m} \right|_{u,L} , \tag{7.6.1}$$

which can then be used to assign a systematic uncertainty to $\Sigma_{\rm P}$ as

$$\delta_{\kappa_{\rm c}} \Sigma_{\rm P} = \rho_{\kappa_{\rm c}} {\rm tol}(Lm) \, , \tag{7.6.2}$$

where ${\rm tol}(Lm) = 0.001$ is our tolerance for defining the critical point. We obtain $\rho_{\kappa_{\rm c}} = -0.15(15)$, which implies that the systematic uncertainty can be estimated as $\delta_{\kappa_{\rm c}} \Sigma_{\rm P} = 0.00015(15)$.[7]

Besides being compatible with zero within 1σ, the central value is more than four times smaller than the statistical uncertainty quoted for $\Sigma_{\rm P}(2.0120, L/a = 6)$ in Table 7.5. For larger lattices or smaller values of the renormalised coupling this systematics is expected to decrease further. On the other hand, it will be larger as the value of the renormalised coupling is increased, but there is no obvious reason why its relative size with respect to the statistical uncertainty may grow as well. We thus conclude that the systematic uncertainty related to the tuning to zero quark mass is negligible at the level of precision we attain in the computation of $\sigma_{\rm P}$.

[7] Our value for the slope $\rho_{\kappa_{\rm c}}$ is in the same ballpark as the ones obtained in [72], where a similar study using $N_{\rm f} = 2$ simulations was performed at values of the SF coupling $u_{\rm SF} = 0.9793$ and $u_{\rm SF} = 2.4792$, finding $\rho_{\kappa_{\rm c}} = -0.0755(10)$ and $\rho_{\kappa_{\rm c}} = -0.1130(27)$, respectively.

7.6.2 Tuning of the gauge coupling

Our lines of constant physics are formally defined by a nominal value of either the SF or the GF coupling, that is to be kept fixed in the lattices at which the denominator of Eq. (7.2.7) is computed. In practice, this is so only within some finite precision, due to two different reasons:

(i) The value of either $u_{\rm SF}$ or $u_{\rm GF}$ is itself computed to within some finite precision.

(ii) In the computations in the SF $-$ SF scheme, the value of the coupling, and the corresponding tuning of β and κ, is performed using independent ensembles with respect to the ones employed for the computation of $Z_{\rm P}$, due to the need to work at non-vanishing background field. The resulting lines of constant physics are expected to differ by $\mathrm{O}(a^2)$ effects.

In order to assess whether the finite precision on the value of the gauge coupling has an impact on the computation of the continuum $\sigma_{\rm P}$, we have

(i) repeated the continuum-limit extrapolations of $\Sigma_{\rm P}$ at fixed u, introducing a horizontal error on the value of $(a/L)^2$ propagated from the uncertainty on u at each value of a/L. To that purpose one can use either the perturbative relation between u and L, or the known non-perturbative β functions [97, 10], with little practical differences.

(ii) repeated fits to the continuum-extrapolated $\sigma_{\rm P}$ as a function of u, introducing an uncertainty on u that covers the spread of the computed values along that particular line of constant physics.

In either case, we have found that the impact of introducing the additional uncertainties in the final description of $\sigma_{\rm P}$ are negligible within our current level of precision. This source of systematic uncertainty is therefore ignored in our final analyses.

7.6.3 Perturbative values of boundary improvement coefficients

In our computation, we use perturbative values for the coefficients $c_{\rm t}$ and $\tilde{c}_{\rm t}$ that appear in Schrödinger Functional boundary $\mathrm{O}(a)$ improvement counterterms, employing the highest available order for the relevant lattice action. In computations in the high-energy region, where the plaquette gauge action is used, we are able to use the corresponding two-loop value of $c_{\rm t}$ [37]. In the low-energy region, where the gauge action is tree-level Symanzik improved, the two-loop coefficient is not known, and we take the one-loop value. In the case of $\tilde{c}_{\rm t}$, we employ the one-loop value throughout. Contributions from these boundary counterterms to the step-scaling function $\sigma_{\rm P}$ start at two-loop order in perturbation theory, and the effects of perturbative truncation in the values of $c_{\rm t}, \tilde{c}_{\rm t}$ are therefore expected to be small. A careful study of these systematic uncertainties in the SF-SF scheme was carried out in the $N_{\rm f} = 0$ [72] and $N_{\rm f} = 2$ [43] computations. Especially in the former case, a precise statement could be made that perturbative truncation effects do not change the result for the continuum limit of $\Sigma_{\rm P}$ even at the largest values of the coupling. In our computation, we have performed a dedicated analysis at two values of the coupling, to check the size of the resulting effects in both the SF $-$ SF and SF $-$ GF schemes.

In order to have a quantitative handle on the effect from a shift on boundary improvement coefficients, let us formally expand $Z_{\rm P}$, considered as a function of, e.g., $c_{\rm t}$, in a power series of the form

$$Z_{\rm P} + \frac{\partial Z_{\rm P}}{\partial c_{\rm t}} \left(\frac{a}{L}\right) \Delta c_{\rm t} + \ldots \tag{7.6.3}$$

where $\Delta c_{\rm t}$ is the deviation with respect to the value of $c_{\rm t}$ at which $Z_{\rm P}$ is computed. The factor (a/L) is made explicit to stress that the perturbative truncation is leaving uncancelled $\mathcal{O}(a)$ terms, which we are parameterising. By simulating at a number of values of $c_{\rm t}$, keeping all other simulation parameters fixed, it is possible to estimate the slope $(\partial Z_{\rm P}/\partial c_{\rm t})$. A systematic uncertainty can then be assigned to $Z_{\rm P}$ as

$$\delta_{c_{\rm t}} Z_{\rm P} \approx \left|\frac{\partial Z_{\rm P}}{\partial c_{\rm t}}\right| \left(\frac{a}{L}\right) \delta c_{\rm t}\,, \tag{7.6.4}$$

where $\delta c_{\rm t}$ is some conservative estimate of the perturbative truncation error. Linear error propagation then yields the corresponding systematic uncertainty on $\Sigma_{\rm P} = Z_{\rm P}(2L)/Z_{\rm P}(L)$ as

$$\frac{\delta_{c_{\rm t}} \Sigma_{\rm P}}{\Sigma_{\rm P}} \approx \left|\frac{\partial Z_{\rm P}}{\partial c_{\rm t}} \left[\frac{1}{2Z_{\rm P}(2L)} - \frac{1}{Z_{\rm P}(L)}\right]\right| \left(\frac{a}{L}\right) \delta c_{\rm t}\,. \tag{7.6.5}$$

The systematic uncertainty due to the truncation in the value of $\tilde{c}_{\rm t}$ can be estimated in exactly the same way.

We have performed dedicated simulations to estimate $(\partial Z_{\rm P}/\partial c_{\rm t})$ and $(\partial Z_{\rm P}/\partial \tilde{c}_{\rm t})$ in the SF $-$ SF scheme at $u = 2.0120$ and in the SF $-$ GF scheme at $u = 4.4901$, considering several values of $c_{\rm t}$ and $\tilde{c}_{\rm t}$ in an interval given by artificially augmenting the size of the perturbative correction to the tree-level value 1 by factors of up to 4. The simulations are performed in $L/a = 6$ and $L/a = 8$ lattices, which should be affected by the largest uncertainty. The results are illustrated in Fig. 7.10. By fitting the results for $Z_{\rm P}$ linearly in the value of the improvement coefficient we find

$$\left.\frac{\partial Z_{\rm P}}{\partial c_{\rm t}}\right|_{\rm SF-SF;\, L/a=6} = -0.016(15)\,, \qquad \left.\frac{\partial Z_{\rm P}}{\partial \tilde{c}_{\rm t}}\right|_{\rm SF-SF;\, L/a=6} = 0.022(21)\,; \tag{7.6.6}$$

$$\left.\frac{\partial Z_{\rm P}}{\partial c_{\rm t}}\right|_{\rm SF-SF;\, L/a=8} = -0.003(26)\,, \qquad \left.\frac{\partial Z_{\rm P}}{\partial \tilde{c}_{\rm t}}\right|_{\rm SF-SF;\, L/a=8} = -0.074(19)\,; \tag{7.6.7}$$

$$\left.\frac{\partial Z_{\rm P}}{\partial c_{\rm t}}\right|_{\rm SF-GF;\, L/a=8} = 0.110(14)\,, \qquad \left.\frac{\partial Z_{\rm P}}{\partial \tilde{c}_{\rm t}}\right|_{\rm SF-GF;\, L/a=8} = -0.090(4)\,. \tag{7.6.8}$$

If now we use values of $\Delta c_{\rm t}$ and $\Delta \tilde{c}_{\rm t}$ given by $1 - c_{\rm t}^{\rm pert}$ and $1 - \tilde{c}_{\rm t}^{\rm pert}$, respectively — i.e., we assign a 100% uncertainty to the perturbative correction to the tree-level value 1 — we finally obtain

$$u_{\rm SF} = 2.0120\,,\ L/a = 6: \qquad \delta_{c_{\rm t}} \Sigma_{\rm P} \approx 0.00014\,, \quad \delta_{\tilde{c}_{\rm t}} \Sigma_{\rm P} \approx 0.000063\,; \tag{7.6.9}$$

$$u_{\rm SF} = 2.0120\,,\ L/a = 8: \qquad \delta_{c_{\rm t}} \Sigma_{\rm P} \approx 0.000019\,, \quad \delta_{\tilde{c}_{\rm t}} \Sigma_{\rm P} \approx 0.00015\,; \tag{7.6.10}$$

$$u_{\rm GF} = 4.4901\,,\ L/a = 8: \qquad \delta_{c_{\rm t}} \Sigma_{\rm P} \approx 0.00037\,, \quad \delta_{\tilde{c}_{\rm t}} \Sigma_{\rm P} \approx 0.00014\,. \tag{7.6.11}$$

In all cases, these figures are much smaller than the quoted statistical error of $\Sigma_{\rm P}$. This justifies neglecting this source of systematic uncertainty in our analysis.

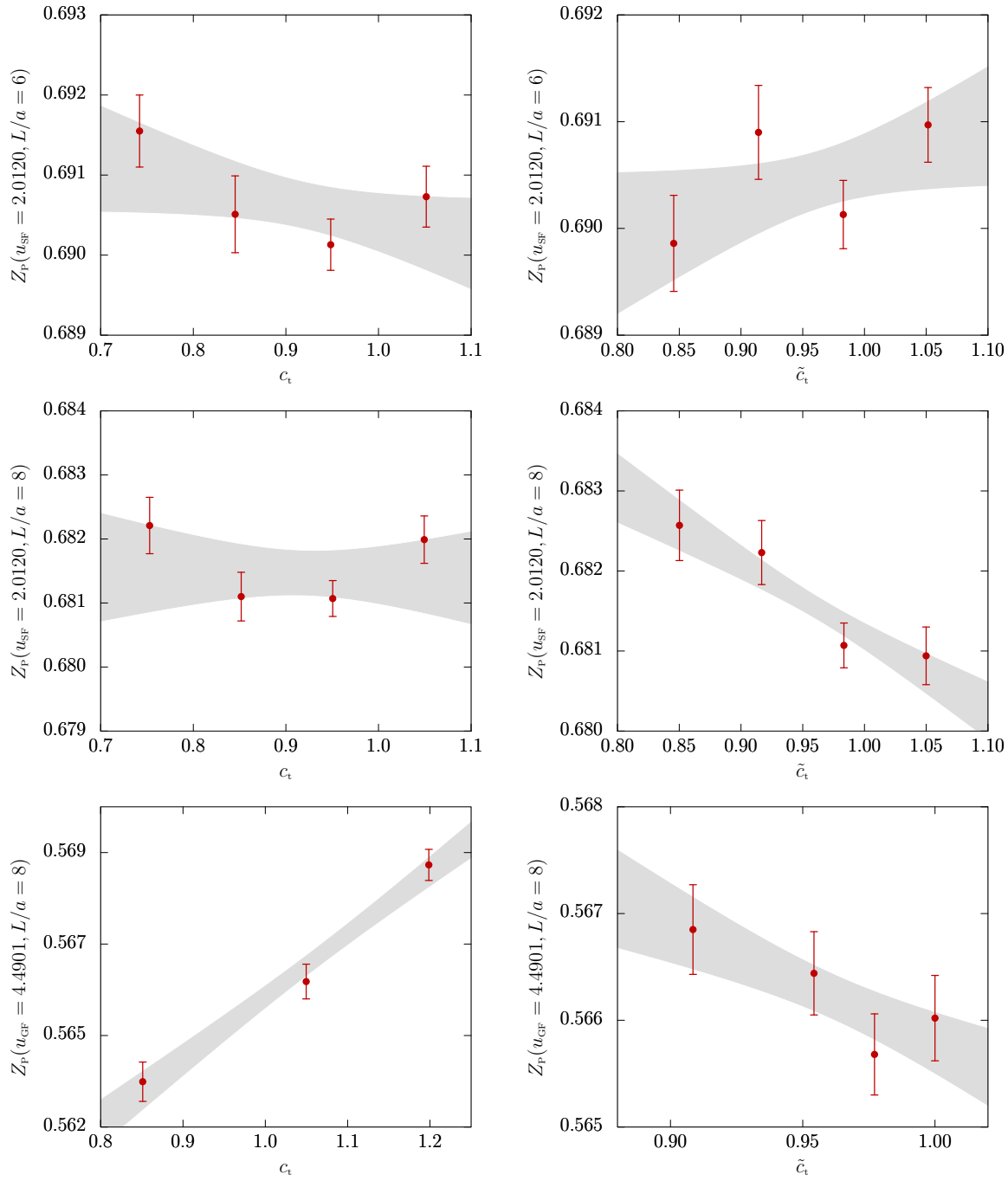

FIGURE 7.10: Variation of $Z_{\rm P}$ with the value of the boundary improvement coefficients $c_{\rm t}$ and $\tilde{c}_{\rm t}$. The shadowed bands are linear fits to the data.

$u_{\rm SF}$	L/a	β	κ	$Z_{\rm P}(g_0^2, L/a)$	$Z_{\rm P}(g_0^2, 2L/a)$	$\Sigma_{\rm P}(g_0^2, L/a)$	$\sigma_{\rm P}(u_{\rm SF})$	$\rho_P(u_{\rm SF})$	χ^2/d.o.f.
	6	8.5403	0.13233610	0.80494(22)	0.76879(24)	0.95587(40)(78)			
1.11000	8	8.7325	0.13213380	0.79640(22)	0.76163(34)	0.95625(50)(10)	0.9577(10)	-0.079(56)	0.64
	12	8.9950	0.13186210	0.78473(29)	0.75167(59)	0.95762(83)(24)			
	6	8.2170	0.13269030	0.79463(25)	0.75594(25)	0.95213(43)(82)			
1.18446	8	8.4044	0.13247670	0.78532(21)	0.74943(39)	0.95420(56)(10)	0.9558(10)	-0.122(58)	0.50
	12	8.6769	0.13217153	0.77426(30)	0.73937(49)	0.95468(73)(25)			
	6	7.9091	0.13305720	0.78344(24)	0.74256(25)	0.94870(44)(88)			
1.26569	8	8.0929	0.13283120	0.77369(23)	0.73483(43)	0.94967(62)(11)	0.9512(10)	-0.093(61)	0.03
	12	8.3730	0.13249231	0.76349(33)	0.72601(49)	0.95064(76)(27)			
	6	7.5909	0.13346930	0.77034(25)	0.72691(26)	0.94457(46)(94)			
1.3627	8	7.7723	0.13322830	0.76036(24)	0.71893(42)	0.94539(63)(11)	0.9482(11)	-0.149(66)	1.11
	12	8.0578	0.13285365	0.74937(35)	0.71036(52)	0.94766(83)(29)			
	6	7.2618	0.13393370	0.75460(27)	0.70808(31)	0.93937(53)(101)			
1.4808	8	7.4424	0.13367450	0.74425(26)	0.70004(33)	0.94047(55)(13)	0.9415(11)	-0.071(66)	0.06
	12	7.7299	0.13326353	0.73515(33)	0.69193(42)	0.94090(72)(31)			
	6	6.9433	0.13442200	0.73740(28)	0.68692(29)	0.93265(52)(110)			
1.6173	8	7.1254	0.13414180	0.72670(26)	0.67983(49)	0.93536(76)(14)	0.9359(15)	-0.086(82)	2.56
	12	7.4107	0.13369922	0.71777(41)	0.67071(75)	0.9341(12)(3)			
	6	6.6050	0.13498290	0.71606(29)	0.65960(32)	0.92237(58)(121)			
1.7943	8	6.7915	0.13467650	0.70597(29)	0.65418(67)	0.9265(10)(2)	0.9298(15)	-0.250(84)	0.63
	12	7.0688	0.13420891	0.69553(40)	0.64543(63)	0.9276(11)(4)			
	6	6.2735	0.13557130	0.69013(32)	0.62979(37)	0.91391(68)(134)			
2.0120	8	6.4680	0.13523620	0.68107(28)	0.62341(43)	0.91518(74)(17)	0.9149(10)	-0.006(69)	0.59
	12	6.72995	0.13475973	0.67113(43)	0.61452(49)	0.91523(93)(41)			
	16	6.93460	0.13441209	0.66627(31)	0.60924(66)	0.9141(11)(3)			

TABLE 7.5: Results for $Z_{\rm P}$, 1-loop corrected $\Sigma_{\rm P}$, and $\sigma_{\rm P}$ in the SF $-$ SF scheme. The first uncertainty on $\Sigma_{\rm P}$ is the statistical error, while the second one is given by the difference between the 1-loop corrected data and raw one, as discussed in the main text. The combination in quadrature of the two source of uncertainty is taken into account in the analysis. The value of $\sigma_{\rm P}$ is obtained from a continuum-limit extrapolation fitting all three points linearly in $(a/L)^2$, subtracting one-loop cutoff effects to all orders in a; and the corresponding slope ρ_P and χ^2.

$u_{\rm GF}$	L/a	β	κ	$Z_{\rm P}(g_0^2, L/a)$	$Z_{\rm P}(g_0^2, 2L/a)$	$\Sigma_{\rm P}(g_0^2, L/a)$	$\sigma_{\rm P}(u_{\rm GF})$	$\rho_P(u_{\rm GF})$	χ^2
2.1269(15)	8	5.371500	0.13362120	0.73275(26)	0.67666(55)	0.92345(82)			
2.1229(12)	12	5.543070	0.13331407	0.71301(33)	0.65748(85)	0.9221 (12)	0.9163(14)	0.47(12)	6.12
2.1257(25)	16	5.700000	0.13304840	0.70248(31)	0.64369(85)	0.9163 (13)			
2.3913(15)	8	5.071000	0.13421678	0.71024(32)	0.64872(59)	0.91338(93)			
2.3912(10)	12	5.242465	0.13387635	0.69064(30)	0.62808(99)	0.9094 (15)	0.9061(16)	0.47(13)	0.003
2.3900(32)	16	5.400000	0.13357851	0.67890(35)	0.61636(95)	0.9079 (15)			
2.7365(14)	8	4.764900	0.13488555	0.68196(32)	0.61339(69)	0.8995 (11)			
2.7390(14)	12	4.938726	0.13450761	0.66137(42)	0.59091(84)	0.8935 (14)	0.8910(17)	0.53(15)	1.33
2.7359(36)	16	5.100000	0.13416889	0.65087(41)	0.58199(92)	0.8942 (15)			
3.2022(16)	8	4.457600	0.13560675	0.64779(34)	0.56891(78)	0.8782 (13)			
3.2053(17)	12	4.634654	0.13519986	0.62622(39)	0.54748(98)	0.8743 (16)	0.8702(20)	0.52(17)	0.14
3.2029(49)	16	4.800000	0.13482139	0.61735(43)	0.5382 (11)	0.8717 (19)			
3.8620(20)	8	4.151900	0.13632589	0.60377(37)	0.51002(78)	0.8447 (14)			
3.8635(21)	12	4.331660	0.13592664	0.58285(49)	0.4887 (14)	0.8384 (26)	0.8366(28)	0.51(22)	0.71
3.8643(64)	16	4.500000	0.13552582	0.57420(48)	0.4822 (14)	0.8398 (25)			
4.4855(25)	8	3.947900	0.13674684	0.56568(39)	0.4570 (11)	0.8079 (21)			
4.4867(28)	12	4.128217	0.13640300	0.54608(62)	0.4331 (10)	0.7931 (21)	0.7824(30)	1.62(27)	0.14
4.4901(75)	16	4.300000	0.13600821	0.54030(55)	0.4266 (16)	0.7895 (30)			
5.2928(28)	8	3.754890	0.13701929	0.52174(43)	0.3928 (29)	0.7528 (57)			
5.2972(36)	12	3.936816	0.13679805	0.50367(57)	0.3642 (21)	0.7231 (41)	0.7033(62)	3.12(65)	0.39
5.301(14)	16	4.100000	0.13647301	0.49847(79)	0.3579 (28)	0.7179 (54)			

TABLE 7.6: Results for $Z_{\rm P}$, $\Sigma_{\rm P}$, $\sigma_{\rm P}$ and $\rho_P(u_{\rm GF})$ in the SF $-$ GF scheme. The last two columns quote the value of $\sigma_{\rm P}$ obtained from a continuum-limit extrapolation fitting all three points linearly in $(a/L)^2$, and the corresponding slope $\rho(u_{\rm GF})$ and χ^2.

Fit	n_s	n_ρ	χ^2/dof	$k=0$	$k=1$	$k=2$	$k=3$	$k=4$	$k=5$
$u_k^{\rm SF}(\ldots, b_3^{\rm eff})$	–	–	–	2.0120	1.7126(31)	1.4939(38)	1.3264(38)	1.1936(35)	1.0856(32)
$u_k^{\rm SF}(\ldots, b_2)$	–	–	–	2.0120	1.71681	1.49909	1.33153	1.19840	1.08997
$u_k(b_0, b_1)$	–	–	–	2.0120	1.71635	1.49848	1.33090	1.19779	1.08939
ubyu									
FITA	4	–	4.7/5	0.91522(98)	0.8528(13)	0.8034(16)	0.7626(17)	0.7280(17)	0.6980(18)
FITA	5	–	4.4/4	0.91500(99)	0.8533(13)	0.8036(15)	0.7624(17)	0.7278(18)	0.6985(19)
FITB	4	–	5.1/6	0.91540(99)	0.8526(13)	0.8030(14)	0.7622(16)	0.7278(17)	0.6982(19)
FITB	5	–	3.3/5	0.91515(97)	0.8529(12)	0.8036(15)	0.7627(16)	0.7280(17)	0.6981(18)
global									
FITA	4	2	19.1/21	0.91682(63)	0.85406(93)	0.8040(12)	0.7625(14)	0.7274(15)	0.6972(16)
FITA	5	3	13.7/19	0.91550(85)	0.8528(12)	0.8031(14)	0.7623(15)	0.7278(17)	0.6982(19)
FITB	4	2	20.2/22	0.91698(72)	0.8540(11)	0.8037(13)	0.7623(15)	0.7273(16)	0.6972(17)
FITB	5	3	13.8/20	0.91551(94)	0.8527(13)	0.8031(15)	0.7623(17)	0.7278(18)	0.6981(19)
global with $L/a > 6$									
FITA	4	2	12.9/13	0.9157(10)	0.8525(16)	0.8021(20)	0.7604(23)	0.7252(24)	0.6948(23)
FITA	5	3	7.7/11	0.9142(11)	0.8514(15)	0.8017(17)	0.7608(20)	0.7264(22)	0.6970(25)
FITB	4	2	14.3/14	0.91595(91)	0.8524(15)	0.8018(18)	0.7602(21)	0.7251(23)	0.6950(24)
FITB	5	3	8.4/12	0.9143(12)	0.8513(16)	0.8016(19)	0.7608(21)	0.7264(24)	0.6967(26)
Anomalous dimension - u-by-u									
FITB	2	–	6.2/7	0.91794(86)	0.8552(13)	0.8051(15)	0.7636(16)	0.7286(17)	0.6984(17)
FITB	3	–	3.5/6	0.9159(11)	0.8533(14)	0.8036(16)	0.7628(17)	0.7282(18)	0.6985(19)
FITB	4	–	3.3/5	0.9156(11)	0.8532(13)	0.8037(16)	0.7629(17)	0.7282(17)	0.6983(18)
FITB	5	–	2.4/4	0.9151(10)	0.8534(13)	0.8036(15)	0.7624(16)	0.7279(16)	0.6984(17)
Anomalous dimension - global									
FITB	2	2	18.9/23	0.91758(87)	0.8547(13)	0.8044(15)	0.7629(17)	0.7278(17)	0.6976(18)
FITB	3	2	18.8/22	0.91749(88)	0.8546(12)	0.8043(15)	0.7628(16)	0.7278(17)	0.6976(18)
FITB	4	2	18.5/21	0.91685(80)	0.8542(11)	0.8040(14)	0.7626(16)	0.7275(17)	0.6972(18)
FITB	2	3	16.4/22	0.91772(85)	0.8549(13)	0.8047(15)	0.7632(16)	0.7282(17)	0.6980(17)
FITB	3	3	13.2/21	0.9155(12)	0.8527(14)	0.8031(16)	0.7623(17)	0.7278(19)	0.6981(20)
Anomalous dimension - global $L/a > 6$									
FITB	2	2	11.9/15	0.9165(11)	0.8530(17)	0.8024(20)	0.7608(21)	0.7256(22)	0.6954(23)
FITB	3	2	11.9/14	0.91661(99)	0.8531(15)	0.8025(18)	0.7608(21)	0.7256(22)	0.6954(24)
FITB	4	2	11.4/13	0.9159(10)	0.8527(15)	0.8023(19)	0.7606(22)	0.7253(23)	0.6950(25)
FITB	2	3	9.7/14	0.9165(11)	0.8532(16)	0.8027(19)	0.7611(21)	0.7259(21)	0.6958(22)
FITB	3	3	7.2/13	0.9144(14)	0.8514(17)	0.8017(18)	0.7609(20)	0.7264(22)	0.6967(24)
Perturbation theory prediction									
s1,s2			13/8	0.90797	0.84057	0.78808	0.74552	0.70998	0.67966

TABLE 7.7: Ratios $R^{(k)} = \bar{m}(2^k\mu_0)/\bar{m}(\mu_0/2)$

Fit	n_f	n_ρ	χ^2/dof	$k=0$	$k=1$	$k=2$	$\bar{m}(\mu_0/2)/\bar{m}(\mu_{\rm had}^A)$	$\bar{m}(\mu_0/2)/\bar{m}(\mu_{\rm had}^B)$
$u_k^{\rm GF}$	–	–	–	2.6723(65)	3.441(16)	4.816(43)		
$u_k(b_0, b_1)$	–	–	–	2.6723	3.517	5.259		
ubyu								
FITA	4	–	1.08	0.8940(8)	0.7667(19)	0.5794(47)	–	–
FITA	5	–	0.97	0.8946(10)	0.7680(21)	0.5790(44)	–	–
Anomalous dimension - global								
FIT1	3	1	1.8	0.89371(91)	0.7642(20)	0.5826(47)	0.5275(55)	0.5540(46)
FIT1	2	1	1.6	0.89366(92)	0.7641(21)	0.5826(48)	0.5272(52)	0.5539(46)
FIT2	2	1	1.2	0.89316(86)	0.7647(19)	0.5854(44)	0.5298(54)	0.5566(46)
FIT2	2	2	1.1	0.89402(91)	0.7645(20)	0.5812(48)	0.5247(53)	0.5519(46)

TABLE 7.8: Ratios $K^{(k)} = \bar{m}(\mu_0/2)/\bar{m}(\mu_0/2^{k+1})$. The hadronic scales $\mu_{\rm had}^{(A,B)}$ correspond respectively to the renormalized squared couplings 9.25 and 8.63. As explained in Sec. 7.5 .

7.7 Summary

To summarise, in this part of the thesis we have presented the strategy and results for the non-perturbative calculation of the running and the anomalous dimension of the quark masses in $N_{\mathrm{f}} = 3$ QCD.
For the first time, we have considered two renormalization schemes, defined on two energy regions, non-perturbatively matched at the intermediate scale $\mu_0/2 \sim m_c$.
In the high-energy region we performed simulations at three value of the lattice spacing ($L/a = 6, 8, 12$) for each of the eight renormalized couplings, while in the low-energy one, taking advantage of the simulations did for computation of the running of the strong coupling, we computed the SSFs three point $L/a = 8, 12, 16$ for seven different scales.
For the first time, we computed non-perturbatively the mass anomalous dimension, presenting a new, more flexible, way to compute the running factor without relying on the SSFs recursion. Our results for the running factors at μ_0 and μ_{had} respectively show a sub-percent and $\sim 1\%$ uncertainty.

As a part of the shared effort between ALPHA and CLS collaborations, we are currently completing the calculation of the bare strange quark mass in large volumes, which, together with the computation of the non-perturbative running presented here will yield to the determination of its physical value.

L/a	β	κ	$u_{\rm GF}$	Lm	$Z_{\rm P}(g_0^2, L/a)$	# cfg
*8	3.3530	0.136423000000000	8.839(10)	0.0088(23)	0.3823(20)	1528
*8	3.3530	0.136497440000000	8.867(10)	-0.0090(23)	0.3790(23)	1683
*8	3.3682	0.136530000000000	8.643(10)	0.0033(23)	0.3879(23)	1645
*8	3.4000	0.136691350000000	8.120(10)	-0.0136(25)	0.4043(23)	1288
10	3.4500	0.136876730000000	8.651(14)	0.0178(18)	0.3723(18)	1521
10	3.4500	0.136935450000000	8.557(14)	-0.0092(28)	0.3715(28)	1170
12	3.5100	0.137078900000000	8.897(18)	-0.0100(40)	0.3584(39)	1575
12	3.5320	0.137101170000000	8.738(18)	-0.0028(28)	0.3652(28)	2812
12	3.5470	0.137113150000000	8.460(10)	-0.0036(35)	0.3723(33)	1938
12	3.5543	0.137118080000000	8.514(25)	-0.0020(47)	0.3711(46)	821
16	3.7000	0.137128980000000	8.633(18)	-0.0020(39)	0.3682(38)	3468
10	3.4000	0.136804050000000	9.282(10)	-0.0221(28)	0.3484(27)	2489
10	3.4110	0.136765000000000	9.290(10)	0.0189(18)	0.3526(18)	4624
12	3.4800	0.137038980000000	9.406(14)	-0.0115(33)	0.3417(32)	1828
12	3.4880	0.137021000000000	9.393(14)	0.0035(25)	0.3430(25)	2667
12	3.4970	0.137062990000000	9.118(18)	-0.0102(40)	0.3487(39)	1491
16	3.6490	0.137157650000000	9.423(18)	-0.0024(35)	0.3430(33)	4560
16	3.6576	0.137154130000000	9.186(18)	-0.0039(33)	0.3492(32)	3079
16	3.6710	0.137147560000000	9.045(28)	0.0009(52)	0.3526(50)	1553
20	3.7900	0.137048000000000	9.251(23)	-0.0008(48)	0.3508(47)	4133
24	3.8934	0.136894444635332	9.382(20)	-0.0001(49)	0.3474(48)	4709
24	3.9122	0.136862164369907	9.132(23)	0.0001(47)	0.3543(47)	5086

TABLE 7.9: Results for $Z_{\rm P}$ in the SF $-$ GF scheme, used to determine quark mass renormalization constants at the two hadronic matching points considered — $u_{\rm had} = 8.63$ (upper panel) and $u_{\rm had} = 9.25$ (lower panel). Alongside the values of $u_{\rm GF}$ and $Z_{\rm P}$, we also quote the value of the PCAC mass m in units of the physical lattice length, and the statistics for each ensemble. $L/a = 8$ lattices carry an asterisk as a reminder that they are excluded from the fit to the interpolating function.

Part IV

Renormalization of Four-Fermion Operators

8 Four-Fermion Operators Renormalization

The renormalization constants of lattice operators are necessary ingredients in the prediction of physical amplitudes from lattice matrix elements. Schematically, the physical amplitude $A_{i\to f}$ associated to the transition from an initial state i to a final state f induced by the composite operator $\mathbf{O}$ is given, in the formalism of the Operator Product Expansion (OPE), by

$$A_{i\to f} = C_W(\mu) Z_{\mathbf{O}}(a\mu) \langle i|\mathbf{O}(a)|f\rangle \tag{8.0.1}$$

where $C_W(\mu)$ is the Wilson Coefficient encoding the high-energy contribution to the amplitude and $\langle i|\mathbf{O}(a)|f\rangle$ is the bare matrix element relevant to the physical process containing the low-energy non-perturbative dynamics of the theory. As usual, μ denote the renormalization scale, and a is the lattice spacing. The renormalization constant $Z_{\mathbf{O}}(a\mu)$ is the connection between the bare operator and its renormalized counterpart in the continuum limit. In this section we focus on the beyond standard model four-fermion operators which play a crucial rôle in putting constraint of the possible extension of the SM. In particular we focus on the operator with a net change in flavour number. The operators are classified according to their discrete symmetries and an operator basis, convenient for our choice, is chosen. The major problem, when dealing with a lattice regularisation which breaks explicitly the chiral symmetry (like Wilson fermions in the current case) is given by the mixing with lower dimensional operators involving then power subtractions.

8.1 Renormalisation of four-quark operators

The mixing under renormalisation of four-quark operators that do not require subtraction of lower-dimensional operators has been determined in full generality in [122]. The absence of subtractions is elegantly implemented by using a formalism in which the operators are made of four different quark flavours; a complete set of Lorentz-invariant operators is

$$\begin{aligned}
Q_1^{\pm} &= \mathcal{O}^{\pm}_{\mathrm{VV+AA}}\,, & \mathcal{Q}_1^{\pm} &= \mathcal{O}^{\pm}_{\mathrm{VA+AV}}\,,\\
Q_2^{\pm} &= \mathcal{O}^{\pm}_{\mathrm{VV-AA}}\,, & \mathcal{Q}_2^{\pm} &= \mathcal{O}^{\pm}_{\mathrm{VA-AV}}\,,\\
Q_3^{\pm} &= \mathcal{O}^{\pm}_{\mathrm{SS-PP}}\,, & \mathcal{Q}_3^{\pm} &= \mathcal{O}^{\pm}_{\mathrm{PS-SP}}\,,\\
Q_4^{\pm} &= \mathcal{O}^{\pm}_{\mathrm{SS+PP}}\,, & \mathcal{Q}_4^{\pm} &= \mathcal{O}^{\pm}_{\mathrm{SP+PS}}\,,\\
Q_5^{\pm} &= -2\,\mathcal{O}^{\pm}_{\mathrm{TT}}\,, & \mathcal{Q}_5^{\pm} &= -2\mathcal{O}^{\pm}_{\mathrm{T\tilde{T}}}\,,
\end{aligned} \tag{8.1.1}$$

where

$$\mathcal{O}^{\pm}_{\Gamma_1\Gamma_2} = \frac{1}{2}\left[(\bar\psi_1\Gamma_1\psi_2)(\bar\psi_3\Gamma_2\psi_4) \pm (\bar\psi_1\Gamma_1\psi_4)(\bar\psi_3\Gamma_2\psi_2)\right]\,, \tag{8.1.2}$$

$\mathcal{O}^{\pm}_{\Gamma_1\Gamma_2\pm\Gamma_2\Gamma_1} \equiv \mathcal{O}^{\pm}_{\Gamma_1\Gamma_2} \pm \mathcal{O}^{\pm}_{\Gamma_2\Gamma_1}$, and the labeling is adopted $\mathrm{V} \to \gamma_\mu$, $\mathrm{A} \to \gamma_\mu\gamma_5$, $\mathrm{S} \to \mathbf{1}$, $\mathrm{P} \to \gamma_5$, $\mathrm{T} \to \sigma_{\mu\nu}$, $\bar{\mathrm{T}} \to \frac{1}{2}\varepsilon_{\mu\nu\rho\tau}\sigma_{\rho\tau}$, with $\sigma_{\mu\nu} = \frac{i}{2}[\gamma_\mu, \gamma_\nu]$. In the above expression round parentheses indicate spin and colour scalars, and subscripts are flavour labels. Note that operators $Q^{\pm}_k$ are parity-even, and $\mathcal{Q}^{\pm}_k$ are parity-odd.

It is important to stress that this framework is fairly general. For instance, with the assignments

$$\psi_1 = \psi_3 = s\,, \qquad \psi_2 = \psi_4 = d \tag{8.1.3}$$

the operators Q^-_k vanish, while Q^+_1 enters the SM amplitude for K^0–$\bar{K}^0$ mixing, and $Q^+_{2,\dots,5}$ the contributions to the same amplitude from arbitrary extensions of the SM. Idem for $B^0_{(s)}$–$\bar{B}^0_{(s)}$ mixing with

$$\psi_1 = \psi_3 = b\,, \qquad \psi_2 = \psi_4 = d/s\,. \tag{8.1.4}$$

If one instead chooses the assignments

$$\begin{aligned} &\psi_1 = s\,, \quad \psi_2 = d\,, \quad \psi_3 = \psi_4 = u, c\,, \\ &\psi_1 = s\,, \quad \psi_4 = d\,, \quad \psi_2 = \psi_3 = u, c\,, \end{aligned} \tag{8.1.5}$$

the resulting $Q^{\pm}_1$ will be the operators in the SM $\Delta S = 1$ effective weak Hamiltonian with an active charm quark, which, in the chiral limit, do not mix with lower-dimensional operators. By proceeding in this way, essentially all possible four-quark effective interactions with net flavour change can be easily seen to be comprised within our scope.

In the following we will assume a mass-independent renormalisation scheme. Renormalised operators can be written as

$$\begin{aligned} \bar{Q}^{\pm}_k &= Z_{kl}(\delta_{lm} + \Delta_{lm})Q^{\pm}_m\,, \\ \bar{\mathcal{Q}}^{\pm}_k &= \mathcal{Z}_{kl}(\delta_{lm} + \mathit{\Pi}_{lm})\mathcal{Q}^{\pm}_m \end{aligned} \tag{8.1.6}$$

(summations over l, m are implied), where the matrices $Z, \mathcal{Z}$ are scale-dependent and reabsorb logarithmic divergences, while $\Delta, \mathit{\Pi}$ are (possible) finite subtraction coefficients that only depend on the bare coupling. They have the generic structure

$$Z = \begin{pmatrix} Z_{11} & 0 & 0 & 0 & 0 \\ 0 & Z_{22} & Z_{23} & 0 & 0 \\ 0 & Z_{32} & Z_{33} & 0 & 0 \\ 0 & 0 & 0 & Z_{44} & Z_{45} \\ 0 & 0 & 0 & Z_{54} & Z_{55} \end{pmatrix}, \qquad \Delta = \begin{pmatrix} 0 & \Delta_{12} & \Delta_{13} & \Delta_{14} & \Delta_{15} \\ \Delta_{21} & 0 & 0 & \Delta_{24} & \Delta_{25} \\ \Delta_{31} & 0 & 0 & \Delta_{34} & \Delta_{35} \\ \Delta_{41} & \Delta_{42} & \Delta_{43} & 0 & 0 \\ \Delta_{51} & \Delta_{52} & \Delta_{53} & 0 & 0 \end{pmatrix}, \tag{8.1.7}$$

and similarly in the parity-odd sector. If chiral symmetry is preserved by the regularization, both Δ and $\mathit{\Pi}$ vanish. The main result of [122] is that $\mathit{\Pi} = 0$ even if chiral symmetry is broken explicitly by a Wilson term, due to residual discrete flavour symmetries that are preserved by the latter. In particular, the left-left operators $\mathcal{Q}^{\pm}_{\mathrm{VA+AV}}$ that mediate Standard Model-allowed transitions renormalise multiplicatively, while operators that appear as effective interactions in extensions of the Standard Model do always mix.[1]

Interestingly, in [122] some identities relate the renormalisation matrices for $(\mathcal{Q}^+_2, \mathcal{Q}^+_3)$ and $(\mathcal{Q}^-_2, \mathcal{Q}^-_3)$ in RI-MOM schemes. In Appendix B we discuss the underlying symmetry

[1] The use of twisted mass Wilson regularisations leads to a different chiral symmetry breaking pattern, which changes the mixing properties. This can be exploited in specific cases to achieve favorable mixing patterns, see e.g. [122].

structure in some more detail, and show how it can be used to derive constraints between matrices of anomalous dimensions in generic schemes.

Reminding the notation presented in Chapter 2, we have

$$q\frac{\partial}{\partial q}\overline{O}_j(q) = \sum_k \gamma_{jk}(\bar{g}(q))\,\overline{O}_k(q) \tag{8.1.8}$$

and the perturbative expansion of the anomalous dimension matrix γ as

$$\gamma(g) \underset{g\sim 0}{\approx} -g^2(\gamma_0 + \gamma_1 g^2 + \ldots)\,. \tag{8.1.9}$$

The universal, one-loop coefficients of the anomalous dimension matrix for four-fermion operators were first computed in [25, 123] and [124]. With our notational conventions the non-zero entries read

$$\begin{aligned}
\gamma_{11}^{+,(0)} &= \left(6 - \frac{6}{N}\right)(4\pi)^{-2}\,, & \gamma_{11}^{-,(0)} &= \left(-6 - \frac{6}{N}\right)(4\pi)^{-2}\,,\\
\gamma_{22}^{+,(0)} &= \left(\frac{6}{N}\right)(4\pi)^{-2}\,, & \gamma_{22}^{-,(0)} &= \left(\frac{6}{N}\right)(4\pi)^{-2}\,,\\
\gamma_{23}^{+,(0)} &= 12(4\pi)^{-2}\,, & \gamma_{23}^{-,(0)} &= -12(4\pi)^{-2}\,,\\
\gamma_{33}^{+,(0)} &= \left(-6N + \frac{6}{N}\right)(4\pi)^{-2}\,, & \gamma_{33}^{-,(0)} &= \left(-6N + \frac{6}{N}\right)(4\pi)^{-2}\,,\\
\gamma_{44}^{+,(0)} &= \left(6 - 6N + \frac{6}{N}\right)(4\pi)^{-2}\,, & \gamma_{44}^{-,(0)} &= \left(-6 - 6N + \frac{6}{N}\right)(4\pi)^{-2}\,,\\
\gamma_{45}^{+,(0)} &= \left(\frac{1}{2} - \frac{1}{N}\right)(4\pi)^{-2}\,, & \gamma_{45}^{-,(0)} &= \left(-\frac{1}{2} - \frac{1}{N}\right)(4\pi)^{-2}\,,\\
\gamma_{54}^{+,(0)} &= \left(-24 - \frac{48}{N}\right)(4\pi)^{-2}\,, & \gamma_{54}^{-,(0)} &= \left(24 - \frac{48}{N}\right)(4\pi)^{-2}\,,\\
\gamma_{55}^{+,(0)} &= \left(6 + 2N - \frac{2}{N}\right)(4\pi)^{-2}\,, & \gamma_{55}^{-,(0)} &= \left(-6 + 2N - \frac{2}{N}\right)(4\pi)^{-2}\,.
\end{aligned} \tag{8.1.10}$$

8.1.1 Perturbative expansion of RG evolution functions

As discussed in chapter 2 the definition of the RGI for mixing operators cannot be simply generalised from the one for multiplicative renormalizable operators. The matrix $W(\mu)$ defined in Eq. (2.1.16) which contains all the corrections beyond LO can be expanded perturbatively, with[2]

$$W(\mu) \approx \mathbf{1} + \bar{g}^2(\mu)J_1 + \bar{g}^4(\mu)J_2 + \bar{g}^6(\mu)J_3 + \bar{g}^8(\mu)J_4 + \ldots \tag{8.1.11}$$

[2]It is easy to check that this is indeed the correct form of the expansion for W. If terms with odd powers $\bar{g}^{2k+1}$, $k = 0, 1, \ldots$ are allowed, the consistency between the left- and right-hand sides of Eq. (2.1.16) requires them to vanish. The same applies if a dependence of J_n on μ is allowed — consistency then requires $\frac{\partial J_n}{\partial \mu} = 0$.

we find for the first four orders in the expansion the conditions

$$2b_0 J_1 - [\gamma_0, J_1] = \frac{b_1}{b_0}\gamma_0 - \gamma_1 \,, \tag{8.1.12}$$

$$4b_0 J_2 - [\gamma_0, J_2] = J_1\left(\frac{b_1}{b_0}\gamma_0 - \gamma_1\right) + \left(\frac{b_2}{b_0} - \frac{b_1^2}{b_0^2}\right)\gamma_0 + \frac{b_1}{b_0}\gamma_1 - \gamma_2 \,, \tag{8.1.13}$$

$$\begin{aligned} 6b_0 J_3 - [\gamma_0, J_3] = {} & J_2\left(\frac{b_1}{b_0}\gamma_0 - \gamma_1\right) + J_1\left\{\left(\frac{b_2}{b_0} - \frac{b_1^2}{b_0^2}\right)\gamma_0 + \frac{b_1}{b_0}\gamma_1 - \gamma_2\right\} + \\ & + \left(\frac{b_3}{b_0} - \frac{2b_2 b_1}{b_0^2} + \frac{b_1^3}{b_0^3}\right)\gamma_0 + \left(\frac{b_2}{b_0} - \frac{b_1^2}{b_0^2}\right)\gamma_1 + \frac{b_1}{b_0}\gamma_2 - \gamma_3 \,, \end{aligned} \tag{8.1.14}$$

$$\begin{aligned} 8b_0 J_4 - [\gamma_0, J_4] = {} & J_3\left(\frac{b_1}{b_0}\gamma_0 - \gamma_1\right) + J_2\left\{\left(\frac{b_2}{b_0} - \frac{b_1^2}{b_0^2}\right)\gamma_0 + \frac{b_1}{b_0}\gamma_1 - \gamma_2\right\} + \\ & + J_1\left\{\left(\frac{b_3}{b_0} - \frac{2b_2 b_1}{b_0^2} + \frac{b_1^3}{b_0^3}\right)\gamma_0 + \left(\frac{b_2}{b_0} - \frac{b_1^2}{b_0^2}\right)\gamma_1 + \frac{b_1}{b_0}\gamma_2 - \gamma_3\right\} + \\ & + \left(-\frac{b_1^4}{b_0^4} + 3\frac{b_1^2 b_2}{b_0^3} - \frac{b_2^2}{b_0^2} - 2\frac{b_1 b_3}{b_0^2} + \frac{b_4}{b_0}\right)\gamma_0 + \left(\frac{b_3}{b_0} - \frac{2b_2 b_1}{b_0^2} + \frac{b_1^3}{b_0^3}\right)\gamma_1 + \\ & + \left(\frac{b_2}{b_0} - \frac{b_1^2}{b_0^2}\right)\gamma_2 + \frac{b_1}{b_0}\gamma_3 - \gamma_4 \,. \end{aligned} \tag{8.1.15}$$

Modulo sign and normalisation conventions (involving powers of 4π related to expanding in $\bar{g}^2$ rather than $\alpha/(4\pi)$), and the dependence on gauge fixing (which does not apply to our context), Eq. (8.1.12) coincides with Eq. (24) of [25]. All four equations, as well as those for higher orders, can be easily solved to obtain J_n for given values the coefficients in the perturbative expansion of γ. The LO, NLO, and NNLO and NNNLO matching for the RGI operators is thus obtained from Eq. (2.1.20) by using the expansion in powers of $\bar{g}^2$ in Eq. (8.1.11) up to zeroth, first, second, and third order, respectively.

8.2 Anomalous dimensions in SF schemes

8.2.1 Strategy for the computation of NLO anomalous dimensions in SF schemes

The technology to match two renormalization scheme at one-loop has been introduced in the context of the tensor renormalization, we then refer for the details to chapter 6. Following what we did for the tensor current, Eq. (6.3.12) is the key ingredient for our computation of (matrix) anomalous dimensions to two loops in SF schemes, using as starting point known two-loop results in $\overline{\text{MS}}$ or RI schemes. Indeed, our strategy will be to compute the one-loop matching coefficient between the SF schemes that we will introduce presently, and the continuum schemes where $\gamma^{(1)}$ is known. $\gamma^{(1);\overline{\text{MS}}}$ can be found in [125, 126, 24], while $\gamma^{(1);\text{RI}}$ can be computed from both [25] and [24]; we gather them in Appendix C.

The one-loop matching coefficients $[\mathcal{X}_O^{(1)}]_{\text{cont;lat}}$ required by Eq. (6.3.15) can be extracted from the literature. For the RI-MOM scheme they can be found in [127], while for the $\overline{\text{MS}}$ scheme they can be extracted from [128, 129, 108] [3]). We gather the RI-MOM results in Landau gauge in Appendix E. $\chi_{\text{g}}^{(1)}$ can be found in [54].

[3] We are grateful to S. Sharpe for having converted for us, in the case of Fierz + operators, the $\overline{\text{MS}}$ scheme used in [128] to the one defined in [24].

8.3 SF renormalisation conditions

We now consider the problem of specifying suitable renormalisation conditions on four-quark operators, using the SF formalism. In this context, the first applications involved the multiplicatively renormalisable operators $\mathcal{Q}_1^{\pm}$ of Eq. (8.1.1) (which, as explained above, enter Standard Model effective Hamiltonians for $\Delta F = 1$ and $\Delta F = 2$ processes) [88, 89, 90, 91], as well as generic $\Delta B = 2$ operators in the static limit [92, 91]. The latter studies are extended in this paper to cover the full set of relativistic operators. It is important to stress that, while these schemes will be ultimately employed in the context of a non-perturbative lattice computation of renormalisation constants and anomalous dimensions, the definition of the schemes is fully independent of any choice of regulator.

We use the standard SF setup as described in [107], where the reader is referred for full details including unexplained notation. We will work on boxes with spacial extent L and time extent T; in practice, $T = L$ will always be set. Source fields are made up of boundary quarks and antiquarks,

$$\mathcal{O}_{\alpha\beta}[\Gamma] = a^6 \sum_{\mathbf{y},\mathbf{z}} \bar{\zeta}_\alpha(\mathbf{y})\Gamma\zeta_\beta(\mathbf{z})\,, \tag{8.3.1}$$

$$\mathcal{O}'_{\alpha\beta}[\Gamma] = a^6 \sum_{\mathbf{y},\mathbf{z}} \bar{\zeta}'_\alpha(\mathbf{y})\Gamma\zeta'_\beta(\mathbf{z})\,, \tag{8.3.2}$$

where α, β are flavour indices, unprimed (primed) fields live at the $x_0 = 0$ ($x_0 = T$) boundary, and Γ is a spin matrix that must anticommute with γ_0, so that the boundary fermion field does not vanish. This is a consequence of the structure of the conditions imposed on boundary fields,

$$\zeta(\mathbf{x}) = \tfrac{1}{2}(\mathbf{1} - \gamma_0)\zeta(\mathbf{x})\,, \qquad \bar{\zeta}(\mathbf{x}) = \bar{\zeta}(\mathbf{x})\tfrac{1}{2}(\mathbf{1} + \gamma_0)\,, \tag{8.3.3}$$

and similarly for primed fields. The resulting limitations on the possible Dirac structures for these operators imply e.g. that it is not possible to use scalar bilinear operators, unless non-vanishing angular momenta are introduced. This can however be expected to lead to poor numerical behaviour; thus, following our earlier studies [88, 89, 92, 91], we will work with zero-momentum bilinears and combine them suitable to produce the desired quantum numbers.

Renormalisation conditions will be imposed in the massless theory, in order to obtain a mass-independent scheme by construction. They will furthermore be imposed on parity-odd four-quark operators, since working in the parity-even sector would entail dealing with the extra mixing due to explicit chiral symmetry breaking with Wilson fermions, cf. Eq. (8.1.7). In order to obtain non-vanishing SF correlation functions, we will then need a product of source operators with overall negative parity; taking into account the above observation about boundary fields, and the need to saturate flavour indices, the minimal structure involves three boundary bilinear operators and the introduction of an extra, "spectator" flavour (labeled as number 5, keeping with the notation in Eq. (8.1.2)). We thus end up with correlation functions of the generic form

$$F^{\pm}_{k;s}(x_0) = \langle \mathcal{Q}^{\pm}_k(x)\mathcal{S}_s\rangle\,, \tag{8.3.4}$$

$$G^{\pm}_{k;s}(x_0) = \eta_k\langle \mathcal{Q}^{\pm}_k(x)\mathcal{S}'_s\rangle\,, \tag{8.3.5}$$

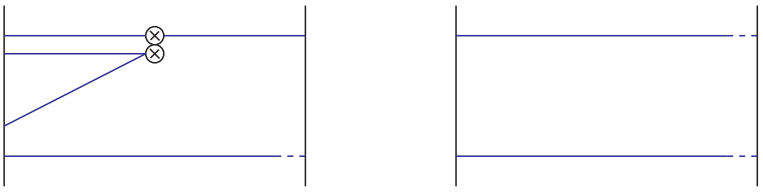

FIGURE 8.1: Feynman diagrams for the four-quark correlation functions $F^{\pm}_{k;s}$ and the boundary-to-boundary correlators f_1, k_1 at tree level. Euclidean time goes from left to right. The double blob indicates the four-quark operator insertion, and dashed lines indicate the explicit time-like link variable involved in boundary-to-boundary quark propagators.

where $\mathcal{S}_s$ is one of the five source operators

$$\mathcal{S}_1 = \mathcal{W}[\gamma_5, \gamma_5, \gamma_5]\,, \tag{8.3.6}$$

$$\mathcal{S}_2 = \frac{1}{6}\sum_{k,l,m=1}^{3} \epsilon_{klm}\mathcal{W}[\gamma_k, \gamma_l, \gamma_m]\,, \tag{8.3.7}$$

$$\mathcal{S}_3 = \frac{1}{3}\sum_{k=1}^{3} \mathcal{W}[\gamma_5, \gamma_k, \gamma_k]\,, \tag{8.3.8}$$

$$\mathcal{S}_4 = \frac{1}{3}\sum_{k=1}^{3} \mathcal{W}[\gamma_k, \gamma_5, \gamma_k]\,, \tag{8.3.9}$$

$$\mathcal{S}_5 = \frac{1}{3}\sum_{k=1}^{3} \mathcal{W}[\gamma_k, \gamma_k, \gamma_5] \tag{8.3.10}$$

with

$$\mathcal{W}[\Gamma_1, \Gamma_2, \Gamma_3] = L^{-3}\mathcal{O}'_{21}[\Gamma_1]\mathcal{O}'_{45}[\Gamma_2]\mathcal{O}_{53}[\Gamma_3]\,, \tag{8.3.11}$$

and similarly for $\mathcal{S}'_s$. The constant η_k is a sign that ensures $F^{\pm}_{k;s}(x_0) = G^{\pm}_{k;s}(x_0)$ for all possible indices; it is easy to check that $\eta_2 = -1$, $\eta_{s\neq 2} = +1$.[4] We will also use the two-point functions of boundary sources

$$f_1 = -\frac{1}{2L^6}\langle \mathcal{O}'_{21}[\gamma_5]\mathcal{O}_{12}[\gamma_5]\rangle\,, \tag{8.3.12}$$

$$k_1 = -\frac{1}{6L^6}\sum_{k=1}^{3}\langle \mathcal{O}'_{21}[\gamma_k]\mathcal{O}_{12}[\gamma_k]\rangle\,. \tag{8.3.13}$$

Finally, we define the ratios

$$\mathcal{A}^{\pm}_{k;s,\alpha} = \frac{F^{\pm}_{1;s}(T/2)}{f_1^{\frac{3}{2}-\alpha}k_1^{\alpha}}\,, \tag{8.3.14}$$

where α is an arbitrary real parameter. The structure of $F^{\pm}_{k;s}$ and f_1, k_1 is illustrated in Fig. 8.1.

[4]Since the correlation functions F and G are related by invariance under time reversal, and are thus identical only after integration over the whole ensemble of gauge fields, computing both of them in a numerical simulation and averaging the results will allow to reduce statistical noise at negligible computational cost. From now on, we will proceed by using only F, and leave possible usage of G at the numerical level, or for cross-checks of results, implicit.

We then proceed to impose renormalisation conditions at bare coupling g_0 and scale $\mu = 1/L$ by generalising the condition introduced in [88, 89] for the renormalisable multiplicative operators $\mathcal{Q}_1^{\pm}$: the latter reads

$$Z^{\pm}_{1;s,\alpha}\,\mathcal{A}^{\pm}_{k;s,\alpha} = \mathcal{A}^{\pm}_{k;s,\alpha}\Big|_{g_0^2=0}\,, \tag{8.3.15}$$

while for operators that mix in doublets, we impose[5]

$$\begin{pmatrix} Z^{\pm}_{22;s_1,s_2,\alpha} & Z^{\pm}_{23;s_1,s_2,\alpha} \\ Z^{\pm}_{32;s_1,s_2,\alpha} & Z^{\pm}_{33;s_1,s_2,\alpha} \end{pmatrix} \begin{pmatrix} \mathcal{A}^{\pm}_{2;s_1,\alpha} & \mathcal{A}^{\pm}_{2;s_2,\alpha} \\ \mathcal{A}^{\pm}_{3;s_1,\alpha} & \mathcal{A}^{\pm}_{3;s_2,\alpha} \end{pmatrix} = \begin{pmatrix} \mathcal{A}^{\pm}_{2;s_1,\alpha} & \mathcal{A}^{\pm}_{2;s_2,\alpha} \\ \mathcal{A}^{\pm}_{3;s_1,\alpha} & \mathcal{A}^{\pm}_{3;s_2,\alpha} \end{pmatrix}_{g_0^2=0}\,, \tag{8.3.16}$$

and similarly for $\mathcal{Q}^{\pm}_{4,5}$. The products of boundary-to-boundary correlators in the denominator of Eq. (8.3.14) cancels the renormalisation of the boundary operators in $F^{\pm}_{k;s}$, and therefore $Z^{\pm}_{k;s,\alpha}$ only contains anomalous dimensions of four-fermion operators. Following [72, 88, 91], conditions are imposed on renormalisation functions evaluated at $x_0 = T/2$, and the phase that parameterises spatial boundary conditions on fermion fields is fixed to $\theta = 0.5$. Together with the $L = T$ geometry of our finite box, this fixes the renormalisation scheme completely, up to the choice of boundary source, indicated by the index s, and the parameter α. The latter can in principle take any value, but we will restrict to the choices $\alpha = 0, 1, 3/2$.

One still has to check that renormalisation conditions are well-defined at tree-level. While this is straightforward for Eq. (8.3.15), it is not so for Eq. (8.3.16): it is still possible that the matrix of ratios $\mathcal{A}$ has zero determinant at tree-level, rendering the system of equations for the matrix of renormalisation constants ill-conditioned. This is indeed the obvious case for $s_1 = s_2$, but the determinant turns out to be zero also for other non-trivial choices $s_1 \neq s_2$. In practice, out of the ten possible schemes one is only left with six, viz.[6]

$$(s_1, s_2) \in \{(1,2), (1,4), (1,5), (2,3), (3,4), (3,5)\}\,. \tag{8.3.17}$$

It has to be stressed that this property is independent of the choice of θ and α. Thus, we are left with a total of 15 schemes for $\mathcal{Q}_1^{\pm}$, and 18 for each of the pairs $(\mathcal{Q}_2^{\pm}, \mathcal{Q}_3^{\pm})$ and $(\mathcal{Q}_4^{\pm}, \mathcal{Q}_5^{\pm})$.

8.3.1 One-loop results in the SF

Let us now carry out a perturbative computation of the SF renormalisation matrices introduced above, using a lattice regulator. For any of the correlation functions as already discussed in chapter 6, the perturbative expansion (even in the matrix case) reads

$$X = X^{(0)} + g_0^2 \left[X^{(1)} + m_{\rm cr}^{(1)} \frac{\partial X^{(0)}}{\partial m_0} \right] + \mathcal{O}(g_0^4)\,, \tag{8.3.18}$$

where X is one of $F^{\pm}_{k;s}(x_0),\ f_1,\ k_1$, or some combination thereof; where m_0 is the bare quark mass; and $m_{\rm cr}^{(1)}$ the one-loop coefficient in the perturbative expansion of the critical mass. The derivative term in the square bracket is needed to set the correlation function X to zero renormalised quark mass, when every term in the r.h.s. of the equation is computed at vanishing bare mass. Also in this context, we use the values for the critical

[5] These renormalisation conditions were first introduced by S. Sint [130].

[6] Note that schemes obtained by exchanging $s_1 \leftrightarrow s_2$ are trivially related to each other.

mass (e.g. see [131]),

$$\begin{aligned} m_{\rm cr}^{(1)} &= -0.20255651209\, C_{\rm F} \quad (c_{\rm sw}=1)\,, \\ m_{\rm cr}^{(1)} &= -0.32571411742\, C_{\rm F} \quad (c_{\rm sw}=0)\,, \end{aligned} \tag{8.3.19}$$

with $C_{\rm F} = (N^2-1)/(2N)$, and the (tree-level) value of the Sheikholeslami-Wohlert (SW) coefficient $c_{\rm sw}$ indicating whether the computation is performed with or without an O(a)-improved action.

The entries of the renormalisation matrix admit a similar expansion,

$$Z(g_0, L/a) = 1 + g_0^2 Z^{(1)}(L/a) + \mathcal{O}(g_0^4)\,, \tag{8.3.20}$$

where we have indicated explicitly the dependence of the quantities on the bare coupling and the lattice spacing-rescaled renormalisation scale $a\mu = a/L$. The explicit expression of the one-loop order coefficient $Z^{(1)}$ for the multiplicatively renormalisable operators $\mathcal{Q}_1^{\pm}$ is

$$\begin{aligned} Z^{(1)} = &- \left\{ \frac{F^{(1)}}{F^{(0)}} + \frac{F_b^{(1)}}{F^{(0)}} + m_{\rm cr}^{(1)} \frac{\partial}{\partial m_0} \log F^{(0)} \right\} \\ &+ \left(\frac{3}{2} - \alpha\right) \left[\frac{f_1^{(1)}}{f_1^{(0)}} + \frac{f_{1;b}^{(1)}}{f_1^{(0)}} + m_{\rm cr}^{(1)} \frac{\partial}{\partial m_0} \log f_1^{(0)} \right] \\ &+ \alpha \left[\frac{k_1^{(1)}}{k_1^{(0)}} + \frac{k_{1;b}^{(1)}}{k_1^{(0)}} + m_{\rm cr}^{(1)} \frac{\partial}{\partial m_0} \log k_1^{(0)} \right]\,, \end{aligned} \tag{8.3.21}$$

while for the entries of each 2×2 submatrix that renormalises operator pairs one has

$$Z_{ij}^{(1)} = -\mathcal{A}_{ik}^{(1)} \left[\left(\mathcal{A}^{(0)} \right)^{-1} \right]_{kj}\,, \tag{8.3.22}$$

with

$$\begin{aligned} \mathcal{A}_{ij}^{(0)} =& \frac{F_{ij}^{(0)}}{\left[f_1^{(0)}\right]^{3/2-\alpha} \left[k_1^{(0)}\right]^{\alpha}}\,, \\ \mathcal{A}_{ij}^{(1)} =& \left\{ \left[F_{ij}^{(1)} + F_{ij;b}^{(1)} + m_{\rm cr}^{(1)} \frac{\partial}{\partial m_0} F_{ij}^{(0)} \right] \right. \\ &- \left(\frac{3}{2} - \alpha\right) \left[\frac{f_1^{(1)}}{f_1^{(0)}} + \frac{f_{1;b}^{(1)}}{f_1^{(0)}} + m_{\rm cr}^{(1)} \frac{\partial}{\partial m_0} \log f_1^{(0)} \right] F_{ij}^{(0)} \\ &\left. - \alpha \left[\frac{k_1^{(1)}}{k_1^{(0)}} + \frac{k_{1;b}^{(1)}}{k_1^{(0)}} + m_{\rm cr}^{(1)} \frac{\partial}{\partial m_0} \log k_1^{(0)} \right] F_{ij}^{(0)} \right\} \left[f_1^{(0)}\right]^{\alpha-3/2} \left[k_1^{(0)}\right]^{-\alpha}\,. \end{aligned} \tag{8.3.23}$$

Contributions with the label "b" arise from the boundary terms that are needed in addition to the SW term in order to achieve full O(a) improvement of the action in the SF [107]. They are neglected in the unimproved case. We will set them to zero in the improved case as well, since they vanish in the continuum limit and thus will not contribute to our results for NLO anomalous dimensions.[7]

[7] These terms do enter perturbative cutoff effects. Note however that we will not include in our computation the required subtractions of dimension 7 operators to render correlation functions O(a) improved,

The computation of the r.h.s. of the four-quark operator correlators $F^{\pm}_{k;s}$ requires the evaluation of the Feynman diagrams in Figure 8.1 at tree level, and of those in Figures 8.2 and 8.3 at one loop. The one-loop expansion of the boundary-to-boundary correlators f_1 is known from [101] and k_1 from [89]. Each diagram can be written as a loop sum of a Dirac trace in time-momentum representation, where the Fourier transform is taken over space only. The sums have been performed numerically in double precision arithmetics using a Fortran 90 code, for all even lattice sizes ranging from $L/a = 4$ to $L/a = 48$. The results have been cross-checked against those of an independent C++ code, also employing double precision arithmetics.

The expected asymptotic expansion for the one-loop (matrix) coefficient of renormalisation constants is (operator and scheme indices not explicit), as in the multiplicative renormalizable case,

$$Z^{(1)}(L/a) = \sum_{n=0}^{\infty} \left(\frac{a}{L}\right)^n \{r_n + s_n \, \ln(L/a)\} \; . \tag{8.3.24}$$

In particular, the coefficient s_0 of the log that survives the continuum limit will be the corresponding entry of the anomalous dimension matrix, while the finite part r_0 will contribute to the one-loop matching coefficients we are interested in. In particular, one has

$$[\mathcal{X}_O^{(1)}]_{\rm SF;lat} = r_0 \, , \tag{8.3.25}$$

which is the required input for the matching condition in Eq. (6.3.15). We thus proceed as follows:

(i) Compute tree-level and one-loop diagrams for all correlation functions.

(ii) Construct one-loop renormalisation constants using Eq. (8.3.21) and Eq. (8.3.22).

(iii) Fit the results to the ansatz in Eq. (8.3.24) as a function of (a/L), using the known value of the entries of the leading-order anomalous dimension matrix $\gamma^{(0)}$ as fixed parameters, and extract r_0.

The description of the procedure employed to extract the finite parts as well as our results are provided in Appendix F.

8.3.2 NLO SF anomalous dimensions

Having collected $[\mathcal{X}_O^{(1)}]_{\rm SF;lat}$, $[\mathcal{X}_O^{(1)}]_{\rm cont;lat}$, $\gamma^{(1);\rm cont}$ and $\mathcal{X}_{\rm g}^{(1)}$ we have finally been able to compute the matrix $\gamma^{(1);\rm SF}$ for both the "+" and the "-" operator basis and for all the 18 schemes presented in Section 8.3. The results are collected in Appendix G.

We have performed two strong consistency checks of our calculation:

- In our one-loop perturbative computation, we have obtained $[\mathcal{X}_O^{(1)}]_{\rm SF;lat}$ for both $c_{\rm sw} = 0$ and $c_{\rm sw} = 1$ values. The results for $[\mathcal{X}_O^{(1)}]_{\rm cont;lat}$ are known for generic values of $c_{\rm sw}$. We have thus been able to compute $[\mathcal{X}_O^{(1)}]_{\rm SF;cont}$ for both $c_{\rm sw} = 0$ and $c_{\rm sw} = 1$ in such a way to check its independence from $c_{\rm sw}$.

- For the "+" operators, we have checked the independence of $\gamma^{(1);\rm SF}$ from the reference scheme used (either the RI-MOM or the $\overline{\rm MS}$). This is a strong check of the

and therefore the scaling to the continuum limit will be dominated by terms linear in a up to logarithms — cf. Eq. (8.3.24) below. The missing boundary contributions are actually expected to be subdominant with respect to the missing counterterms to four-fermion operators.

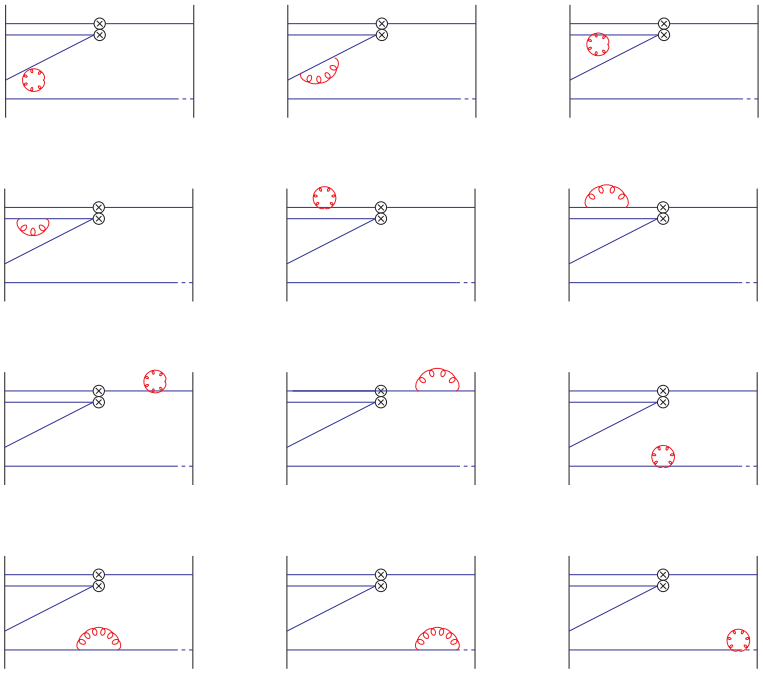

FIGURE 8.2: Feynman diagrams of the self-energy type entering the one-loop computation of $F^{\pm}_{k;s}$.

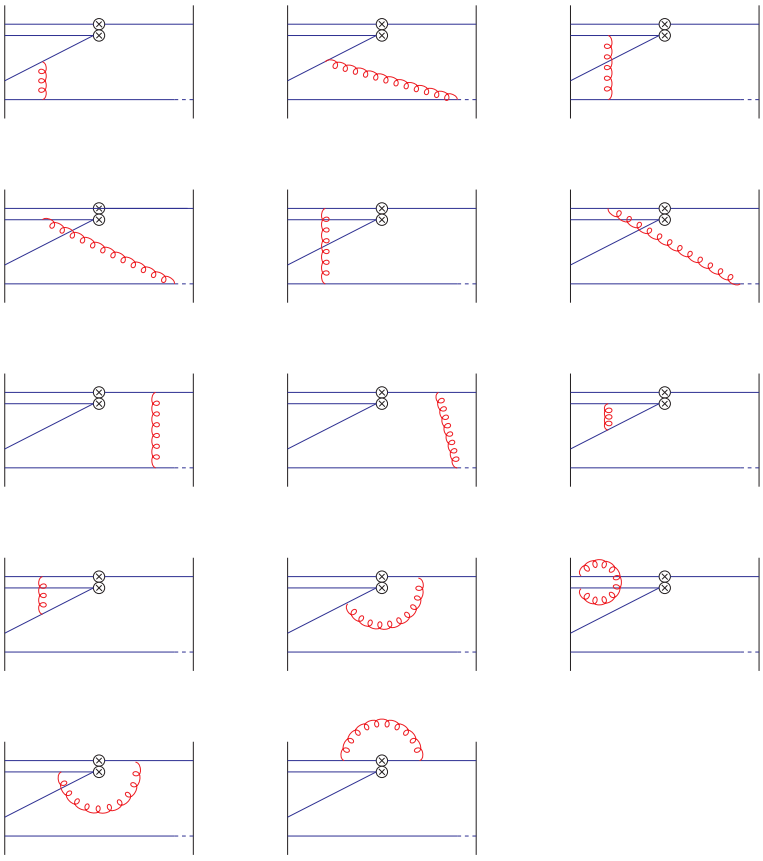

FIGURE 8.3: Feynman diagrams with gluon exchanges between quark lines entering the one-loop computation of $F^{\pm}_{k;s}$.

calculations from the literature of the NLO anomalous dimensions $\gamma^{(1);\mathrm{cont}}$ and one-loop matching coefficients $[\mathcal{X}_O^{(1)}]_{\mathrm{cont;lat}}$ in both the RI-MOM and $\overline{\mathrm{MS}}$ scheme.

The resulting values of $\gamma^{(1)}$ exhibit a strong scheme dependence. In order to define a reference scheme for each operator, we have devised a criterion that singles out those schemes with the smallest NLO corrections: given the matrix

$$16\pi^2\,\gamma^{(1);\mathrm{SF}}\,(\gamma^{(0)})^{-1}\,, \tag{8.3.26}$$

we compute the the trace and the determinant of each non-trivial submatrix, and look for the smallest absolute value of both quantities. Remarkably, in all cases (2-3 and 4-5 operator doublets, both in the Fierz $+$ and $-$ sectors) this is satisfied by the scheme given by $s = 6,\ \alpha = 3/2$.

8.4 Renormalisation group running in perturbation theory

In this section we will discuss the perturbative computation of the RG running factor $\tilde{U}(\mu)$ in Eq. (2.1.20). The main purpose of this exercise is to understand the systematic of perturbative truncation, both in view of our own non-perturbative computation of the RG running factor [93] (which involves a matching to NLO perturbation theory around the electroweak scale), and in order to assess the extensive use of NLO RG running down to hadronic scales in the phenomenological literature. In view of our upcoming publication of a non-perturbative determination of the anomalous dimensions for QCD with $N_\mathrm{f} = 2$, the analysis below will be performed for that case; the qualitative conclusions are independent of the precise value of N_f. The scale will be fixed using the value $\Lambda_{\mathrm{QCD}}^{\overline{\mathrm{MS}};N_\mathrm{f}=2} = 310(20)\ \mathrm{MeV}$ quoted in [132].

At leading order in perturbation theory the running factor is given by U_{LO} in Eq. (2.1.13). Beyond LO, the running factor is given by Eq. (2.1.14), where $W(\mu)$ satisfies Eq. (2.1.16). In the computation of W, the β and the γ functions are known only up to 3 loops and 2 loops, respectively. In order to asses the systematic, we will compute the running factor for several approximations that will be labeled through a pair of numbers "n_γ/n_β" where n_γ is the order used for the γ function while n_β is the order used for the β function. We will consider the following cases:

(i) "1/1", i.e. the LO approximation in which $W \equiv 1$;

(ii) "2/2", in which both γ and β are taken at NLO;

(iii) "2/3", in which β is taken at NNLO and γ at NLO;

(iv) "+3/3", in which β is taken at NNLO and for the NNLO coefficient γ_2 we use a guesstimate given by $\gamma_2\gamma_1^{-1} = \gamma_1\gamma_0^{-1}$;

(v) "-3/3", in which β is taken at the NNLO and for the NNLO coefficient γ_2 we use a guesstimate given by $\gamma_2\gamma_1^{-1} = -\gamma_1\gamma_0^{-1}$;

Beyond LO we have first computed the perturbative expansion of the running factor, Eq. (2.1.14) and Eq. (8.1.11), by including all the J_n's corresponding to the highest order used in the combinations of β/γ functions chosen above. The J_n have been computed from Eq. (8.1.12) and Eq. (8.1.13) setting the unknown coefficients to zero. Namely: J_1 in the 2/2 case, J_1 and J_2 (with $\gamma_2 = 0$) in the 2/3 case, J_1 and J_2 with γ_2 set to the guesstimates above in the +3/3 and -3/3 cases. We have compared these results with the numerical solution of Eq. (2.1.16) in which the perturbative expansions for γ and β at the chosen orders are plugged in. We have chosen two cases in which perturbation theory seems particularly ill-behaved, namely the matrix for operators 4 and 5 with both Fierz + and - in the RI-MOM scheme, and we show the comparison in Fig. 8.4. As one can see, the two methods

are not in very good agreement in the region of few GeV scales. This is obvious, because by expanding W in powers of g^2 and including only the first/second coefficients J_1, J_2, substantial information is lost.

We have then included in the perturbative expansion the next order, computed from Eq. (8.1.13) and Eq. (8.1.14), setting again the unknown coefficients to zero. Namely: J_2 (with $b_2 = \gamma_2 = 0$) in the 2/2 case, J_3 (with $b_3 = \gamma_3 = \gamma_2 = 0$) in the 2/3 case, J_3 (with $b_3 = \gamma_3 = 0$ and γ_2 set to the guesstimates above) in the +3/3 and -3/3 cases. The comparison, again with the corresponding numerical solution of Eq. (2.1.16) (which remains unchanged), is shown in Fig. 8.5 and shows a reasonable agreement for the Fierz + matrix while still noticeable desagreement for some of the Fierz - matrix elements.

In the the Fierz - case we have thus proceeded by introducing the next order, namely: J_3 (with $b_2 = \gamma_2 = b_3 = \gamma_3 = 0$) in the 2/2 case, J_4 (with $b_4 = b_3 = \gamma_4 = \gamma_3 = \gamma_2 = 0$) in the 2/3 case, J_4 (with $b_4 = b_3 = \gamma_4 = \gamma_3 = 0$ and γ_2 set to the guesstimates above) in the +3/3 and -3/3 cases. The comparison, again with the corresponding numerical solution of Eq. (2.1.16), is shown in Fig. 8.6a. The agreement between the numerical solution and the perturbative expansion further improves in all cases except for the 55 matrix element in the $\pm 3/3$ cases where the perturbative expansion further moves away from the numerical solution. From both examples of Fierz $\pm$ 4-5 matrix, we understand that by including more and more orders in the perturbative expansion of $W(\mu)$ Eq. (8.1.11), we approximate better and better the numerical solution of Eq. (2.1.16) [8], which can thus be considered the best approximation of the running factor given a fixed order computation of the β and γ functions.

There is still a subtle technical issue concerning the numerical integration of Eq. (2.1.16) which needs to be discussed, because it becomes relevant in practice. Since γ and β have simple expressions in terms of $\bar{g}(\mu)$ rather than in terms of μ, Eq. (2.1.16) is most easily solved by rewriting it in terms of the derivative with respect to the coupling, viz.

$$\widetilde{W}'(g) = -\widetilde{W}(g)\,\frac{\gamma(g)}{\beta(g)} + \frac{\gamma_0}{b_0 g}\,\widetilde{W}(g)\,, \tag{8.4.1}$$

where $\widetilde{W}(\bar{g}(\mu)) \equiv W(\mu)$. While both terms on the right hand side diverge as $g \to 0$, the divergence cancels in the sum due to Eq. (2.1.17). However, it is not straightforward to implement this latter initial condition at the level of the numerical solution to Eq. (8.4.1): a stable numerical solution requires fixing the initial condition Eq. (2.1.17) at an extremely small value of the coupling, and consequently the use of a sophisticated and computationally expensive integrator. A simpler solution is to substitute Eq. (2.1.17) by an initial condition of the form

$$\widetilde{W}(g_{\rm i}) = \mathbf{1} + g_{\rm i}^2 J_1 + g_{\rm i}^4 J_2 + g_{\rm i}^6 J_3 + g_{\rm i}^8 J_4 + \dots\,, \tag{8.4.2}$$

at some very perturbative coupling $g_{\rm i}$ (but still a significantly larger value than required by Eq. (2.1.17)), where we include exactly the same coefficients J_n, $n = 1, \dots$ that we use in the perturbative expansion of the running factor, and which are computed by using the same amount of perturbative information employed in the ratio γ/β used for the numerical integration.[9] Note that indeed the numerical value of $g_{\rm i}$ needs not be extremely small for this to make physical sense, e.g. for $N_{\rm f} = 2$ (which will be of particular interest to us) and at the Planck scale one has $\bar{g}^2_{\overline{\rm MS}}(M_P) \approx 0.221 \leftrightarrow \alpha_{\rm s}^{\overline{\rm MS}}(M_P) \approx 0.0176$ and $\bar{g}^2_{\rm SF}(M_P)$ differs with respect to $\bar{g}^2_{\overline{\rm MS}}(M_P)$ only on the third decimal digit.

[8] Except for the 55 matrix element where, in presence of a non-zero γ_2 the expansion looks like an alternating series.

[9] For $N_{\rm f} = 3$ Eq. (8.4.2) is not practical, and Eq. (2.1.17) becomes mandatory, cf. Appendix D.

In Fig. 8.6b we compare the results for the numerical integration of $W(\mu)$ when matched at $g_{\rm i}$ with the perturbative expansion at the order used in Fig. 8.4 and Fig. 8.5 respectively and the results turn out to be indistiguishable. We have also changed the value of the coupling chosen for the matching in a broad range of $\bar{g}^2$ without observing any noticeable difference in the solution. These checks prove the stability of the numerical procedure and give us confidence in the corresponding results, which will be used below to assess the systematic uncertainties. In the following we won't consider anymore the perturbative expansion of the running factor except for the 2/2 case where only J_1 is included (we will call this $2/2$ at $\mathrm{O}(g^2)$), which is the case usually considered in literature, both for phenomenological application and in lattice computations.

According to the previous discussion, we have chosen to quote as our best estimate of the running factors the 2/3 results (which encode the maximum of information at our disposal for the β and γ functions) obtained through numerical integration. They are presented in Tab. 8.9 at the scale $\mu = 3\,\mathrm{GeV}$. In alternative we quote also the results for the 2/2 case perturbatively expanded at $\mathrm{O}(g^2)$ (i.e. including J_1 only), which are the results usually considered in literature. We present them in Tab. 8.10 again at the scale $\mu = 3\,\mathrm{GeV}$.

The systematic uncertainties in Tab. 8.9 (respectively Tab. 8.10) are estimated by considering the maximal deviation of the 2/3 case (respectively the 2/2, $\mathrm{O}(g^2)$ case) from the other 3 (respectively 4) numerical cases.

The results for the LO running factor $U_{\rm LO}(\mu)$ Eq. (2.1.13) and the numerically integrated $\tilde{U}(\mu)$ running factors beyond LO (ii)-(v) described above are illustrated in Figs. (8.15), (8.16), (8.17), (8.18), (8.19), (8.20) together with the 2/2 $\mathrm{O}(g^2)$ perturbative expansion, for the four doublets of operators and three different schemes ($\overline{\rm MS}$, RI and a chosen SF scheme).

Some important observations are:

- The convergence of LO respect to NLO and NNLO seems to be slow in all the schemes under investigation for almost all the operators. In particular, for the matrix elements involving tensor current (4-5 sub-matrices) the convergence is very poor. Note that the LO anomalous dimensions for these submatrices are already very large compared with the others.

- the 2/3 numerical running factors have always symmetric systematic errors, because most of the systematics is due to the inclusion of the guesstimate for γ_2 with + and - sign, and these effects turn out to be always symmetric with respect to the 2/3 (and also 2/2) cases.

- the 2/2 $\mathrm{O}(g^2)$ running factors are, for several matrix elements, quite far from the 2/3 (and also the 2/2) numerical ones. Possibly even further away than the $\pm 3/3$ and have thus very large, asymmetric errors.

- For both 4-5 sub-matrices (Fierz + and -) the ratio $\gamma_1\gamma_0^{-1}$ turns out to have large matrix elements. As a consequence, our plausibility argument for the guesstimates $\gamma_2\gamma_1^{-1} = \pm\gamma_1\gamma_0^{-1}$ leads to large systematic uncertainties. In particular, for the 54 matrix element the error is huge in the RI scheme and large also in the $\overline{\rm MS}$ and SF schemes, already for the 2/3 numerical solution (for the 2/2 $\mathrm{O}(g^2)$ perturbative expansion the situation is much worse). This obviously poses serious doubts on all the computations of $\Delta F = 2$ matrix elements beyond the Standard Model which use perturbative running (in all cases through the 2/2 $\mathrm{O}(g^2)$ expansion) down to scales of 3 GeV or less.

8.5 One-loop cutoff effects in the step scaling function

As an outcome of the perturbative calculation carried out in the previous section ([94]) we can compute the $\mathcal{O}(ag^2)$ effects on the SSFs[10]. Following the same conventions used in [101], at one-loop order in perturbation theory the lattice (matrix) SSFs read

$$\Sigma_O(g^2, a/L) = \mathbf{1} + k(L/a)g^2 + \mathcal{O}(g^2) \tag{8.5.1}$$

with

$$k(L/a) = Z^{(1)}(2L/a) - Z^{(1)}(L/a) \tag{8.5.2}$$

where k and Z are matrices.
In order to see the relative deviation from the perturbative prediction, we define

$$k(\infty) = \gamma^{(0)} \log(2). \tag{8.5.3}$$

The 1-loop cutoff effect for the SSFs is then given by

$$\delta_k(L/a) = k(L/a)[k(\infty)]^{-1} - \mathbf{1}. \tag{8.5.4}$$

Numerical values and plots are reported in Appendix A. The chosen scheme $\alpha = 3/2$,$(s_1, s_2) = (4, 5)$ is plotted with a blue "triangle" marker).

8.6 Perturbative expansion of step-scaling functions

Step-scaling functions for four-quark operators are given by

$$\sigma_O(\bar{g}^2(\mu)) = U(\mu/2, \mu) = T \exp\left\{ \int_{\bar{g}(\mu)}^{\bar{g}(\mu/2)} \mathrm{d}g \, \frac{1}{\beta(g)} \, \gamma(g) \right\}, \tag{8.6.1}$$

Taking advantage of the factorisation of LO and NLO, the SSFs can be rewritten as

$$\sigma_O(\bar{g}^2(\mu)) = U(\mu/2, \mu) \equiv [W(\mu/2)]^{-1} \, U_{\mathrm{LO}}(\mu/2, \mu) W(\mu) \,. \tag{8.6.2}$$

Furthermore, the step-scaling function σ for the gauge coupling, is as usual defined as

$$-\ln 2 = \int_{\sqrt{u}}^{\sqrt{\sigma(u)}} \frac{\mathrm{d}g}{\beta(g)} \,. \tag{8.6.3}$$

Defining the perturbative expansions, up to two loops, as

$$\sigma(u) = u(1 + s_1 u + s_2 u^2) \,, \tag{8.6.4}$$

$$\sigma_O(u) = \mathbf{1} + r_1 u + r_2 u^2 \,, \tag{8.6.5}$$

one finds for the coefficients of the coupling step-scaling function the expressions

$$s_1 = 2b_0 \ln 2 \,, \tag{8.6.6}$$

$$s_2 = 2b_1 \ln 2 + 4b_0^2 \ln^2 2 \,. \tag{8.6.7}$$

[10] While $\mathcal{O}(a^2)$ scaling toward the continuum is guaranteed for the fermionic and gauge actions by the presence of bulk and boundary counter terms, there is a remainder $\mathcal{O}(a)$ contribution coming from the four-fermions correlation functions whose counterterm have never been computed.

u	$\sigma_{(23)}^{\alpha=3/2,(3,5),+}(u)$	$\sigma_{(23)}^{\alpha=3/2,(3,5),-}(u)$
0.9793	$\begin{pmatrix} 1.0112(71) & 0.067(21) \\ 0.0095(40) & 0.9227(100) \end{pmatrix}$	$\begin{pmatrix} 1.0003(74) & -0.074(11) \\ -0.0094(41) & 0.918(11) \end{pmatrix}$
1.1814	$\begin{pmatrix} 1.0167(90) & 0.054(23) \\ 0.0073(44) & 0.919(10) \end{pmatrix}$	$\begin{pmatrix} 1.0098(83) & -0.059(11) \\ -0.0055(40) & 0.918(12) \end{pmatrix}$
1.5078	$\begin{pmatrix} 1.016(12) & 0.065(30) \\ 0.0116(57) & 0.882(14) \end{pmatrix}$	$\begin{pmatrix} 1.007(12) & -0.089(17) \\ -0.0106(60) & 0.883(18) \end{pmatrix}$
2.0142	$\begin{pmatrix} 1.0061(100) & 0.101(33) \\ 0.0186(55) & 0.829(11) \end{pmatrix}$	$\begin{pmatrix} 0.9952(85) & -0.117(11) \\ -0.0213(55) & 0.835(14) \end{pmatrix}$
2.4792	$\begin{pmatrix} 0.988(20) & 0.087(42) \\ 0.0171(76) & 0.794(22) \end{pmatrix}$	$\begin{pmatrix} 0.986(14) & -0.095(14) \\ -0.0200(75) & 0.812(21) \end{pmatrix}$
3.3340	$\begin{pmatrix} 0.990(30) & 0.138(55) \\ 0.049(11) & 0.691(20) \end{pmatrix}$	$\begin{pmatrix} 0.950(19) & -0.141(21) \\ -0.0500(95) & 0.716(22) \end{pmatrix}$

TABLE 8.1: Continuum SSFs for Op $2,3$ in the specific renormalization scheme $(s_1, s_2) = (3, 5)$.

Thus the three pieces on r.h.s. of Eq. (8.6.2) can be expanded

$$\begin{aligned} U_{\rm LO}(\mu/2, /mu) &= \exp\left\{\frac{\gamma^{(0)}}{2b_0}\ln\left[\frac{\sigma(u)}{u}\right]\right\} \\ &\approx \mathbf{1} + u\gamma^{(0)}\ln 2 + u^2\left[\left(b_0\ln 2 + \frac{b_1}{b_0}\right)\gamma^{(0)}\ln 2 + \frac{\ln^2 2}{2}\left(\gamma^{(0)}\right)^2\right], \end{aligned} \tag{8.6.8}$$

and ,

$$W(\mu) \approx \mathbf{1} + uJ + cu^2 + \dots, \tag{8.6.9}$$

$$[W(\mu/2)]^{-1} \approx \mathbf{1} - \sigma(u)J \approx \mathbf{1} - uJ - u^2 s_1 J + u^2 J^2 - cu^2 + \dots \tag{8.6.10}$$

In these latter expressions, cu^2 is the $\mathcal{O}(u^2)$ correction to Eq. (8.1.11), while the other u^2 terms in $[W(\mu/2)]^{-1}$ come from the power-series expansion of $\sigma(u)$ and the inverse matrix. By putting everything together one finally finds

$$r_1 = \gamma^{(0)}\ln 2\,, \tag{8.6.11}$$

$$r_2 = \gamma^{(1)}\ln 2 + b_0\gamma^{(0)}\ln^2 2 + \frac{1}{2}\left(\gamma^{(0)}\right)^2\ln^2 2\,, \tag{8.6.12}$$

where we have used Eq. (8.1.12) to simplify the term $[\gamma^{(0)}, J]$. We thus see explicitly that $\mathcal{O}(u^2)$ corrections to W do not contribute to r_2, consistently with the fact that the $\mathcal{O}(u)$ correction already contains all NLO contributions. Remarkably, the above expression is the same one found for operators that renormalise multiplicatively, cf. e.g. Eq. (6.6) in [89].

8.7 Non-perturbative results

We use here the same $N_{\rm f} = 2$ gauge ensembles introduced in the context of the renormalization of the tensor currents in chapter 6.[11] Concerning the statistical analysis, since it involves the computation several correlation functions which are then combined together in order to extract the (matrix) renormalization coefficient, a robust analysis that takes into account the autocorrelations is crucial. In order to achieve that, we proceeded with a

[11] As in [91], for $u = 1.578$ we neglected the different perturbative orders of $c_{\rm t}$, keeping only the data with highest order. We observed that this approximation does not have any relevant impact in our analysis with respect to our accuracy.

block bootstrap analysis and the Gamma Method [112] choosing the same bin-length (or window size in the case of the latter) for all the matrix elements, choosed conservatively to be the largest among them. We have found a very good agreement between the two procedures. An interesting proof of the robustness of our technique to estimate the error is provided by the agreement of the bin-length estimated starting from the integrate autocorrelation time $\tau_{\rm int}$ and one given from blocking. Using Eq. (8.3.16) we compute the (matrix) renormalization constants, $Z(g_0, a/L)$ and its double-size $Z(g_0, a/2L)$, numerical values are collected in Tab. 8.7, 8.8.

We define the lattice SSFs as

$$\Sigma_O(g_0, a/L) = [Z(g_0, a/2L)][Z(g_0, a/L)]^{-1}\,, \tag{8.7.1}$$

Notice that in Eq. (8.7.1) we have chosen to multiply with Z^{-1} to the right. This imply the ordering which enter the definition of the evolution coefficient (as we will see).

8.7.1 Lattice computation of step-scaling functions

In the lattice setup employed for this work the O(a) counter terms for the four-fermion operators have not been included. A preliminary study [133, 134] on the $\mathcal{O}(1/m)$ counterterms for the static four-fermion operators entering in HQET computations, which share a similar structure to the ones required for achieving $\mathcal{O}(a)$ improvement, reasonably suggests that ≥ 10 improvement parameters would need to be tuned. A possible solution, which simplify enormously the task is given by the Chirally Rotated Schrödinger Function (χSF). It has been proved [135], that the employment of this slightly different renormalization scheme [12] provides an *automatic* $\mathcal{O}(a)$-improvement. Preliminary study in this directions are ongoing [136], but out of the scope of this thesis.

The only linear cutoff effects which are removed from $\Sigma(u, a/L)$ are those cancelled by the non-perturbative improvement of the fermion action, and by the boundary improvements as discussed above.
We therefore expect linear cut-off effects to be still present and correspondingly we fit to the ansatz

$$[\Sigma_O(u, a/L)]_{ij} = [\sigma_O]_{ij}(u) + [\rho_O]_{ij}(u)(a/L)\,, \tag{8.7.2}$$

where the subscripts i, j denote elements of the matrices Σ_O, the continuum SSF σ_O and slope ρ_O. In practice, to remove part of the linear cutoff effects at $\mathcal{O}(ag^2)$ we define a "subtracted" matrix SSF as

$$\tilde{\Sigma}_O(u, a/L) = [\Sigma_O(u, a/L)][\mathbf{1} + u\log(2)\delta_k(a/L)\gamma^{(0)}]^{-1}\Big|_{u=g^2_{\rm SF}(L)} \tag{8.7.3}$$

the details about the definition of the relative 1-loop cutoff effects $[\delta_k(a/L)]_{ij}$ are provided in section 8.5 and numerical values in Appendix A. In order to have a good control about the continuum $\sigma_O(u)$ we performed the extrapolation on both the Σ_O and $\tilde{\Sigma}_O$, leading to a good agreement within one standard deviation for all the matrix elements except for the ones with a very large LO anomalous dimensions (e.g. $O_{5,4}$). We have checked that, in most case, in particular at large coupling, linear fits to all three data-points and weighted averages of the two results from the finest lattices lead to continuum limit estimates compatible within one standard deviation. However this is not true at the smallest coupling where the statistical error is smaller. Conservatively we then quote, as our best results, those obtained from linear extrapolation involving all three data-points of the "subtracted" SSF with a systematic error added in quadrature to the

[12] Which require completely different correlation functions respect to the ones in the "standard" SF

u	$\sigma^{\alpha=3/2,(3,5),+}_{(45)}(u)$	$\sigma^{\alpha=3/2,(3,5),-}_{(45)}(u)$
0.9793	$\begin{pmatrix} 0.9554(90) & -0.00212(78) \\ -0.256(41) & 1.0479(76) \end{pmatrix}$	$\begin{pmatrix} 0.8870(94) & -0.00092(79) \\ 0.093(37) & 1.0040(66) \end{pmatrix}$
1.1814	$\begin{pmatrix} 0.957(12) & -0.0005(10) \\ -0.195(56) & 1.076(11) \end{pmatrix}$	$\begin{pmatrix} 0.883(11) & -0.0024(10) \\ 0.009(46) & 1.0012(95) \end{pmatrix}$
1.5078	$\begin{pmatrix} 0.930(16) & -0.0016(15) \\ -0.252(76) & 1.089(16) \end{pmatrix}$	$\begin{pmatrix} 0.833(18) & -0.0026(13) \\ 0.022(62) & 0.994(10) \end{pmatrix}$
2.0142	$\begin{pmatrix} 0.896(14) & -0.0034(11) \\ -0.355(67) & 1.105(12) \end{pmatrix}$	$\begin{pmatrix} 0.763(11) & -0.0021(12) \\ 0.046(55) & 0.988(12) \end{pmatrix}$
2.4792	$\begin{pmatrix} 0.874(18) & -0.0020(14) \\ -0.288(82) & 1.136(17) \end{pmatrix}$	$\begin{pmatrix} 0.718(19) & -0.0039(18) \\ -0.066(67) & 0.959(17) \end{pmatrix}$
3.3340	$\begin{pmatrix} 0.812(25) & -0.0098(32) \\ -0.52(13) & 1.204(36) \end{pmatrix}$	$\begin{pmatrix} 0.587(20) & 0.0012(23) \\ -0.056(92) & 0.948(22) \end{pmatrix}$

TABLE 8.2: Continuum SSFs for Op $4,5$ in the specific renormalization scheme $(s_1, s_2) = (3, 5)$.

one from the fit given from the discrepancy of the extrapolated values between the raw data and the "subtracted" ones. The results of continuum extrapolation of Σ_O can be found in Tab. 8.1, 8.2, and plots for a specific renormalization scheme are provided in in Fig. (8.11,8.12,8.13,8.14).

8.7.2 Non-perturbative running in the continuum

In order to compute the RG running of the operators in the continuum limit, the continuum SSFs have to be fitted to the functional form showed below in Appendix 8.6.
We performed the fit with different Ansatz, considering different orders in the polynomial expansion and keeping different combination of parameter fixed to their perturbative values,

$$[\sigma_O(u)]_{ij} = \delta_{ij} + [r_1]_{O,ij}u + [r_2]_{O,ij}u^2 + [r_3]_{O,ij}u^3 + O(u^4)\,, \tag{8.7.4}$$

but we quote as best Ansatz the one at $O(u^3)$ with matrices of parameters r_1 and r_2 fixed to their perturbative values and r_3 left as free parameters. As a check we found that fitted values of r_2 turned out to be close to the perturbative prediction of Eq. (8.6.12).
An important remark here is that since the deviations from LO are large for some matrix elements (in particular σ^+_{54}) the knowledge of the NLO anomalous dimension $\gamma^{(1)}_{\rm SF}$ from perturbative calculations is necessary in order to have a good convergence of the fit since it enters in the definition of r_2. The plots of the SSFs for an example scheme are collected in Fig. (8.7,8.8). In practice, as stressed several times in this thesis, the SSFs allow to access to RG evolution, in fact, using Eq. (8.6.2) we can compute the evolution by taking product of SSFs as

$$U(\mu_{\rm had}, 2^n\mu_{\rm had}) = \sigma_O(u_0)\sigma_O(u_1)\cdots\sigma_O(u_{n-1})\,, \tag{8.7.5}$$

with

$$\sigma(u_0) = 4.61 = u(\mu_{\rm had})\,, \tag{8.7.6}$$

$$u_k = \sigma(u_{k-1})\,. \tag{8.7.7}$$

The running factor (expressed in terms of renormalization constants) from the hadronic scale $\mu_{\rm had}$ to a formal infinite scale then is given by

$$\tilde{U}(\mu_{\rm had}) = \left[\frac{\bar{g}^2(\mu_{\rm pt})}{4\pi}\right]^{-\frac{\gamma^{(0)}}{2b_0}} W(\mu_{\rm pt})\,[U(\mu_{\rm had},\mu_{\rm pt})]^{-1}\,, \tag{8.7.8}$$

It is easy to see from the above equation that $\mu_{\rm pt}$ plays no rôle to the formal definition of the running once the scale is taken to be large enough to apply safely PT. The effect of varying the perturbative matching point in a specific scheme is described in Tab. (8.3,8.4). In the present work, as a consequence of the recursive SSFs procedure, the perturbative matching point is defined to be $\mu_{\rm pt} = 2^n\mu_{\rm had}$. In the current work, we use $n = 8$ which is the maximum possible without extrapolating from our non-perturbative data. Playing the reverse game, i.e. keeping $\mu_{\rm pt} = 2^8\mu_{\rm had}$ and changing the value of $\mu_{\rm had}$ in Eq. (8.7.8) yields to Fig. (8.9, 8.10). In Tables 8.3, 8.4 is showed the dependence on the perturbative matching point in the running from $\mu_{\rm had}$. We observe that for $n > 5$ the value stabilises and the PT systematics became negligible. In implementing Eq. (8.7.8), we used the numerical integration as described in section 8.4.

8.7.3 Hadronic Matching

Having computed the universal NLO evolution factors defined through Eq. (8.7.8), which provide the RG-running from the low energy matching scale μ_{had} to a formally infinite one, we proceeded to establish the connection between bare lattice operators and their RGI counterparts. As showed in previous sections, Z_{RGI} factors do not depend on any renormalisation scale and carries a dependence upon the renormalization condition only via cutoff effects.
In order to obtain $Z(g_0, a\mu_{had})$ we computed $Z(g_0, a\mu)$ at three values of the lattice spacing, namely $\beta = \{5.20, 5.29, 5.40\}$, which belong to range of inverse couplings commonly used for simulations of two-flavours QCD in physically large volumes. The numerical values are listed in Tab. (8.7,8.8). In order to interpolate $u(\mu_{had}) = 4.61$ we performed an interpolation (whose parameters are available upon request) with a global fit given by

$$[Z_{\rm had}(\beta,u)]_{ij} = \sum_{n=0}^{N_\beta} a_{i,j}^{(n)}[\beta-5,20]^n + \sum_{m=1}^{N_u} b_{i,j}^{(m)}[u]^m + \sum_{k=1}^{N_{\log}} c_{i,j}^{(k)}[\log(u)]^k + \text{mixed terms}\,. \tag{8.7.9}$$

In the current case, given the limited statistics and quality of the hadronic renormalization constant we found as the following ansatz to describe better our data

$$\begin{aligned} &a_{i,j}^{(0)} + a_{i,j}^{(1)}[\beta-5.20] + a_{i,j}^{(2)}[\beta-5.20]^2 \\ &+ b_{i,j}^{(1)}u + c_{i,j}^{(1)}\log(u) + [\beta-5.20](d_{i,j}^{(1)}u + e_{i,j}^{(1)}\log(u)) + d_{i,j}^{(2)}u^2[\beta-5.20]^2\,. \end{aligned} \tag{8.7.10}$$

n	$\tilde{U}^{+}_{23}(2^n\mu_{\rm had})$	$\tilde{U}^{-}_{23}(2^n\mu_{\rm had})$
0	$\begin{pmatrix} 1.215505 & -0.363611 \\ -0.077786 & 0.472123 \end{pmatrix}$	$\begin{pmatrix} 1.132141 & -0.607507 \\ 0.063161 & 0.431281 \end{pmatrix}$
1	$\begin{pmatrix} 1.2016(190) & -0.1649(270) \\ -0.0532(22) & 0.4562(80) \end{pmatrix}$	$\begin{pmatrix} 1.1837(126) & -0.6972(172) \\ 0.0484(24) & 0.4185(67) \end{pmatrix}$
2	$\begin{pmatrix} 1.2022(283) & -0.0773(425) \\ -0.0476(29) & 0.4580(112) \end{pmatrix}$	$\begin{pmatrix} 1.2057(186) & -0.7419(277) \\ 0.0452(32) & 0.4200(94) \end{pmatrix}$
3	$\begin{pmatrix} 1.2030(336) & -0.0212(499) \\ -0.0453(32) & 0.4595(129) \end{pmatrix}$	$\begin{pmatrix} 1.2177(221) & -0.7693(344) \\ 0.0440(36) & 0.4213(110) \end{pmatrix}$
4	$\begin{pmatrix} 1.2035(369) & 0.0212(559) \\ -0.0441(34) & 0.4599(138) \end{pmatrix}$	$\begin{pmatrix} 1.2250(243) & -0.7886(387) \\ 0.0433(38) & 0.4216(118) \end{pmatrix}$
5	$\begin{pmatrix} 1.2035(395) & 0.0542(609) \\ -0.0434(35) & 0.4595(144) \end{pmatrix}$	$\begin{pmatrix} 1.2298(258) & -0.8027(422) \\ 0.0428(40) & 0.4212(124) \end{pmatrix}$
6	$\begin{pmatrix} 1.2033(412) & 0.0808(644) \\ -0.0429(35) & 0.4588(147) \end{pmatrix}$	$\begin{pmatrix} 1.2333(268) & -0.8135(447) \\ 0.0424(41) & 0.4206(127) \end{pmatrix}$
7	$\begin{pmatrix} 1.2031(426) & 0.1022(674) \\ -0.0425(36) & 0.4580(150) \end{pmatrix}$	$\begin{pmatrix} 1.2358(276) & -0.8220(468) \\ 0.0422(41) & 0.4200(130) \end{pmatrix}$
8	$\begin{pmatrix} 1.2028(436) & 0.1202(692) \\ -0.0423(36) & 0.4572(152) \end{pmatrix}$	$\begin{pmatrix} 1.2377(281) & -0.8289(486) \\ 0.0420(42) & 0.4192(131) \end{pmatrix}$

TABLE 8.3: Dependence on the perturbative matching scale for Op $2, 3$.

n	$\tilde{U}^{+}_{45}(2^n\mu_{\rm had})$	$\tilde{U}^{-}_{45}(2^n\mu_{\rm had})$
0	$\begin{pmatrix} 0.522119 & 0.028246 \\ 2.648160 & 2.098693 \end{pmatrix}$	$\begin{pmatrix} 0.492746 & -0.032468 \\ -2.607554 & 0.771786 \end{pmatrix}$
1	$\begin{pmatrix} 0.5417(73) & 0.0242(7) \\ 2.3620(1360) & 2.1229(300) \end{pmatrix}$	$\begin{pmatrix} 0.4531(96) & -0.0304(5) \\ -2.2066(850) & 0.8223(81) \end{pmatrix}$
2	$\begin{pmatrix} 0.5537(106) & 0.0232(9) \\ 2.2306(2151) & 2.1222(446) \end{pmatrix}$	$\begin{pmatrix} 0.4474(134) & -0.0305(7) \\ -2.0604(1298) & 0.8502(119) \end{pmatrix}$
3	$\begin{pmatrix} 0.5602(126) & 0.0228(10) \\ 2.1242(2675) & 2.1205(534) \end{pmatrix}$	$\begin{pmatrix} 0.4443(159) & -0.0307(8) \\ -1.9636(1558) & 0.8670(142) \end{pmatrix}$
4	$\begin{pmatrix} 0.5636(136) & 0.0226(11) \\ 2.0255(3040) & 2.1214(585) \end{pmatrix}$	$\begin{pmatrix} 0.4411(172) & -0.0309(8) \\ -1.8862(1750) & 0.8779(154) \end{pmatrix}$
5	$\begin{pmatrix} 0.5652(143) & 0.0225(11) \\ 1.9411(3365) & 2.1237(619) \end{pmatrix}$	$\begin{pmatrix} 0.4379(181) & -0.0311(8) \\ -1.8213(1884) & 0.8854(163) \end{pmatrix}$
6	$\begin{pmatrix} 0.5656(150) & 0.0225(11) \\ 1.8581(3668) & 2.1266(643) \end{pmatrix}$	$\begin{pmatrix} 0.4350(186) & -0.0312(9) \\ -1.7669(2009) & 0.8905(168) \end{pmatrix}$
7	$\begin{pmatrix} 0.5659(154) & 0.0224(11) \\ 1.7872(3884) & 2.1292(663) \end{pmatrix}$	$\begin{pmatrix} 0.4322(191) & -0.0314(9) \\ -1.7212(2105) & 0.8947(174) \end{pmatrix}$
8	$\begin{pmatrix} 0.5657(158) & 0.0224(11) \\ 1.7245(4070) & 2.1317(679) \end{pmatrix}$	$\begin{pmatrix} 0.4297(195) & -0.0315(9) \\ -1.6825(2182) & 0.8976(176) \end{pmatrix}$

TABLE 8.4: Dependence on the perturbative matching scale for Op $4, 5$.

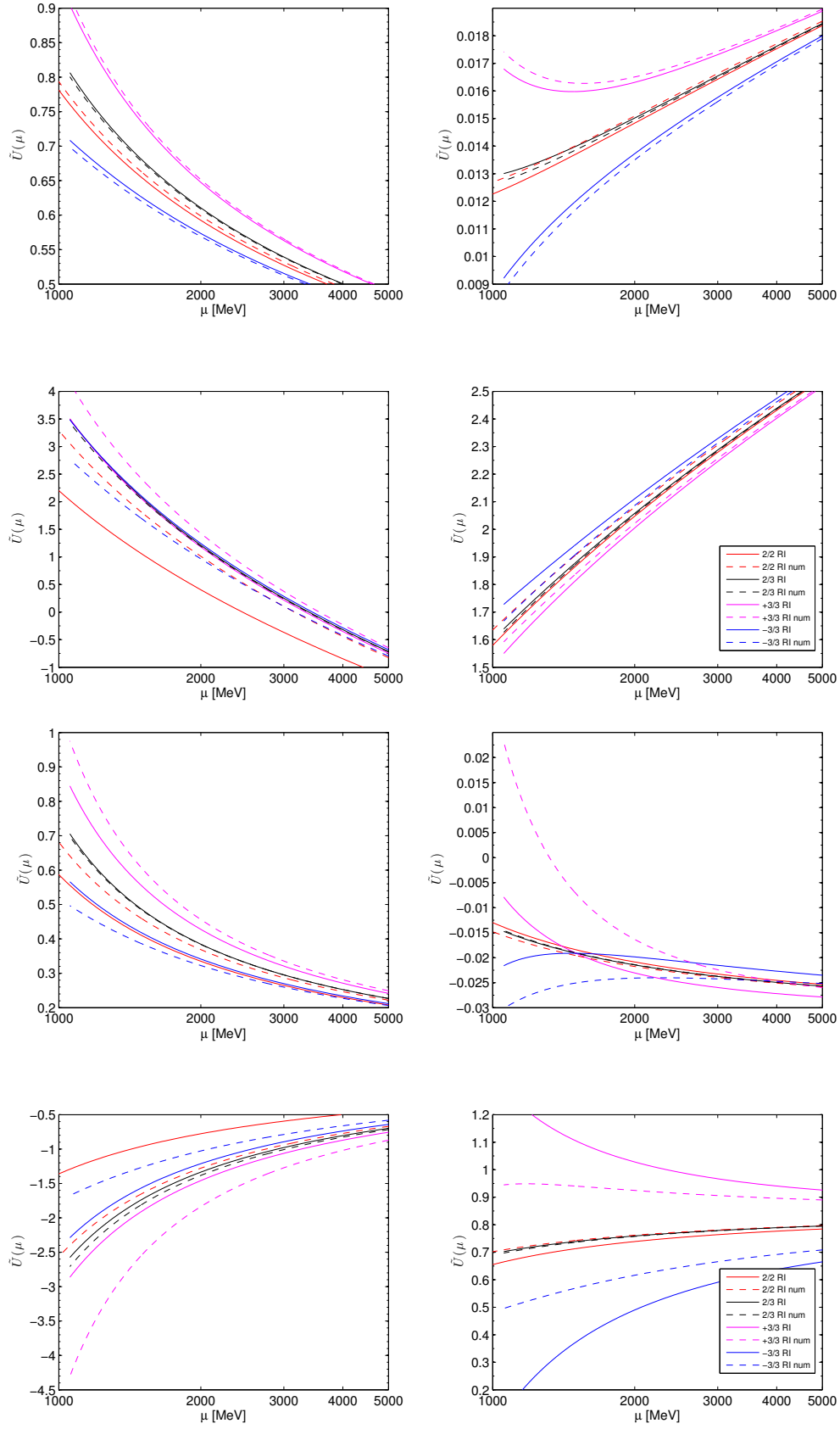

FIGURE 8.4: RG running matrix for the Op $4,5$ in the RI scheme. Top half (a): Fierz $+$. Bottom half (b): Fierz $-$. The four cases $n_\gamma/n_\beta = \{2/2, 2/3, +3/3, -3/3\}$ are plotted respectively in red, black, magenta and blue. Dashed lines correspond to the numerical integration of $W(\mu)$. Solid lines correspond to the perturbative expansion up to $\mathrm{O}(g^2)$ (i.e. J_1) for the $2/2$ case and up to $\mathrm{O}(g^4)$ (i.e. J_2) for the $2/3$, $+3/3$ and $-3/3$ cases.

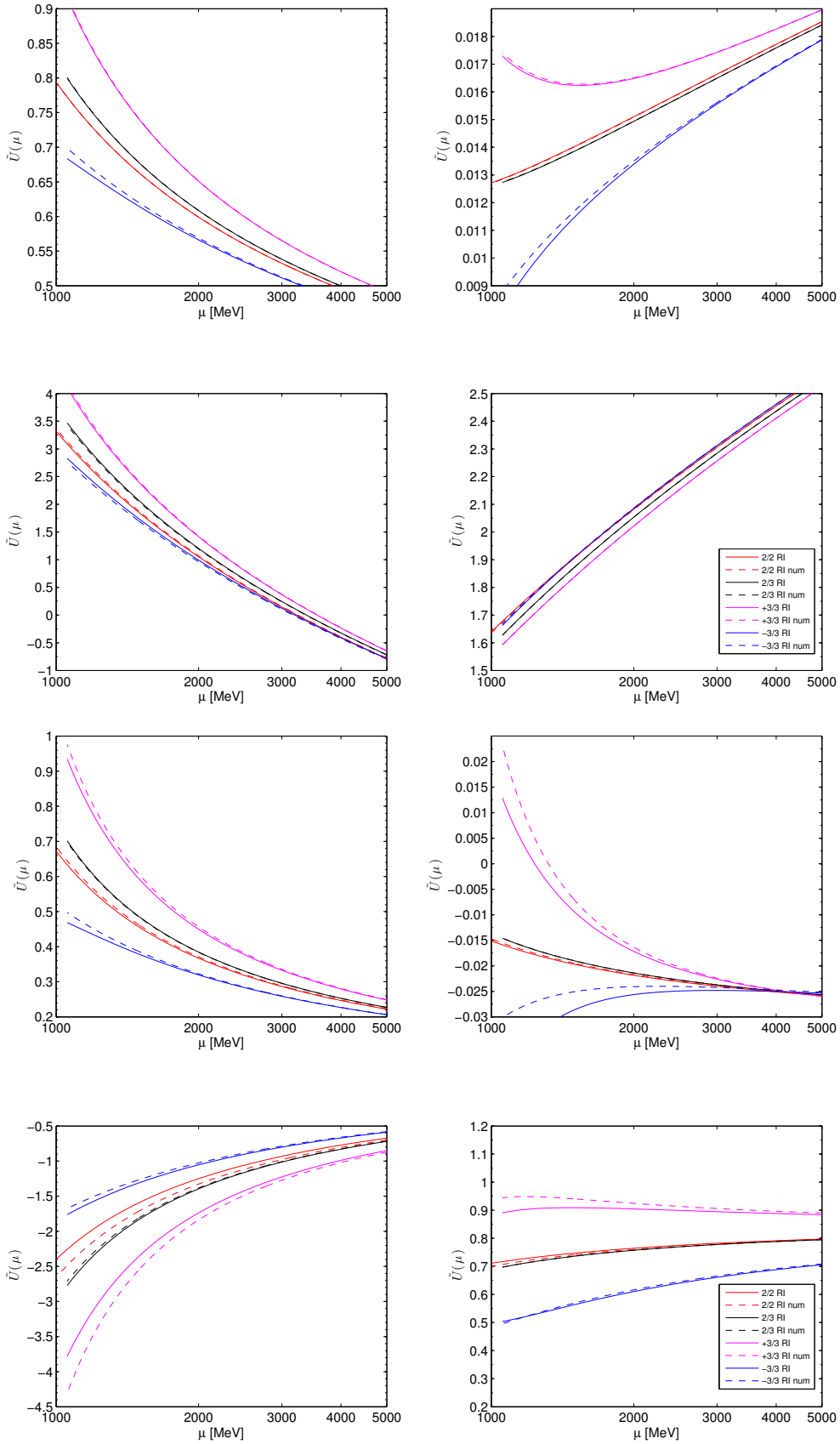

FIGURE 8.5: RG running matrix for the Op $4,5$ in the RI scheme. Top half (a): Fierz $+$. Bottom half (b): Fierz $-$. The four cases $n_\gamma/n_\beta = \{2/2, 2/3, +3/3, -3/3\}$ are plotted respectively in red, black, magenta and blue. Dashed lines correspond to the numerical integration of $W(\mu)$. Solid lines correspond to the perturbative expansion up to $\mathrm{O}(g^4)$ (i.e. J_2) for the $2/2$ case and up to $\mathrm{O}(g^6)$ (i.e. J_3) for the $2/3$, $+3/3$ and $-3/3$ cases.

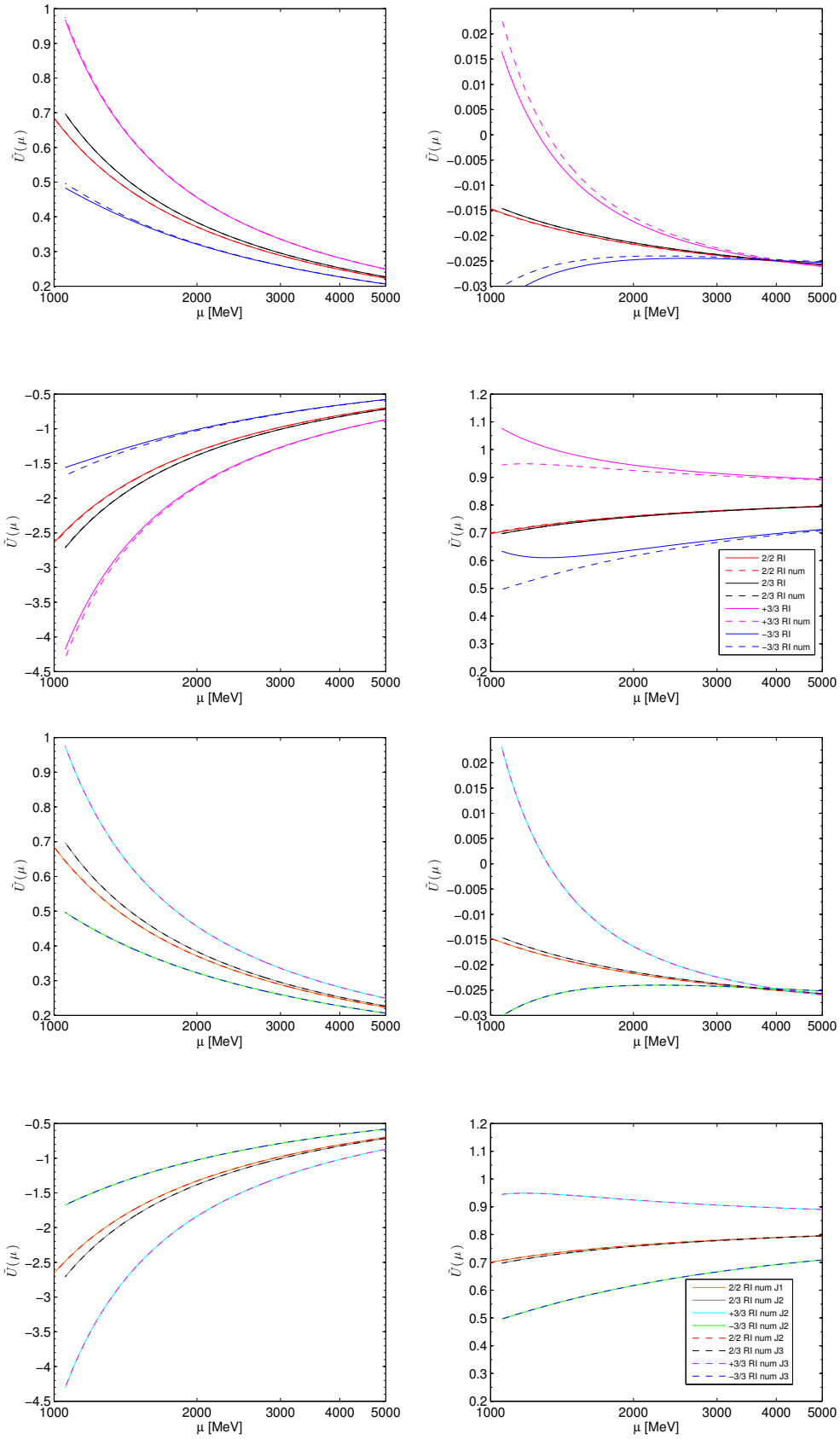

FIGURE 8.6: RG running matrix for the Op $4,5$ Fierz $-$ in the RI scheme. Top half (a): the four cases $n_\gamma/n_\beta = \{2/2, 2/3, +3/3, -3/3\}$ are plotted respectively in red, black, magenta and blue. Dashed lines correspond to the numerical integration of $W(\mu)$. Solid lines correspond to the perturbative expansion up to $\mathrm{O}(g^6)$ (i.e. J_3) for the $2/2$ case and up to $\mathrm{O}(g^8)$ (i.e. J_4) for the $2/3$, $+3/3$ and $-3/3$ cases. Bottom half (b): comparison of the results for the numerical integration of $W(\mu)$ when matched at $\bar{g}^2_{\overline{\mathrm{MS}}}(M_P)$ with the perturbative expansion at the order used in Fig. 8.4 (solid lines) and Fig. 8.5 (dashed lines).

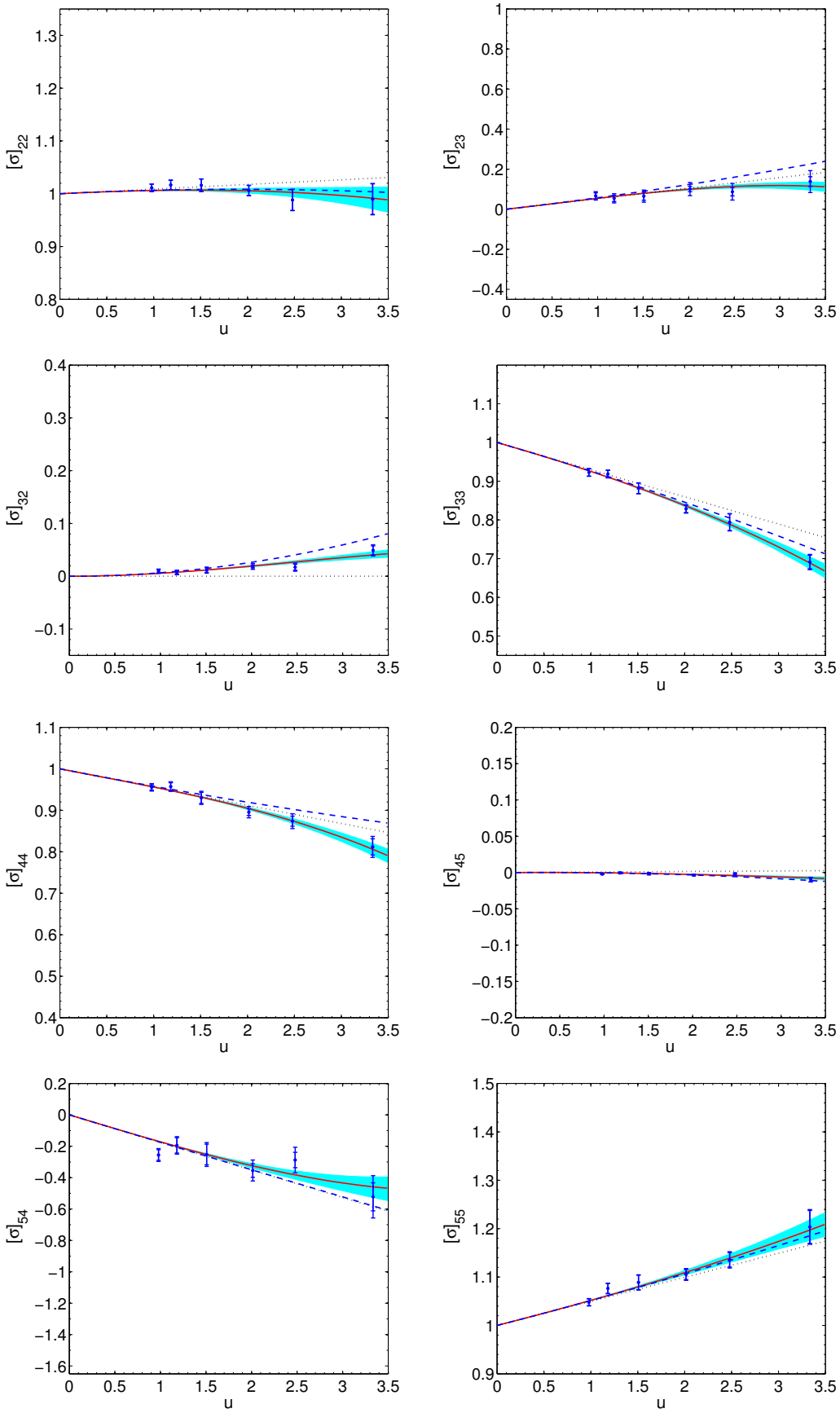

FIGURE 8.7: Continuum matrix SSFs for Op $2, 3$ top, $4, 5$ bottom with fierz "+". LO approximation $\mathcal{O}(u)$ is represented by the dotted black line, while NLO $\mathcal{O}(u^2)$ is given by the dashed blue line. Red line is the fit $\mathcal{O}(u^3)$ with a correspondent error band.

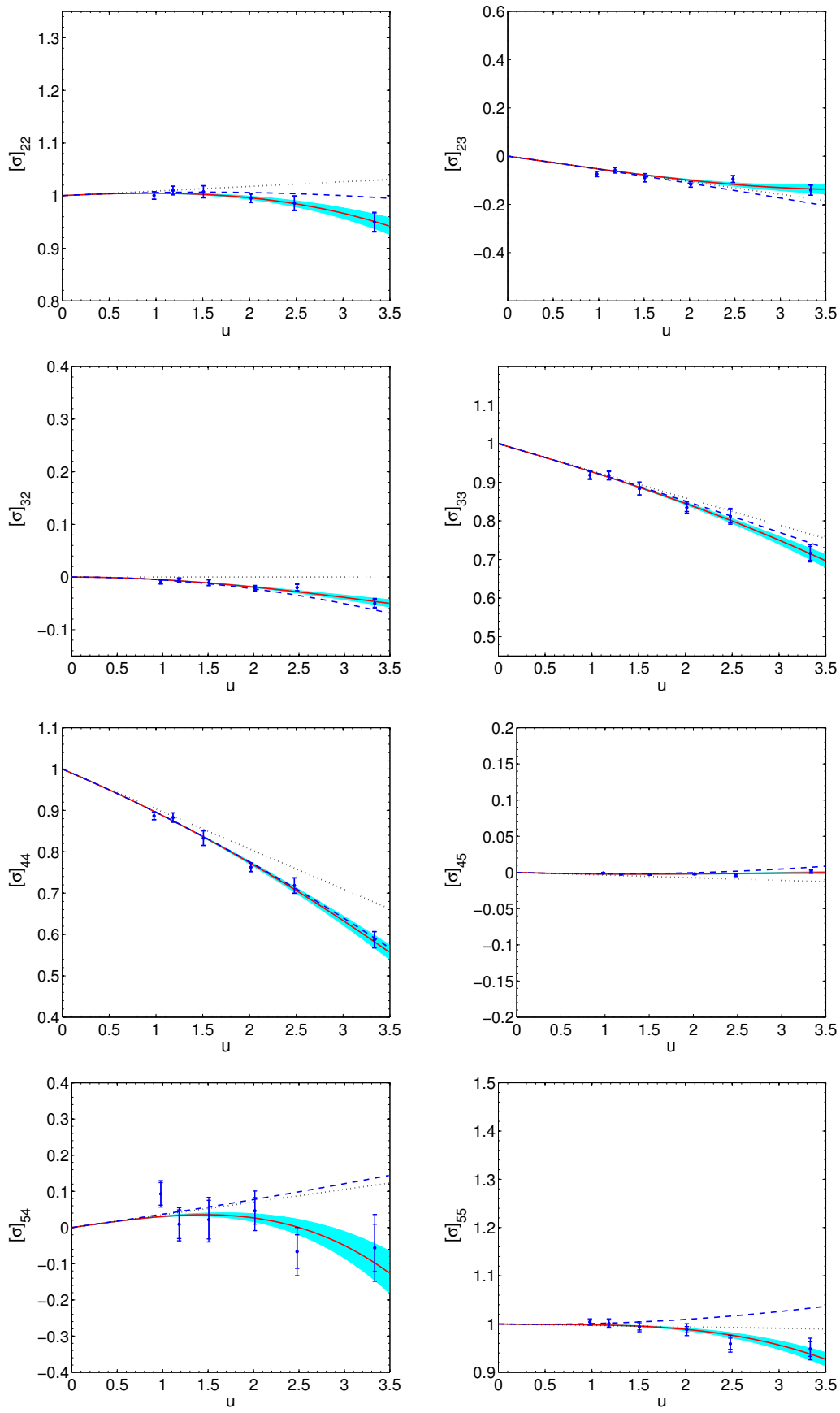

FIGURE 8.8: Continuum matrix SSFs for Op $2,3$ top, $4,5$ bottom with fierz "-". LO approximation $\mathcal{O}(u)$ is represented by the dotted black line, while NLO $\mathcal{O}(u^2)$ is given by the dashed blue line. Red line is the fit $\mathcal{O}(u^3)$ with a correspondent error band.

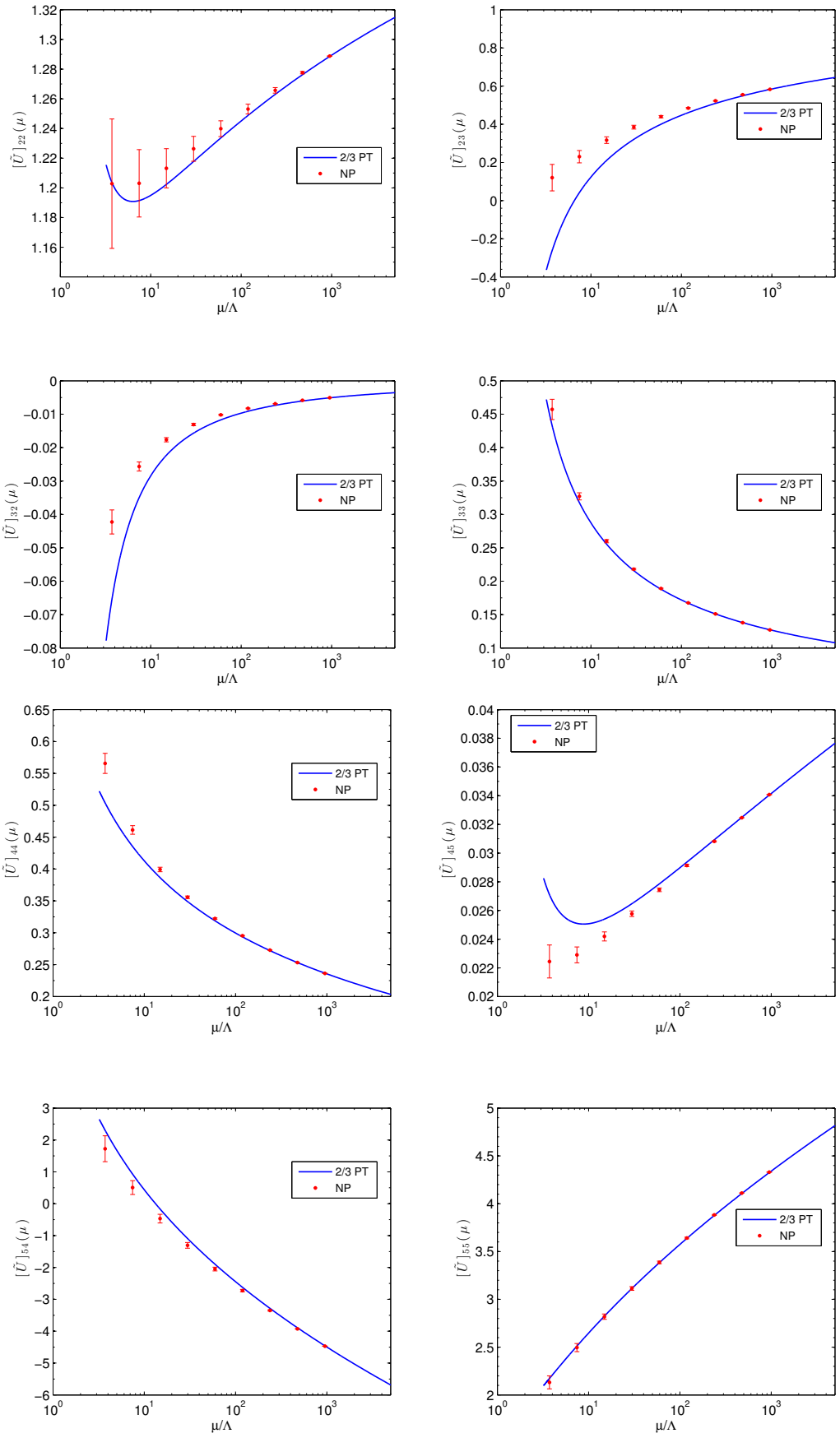

FIGURE 8.9: Non-perturbative running of Op 2, 3 (Op 4, 5) on the top (bottom) with fierz "+". Results are compared with the perturbative ones obtained from a numerical integration of the evolution coefficient with 2-loops γ and 3-loops β which is the highest order known for the SF renormalization scheme.

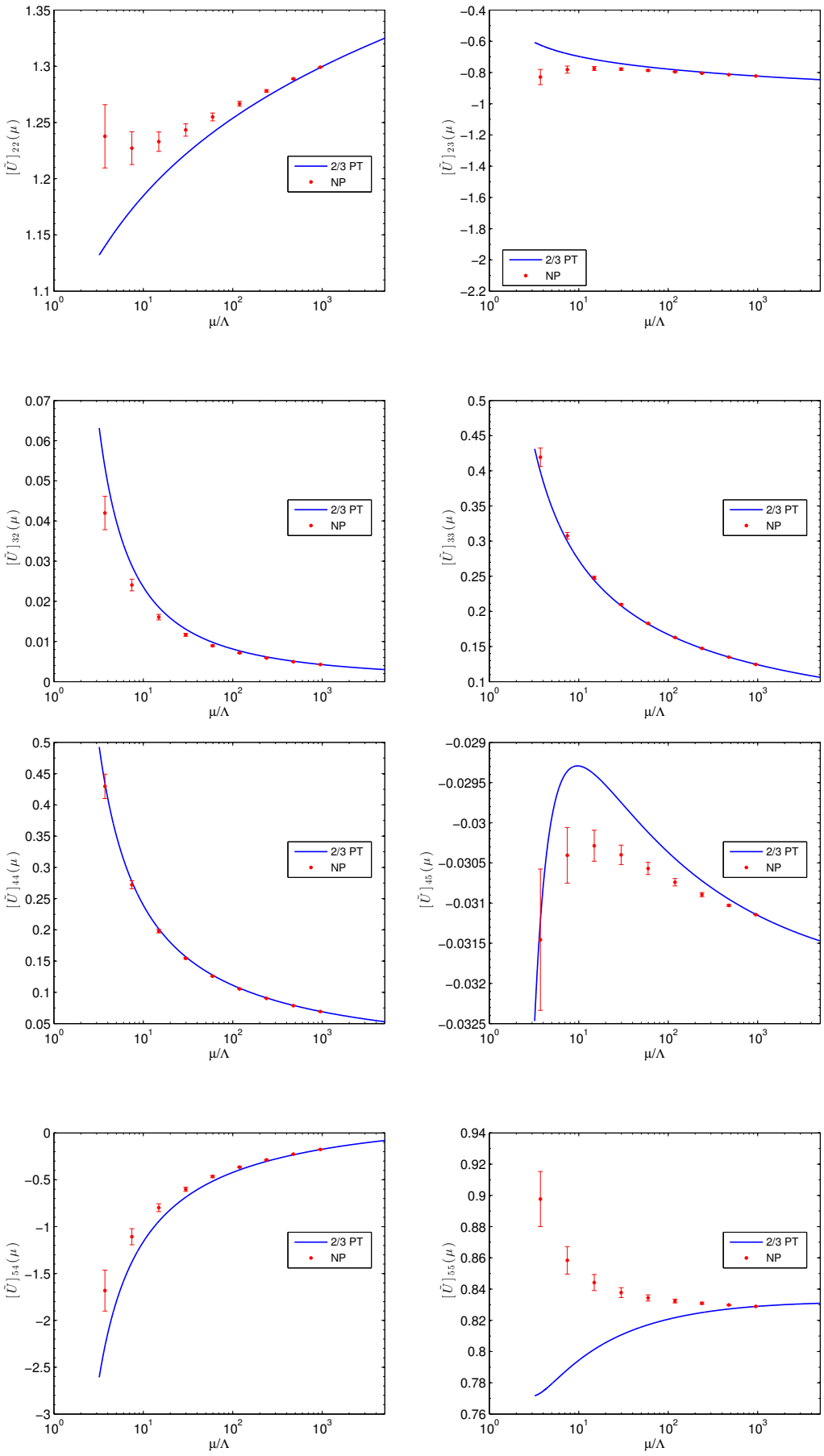

FIGURE 8.10: Non-perturbative running of Op $2,3$ (Op $4,5$) on the top (bottom) with fierz ″-″. Results are compared with the perturbative ones obtained from a numerical integration of the evolution coefficient with 2-loops γ and 3-loops β which is the highest order known for the SF renormalization scheme.

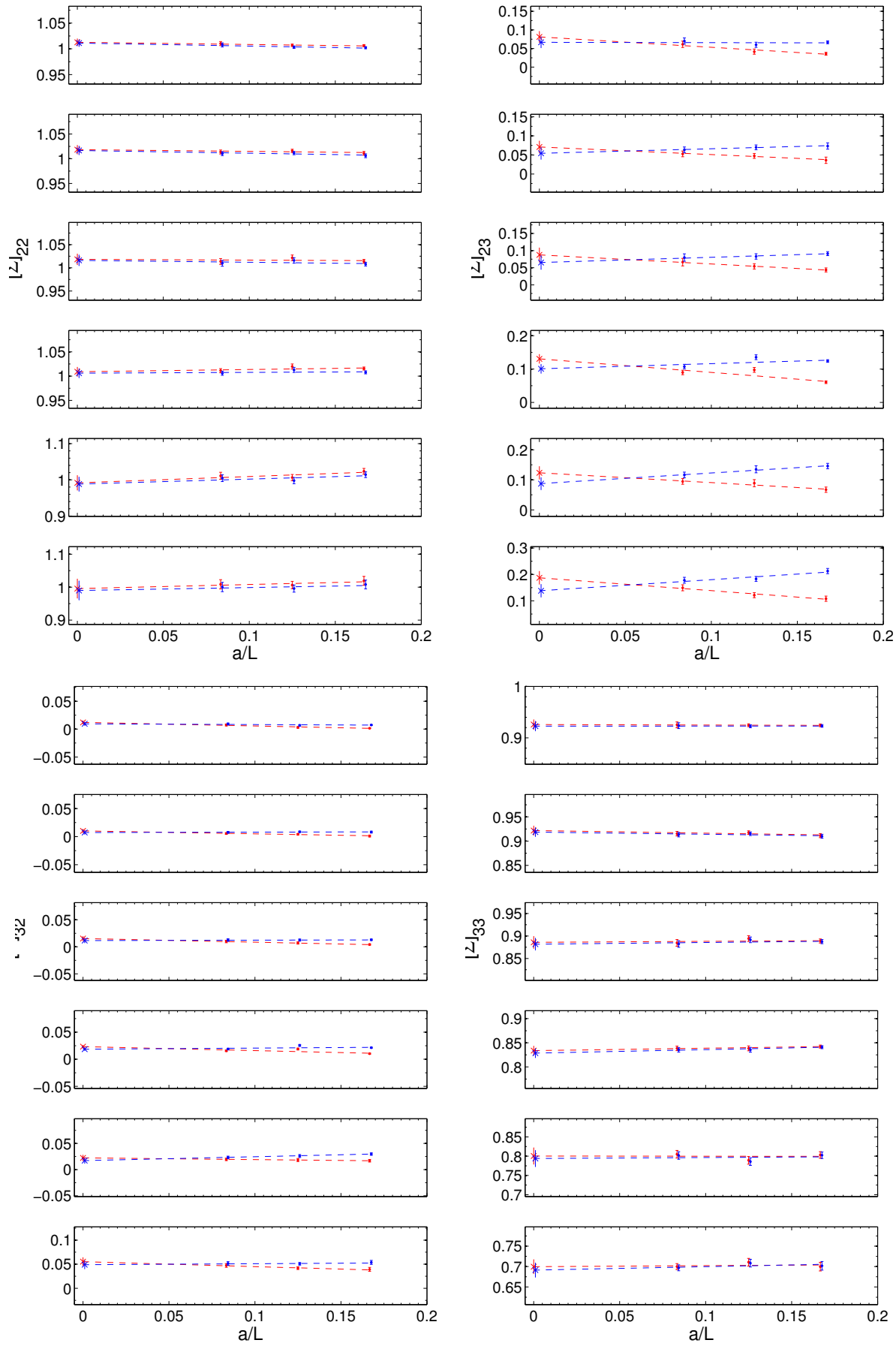

FIGURE 8.11: Linear continuum extrapolation of $\Sigma(u, a/L)$ in red and $\tilde{\Sigma}(u, a/L)$ in blue for Op 2, 3 fierz "+". The renormalized coupling u grows from the top to the bottom for each element of the SSFs.

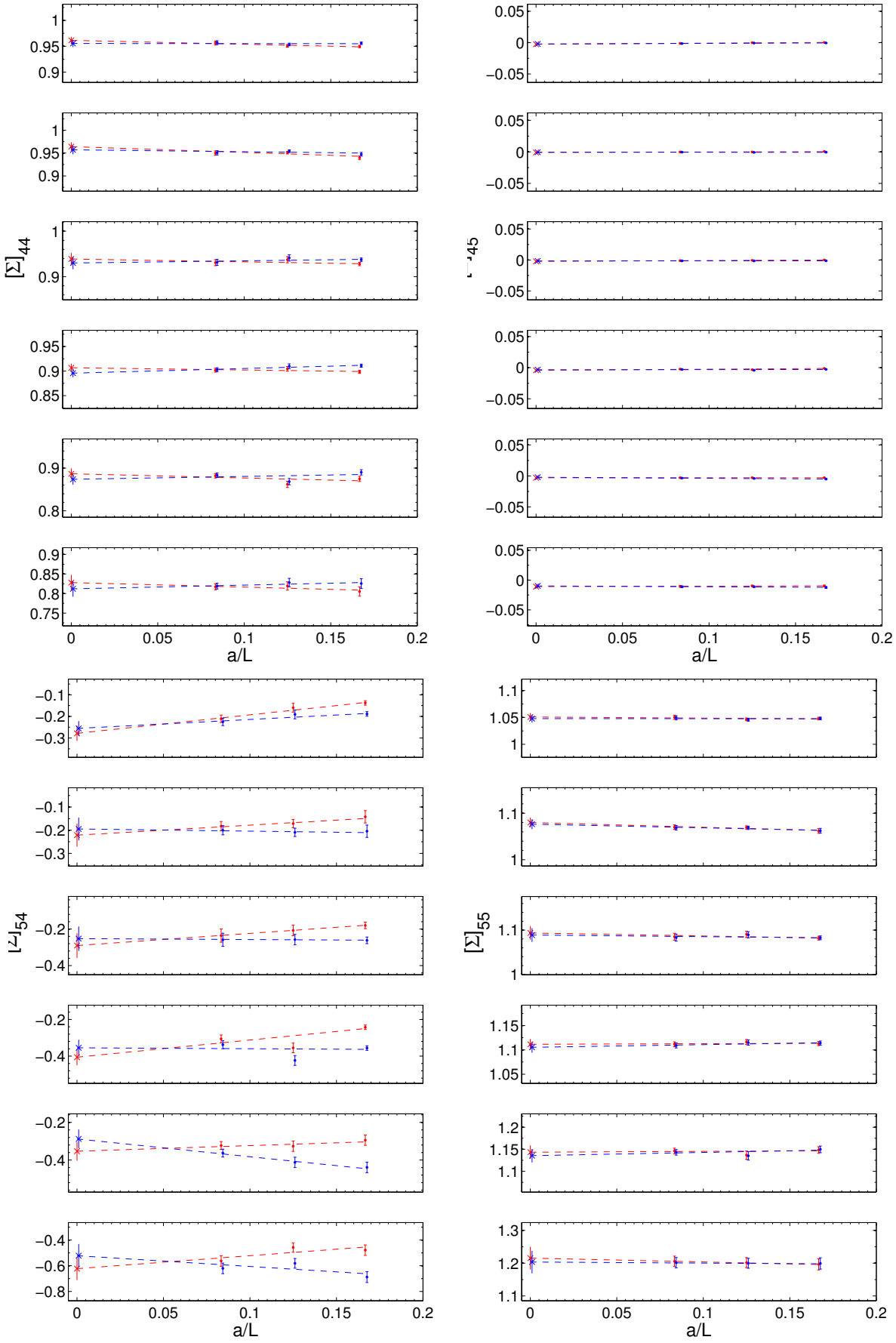

FIGURE 8.12: Linear continuum extrapolation of $\Sigma(u, a/L)$ in red and $\tilde{\Sigma}(u, a/L)$ in blue for Op $4, 5$ fierz "+". The renormalized coupling u grows from the top to the bottom for each element of the SSFs.

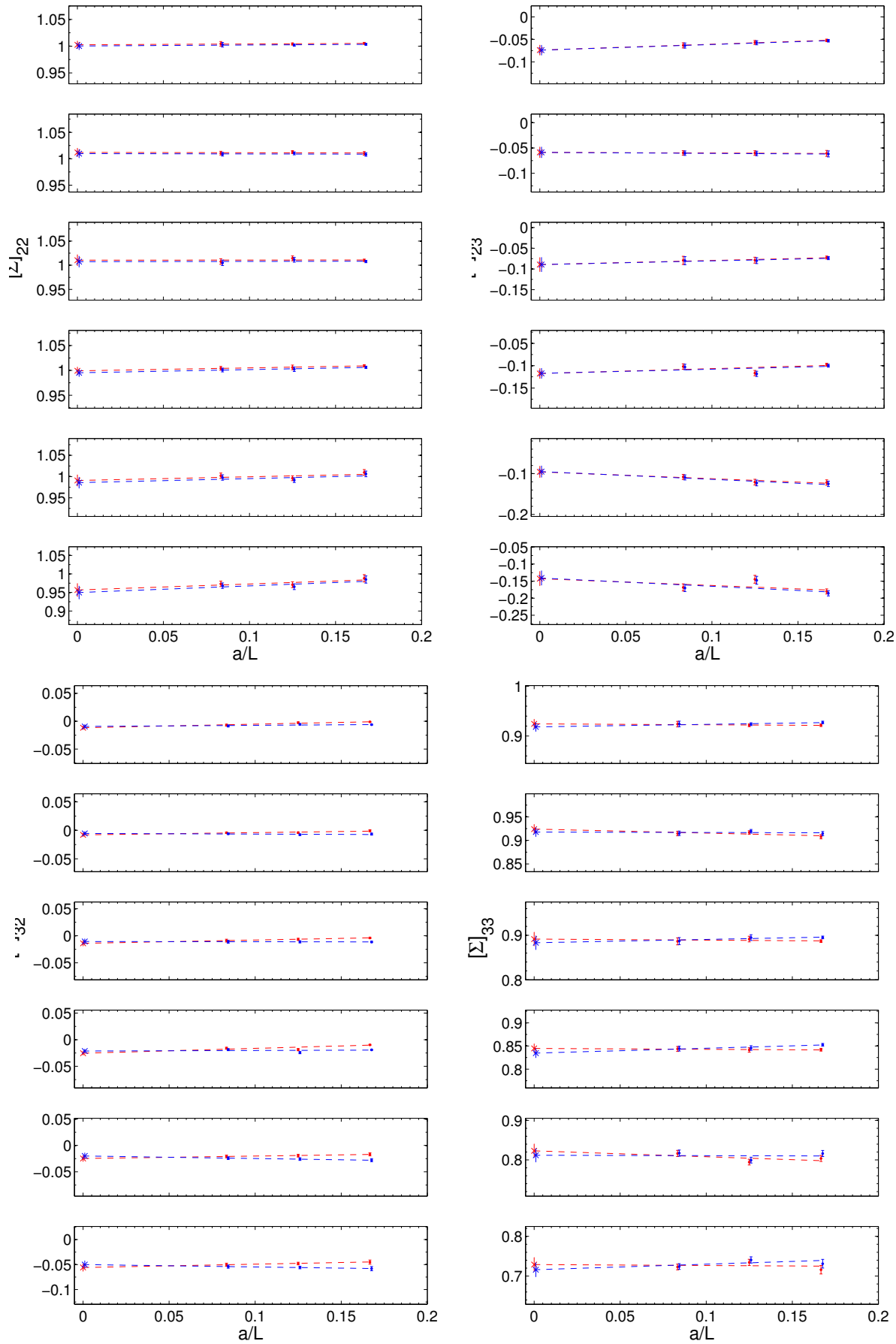

FIGURE 8.13: Linear continuum extrapolation of $\Sigma(u, a/L)$ in red and $\tilde{\Sigma}(u, a/L)$ for Op 2, 3 fierz ″-″. The renormalized coupling u grows from the top to the bottom for each element of the SSFs.

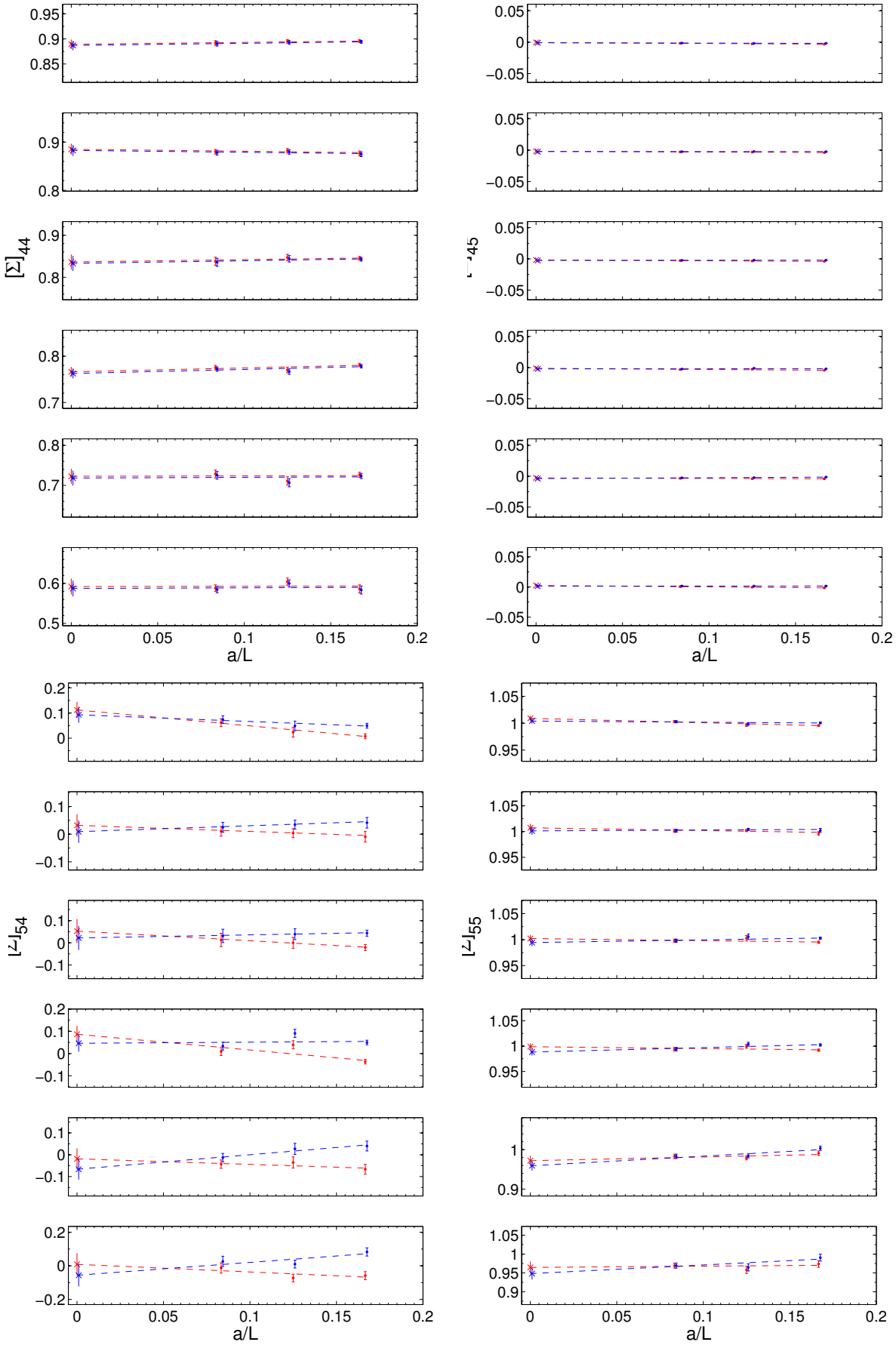

FIGURE 8.14: Linear continuum extrapolation of $\Sigma(u, a/L)$ in red and $\tilde{\Sigma}(u, a/L)$ for Op $4, 5$ fierz "-". The renormalized coupling u grows from the top to the bottom for each element of the SSFs.

$\bar{g}^2_{SF}(L)$	β	k_{cr}	L/a	$\left[Z^{\alpha=3/2,(3,5),+}_{(23)}(g_0,a/L)\right]^{-1}$	$Z^{\alpha=3/2,(3,5),+}_{(23)}(g_0,a/2L)$	$\Sigma^{\alpha=3/2,(3,5),+}_{(23)}(g_0,a/L)$
0.9793	9.50000	0.131532	6	$\begin{pmatrix} 1.2133(17) & -0.3792(35) \\ -0.05744(71) & 1.4505(27) \end{pmatrix}$	$\begin{pmatrix} 0.8410(13) & 0.2446(20) \\ 0.03188(52) & 0.6457(13) \end{pmatrix}$	$\begin{pmatrix} 1.0063(20) & 0.0358(39) \\ 0.00157(79) & 0.9244(26) \end{pmatrix}$
	9.73410	0.131305	8	$\begin{pmatrix} 1.2049(16) & -0.3904(39) \\ -0.05411(82) & 1.4807(27) \end{pmatrix}$	$\begin{pmatrix} 0.8470(17) & 0.2516(42) \\ 0.0310(10) & 0.6326(15) \end{pmatrix}$	$\begin{pmatrix} 1.0069(24) & 0.0416(69) \\ 0.0030(14) & 0.9246(28) \end{pmatrix}$
	10.05755	0.131069	12	$\begin{pmatrix} 1.1897(14) & -0.4106(34) \\ -0.05176(66) & 1.5153(25) \end{pmatrix}$	$\begin{pmatrix} 0.8612(30) & 0.2740(47) \\ 0.0332(14) & 0.6196(34) \end{pmatrix}$	$\begin{pmatrix} 1.0102(39) & 0.0613(84) \\ 0.0075(18) & 0.9253(57) \end{pmatrix}$
1.1814	8.50000	0.132509	6	$\begin{pmatrix} 1.2566(16) & -0.4655(35) \\ -0.07279(84) & 1.5573(30) \end{pmatrix}$	$\begin{pmatrix} 0.8200(29) & 0.2682(50) \\ 0.0353(13) & 0.5956(23) \end{pmatrix}$	$\begin{pmatrix} 1.0110(38) & 0.0361(82) \\ 0.0010(17) & 0.9113(41) \end{pmatrix}$
	8.72230	0.132291	8	$\begin{pmatrix} 1.2436(26) & -0.4875(58) \\ -0.0713(13) & 1.5927(42) \end{pmatrix}$	$\begin{pmatrix} 0.8332(18) & 0.2850(33) \\ 0.03712(84) & 0.5874(18) \end{pmatrix}$	$\begin{pmatrix} 1.0159(33) & 0.0475(64) \\ 0.0042(13) & 0.9175(38) \end{pmatrix}$
	8.99366	0.131975	12	$\begin{pmatrix} 1.2249(19) & -0.5071(46) \\ -0.06697(100) & 1.6373(34) \end{pmatrix}$	$\begin{pmatrix} 0.8436(32) & 0.2934(44) \\ 0.0356(11) & 0.5700(26) \end{pmatrix}$	$\begin{pmatrix} 1.0137(40) & 0.0528(75) \\ 0.0055(15) & 0.9154(46) \end{pmatrix}$
1.5078	7.54200	0.133705	6	$\begin{pmatrix} 1.3140(20) & -0.5896(40) \\ -0.09652(87) & 1.7162(33) \end{pmatrix}$	$\begin{pmatrix} 0.7937(27) & 0.2981(30) \\ 0.04239(88) & 0.5325(23) \end{pmatrix}$	$\begin{pmatrix} 1.0142(40) & 0.0435(59) \\ 0.0043(13) & 0.8890(45) \end{pmatrix}$
	7.72060	0.133497	8	$\begin{pmatrix} 1.3037(39) & -0.6279(73) \\ -0.0959(17) & 1.7721(65) \end{pmatrix}$	$\begin{pmatrix} 0.8071(43) & 0.3162(42) \\ 0.0437(14) & 0.5201(34) \end{pmatrix}$	$\begin{pmatrix} 1.0216(59) & 0.0541(78) \\ 0.0070(20) & 0.8943(63) \end{pmatrix}$
	8.02599	0.133063	12	$\begin{pmatrix} 1.2785(49) & -0.660(12) \\ -0.0924(25) & 1.826(11) \end{pmatrix}$	$\begin{pmatrix} 0.8166(40) & 0.3313(55) \\ 0.0439(16) & 0.5001(31) \end{pmatrix}$	$\begin{pmatrix} 1.0138(62) & 0.066(11) \\ 0.0099(23) & 0.8846(74) \end{pmatrix}$
2.0142	6.60850	0.135260	6	$\begin{pmatrix} 1.4150(27) & -0.8110(54) \\ -0.1425(12) & 2.0090(49) \end{pmatrix}$	$\begin{pmatrix} 0.7514(19) & 0.3335(15) \\ 0.05167(57) & 0.4401(13) \end{pmatrix}$	$\begin{pmatrix} 1.0157(31) & 0.0605(40) \\ 0.01041(96) & 0.8421(32) \end{pmatrix}$
	6.82170	0.134891	8	$\begin{pmatrix} 1.3812(53) & -0.814(11) \\ -0.1295(26) & 2.043(10) \end{pmatrix}$	$\begin{pmatrix} 0.7719(23) & 0.3554(27) \\ 0.05420(98) & 0.4320(17) \end{pmatrix}$	$\begin{pmatrix} 1.0199(52) & 0.0974(74) \\ 0.0189(17) & 0.8385(51) \end{pmatrix}$
	7.09300	0.134432	12	$\begin{pmatrix} 1.3519(40) & -0.8891(89) \\ -0.1335(22) & 2.1328(77) \end{pmatrix}$	$\begin{pmatrix} 0.7844(26) & 0.3691(25) \\ 0.05261(86) & 0.4150(18) \end{pmatrix}$	$\begin{pmatrix} 1.0113(43) & 0.0897(67) \\ 0.0157(14) & 0.8385(47) \end{pmatrix}$
2.4792	6.13300	0.136110	6	$\begin{pmatrix} 1.4969(45) & -1.0111(81) \\ -0.1878(20) & 2.2820(81) \end{pmatrix}$	$\begin{pmatrix} 0.7280(50) & 0.3519(39) \\ 0.0587(16) & 0.3780(35) \end{pmatrix}$	$\begin{pmatrix} 1.0236(79) & 0.0672(88) \\ 0.0169(25) & 0.8031(86) \end{pmatrix}$
	6.32290	0.135767	8	$\begin{pmatrix} 1.4557(36) & -1.0256(76) \\ -0.1743(20) & 2.3371(71) \end{pmatrix}$	$\begin{pmatrix} 0.7340(53) & 0.3602(44) \\ 0.0558(17) & 0.3621(39) \end{pmatrix}$	$\begin{pmatrix} 1.0063(86) & 0.089(12) \\ 0.0183(29) & 0.7893(99) \end{pmatrix}$
	6.63164	0.135227	12	$\begin{pmatrix} 1.4076(47) & -1.078(10) \\ -0.1677(28) & 2.401(10) \end{pmatrix}$	$\begin{pmatrix} 0.7640(65) & 0.3826(32) \\ 0.0569(15) & 0.3608(41) \end{pmatrix}$	$\begin{pmatrix} 1.0111(96) & 0.0945(94) \\ 0.0195(23) & 0.8051(98) \end{pmatrix}$
3.3340	5.62150	0.136665	6	$\begin{pmatrix} 1.6592(74) & -1.411(13) \\ -0.2842(37) & 2.863(15) \end{pmatrix}$	$\begin{pmatrix} 0.6776(84) & 0.3716(53) \\ 0.0714(29) & 0.2796(41) \end{pmatrix}$	$\begin{pmatrix} 1.019(14) & 0.1080(98) \\ 0.0392(41) & 0.700(10) \end{pmatrix}$
	5.80970	0.136608	8	$\begin{pmatrix} 1.5838(67) & -1.415(16) \\ -0.2655(46) & 2.888(16) \end{pmatrix}$	$\begin{pmatrix} 0.7001(70) & 0.3851(43) \\ 0.0738(19) & 0.2822(31) \end{pmatrix}$	$\begin{pmatrix} 1.006(11) & 0.1215(95) \\ 0.0419(28) & 0.7107(94) \end{pmatrix}$
	6.11816	0.136139	12	$\begin{pmatrix} 1.5063(82) & -1.424(20) \\ -0.2385(57) & 2.907(19) \end{pmatrix}$	$\begin{pmatrix} 0.7347(86) & 0.4113(46) \\ 0.0755(26) & 0.2776(29) \end{pmatrix}$	$\begin{pmatrix} 1.009(14) & 0.149(11) \\ 0.0474(38) & 0.6999(72) \end{pmatrix}$

$\bar{g}^2_{SF}(L)$	β	k_{cr}	L/a	$\left[Z^{\alpha=3/2,(3,5),-}_{(23)}(g_0,a/L)\right]^{-1}$	$Z^{\alpha=3/2,(3,5),-}_{(23)}(g_0,a/2L)$	$\Sigma^{\alpha=3/2,(3,5),-}_{(23)}(g_0,a/L)$
0.9793	9.50000	0.131532	6	$\begin{pmatrix} 1.2280(14) & 0.1801(22) \\ 0.05161(71) & 1.4101(23) \end{pmatrix}$	$\begin{pmatrix} 0.8246(12) & -0.1423(16) \\ -0.02854(53) & 0.6572(14) \end{pmatrix}$	$\begin{pmatrix} 1.0052(19) & -0.0522(28) \\ -0.00113(82) & 0.9217(25) \end{pmatrix}$
	9.73410	0.131305	8	$\begin{pmatrix} 1.2186(14) & 0.2053(27) \\ 0.04869(82) & 1.4443(23) \end{pmatrix}$	$\begin{pmatrix} 0.8302(14) & -0.1575(27) \\ -0.0277(10) & 0.6420(16) \end{pmatrix}$	$\begin{pmatrix} 1.0040(21) & -0.0568(45) \\ -0.0026(14) & 0.9215(28) \end{pmatrix}$
	10.05755	0.131069	12	$\begin{pmatrix} 1.2029(14) & 0.2361(27) \\ 0.04650(80) & 1.4813(25) \end{pmatrix}$	$\begin{pmatrix} 0.8418(32) & -0.1770(34) \\ -0.0302(13) & 0.6284(34) \end{pmatrix}$	$\begin{pmatrix} 1.0044(42) & -0.0633(57) \\ -0.0070(18) & 0.9239(56) \end{pmatrix}$
1.1814	8.50000	0.132509	6	$\begin{pmatrix} 1.2763(15) & 0.2281(25) \\ 0.06654(82) & 1.5057(24) \end{pmatrix}$	$\begin{pmatrix} 0.8000(23) & -0.1615(34) \\ -0.0323(13) & 0.6079(25) \end{pmatrix}$	$\begin{pmatrix} 1.0102(34) & -0.0607(59) \\ -0.0008(18) & 0.9078(45) \end{pmatrix}$
	8.72230	0.132291	8	$\begin{pmatrix} 1.2627(26) & 0.2609(42) \\ 0.0644(13) & 1.5455(46) \end{pmatrix}$	$\begin{pmatrix} 0.8110(16) & -0.1758(23) \\ -0.03383(87) & 0.5988(18) \end{pmatrix}$	$\begin{pmatrix} 1.0127(28) & -0.0600(45) \\ -0.0042(14) & 0.9166(38) \end{pmatrix}$
	8.99366	0.131975	12	$\begin{pmatrix} 1.2437(17) & 0.2982(31) \\ 0.06091(98) & 1.5937(30) \end{pmatrix}$	$\begin{pmatrix} 0.8219(26) & -0.1912(22) \\ -0.03184(97) & 0.5797(28) \end{pmatrix}$	$\begin{pmatrix} 1.0107(35) & -0.0597(44) \\ -0.0043(14) & 0.9145(48) \end{pmatrix}$
1.5078	7.54200	0.133705	6	$\begin{pmatrix} 1.3425(17) & 0.2977(28) \\ 0.08950(82) & 1.6457(28) \end{pmatrix}$	$\begin{pmatrix} 0.7646(17) & -0.1822(17) \\ -0.03943(92) & 0.5461(17) \end{pmatrix}$	$\begin{pmatrix} 1.0102(25) & -0.0723(36) \\ -0.0040(13) & 0.8869(30) \end{pmatrix}$
	7.72060	0.133497	8	$\begin{pmatrix} 1.3295(34) & 0.3403(68) \\ 0.0886(21) & 1.7028(62) \end{pmatrix}$	$\begin{pmatrix} 0.7765(30) & -0.2011(34) \\ -0.0405(14) & 0.5319(30) \end{pmatrix}$	$\begin{pmatrix} 1.0143(49) & -0.0787(71) \\ -0.0067(21) & 0.8915(64) \end{pmatrix}$
	8.02599	0.133063	12	$\begin{pmatrix} 1.3040(46) & 0.3987(88) \\ 0.0858(26) & 1.7652(88) \end{pmatrix}$	$\begin{pmatrix} 0.7873(35) & -0.2226(47) \\ -0.0406(17) & 0.5114(36) \end{pmatrix}$	$\begin{pmatrix} 1.0076(57) & -0.0792(98) \\ -0.0089(27) & 0.8864(79) \end{pmatrix}$
2.0142	6.60850	0.135260	6	$\begin{pmatrix} 1.4601(24) & 0.4226(35) \\ 0.1357(12) & 1.8967(42) \end{pmatrix}$	$\begin{pmatrix} 0.7107(13) & -0.2099(13) \\ -0.04891(53) & 0.4548(13) \end{pmatrix}$	$\begin{pmatrix} 1.0092(24) & -0.0978(33) \\ -0.00972(94) & 0.8419(29) \end{pmatrix}$
	6.82170	0.134891	8	$\begin{pmatrix} 1.4195(56) & 0.4610(75) \\ 0.1223(30) & 1.9437(87) \end{pmatrix}$	$\begin{pmatrix} 0.7288(21) & -0.2327(21) \\ -0.0515(12) & 0.4451(16) \end{pmatrix}$	$\begin{pmatrix} 1.0060(46) & -0.1166(59) \\ -0.0187(21) & 0.8414(49) \end{pmatrix}$
	7.09300	0.134432	12	$\begin{pmatrix} 1.3903(33) & 0.5490(66) \\ 0.1259(24) & 2.0377(67) \end{pmatrix}$	$\begin{pmatrix} 0.7451(24) & -0.2508(24) \\ -0.0502(13) & 0.4277(25) \end{pmatrix}$	$\begin{pmatrix} 1.0042(38) & -0.1019(61) \\ -0.0160(19) & 0.8436(53) \end{pmatrix}$
2.4792	6.13300	0.136110	6	$\begin{pmatrix} 1.5594(39) & 0.5362(61) \\ 0.1815(21) & 2.1251(69) \end{pmatrix}$	$\begin{pmatrix} 0.6741(37) & -0.2273(29) \\ -0.0565(18) & 0.3925(32) \end{pmatrix}$	$\begin{pmatrix} 1.0097(68) & -0.1217(65) \\ -0.0169(28) & 0.8037(75) \end{pmatrix}$
	6.32290	0.135767	8	$\begin{pmatrix} 1.5131(30) & 0.6039(49) \\ 0.1678(21) & 2.2016(54) \end{pmatrix}$	$\begin{pmatrix} 0.6854(38) & -0.2428(24) \\ -0.0545(17) & 0.3758(34) \end{pmatrix}$	$\begin{pmatrix} 0.9962(57) & -0.1208(70) \\ -0.0194(26) & 0.7946(73) \end{pmatrix}$
	6.63164	0.135227	12	$\begin{pmatrix} 1.4544(40) & 0.6853(76) \\ 0.1586(30) & 2.2771(86) \end{pmatrix}$	$\begin{pmatrix} 0.7177(41) & -0.2635(17) \\ -0.0553(16) & 0.3752(31) \end{pmatrix}$	$\begin{pmatrix} 1.0019(64) & -0.1080(61) \\ -0.0208(26) & 0.8163(78) \end{pmatrix}$
3.3340	5.62150	0.136665	6	$\begin{pmatrix} 1.7596(65) & 0.7674(91) \\ 0.2862(43) & 2.597(12) \end{pmatrix}$	$\begin{pmatrix} 0.6020(53) & -0.2474(28) \\ -0.0741(28) & 0.2977(42) \end{pmatrix}$	$\begin{pmatrix} 0.9882(98) & -0.1803(75) \\ -0.0450(42) & 0.716(11) \end{pmatrix}$
	5.80970	0.136608	8	$\begin{pmatrix} 1.6746(64) & 0.850(14) \\ 0.2609(51) & 2.664(15) \end{pmatrix}$	$\begin{pmatrix} 0.6190(48) & -0.2516(46) \\ -0.0754(16) & 0.2997(28) \end{pmatrix}$	$\begin{pmatrix} 0.9710(78) & -0.145(12) \\ -0.0479(26) & 0.7344(78) \end{pmatrix}$
	6.11816	0.136139	12	$\begin{pmatrix} 1.5789(79) & 0.924(16) \\ 0.2346(74) & 2.710(18) \end{pmatrix}$	$\begin{pmatrix} 0.6588(47) & -0.2865(40) \\ -0.0755(18) & 0.2924(23) \end{pmatrix}$	$\begin{pmatrix} 0.9733(74) & -0.168(10) \\ -0.0504(32) & 0.7229(72) \end{pmatrix}$

TABLE 8.5: Renormalization constants and lattice SSFs for Op 2, 3 for both fierz "+,-" in the renormalization scheme $\alpha = 3/2$, $(s1, s2) = (3, 5)$.

$\bar{g}^2_{SF}(L)$	β	k_{cr}	L/a	$\left[Z^{\alpha=3/2,(3,5),+}_{(45)}(g_0,a/L)\right]^{-1}$	$Z^{\alpha=3/2,(3,5),+}_{(45)}(g_0,a/2L)$	$\Sigma^{\alpha=3/2,(3,5),+}_{(45)}(g_0,a/L)$
0.9793	9.50000	0.131532	6	$\begin{pmatrix} 1.3013(20) & 0.00768(15) \\ 0.8563(75) & 1.0872(15) \end{pmatrix}$	$\begin{pmatrix} 0.7328(14) & -0.00488(16) \\ -0.7433(64) & 0.9690(19) \end{pmatrix}$	$\begin{pmatrix} 0.9495(23) & 0.00031(20) \\ -0.138(10) & 1.0479(25) \end{pmatrix}$
	9.73410	0.131305	8	$\begin{pmatrix} 1.3213(18) & 0.00683(18) \\ 0.8960(86) & 1.0678(16) \end{pmatrix}$	$\begin{pmatrix} 0.7228(17) & -0.00473(36) \\ -0.789(14) & 0.9851(20) \end{pmatrix}$	$\begin{pmatrix} 0.9508(26) & -0.00011(41) \\ -0.160(20) & 1.0465(27) \end{pmatrix}$
	10.05755	0.131069	12	$\begin{pmatrix} 1.3389(19) & 0.00600(18) \\ 0.9538(82) & 1.0363(15) \end{pmatrix}$	$\begin{pmatrix} 0.7180(25) & -0.00528(31) \\ -0.884(11) & 1.0188(35) \end{pmatrix}$	$\begin{pmatrix} 0.9562(38) & -0.00115(35) \\ -0.211(17) & 1.0505(39) \end{pmatrix}$
1.1814	8.50000	0.132509	6	$\begin{pmatrix} 1.3671(20) & 0.00986(18) \\ 1.0429(87) & 1.1019(15) \end{pmatrix}$	$\begin{pmatrix} 0.6919(27) & -0.00566(47) \\ -0.845(18) & 0.9711(45) \end{pmatrix}$	$\begin{pmatrix} 0.9400(41) & 0.00059(53) \\ -0.142(27) & 1.0618(50) \end{pmatrix}$
	8.72230	0.132291	8	$\begin{pmatrix} 1.3865(33) & 0.00919(29) \\ 1.103(12) & 1.0754(24) \end{pmatrix}$	$\begin{pmatrix} 0.6906(14) & -0.00607(26) \\ -0.9209(87) & 1.0022(20) \end{pmatrix}$	$\begin{pmatrix} 0.9509(30) & -0.00019(36) \\ -0.171(18) & 1.0694(35) \end{pmatrix}$
	8.99366	0.131975	12	$\begin{pmatrix} 1.4106(22) & 0.00796(22) \\ 1.1609(94) & 1.0381(17) \end{pmatrix}$	$\begin{pmatrix} 0.6780(32) & -0.00536(40) \\ -0.984(12) & 1.0382(43) \end{pmatrix}$	$\begin{pmatrix} 0.9501(47) & -0.00017(40) \\ -0.182(20) & 1.0700(48) \end{pmatrix}$
1.5078	7.54200	0.133705	6	$\begin{pmatrix} 1.4600(23) & 0.01299(19) \\ 1.2985(86) & 1.1144(18) \end{pmatrix}$	$\begin{pmatrix} 0.6422(24) & -0.00750(31) \\ -0.998(10) & 0.9825(37) \end{pmatrix}$	$\begin{pmatrix} 0.9278(37) & -0.00002(38) \\ -0.180(18) & 1.0819(43) \end{pmatrix}$
	7.72060	0.133497	8	$\begin{pmatrix} 1.4907(51) & 0.01228(49) \\ 1.381(20) & 1.0858(37) \end{pmatrix}$	$\begin{pmatrix} 0.6360(43) & -0.00776(54) \\ -1.081(15) & 1.0163(55) \end{pmatrix}$	$\begin{pmatrix} 0.9372(68) & -0.00064(61) \\ -0.208(29) & 1.0904(70) \end{pmatrix}$
	8.02599	0.133063	12	$\begin{pmatrix} 1.5172(63) & 0.01140(51) \\ 1.471(23) & 1.0442(45) \end{pmatrix}$	$\begin{pmatrix} 0.6214(33) & -0.00777(69) \\ -1.175(18) & 1.0523(64) \end{pmatrix}$	$\begin{pmatrix} 0.9308(66) & -0.00102(78) \\ -0.236(36) & 1.0849(80) \end{pmatrix}$
2.0142	6.60850	0.135260	6	$\begin{pmatrix} 1.6235(31) & 0.01888(23) \\ 1.7229(97) & 1.1352(20) \end{pmatrix}$	$\begin{pmatrix} 0.5644(17) & -0.01041(21) \\ -1.2111(59) & 1.0006(32) \end{pmatrix}$	$\begin{pmatrix} 0.8983(32) & -0.00114(27) \\ -0.242(12) & 1.1131(42) \end{pmatrix}$
	6.82170	0.134891	8	$\begin{pmatrix} 1.6431(61) & 0.01625(58) \\ 1.743(23) & 1.0896(38) \end{pmatrix}$	$\begin{pmatrix} 0.5624(22) & -0.01143(44) \\ -1.324(11) & 1.0439(36) \end{pmatrix}$	$\begin{pmatrix} 0.9044(48) & -0.00330(56) \\ -0.355(27) & 1.1162(53) \end{pmatrix}$
	7.09300	0.134432	12	$\begin{pmatrix} 1.6778(56) & 0.01590(50) \\ 1.890(18) & 1.0359(35) \end{pmatrix}$	$\begin{pmatrix} 0.5494(19) & -0.01069(34) \\ -1.4154(83) & 1.0946(36) \end{pmatrix}$	$\begin{pmatrix} 0.9016(40) & -0.00233(44) \\ -0.306(22) & 1.1116(51) \end{pmatrix}$
2.4792	6.13300	0.136110	6	$\begin{pmatrix} 1.7653(57) & 0.02424(41) \\ 2.075(17) & 1.1435(34) \end{pmatrix}$	$\begin{pmatrix} 0.5112(34) & -0.01334(62) \\ -1.380(16) & 1.0334(63) \end{pmatrix}$	$\begin{pmatrix} 0.8747(60) & -0.00287(73) \\ -0.294(27) & 1.1484(75) \end{pmatrix}$
	6.32290	0.135767	8	$\begin{pmatrix} 1.7950(40) & 0.02187(39) \\ 2.133(13) & 1.0929(23) \end{pmatrix}$	$\begin{pmatrix} 0.4950(39) & -0.01251(59) \\ -1.452(15) & 1.0690(87) \end{pmatrix}$	$\begin{pmatrix} 0.8621(73) & -0.00284(67) \\ -0.326(28) & 1.1366(96) \end{pmatrix}$
	6.63164	0.135227	12	$\begin{pmatrix} 1.8152(59) & 0.01965(57) \\ 2.224(18) & 1.0303(33) \end{pmatrix}$	$\begin{pmatrix} 0.5009(24) & -0.01228(34) \\ -1.5776(83) & 1.1426(48) \end{pmatrix}$	$\begin{pmatrix} 0.8820(52) & -0.00283(43) \\ -0.323(21) & 1.1463(64) \end{pmatrix}$
3.3340	5.62150	0.136665	6	$\begin{pmatrix} 2.0537(100) & 0.03521(64) \\ 2.720(21) & 1.1637(50) \end{pmatrix}$	$\begin{pmatrix} 0.4202(72) & -0.0213(15) \\ -1.662(33) & 1.079(15) \end{pmatrix}$	$\begin{pmatrix} 0.805(12) & -0.0099(15) \\ -0.479(40) & 1.196(17) \end{pmatrix}$
	5.80970	0.136608	8	$\begin{pmatrix} 2.0571(90) & 0.03204(84) \\ 2.758(27) & 1.0912(47) \end{pmatrix}$	$\begin{pmatrix} 0.4272(61) & -0.0214(11) \\ -1.770(29) & 1.153(14) \end{pmatrix}$	$\begin{pmatrix} 0.819(11) & -0.0097(11) \\ -0.458(36) & 1.202(15) \end{pmatrix}$
	6.11816	0.136139	12	$\begin{pmatrix} 2.052(14) & 0.0275(12) \\ 2.771(37) & 1.0145(70) \end{pmatrix}$	$\begin{pmatrix} 0.4279(39) & -0.0219(13) \\ -1.950(28) & 1.241(14) \end{pmatrix}$	$\begin{pmatrix} 0.8171(75) & -0.0106(13) \\ -0.563(41) & 1.206(16) \end{pmatrix}$

$\bar{g}^2_{SF}(L)$	β	k_{cr}	L/a	$\left[Z^{\alpha=3/2,(3,5),-}_{(45)}(g_0,a/L)\right]^{-1}$	$Z^{\alpha=3/2,(3,5),-}_{(45)}(g_0,a/2L)$	$\Sigma^{\alpha=3/2,(3,5),-}_{(45)}(g_0,a/L)$
0.9793	9.50000	0.131532	6	$\begin{pmatrix} 1.5644(33) & -0.00363(17) \\ -0.5050(81) & 1.1866(11) \end{pmatrix}$	$\begin{pmatrix} 0.5723(14) & -0.00084(12) \\ 0.2759(46) & 0.83999(93) \end{pmatrix}$	$\begin{pmatrix} 0.8957(29) & -0.00308(18) \\ 0.0073(97) & 0.9956(15) \end{pmatrix}$
	9.73410	0.131305	8	$\begin{pmatrix} 1.6118(35) & -0.00099(22) \\ -0.5070(92) & 1.1835(11) \end{pmatrix}$	$\begin{pmatrix} 0.5548(19) & -0.00178(28) \\ 0.280(11) & 0.8424(21) \end{pmatrix}$	$\begin{pmatrix} 0.8952(37) & -0.00267(36) \\ 0.023(19) & 0.9967(26) \end{pmatrix}$
	10.05755	0.131069	12	$\begin{pmatrix} 1.6685(36) & 0.00201(20) \\ -0.5117(99) & 1.17541(97) \end{pmatrix}$	$\begin{pmatrix} 0.5338(26) & -0.00232(23) \\ 0.2988(79) & 0.8526(16) \end{pmatrix}$	$\begin{pmatrix} 0.8920(47) & -0.00166(30) \\ 0.062(15) & 1.0027(21) \end{pmatrix}$
1.1814	8.50000	0.132509	6	$\begin{pmatrix} 1.7063(38) & -0.00486(20) \\ -0.6226(89) & 1.2260(11) \end{pmatrix}$	$\begin{pmatrix} 0.5133(25) & -0.00119(31) \\ 0.291(11) & 0.8139(28) \end{pmatrix}$	$\begin{pmatrix} 0.8766(49) & -0.00395(40) \\ -0.009(19) & 0.9964(36) \end{pmatrix}$
	8.72230	0.132291	8	$\begin{pmatrix} 1.7642(57) & -0.00233(32) \\ -0.643(15) & 1.2165(17) \end{pmatrix}$	$\begin{pmatrix} 0.4994(21) & -0.00162(21) \\ 0.3023(76) & 0.8242(11) \end{pmatrix}$	$\begin{pmatrix} 0.8821(48) & -0.00313(29) \\ 0.004(16) & 1.0019(21) \end{pmatrix}$
	8.99366	0.131975	12	$\begin{pmatrix} 1.8399(44) & 0.00194(25) \\ -0.636(12) & 1.2090(10) \end{pmatrix}$	$\begin{pmatrix} 0.4773(24) & -0.00316(25) \\ 0.2918(91) & 0.8278(24) \end{pmatrix}$	$\begin{pmatrix} 0.8801(49) & -0.00288(33) \\ 0.010(18) & 1.0014(30) \end{pmatrix}$
1.5078	7.54200	0.133705	6	$\begin{pmatrix} 1.9239(42) & -0.00667(20) \\ -0.7804(88) & 1.2815(13) \end{pmatrix}$	$\begin{pmatrix} 0.4388(22) & -0.00085(24) \\ 0.3045(66) & 0.7780(16) \end{pmatrix}$	$\begin{pmatrix} 0.8450(45) & -0.00400(33) \\ -0.021(13) & 0.9950(22) \end{pmatrix}$
	7.72060	0.133497	8	$\begin{pmatrix} 2.0113(90) & -0.00333(55) \\ -0.809(22) & 1.2730(25) \end{pmatrix}$	$\begin{pmatrix} 0.4203(35) & -0.00157(36) \\ 0.3177(100) & 0.7884(38) \end{pmatrix}$	$\begin{pmatrix} 0.8470(77) & -0.00340(53) \\ -0.000(25) & 1.0026(53) \end{pmatrix}$
	8.02599	0.133063	12	$\begin{pmatrix} 2.112(14) & 0.00116(67) \\ -0.844(29) & 1.2565(27) \end{pmatrix}$	$\begin{pmatrix} 0.3959(38) & -0.00270(40) \\ 0.323(12) & 0.7938(21) \end{pmatrix}$	$\begin{pmatrix} 0.8380(97) & -0.00291(53) \\ 0.013(30) & 0.9978(32) \end{pmatrix}$
2.0142	6.60850	0.135260	6	$\begin{pmatrix} 2.3354(67) & -0.01089(30) \\ -1.059(11) & 1.3788(19) \end{pmatrix}$	$\begin{pmatrix} 0.3342(11) & -0.00052(14) \\ 0.3116(33) & 0.7219(12) \end{pmatrix}$	$\begin{pmatrix} 0.7808(38) & -0.00436(22) \\ -0.037(10) & 0.9920(22) \end{pmatrix}$
	6.82170	0.134891	8	$\begin{pmatrix} 2.405(15) & -0.00394(70) \\ -1.025(27) & 1.3541(36) \end{pmatrix}$	$\begin{pmatrix} 0.3200(15) & -0.00089(22) \\ 0.3311(50) & 0.7392(20) \end{pmatrix}$	$\begin{pmatrix} 0.7702(60) & -0.00249(38) \\ 0.039(19) & 0.9996(39) \end{pmatrix}$
	7.09300	0.134432	12	$\begin{pmatrix} 2.570(11) & 0.00073(73) \\ -1.111(22) & 1.3266(27) \end{pmatrix}$	$\begin{pmatrix} 0.3004(15) & -0.00244(21) \\ 0.3275(48) & 0.7489(18) \end{pmatrix}$	$\begin{pmatrix} 0.7751(49) & -0.00303(34) \\ 0.009(18) & 0.9939(35) \end{pmatrix}$
2.4792	6.13300	0.136110	6	$\begin{pmatrix} 2.737(11) & -0.01545(61) \\ -1.300(18) & 1.4600(33) \end{pmatrix}$	$\begin{pmatrix} 0.2654(21) & -0.00006(36) \\ 0.2997(81) & 0.6818(36) \end{pmatrix}$	$\begin{pmatrix} 0.7264(65) & -0.00421(60) \\ -0.067(23) & 0.9909(55) \end{pmatrix}$
	6.32290	0.135767	8	$\begin{pmatrix} 2.8542(96) & -0.00675(53) \\ -1.288(16) & 1.4303(23) \end{pmatrix}$	$\begin{pmatrix} 0.2483(34) & -0.00164(38) \\ 0.2972(87) & 0.6861(34) \end{pmatrix}$	$\begin{pmatrix} 0.711(10) & -0.00401(58) \\ -0.035(26) & 0.9792(51) \end{pmatrix}$
	6.63164	0.135227	12	$\begin{pmatrix} 2.992(14) & 0.00089(77) \\ -1.343(20) & 1.3787(29) \end{pmatrix}$	$\begin{pmatrix} 0.2424(28) & -0.00267(43) \\ 0.3056(54) & 0.7129(36) \end{pmatrix}$	$\begin{pmatrix} 0.7286(98) & -0.00346(62) \\ -0.043(19) & 0.9830(56) \end{pmatrix}$
3.3340	5.62150	0.136665	6	$\begin{pmatrix} 3.640(20) & -0.0259(11) \\ -1.759(25) & 1.6207(53) \end{pmatrix}$	$\begin{pmatrix} 0.1619(27) & 0.00166(52) \\ 0.2764(65) & 0.6050(52) \end{pmatrix}$	$\begin{pmatrix} 0.586(10) & -0.00149(84) \\ -0.058(24) & 0.9736(88) \end{pmatrix}$
	5.80970	0.136608	8	$\begin{pmatrix} 3.750(24) & -0.0150(13) \\ -1.758(36) & 1.5532(45) \end{pmatrix}$	$\begin{pmatrix} 0.1617(23) & 0.00119(34) \\ 0.2714(49) & 0.6194(59) \end{pmatrix}$	$\begin{pmatrix} 0.6044(91) & -0.00055(55) \\ -0.073(23) & 0.9581(96) \end{pmatrix}$
	6.11816	0.136139	12	$\begin{pmatrix} 3.836(26) & -0.0011(17) \\ -1.736(43) & 1.4802(54) \end{pmatrix}$	$\begin{pmatrix} 0.1535(15) & 0.00048(57) \\ 0.2928(68) & 0.6551(37) \end{pmatrix}$	$\begin{pmatrix} 0.5883(80) & 0.00053(92) \\ -0.013(31) & 0.9694(66) \end{pmatrix}$

TABLE 8.6: Renormalization constants and lattice SSFs for Op $4,5$ for both fierz "+,-" in the renormalization scheme $\alpha = 3/2$, $(s1, s2) = (3, 5)$.

β	k_{cr}	L/a	$\bar{g}^2_{SF}(L)$	$Z^{\alpha=3/2,(3,5),+}_{(23)}$		$Z^{\alpha=3/2,(3,5),-}_{(23)}$	
5.20	0.13600	4	3.65	$\begin{pmatrix} 0.5992(11) & 0.31835(83) \\ 0.08539(42) & 0.35980(88) \end{pmatrix}$		$\begin{pmatrix} 0.5048(11) & -0.12417(81) \\ -0.08479(37) & 0.39148(77) \end{pmatrix}$	
		6	4.61	$\begin{pmatrix} 0.6026(12) & 0.34048(59) \\ 0.08647(33) & 0.29400(61) \end{pmatrix}$		$\begin{pmatrix} 0.50745(86) & -0.17402(63) \\ -0.08586(34) & 0.31768(58) \end{pmatrix}$	
5.29	0.13641	4	3.39	$\begin{pmatrix} 0.6179(11) & 0.31837(69) \\ 0.08123(33) & 0.38268(82) \end{pmatrix}$		$\begin{pmatrix} 0.53117(83) & -0.12960(76) \\ -0.08047(41) & 0.41335(68) \end{pmatrix}$	
		6	4.30	$\begin{pmatrix} 0.6212(11) & 0.33681(81) \\ 0.07975(35) & 0.31743(68) \end{pmatrix}$		$\begin{pmatrix} 0.53520(90) & -0.17551(80) \\ -0.07941(40) & 0.34077(70) \end{pmatrix}$	
		8	5.65	$\begin{pmatrix} 0.6274(13) & 0.35466(78) \\ 0.08400(49) & 0.27293(68) \end{pmatrix}$		$\begin{pmatrix} 0.5317(10) & -0.2035(10) \\ -0.08554(50) & 0.29424(62) \end{pmatrix}$	
5.40	0.13669	4	3.19	$\begin{pmatrix} 0.6367(10) & 0.31526(70) \\ 0.07672(32) & 0.40904(83) \end{pmatrix}$		$\begin{pmatrix} 0.55721(81) & -0.13146(75) \\ -0.07610(28) & 0.43891(82) \end{pmatrix}$	
		6	3.86	$\begin{pmatrix} 0.63422(95) & 0.33226(72) \\ 0.07429(37) & 0.34047(67) \end{pmatrix}$		$\begin{pmatrix} 0.55768(81) & -0.17545(73) \\ -0.07358(35) & 0.36360(59) \end{pmatrix}$	
		8	4.75	$\begin{pmatrix} 0.6422(13) & 0.35228(79) \\ 0.07738(41) & 0.29670(64) \end{pmatrix}$		$\begin{pmatrix} 0.55925(84) & -0.20644(70) \\ -0.07761(50) & 0.31681(65) \end{pmatrix}$	

TABLE 8.7: Renormalization constants at hadronic $\beta = [5.20, 5.29, 5.40]$ for Op $2, 3$

β	k_{cr}	L/a	$\bar{g}^2_{SF}(L)$	$Z^{\alpha=3/2,(3,5),+}_{(45)}$		$Z^{\alpha=3/2,(3,5),-}_{(45)}$	
5.20	0.13600	4	3.65	$\begin{pmatrix} 0.4921(11) & -0.02039(13) \\ -1.1531(32) & 0.8350(19) \end{pmatrix}$		$\begin{pmatrix} 0.24875(92) & 0.01084(10) \\ 0.2681(16) & 0.5416(10) \end{pmatrix}$	
		6	4.61	$\begin{pmatrix} 0.4293(10) & -0.02340(19) \\ -1.3971(38) & 0.9190(18) \end{pmatrix}$		$\begin{pmatrix} 0.17779(68) & 0.00886(11) \\ 0.2660(16) & 0.5373(11) \end{pmatrix}$	
5.29	0.13641	4	3.39	$\begin{pmatrix} 0.5133(12) & -0.01910(13) \\ -1.1264(31) & 0.8385(15) \end{pmatrix}$		$\begin{pmatrix} 0.27459(88) & 0.009909(86) \\ 0.2838(16) & 0.56761(95) \end{pmatrix}$	
		6	4.30	$\begin{pmatrix} 0.4509(12) & -0.02075(23) \\ -1.3442(46) & 0.9189(20) \end{pmatrix}$		$\begin{pmatrix} 0.20420(76) & 0.00734(13) \\ 0.2741(19) & 0.5621(11) \end{pmatrix}$	
		8	5.65	$\begin{pmatrix} 0.4120(11) & -0.02498(26) \\ -1.5596(49) & 1.0027(26) \end{pmatrix}$		$\begin{pmatrix} 0.15562(58) & 0.00676(17) \\ 0.2607(14) & 0.5514(11) \end{pmatrix}$	
5.40	0.13669	4	3.19	$\begin{pmatrix} 0.5372(10) & -0.01782(13) \\ -1.0918(31) & 0.8416(15) \end{pmatrix}$		$\begin{pmatrix} 0.30436(89) & 0.008962(76) \\ 0.2935(16) & 0.59197(98) \end{pmatrix}$	
		6	3.86	$\begin{pmatrix} 0.4717(12) & -0.01848(20) \\ -1.2852(44) & 0.9099(19) \end{pmatrix}$		$\begin{pmatrix} 0.23038(72) & 0.006133(95) \\ 0.2827(18) & 0.5833(11) \end{pmatrix}$	
		8	4.75	$\begin{pmatrix} 0.43354(94) & -0.02131(20) \\ -1.4867(41) & 0.9867(18) \end{pmatrix}$		$\begin{pmatrix} 0.18096(60) & 0.00509(12) \\ 0.2753(16) & 0.5788(10) \end{pmatrix}$	

TABLE 8.8: Renormalization constants at hadronic $\beta = [5.20, 5.29, 5.40]$ for Op $4, 5$

$\widetilde{U}^{2/3}_{\mathcal{Q}_1\mathcal{Q}_2}(3\text{ GeV})$	Fierz	RI	$\overline{\text{MS}}$	SF
23	+	$\begin{pmatrix} 1.121\,^{+0.019}_{-0.019} & 0.650\,^{+0.014}_{-0.013} \\ -0.0057\,^{+0.0042}_{-0.0047} & 0.363\,^{+0.032}_{-0.029} \end{pmatrix}$	$\begin{pmatrix} 1.138\,^{+0.011}_{-0.011} & 0.654\,^{+0.006}_{-0.006} \\ -0.0066\,^{+0.0032}_{-0.0032} & 0.305\,^{+0.006}_{-0.006} \end{pmatrix}$	$\begin{pmatrix} 1.212\,^{+0.009}_{-0.009} & 0.283\,^{+0.009}_{-0.009} \\ -0.018\,^{+0.007}_{-0.007} & 0.2292\,^{+0.0038}_{-0.0037} \end{pmatrix}$
	-	$\begin{pmatrix} 1.121\,^{+0.019}_{-0.019} & -0.650\,^{+0.013}_{-0.014} \\ 0.0057\,^{+0.0047}_{-0.0042} & 0.363\,^{+0.032}_{-0.029} \end{pmatrix}$	$\begin{pmatrix} 1.138\,^{+0.011}_{-0.011} & -0.654\,^{+0.006}_{-0.006} \\ 0.0066\,^{+0.0032}_{-0.0032} & 0.305\,^{+0.006}_{-0.006} \end{pmatrix}$	$\begin{pmatrix} 1.2137\,^{+0.0002}_{-0.0002} & -0.7338\,^{+0.0002}_{-0.0002} \\ 0.0148\,^{+0.0025}_{-0.0025} & 0.2202\,^{+0.0010}_{-0.0010} \end{pmatrix}$
45	+	$\begin{pmatrix} 0.539\,^{+0.027}_{-0.026} & 0.0165\,^{+0.0009}_{-0.0009} \\ 0.243\,^{+0.136}_{-0.135} & 2.283\,^{+0.029}_{-0.028} \end{pmatrix}$	$\begin{pmatrix} 0.488\,^{+0.008}_{-0.008} & 0.01414\,^{+0.00024}_{-0.00023} \\ -0.303\,^{+0.061}_{-0.065} & 2.187\,^{+0.057}_{-0.056} \end{pmatrix}$	$\begin{pmatrix} 0.3623\,^{+0.0012}_{-0.0012} & 0.02601\,^{+0.00003}_{-0.00003} \\ -0.754\,^{+0.028}_{-0.028} & 3.005\,^{+0.010}_{-0.010} \end{pmatrix}$
	-	$\begin{pmatrix} 0.296\,^{+0.040}_{-0.036} & -0.0237\,^{+0.0013}_{-0.0005} \\ -1.008\,^{+0.220}_{-0.265} & 0.778\,^{+0.128}_{-0.112} \end{pmatrix}$	$\begin{pmatrix} 0.223\,^{+0.010}_{-0.010} & -0.02644\,^{+0.00026}_{-0.00024} \\ -0.404\,^{+0.053}_{-0.056} & 0.855\,^{+0.025}_{-0.025} \end{pmatrix}$	$\begin{pmatrix} 0.1717\,^{+0.0034}_{-0.0034} & -0.0296\,^{+0.0019}_{-0.0017} \\ -0.771\,^{+0.092}_{-0.096} & 0.807\,^{+0.063}_{-0.061} \end{pmatrix}$

TABLE 8.9: Values for the RG running coefficients at $\mu = 3\,\text{GeV}$ for the four doublets of operators in three different schemes ($\overline{\text{MS}}$, RI and a chosen SF scheme). We quote here, as our best result, the case n_γ/n_β=2/3 obtained by numerical integration. The systematic errors have been estimated by computing the maximal deviation between the central value and the values of the 2/2, +3/3 and -3/3 numerical solutions.

$\widetilde{U}^{2/2,\text{O}(g^2)}_{\mathcal{Q}_1\mathcal{Q}_2}(3\text{ GeV})$	Fierz	RI	$\overline{\text{MS}}$	SF
23	+	$\begin{pmatrix} 1.120\,^{+0.020}_{-0.019} & 0.624\,^{+0.040}_{-0.000} \\ -0.0051\,^{+0.0036}_{-0.0053} & 0.352\,^{+0.043}_{-0.018} \end{pmatrix}$	$\begin{pmatrix} 1.139\,^{+0.009}_{-0.012} & 0.648\,^{+0.012}_{-0.000} \\ -0.0066\,^{+0.0032}_{-0.0032} & 0.301\,^{+0.010}_{-0.003} \end{pmatrix}$	$\begin{pmatrix} 1.184\,^{+0.038}_{-0.000} & 0.290\,^{+0.002}_{-0.015} \\ -0.018\,^{+0.007}_{-0.007} & 0.2292\,^{+0.0038}_{-0.0037} \end{pmatrix}$
	-	$\begin{pmatrix} 1.120\,^{+0.020}_{-0.019} & -0.624\,^{+0.000}_{-0.040} \\ 0.0051\,^{+0.0053}_{-0.0036} & 0.352\,^{+0.043}_{-0.018} \end{pmatrix}$	$\begin{pmatrix} 1.139\,^{+0.009}_{-0.012} & -0.648\,^{+0.000}_{-0.012} \\ 0.0066\,^{+0.0032}_{-0.0032} & 0.305\,^{+0.010}_{-0.003} \end{pmatrix}$	$\begin{pmatrix} 1.219\,^{+0.000}_{-0.005} & -0.7346\,^{+0.0009}_{-0.0000} \\ 0.0154\,^{+0.0019}_{-0.0030} & 0.2203\,^{+0.0009}_{-0.0011} \end{pmatrix}$
45	+	$\begin{pmatrix} 0.528\,^{+0.038}_{-0.015} & 0.0164\,^{+0.0010}_{-0.0008} \\ -0.358\,^{+0.737}_{-0.000} & 2.276\,^{+0.036}_{-0.021} \end{pmatrix}$	$\begin{pmatrix} 0.484\,^{+0.013}_{-0.003} & 0.01413\,^{+0.00025}_{-0.00023} \\ -0.533\,^{+0.291}_{-0.000} & 2.179\,^{+0.065}_{-0.048} \end{pmatrix}$	$\begin{pmatrix} 0.3629\,^{+0.0006}_{-0.0018} & 0.02605\,^{+0.00000}_{-0.00008} \\ -0.382\,^{+0.000}_{-0.400} & 2.945\,^{+0.070}_{-0.000} \end{pmatrix}$
	-	$\begin{pmatrix} 0.266\,^{+0.070}_{-0.006} & -0.0233\,^{+0.0008}_{-0.0010} \\ -0.596\,^{+0.000}_{-0.678} & 0.764\,^{+0.143}_{-0.098} \end{pmatrix}$	$\begin{pmatrix} 0.215\,^{+0.018}_{-0.001} & -0.02644\,^{+0.00026}_{-0.00025} \\ -0.294\,^{+0.000}_{-0.166} & 0.851\,^{+0.029}_{-0.022} \end{pmatrix}$	$\begin{pmatrix} 0.168\,^{+0.007}_{-0.000} & -0.0285\,^{+0.0008}_{-0.0028} \\ -0.670\,^{+0.000}_{-0.197} & 0.777\,^{+0.094}_{-0.030} \end{pmatrix}$

TABLE 8.10: Values for the RG running coefficients at $\mu = 3\,\text{GeV}$ for the four doublets of operators in three different schemes ($\overline{\text{MS}}$, RI and a chosen SF scheme). We quote here the 2/2 result from the perturbative expansion at $\text{O}(g^2)$, which is the case usually considered in literature, both for phenomenological application and in lattice computations. The systematic errors have been estimated by computing the maximal deviation between the central value and the values of the 2/2, 2/3, +3/3 and -3/3 numerical solutions. It is worth noticing the large asymmetric errors which occour in particular in the 45 Fierz $+$ and $-$ matrices (especially in the RI scheme).

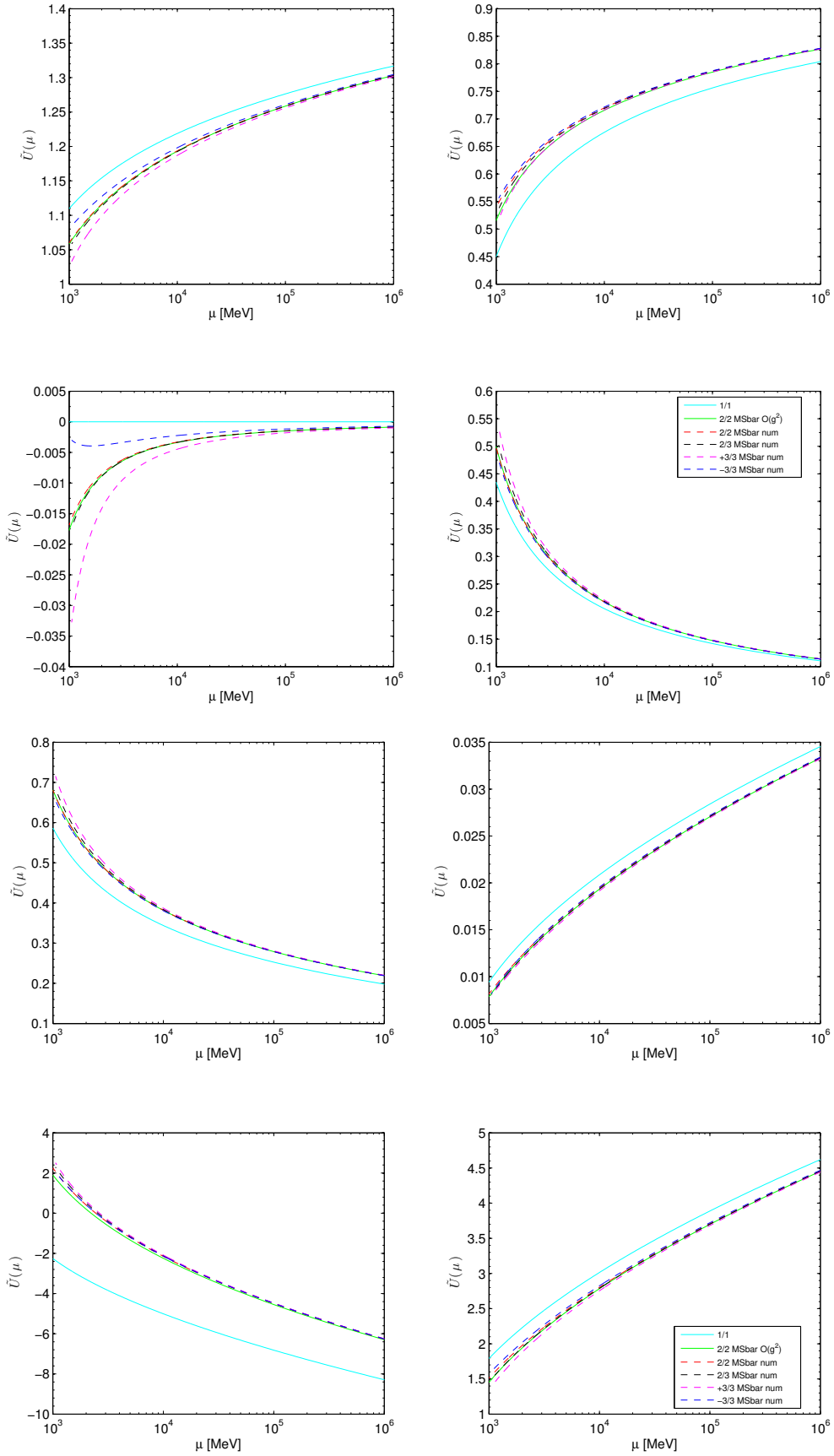

FIGURE 8.15: RG running matrices for the Fierz + Op. $2, 3$ (top half) and Op. $4, 5$ (bottom half) in the $\overline{\text{MS}}$ scheme. Solid lines correspond to the LO plotted (cyan) and the perturbative expansion for the NLO $2/2$ case up to $\text{O}(g^2)$ - i.e. including J_1 (green). Dashed lines correspond to the numerical solution for $W(\mu)$ in the cases $n_\gamma/n_\beta = \{2/2, 2/3, +3/3, -3/3\}$ respectively in red, black, magenta and blue.

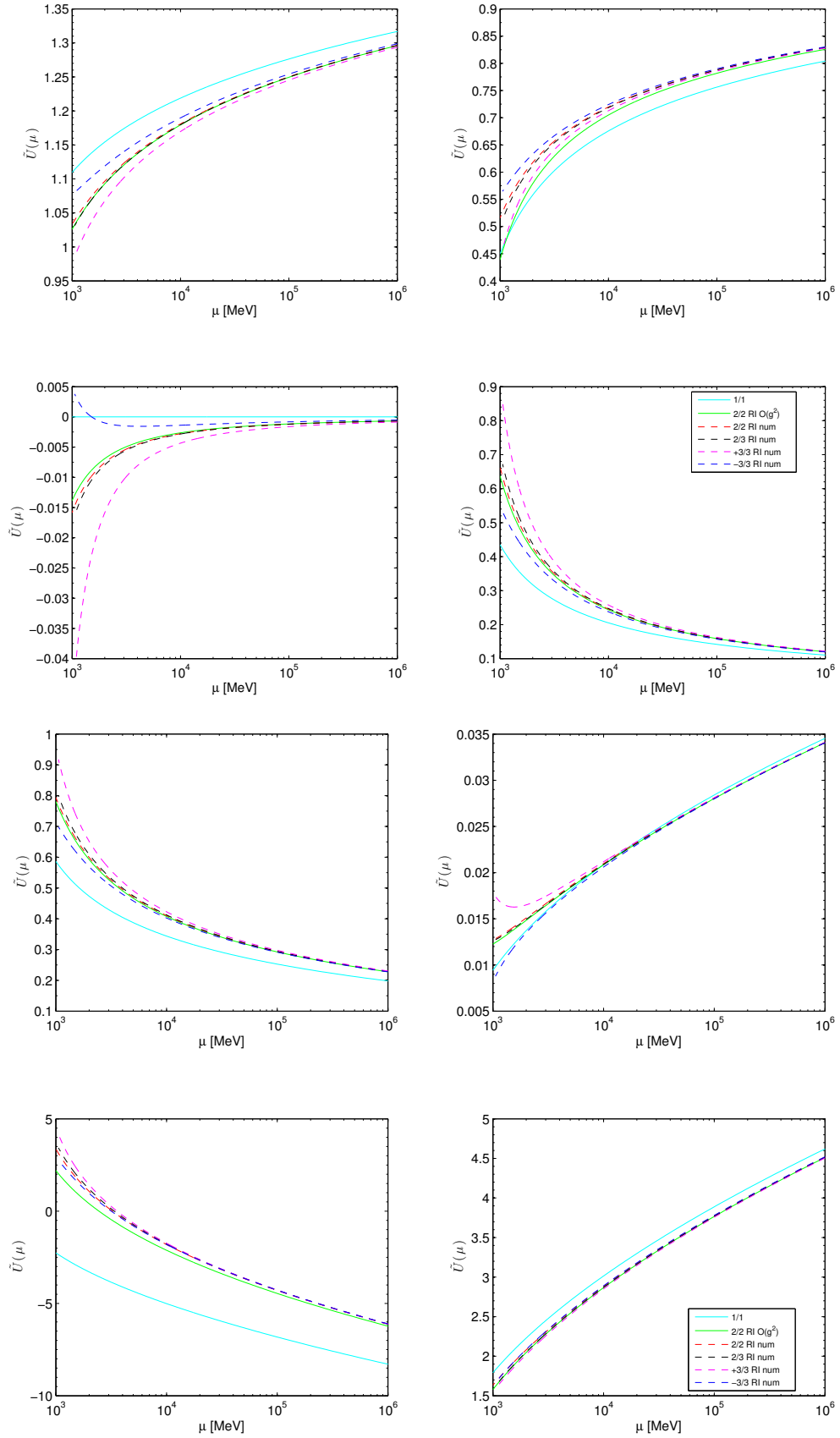

FIGURE 8.16: RG running matrices for the Fierz + Op. $2,3$ (top half) and Op. $4,5$ (bottom half) in the RI scheme. Solid lines correspond to the LO (cyan) and the perturbative expansion for the NLO $2/2$ case up to $\mathrm{O}(g^2)$ - i.e. including J_1 (green). Dashed lines correspond to the numerical solution for $W(\mu)$ in the cases $n_\gamma/n_\beta = \{2/2, 2/3, +3/3, -3/3\}$ respectively in red, black, magenta and blue.

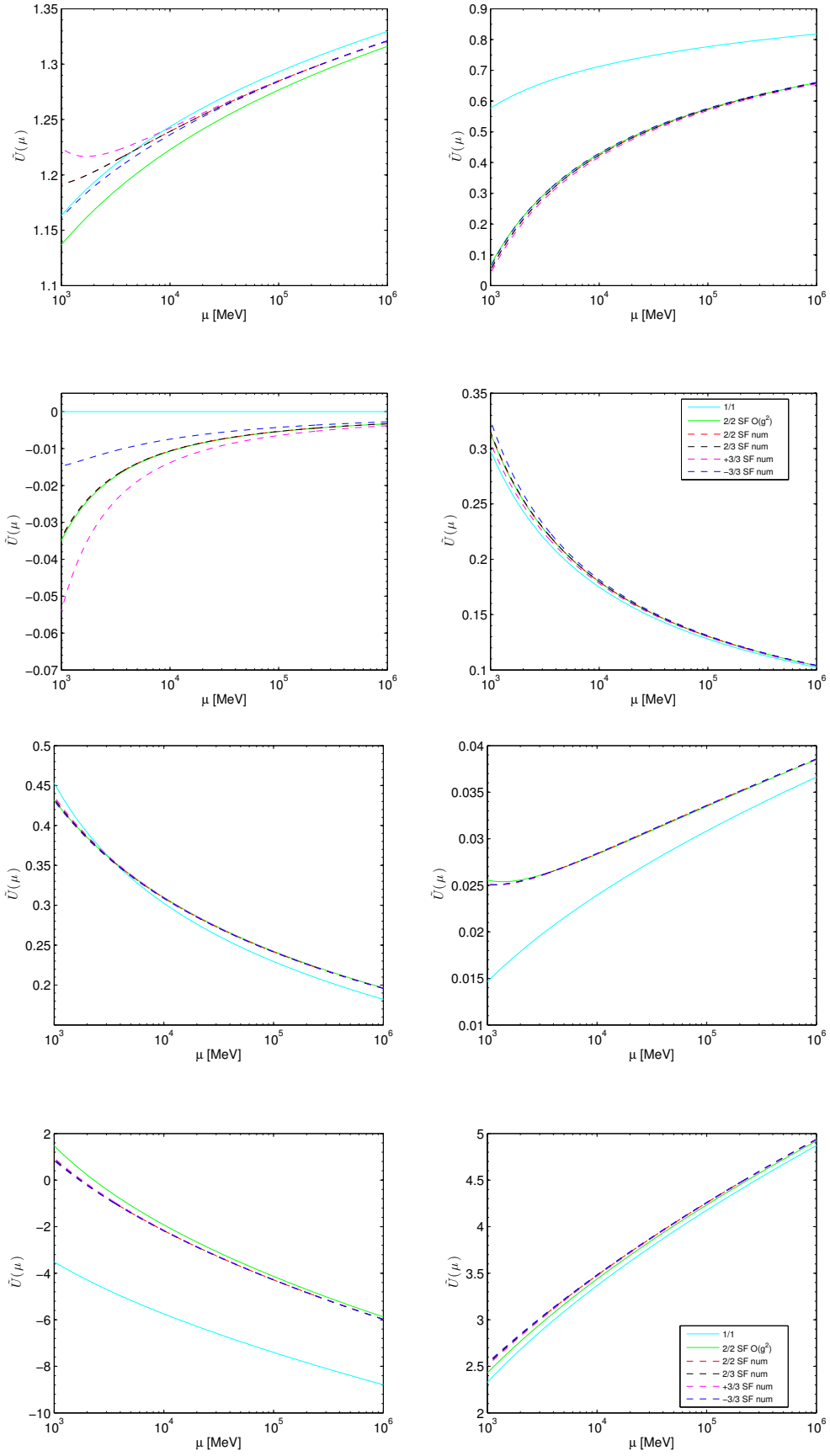

FIGURE 8.17: RG running matrices for the Fierz + Op. $2, 3$ (top half) and Op. $4, 5$ (bottom half) in the SF scheme. Solid lines correspond to the LO (cyan) and the perturbative expansion for the NLO $2/2$ case up to $\mathrm{O}(g^2)$ - i.e. including J_1 (green). Dashed lines correspond to the numerical solution for $W(\mu)$ in the cases $n_\gamma/n_\beta = \{2/2, 2/3, +3/3, -3/3\}$ respectively in red, black, magenta and blue.

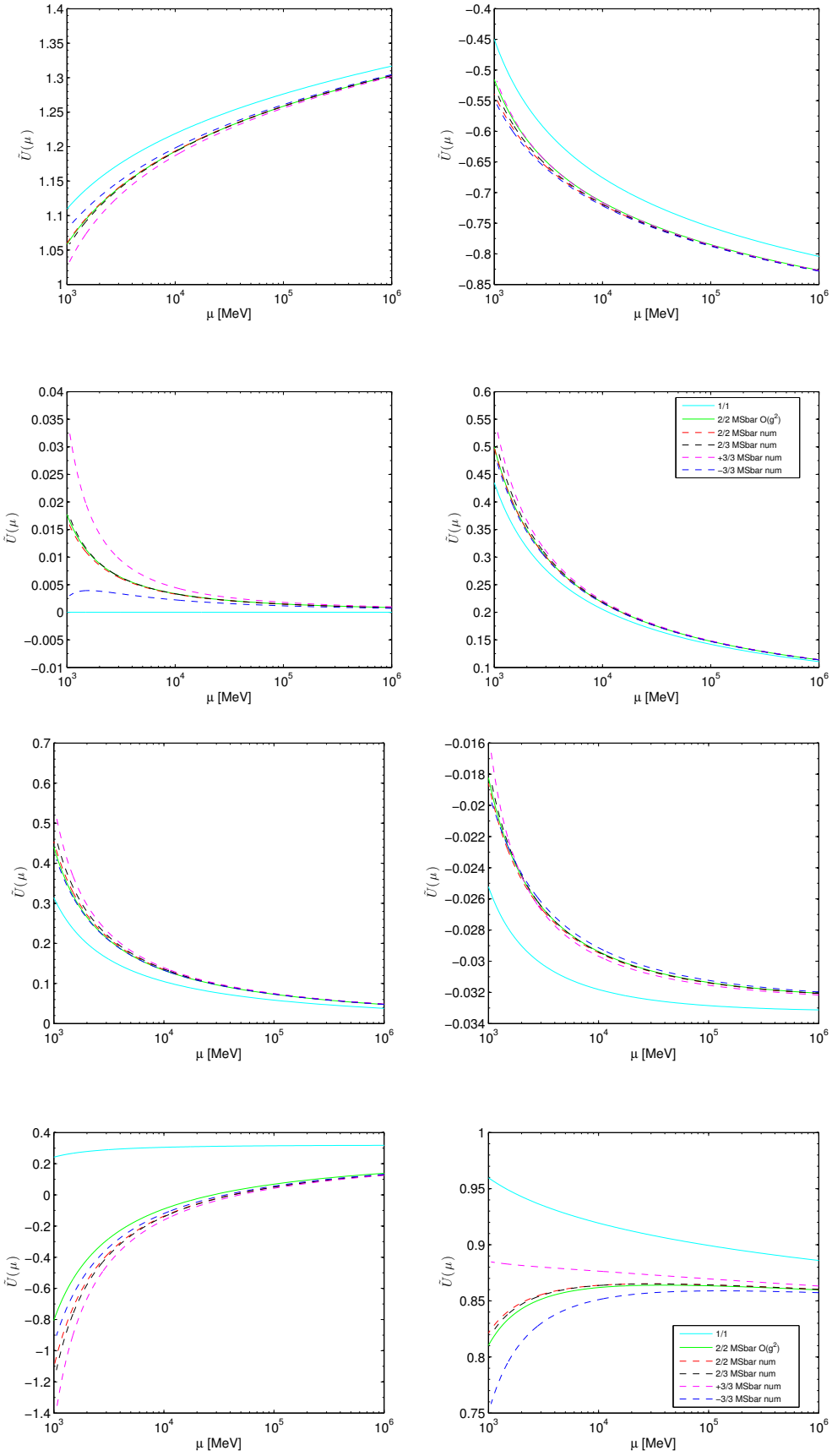

FIGURE 8.18: RG running matrices for the Fierz − Op. $2, 3$ (top half) and Op. $4, 5$ (bottom half) in the $\overline{\text{MS}}$ scheme. Solid lines correspond to the LO (cyan) and the perturbative expansion for the NLO $2/2$ case up to $\text{O}(g^2)$ - i.e. including J_1 (green). Dashed lines correspond to the numerical solution for $W(\mu)$ in the cases $n_\gamma/n_\beta = \{2/2, 2/3, +3/3, -3/3\}$ respectively in red, black, magenta and blue.

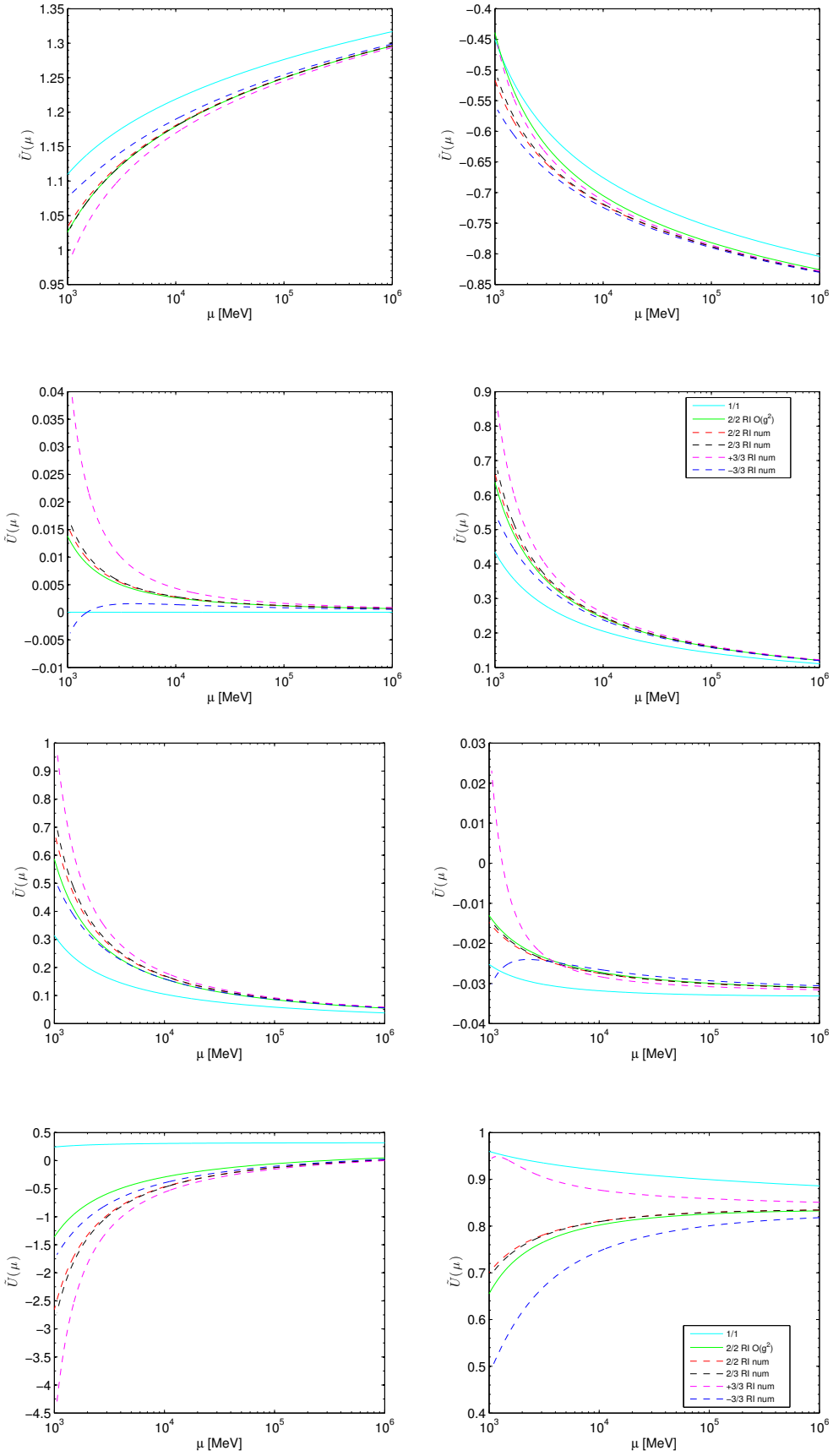

FIGURE 8.19: RG running matrices for the Fierz − Op. $2,3$ (top half) and Op. $4,5$ (bottom half) in the RI scheme. Solid lines correspond to the LO (cyan) and the perturbative expansion for the NLO $2/2$ case up to O(g^2) - i.e. including J_1 (green). Dashed lines correspond to the numerical solution for $W(\mu)$ in the cases $n_\gamma/n_\beta = \{2/2, 2/3, +3/3, -3/3\}$ respectively in red, black, magenta and blue.

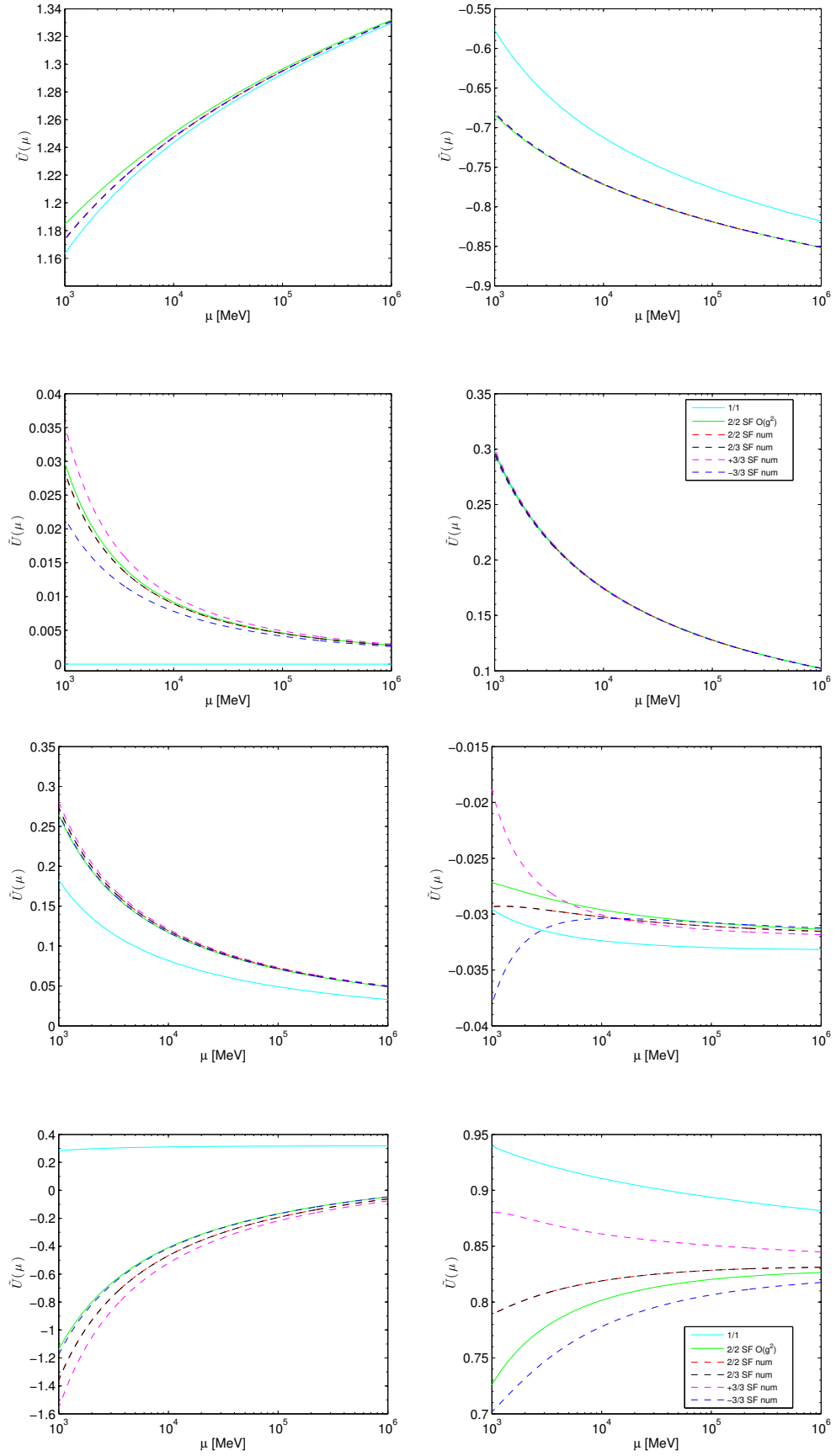

FIGURE 8.20: RG running matrices for the Fierz − Op. $2, 3$ (top half) and Op. $4, 5$ (bottom half) in the SF scheme. Solid lines correspond to the LO (cyan) and the perturbative expansion for the NLO 2/2 case up to O(g^2) - i.e. including J_1 (green). Dashed lines correspond to the numerical solution for $W(\mu)$ in the cases $n_\gamma/n_\beta = \{2/2, 2/3, +3/3, -3/3\}$ respectively in red, black, magenta and blue.

8.8 Summary

In this part of the thesis we have reviewed the renormalisation and RG running properties of the four-quark operators relevant for BSM analyses, and introduced a family of SF schemes that allow to compute them in a fully non-perturbative way. Our non-perturbative results for $N_{\rm f} = 2$ QCD will be presented in a separate publication [137].[13] Here we have focused on the perturbative matching of our schemes to commonly used perturbative schemes and to RGI operators. One of our main results in this context is the full set of NLO operator anomalous dimensions in our SF schemes.

We have also conducted a detailed analysis of perturbative truncation effects in operator RG running in both the SF schemes introduced here, and in commonly used $\overline{\rm MS}$ and RI-MOM schemes. We conclude that when NLO perturbation theory is used to run the operators from high-energy scales down to the few GeV range, large truncation effects appear. One striking example is the mixing of tensor-tensor and scalar-scalar operators, where all the available indications point to extremely large anomalous dimensions and very poor perturbative convergence. One important point worth stressing is that, in the computation of the running factor $W(\mu)$, the use of the truncated perturbative expansion in Eq. (8.1.11) leads to a significantly worse behaviour than the numerical integration of Eq. (2.1.16) with the highest available orders for γ and β.

A context where these findings might have an important impact is e.g. the computation of BSM contributions to neutral kaon mixing. At present, few computations of the relevant $\Delta S = 2$ operators exist with dynamical fermions [139, 140, 141, 142, 143], all of which use perturbative RG running (and, in the case of [142], perturbative operator renormalisation as well). There are substantial discrepancies between the various results in [139, 140, 141, 142, 143], which may be speculated to stem, at least in part, from perturbative truncation effects. Another possible contribution to the discrepancy is the delicate pole subtraction required in the RI-MOM scheme — indeed, results involving perturbative renormalisation and non-perturbative renormalisation constants in RI-SMOM schemes are consistent. At any rate, future efforts to settle this issue, as well as similar studies for $\Delta B = 2$ amplitudes, should put a strong focus on non-perturbative renormalisation.

Moreover, we performed a set of simulations in $N_{\rm f} = 2$ QCD at three value of the lattice spacing for 6 energy scales, allowing us to obtain the (matrix) SSFs. The latter have been used to compute the non-perturbative running over ~ 250 energy scales. As emerged by the perturbative calculations, we confirm large non-perturbative effects. This exploratory work is the first application of the SF recursive technique to operators with mixing. All the technology developed to achieve the computation will be an essential material for future calculations in $N_{\rm f} = 3$ QCD

[13] A comparison of perturbative and non-perturbative results for the running of these operators in RI-MOM schemes for a small region in the few-GeV ballpark can be found in [138].

Conclusions

In this thesis we have computed the non-perturbative running for a set of composite operators, namely, the quark masses ($N_{\rm f} = 2+1$), the tensor currents ($N_{\rm f} = 0$,$N_{\rm f} = 2$) and four-fermion operators with $\Delta F = 1, 2$ ($N_{\rm f} = 2$). The first case is a shared effort with the running coupling project [10] which proceeded in parallel during the realisation of this work. For the first time two renormalization schemes have been adopted for the high and low energy region allowing us to cover a largest range of energy scales respect to the past while obtaining an unprecedented accuracy, where all the source of systematic errors have been carefully taken into account. The quark mass running, together with the value of the renormalization constants computed at the hadronic scales are provided in this work, making a step toward the ongoing computation of the strange quark mass. The latter constitute a natural development of this work whose results will be available in a short time.

Another important results of this work is the running of tensor currents. In this case, taking advantage of 1-loop perturbative computations we have computed, for the first time, the NLO anomalous dimension for the tensor in the SF scheme and 1-loop cutoff effects of the SSFs. This, together with the non-perturbative computation of the running on the ensemble $N_{\rm f} = 0$ and $N_{\rm f} = 2$ provide a complete analysis on this topic, preparing the ground for a $N_{\rm f} = 2 + 1$ calculation which is ongoing. The last, but not least, result concerns the four-fermion operators. On the same line as for the tensor, we discussed the renormalization properties in perturbation theory, extracting for the first time 1-loop SSFs cutoff effects and NLO anomalous dimensions. We then discussed the definition of the RGI, overcoming the difficulties posed by the mixing, which do not allow for a straightforward extension respect to operators which renormalise multiplicatively. We observed large perturbative systematics at around charm mass for a variety of schemes (lattice, and continuum). We then provided a non-perturbative study of the running, which exhibit strong deviation respect to perturbative description in the low energy. This, together with the strong perturbative systematics speaks in favour of treating these operators with a full non-perturbative approach, or at least to apply perturbation theory at a very high scale. Also in this case, our results are essential for further extension to $N_{\rm f} = 2 + 1$.

Conclusiones

En esta tesis hemos calculado el running no perturbativo de un conjunto de operadores compuestos, a saber, las masas de quark ($N_{\rm f} = 2 + 1$), corrientes tensoriales ($N_{\rm f} = 0$,$N_{\rm f} = 2$), y operadores de cuatro fermiones con $\Delta F = 1, 2$ ($N_{\rm f} = 2$).

El primer cálculo es parte de un proyecto conjunto con el cálculo del acoplamiento renormalizado [10], que ha tenido lugar en paralelo durante el desarrollo de este trabajo. Por primera vez han sido adoptados dos esquemas distintos para las regiones de alta y baja energía, lo que nos permite cubrir un rango mayor de escalas energía respecto a estudios anteriores, manteniendo al mismo tiempo una precisión mayor, con todas las incertidumbres sistemáticas tenidas en cuenta de manera cuidadosa. El running de las masas de quark, junto con el valor de las constantes de renormalización calculadas en escalas hadrónicas, son los resultados de este trabajo, y constituyen un paso crucial para el cálculo en curso de la masa del quark extraño. Este último es un desarrollo natural de este trabajo, y será completado en un plazo breve.

Otro importante resultado de este trabajo es el running de las corrientes tensoriales. En este caso, gracias a nuestros cálculos a un loop, hemos determinado por primera vez la dimensión anómala NLO del tensor en esquemas SF, y los efectos de cutoff a un loop en las SSF. Esto, junto a un cálculo no perturbativo del running para $N_{\rm f} = 0$ y $N_{\rm f} = 2$, dan lugar a un análisis completo de este problema, preparando el terreno para un cálculo $N_{\rm f} = 2 + 1$ en curso.

El último, pero no menos importante resultado concierne operadores de cuatro fermiones. En la misma línea que para el tensor, hemos discutido las propiedades de renormalización en teoría de perturbaciones, extrayendo por primera vez efectos de cutoff de las SSF y las dimensiones anómalas NLO en nuestros esquemas. También hemos discutido la definición de RGI, superando las dificultades planteadas por la mezcla de operadores, que no permite una extensión trivial del caso multiplicativamente renormalizable. Hemos observado una sistemática perturbativa grande alrededor de la masa del charm para una gran variedad de esquemas. A continuación hemos presentado un estudio no perturbativo del running, que a bajas energías exhibe grandes desviaciones respecto a la descripción perturbativa. Esto, junto a la sistemática perturbativa, es una fuerte motivación para tratar estos operadores de manera completamente no perturbativa, o al menos de la aplicación de teoría de perturbaciones sólo a escalas muy altas. También en este caso nuestros resultados son esenciales en vista de una extensión a $N_{\rm f} = 2 + 1$.

Appendices

A One-loop cutoff effects in the step scaling function

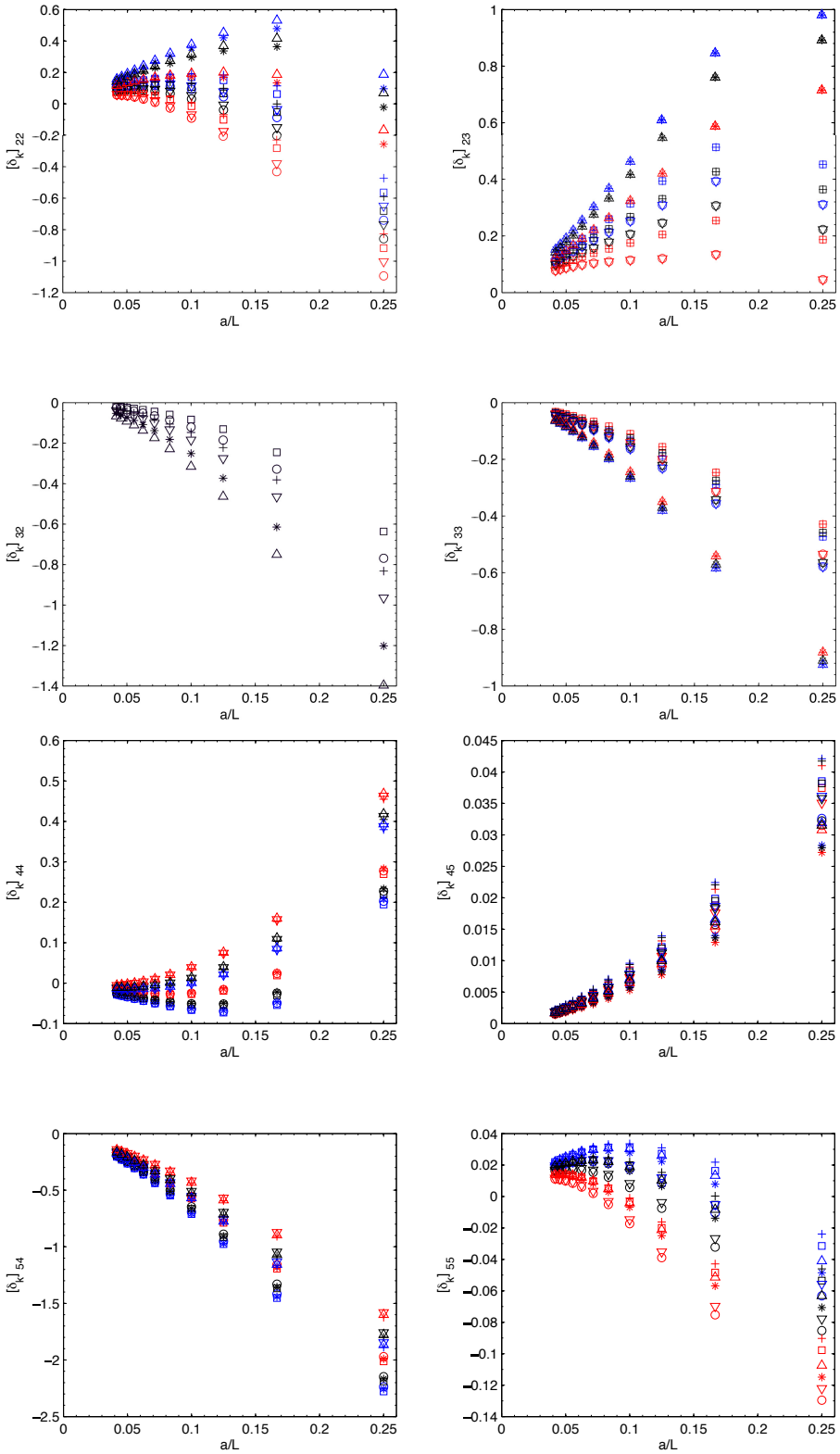

FIGURE A.1: Matrix of the 1-loop cutoff effects with $c_{\rm sw} = 1$ of the SSF for Op $2, 3$ $(4, 5)$ fierz "$+$" on the top (bottom). Color denote the different choice of α and markers are sources s.

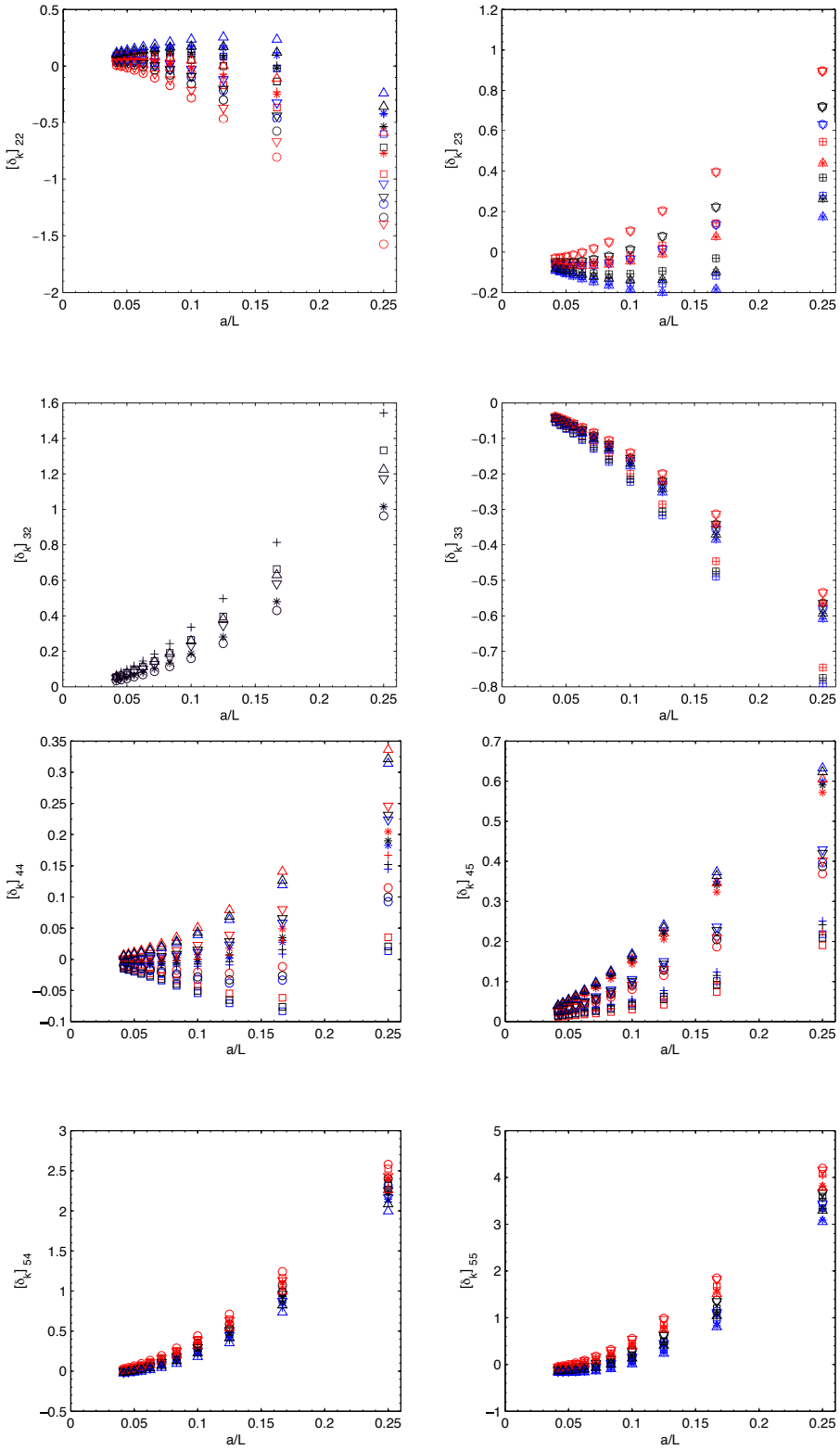

FIGURE A.2: Matrix of the 1-loop cutoff effects with $c_{\rm sw} = 1$ of the SSF for Op $2, 3$ $(4, 5)$ fierz "$-$" on the top (bottom). Color denote the different choice of α and markers are sources s.

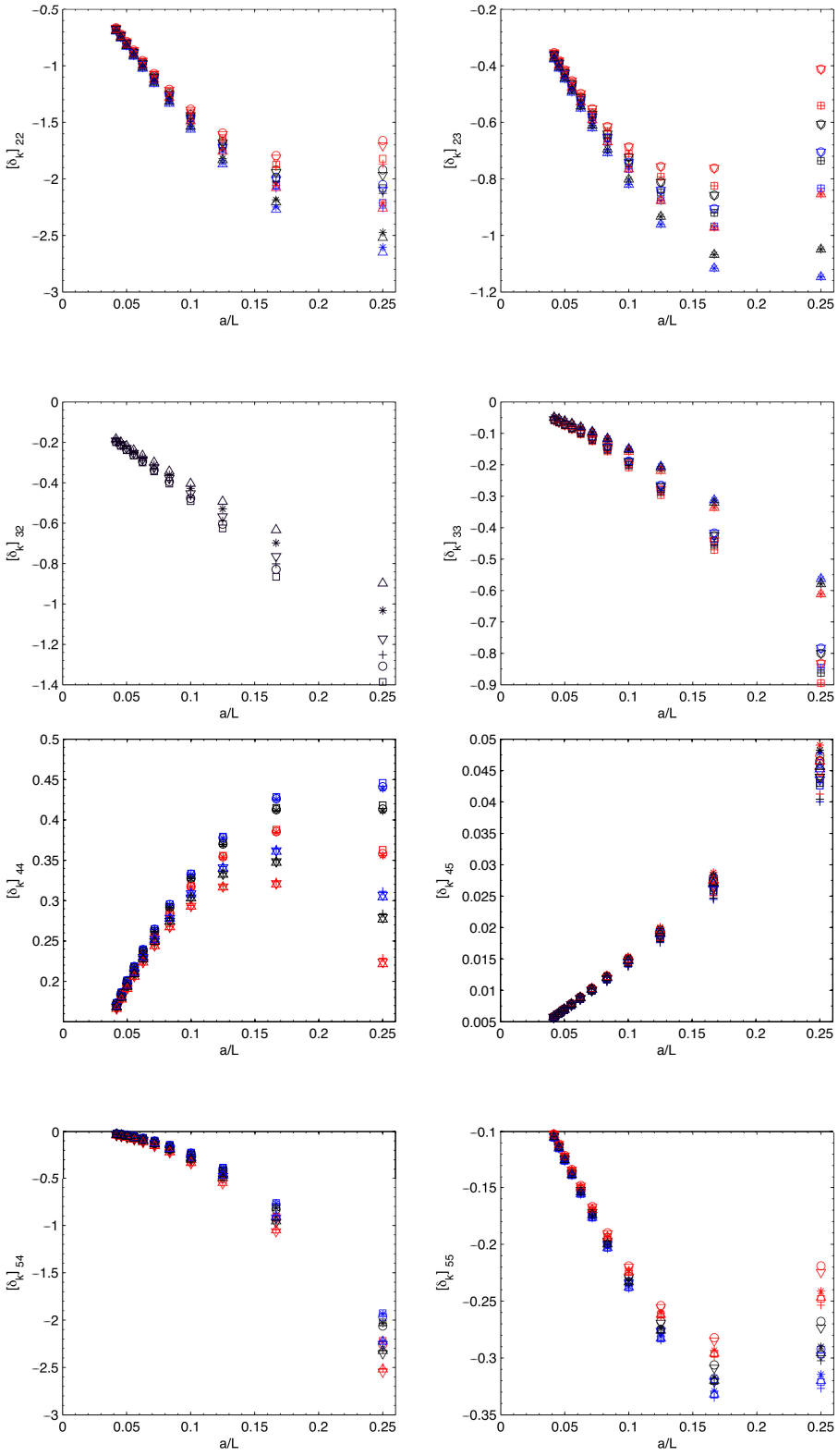

FIGURE A.3: Matrix of the 1-loop cutoff effects with $c_{\rm sw} = 0$ of the SSF for Op $2, 3$ $(4, 5)$ fierz "$+$" on the top (bottom). Color denote the different choice of α and markers are sources s.

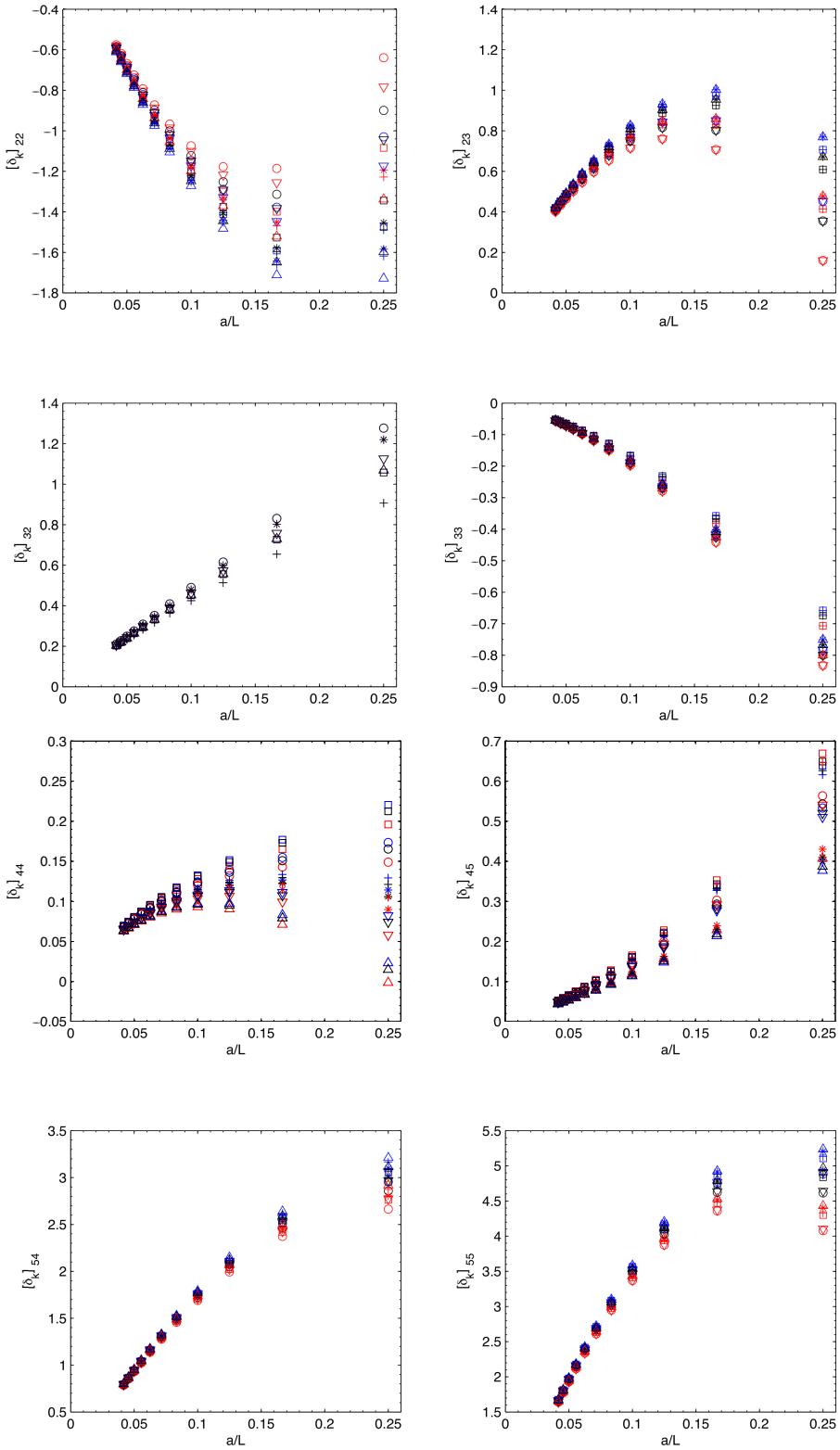

FIGURE A.4: Matrix of the 1-loop cutoff effects with $c_{\rm sw} = 0$ of the SSF for Op $2, 3$ $(4, 5)$ fierz "$-$" on the top (bottom). Color denote the different choice of α and markers are sources s.

L/a	$[\delta_k]_{23}^{(+;c_{\rm sw}=0)}$	$[\delta_k]_{23}^{(-;c_{\rm sw}=0)}$	$[\delta_k]_{23}^{(+;c_{\rm sw}=1)}$	$[\delta_k]_{23}^{(-;c_{\rm sw}=1)}$
4	$\begin{pmatrix} -2.649644 & -1.146696 \\ -0.897521 & -0.562903 \end{pmatrix}$	$\begin{pmatrix} -1.728316 & 0.769175 \\ 1.068844 & -0.750880 \end{pmatrix}$	$\begin{pmatrix} 0.187434 & 0.980468 \\ -1.397054 & -0.925080 \end{pmatrix}$	$\begin{pmatrix} -0.239029 & 0.172755 \\ 1.224870 & -0.608259 \end{pmatrix}$
6	$\begin{pmatrix} -2.270147 & -1.115956 \\ -0.633302 & -0.312431 \end{pmatrix}$	$\begin{pmatrix} -1.712244 & 1.002450 \\ 0.730167 & -0.401243 \end{pmatrix}$	$\begin{pmatrix} 0.531248 & 0.846324 \\ -0.750504 & -0.584800 \end{pmatrix}$	$\begin{pmatrix} 0.235172 & -0.183865 \\ 0.630602 & -0.384869 \end{pmatrix}$
8	$\begin{pmatrix} -1.869882 & -0.960863 \\ -0.492422 & -0.204899 \end{pmatrix}$	$\begin{pmatrix} -1.482077 & 0.931524 \\ 0.556962 & -0.255909 \end{pmatrix}$	$\begin{pmatrix} 0.453106 & 0.609325 \\ -0.463794 & -0.381264 \end{pmatrix}$	$\begin{pmatrix} 0.255353 & -0.199539 \\ 0.382567 & -0.251823 \end{pmatrix}$
10	$\begin{pmatrix} -1.562385 & -0.819867 \\ -0.404426 & -0.149062 \end{pmatrix}$	$\begin{pmatrix} -1.271702 & 0.826113 \\ 0.452405 & -0.182018 \end{pmatrix}$	$\begin{pmatrix} 0.377981 & 0.462327 \\ -0.315184 & -0.267748 \end{pmatrix}$	$\begin{pmatrix} 0.235681 & -0.184042 \\ 0.258383 & -0.178388 \end{pmatrix}$
12	$\begin{pmatrix} -1.333472 & -0.707992 \\ -0.343891 & -0.115961 \end{pmatrix}$	$\begin{pmatrix} -1.105124 & 0.731935 \\ 0.382266 & -0.138962 \end{pmatrix}$	$\begin{pmatrix} 0.320224 & 0.367452 \\ -0.228612 & -0.199372 \end{pmatrix}$	$\begin{pmatrix} 0.211516 & -0.165182 \\ 0.187365 & -0.134313 \end{pmatrix}$
14	$\begin{pmatrix} -1.159958 & -0.620313 \\ -0.299573 & -0.094449 \end{pmatrix}$	$\begin{pmatrix} -0.974682 & 0.653858 \\ 0.331822 & -0.111397 \end{pmatrix}$	$\begin{pmatrix} 0.275829 & 0.302158 \\ -0.173803 & -0.155093 \end{pmatrix}$	$\begin{pmatrix} 0.189124 & -0.147796 \\ 0.142824 & -0.105725 \end{pmatrix}$
16	$\begin{pmatrix} -1.024995 & -0.550700 \\ -0.265671 & -0.079507 \end{pmatrix}$	$\begin{pmatrix} -0.871044 & 0.589677 \\ 0.293718 & -0.092508 \end{pmatrix}$	$\begin{pmatrix} 0.241149 & 0.254939 \\ -0.136903 & -0.124728 \end{pmatrix}$	$\begin{pmatrix} 0.169756 & -0.132789 \\ 0.112970 & -0.086034 \end{pmatrix}$
18	$\begin{pmatrix} -0.917432 & -0.494446 \\ -0.238873 & -0.068599 \end{pmatrix}$	$\begin{pmatrix} -0.787148 & 0.536519 \\ 0.263869 & -0.078883 \end{pmatrix}$	$\begin{pmatrix} 0.213561 & 0.219466 \\ -0.110860 & -0.102950 \end{pmatrix}$	$\begin{pmatrix} 0.153325 & -0.120063 \\ 0.091934 & -0.071829 \end{pmatrix}$
20	$\begin{pmatrix} -0.829877 & -0.448202 \\ -0.217139 & -0.060320 \end{pmatrix}$	$\begin{pmatrix} -0.718006 & 0.491978 \\ 0.239821 & -0.068657 \end{pmatrix}$	$\begin{pmatrix} 0.191226 & 0.191997 \\ -0.091780 & -0.086762 \end{pmatrix}$	$\begin{pmatrix} 0.139416 & -0.109285 \\ 0.076522 & -0.061199 \end{pmatrix}$
22	$\begin{pmatrix} -0.757313 & -0.409593 \\ -0.199147 & -0.053840 \end{pmatrix}$	$\begin{pmatrix} -0.660112 & 0.454212 \\ 0.220008 & -0.060735 \end{pmatrix}$	$\begin{pmatrix} 0.172850 & 0.170193 \\ -0.077372 & -0.074372 \end{pmatrix}$	$\begin{pmatrix} 0.127590 & -0.100114 \\ 0.064873 & -0.053007 \end{pmatrix}$
24	$\begin{pmatrix} -0.696242 & -0.376917 \\ -0.183999 & -0.048639 \end{pmatrix}$	$\begin{pmatrix} -0.610956 & 0.421828 \\ 0.203386 & -0.054436 \end{pmatrix}$	$\begin{pmatrix} 0.157511 & 0.152526 \\ -0.066218 & -0.064659 \end{pmatrix}$	$\begin{pmatrix} 0.117464 & -0.092254 \\ 0.055837 & -0.046540 \end{pmatrix}$
L/a	$[\delta_k]_{45}^{(+;c_{\rm sw}=0)}$	$[\delta_k]_{45}^{(-;c_{\rm sw}=0)}$	$[\delta_k]_{45}^{(+;c_{\rm sw}=1)}$	$[\delta_k]_{45}^{(-;c_{\rm sw}=1)}$
4	$\begin{pmatrix} 0.304518 & 0.045248 \\ -2.225718 & -0.320010 \end{pmatrix}$	$\begin{pmatrix} 0.023085 & 0.376880 \\ 3.211378 & 5.236303 \end{pmatrix}$	$\begin{pmatrix} 0.393235 & 0.031881 \\ -1.865444 & -0.041070 \end{pmatrix}$	$\begin{pmatrix} 0.314036 & 0.632269 \\ 1.996419 & 3.051790 \end{pmatrix}$
6	$\begin{pmatrix} 0.360832 & 0.026906 \\ -0.907110 & -0.331808 \end{pmatrix}$	$\begin{pmatrix} 0.083096 & 0.213740 \\ 2.639245 & 4.926161 \end{pmatrix}$	$\begin{pmatrix} 0.086802 & 0.016542 \\ -1.156020 & 0.013281 \end{pmatrix}$	$\begin{pmatrix} 0.119120 & 0.373079 \\ 0.736291 & 0.802921 \end{pmatrix}$
8	$\begin{pmatrix} 0.340234 & 0.018988 \\ -0.466335 & -0.282722 \end{pmatrix}$	$\begin{pmatrix} 0.097391 & 0.147874 \\ 2.149300 & 4.203452 \end{pmatrix}$	$\begin{pmatrix} 0.022327 & 0.010258 \\ -0.776005 & 0.025993 \end{pmatrix}$	$\begin{pmatrix} 0.063469 & 0.240718 \\ 0.351217 & 0.234227 \end{pmatrix}$
10	$\begin{pmatrix} 0.308242 & 0.014678 \\ -0.277130 & -0.237795 \end{pmatrix}$	$\begin{pmatrix} 0.097575 & 0.113428 \\ 1.790539 & 3.583070 \end{pmatrix}$	$\begin{pmatrix} 0.000572 & 0.007095 \\ -0.569481 & 0.030288 \end{pmatrix}$	$\begin{pmatrix} 0.039145 & 0.168897 \\ 0.180364 & 0.008998 \end{pmatrix}$
12	$\begin{pmatrix} 0.278023 & 0.011975 \\ -0.180140 & -0.203058 \end{pmatrix}$	$\begin{pmatrix} 0.093222 & 0.092219 \\ 1.527657 & 3.099067 \end{pmatrix}$	$\begin{pmatrix} -0.008433 & 0.005262 \\ -0.443270 & 0.030817 \end{pmatrix}$	$\begin{pmatrix} 0.026045 & 0.125824 \\ 0.092686 & -0.093092 \end{pmatrix}$
14	$\begin{pmatrix} 0.251877 & 0.010121 \\ -0.124242 & -0.176481 \end{pmatrix}$	$\begin{pmatrix} 0.087627 & 0.077803 \\ 1.329668 & 2.722092 \end{pmatrix}$	$\begin{pmatrix} -0.012424 & 0.004096 \\ -0.359273 & 0.029790 \end{pmatrix}$	$\begin{pmatrix} 0.018172 & 0.097923 \\ 0.043715 & -0.141307 \end{pmatrix}$
16	$\begin{pmatrix} 0.229686 & 0.008772 \\ -0.089343 & -0.155782 \end{pmatrix}$	$\begin{pmatrix} 0.081969 & 0.067351 \\ 1.176128 & 2.423499 \end{pmatrix}$	$\begin{pmatrix} -0.014147 & 0.003303 \\ -0.299932 & 0.028210 \end{pmatrix}$	$\begin{pmatrix} 0.013104 & 0.078774 \\ 0.014706 & -0.163650 \end{pmatrix}$
18	$\begin{pmatrix} 0.210851 & 0.007745 \\ -0.066253 & -0.139304 \end{pmatrix}$	$\begin{pmatrix} 0.076660 & 0.059420 \\ 1.053939 & 2.182368 \end{pmatrix}$	$\begin{pmatrix} -0.014760 & 0.002737 \\ -0.256116 & 0.026503 \end{pmatrix}$	$\begin{pmatrix} 0.009676 & 0.065031 \\ 0.003208 & -0.172802 \end{pmatrix}$
20	$\begin{pmatrix} 0.194763 & 0.006937 \\ -0.050289 & -0.125917 \end{pmatrix}$	$\begin{pmatrix} 0.071819 & 0.053193 \\ 0.954545 & 1.984093 \end{pmatrix}$	$\begin{pmatrix} -0.014807 & 0.002317 \\ -0.222634 & 0.024843 \end{pmatrix}$	$\begin{pmatrix} 0.007267 & 0.054810 \\ 0.014590 & -0.174959 \end{pmatrix}$
22	$\begin{pmatrix} 0.180910 & 0.006285 \\ -0.038863 & -0.114844 \end{pmatrix}$	$\begin{pmatrix} 0.067455 & 0.048172 \\ 0.872187 & 1.818430 \end{pmatrix}$	$\begin{pmatrix} -0.014560 & 0.001995 \\ -0.196335 & 0.023295 \end{pmatrix}$	$\begin{pmatrix} 0.005523 & 0.046986 \\ 0.021945 & -0.173333 \end{pmatrix}$
24	$\begin{pmatrix} 0.168880 & 0.005748 \\ -0.030454 & -0.105542 \end{pmatrix}$	$\begin{pmatrix} 0.063534 & 0.044036 \\ 0.802870 & 1.678076 \end{pmatrix}$	$\begin{pmatrix} -0.014162 & 0.001743 \\ -0.175208 & 0.021879 \end{pmatrix}$	$\begin{pmatrix} 0.004229 & 0.040850 \\ 0.026729 & -0.169666 \end{pmatrix}$

TABLE A.1: SSFs 1-loop cutoff for Op.$2,3$ and $4,5$ for the scheme denoted by $\alpha = 3/2$ and $(s_1, s_2) = (3, 5)$

B Constraints on anomalous dimensions from chiral symmetry

In section 5.3 of [122] the authors derive an identity between the the renormalisation matrices for $(\mathcal{Q}_2^+, \mathcal{Q}_3^+)$ and $(\mathcal{Q}_2^-, \mathcal{Q}_3^-)$, valid in the RI-MOM scheme considered in that paper. Here we discuss how such an identity can be derived from generic considerations based on chiral symmetry, and how (or, rather, under which conditions) it can be generalised to other renormalisation schemes.

Let us consider a renormalised matrix element of the form $\langle f|\bar{Q}_k^{\pm}|i\rangle$, where $Q_k^{\pm}$ is a parity-even operator and $|i, f\rangle$ are stable hadron states with the same, well-defined parity. Simple examples would be the matrix elements of $\Delta F = 2$ operators providing the hadronic contribution to K^0–$\bar{K}^0$ or B^0–$\bar{B}^0$ oscillation amplitudes (cf. Section **??**). Bare matrix elements can be extracted from suitable three-point Euclidean correlation functions

$$\langle \mathcal{O}_f(x)\, Q_k^{\pm}(0)\, \mathcal{O}_i(y)\rangle = \frac{1}{\mathcal{Z}} \int D[\psi]D[\bar{\psi}]D[A]\, e^{-S}\, \mathcal{O}_f(x)\, Q_k^{\pm}(0)\, \mathcal{O}_i(y) \tag{B.0.1}$$

where $\mathcal{O}_{i,f}$ are interpolating operators for the external states $|i, f\rangle$. If we perform a change of fermion variables of the form

$$\psi \to \psi' = e^{i\gamma_5 T}\psi\,, \qquad \bar{\psi} \to \bar{\psi}' = \bar{\psi} e^{i\gamma_5 T}\,, \tag{B.0.2}$$

where ψ is a fermion field with N_{f} flavour components and T is a traceless matrix acting on flavour space, this will induce a corresponding transformation $Q_k^{\pm} \to {Q'_k}^{\pm}$, $\mathcal{O}_{i,f} \to \mathcal{O}'_{i,f}$ of the involved composite operators. If the regularised theory employed to define the path integral preserves exactly the $\mathrm{SU}(N_{\mathrm{f}})_{\mathrm{A}}$ axial chiral symmetry of the formal continuum theory, the equality $\langle \mathcal{O}_f(x)\, Q_k^{\pm}(0)\, \mathcal{O}_i(y)\rangle = \langle \mathcal{O}'_f(x)\, {Q'_k}^{\pm}(0)\, \mathcal{O}'_i(y)\rangle$ will hold exactly; otherwise, it will only hold upon renormalisation and removal of the cutoff. At the level of matrix elements, one will then have

$$\langle f|\bar{Q}_k^{\pm}|i\rangle_{(\psi,\bar{\psi})} = \langle f|\bar{Q'_k}^{\pm}|i\rangle_{(\psi',\bar{\psi}')}\,, \tag{B.0.3}$$

where the subscript remarks that the interpretation of the operator depends on the fermion variables used on each side of the equation. If the flavour matrix T is not traceless, the argument will still hold if the fermion fields entering composite operators are part of a valence sector, employed only for the purpose of defining suitable correlation functions.

The result in Eq. (B.0.2) is at the basis e.g. of the definition of twisted-mass QCD lattice regularisations, and is discussed in more detail in [121, 144, 145]. Indeed, the rotation in Eq. (B.0.2) will in general transform the mass term of the action. One crucial remark at this point is that, if a mass-independent renormalisation scheme is used, renormalisation constants for any given composite operator will be independent of which fermion variables are employed in the computation of the matrix element.

Let us now consider a particular case of Eq. (B.0.2) given by

$$T = \frac{\pi}{4}\begin{pmatrix} 1 & 0 & 0 & 0 \\ 0 & 1 & 0 & 0 \\ 0 & 0 & 1 & 0 \\ 0 & 0 & 0 & -1 \end{pmatrix}, \tag{B.0.4}$$

where $\psi = (\psi_1, \psi_2, \psi_3, \psi_4)^T$ comprises the four, formally distinct flavours that enter $Q_k^\pm, \mathcal{Q}_k^\pm$. Under this rotation, the ten operators of the basis in Eq. (8.1.1) transform as

$$\begin{aligned} Q_1^\pm &\to i\mathcal{Q}_1^\pm\,, \\ Q_2^\pm &\to -i\mathcal{Q}_2^\mp\,, \\ Q_3^\pm &\to i\mathcal{Q}_3^\mp\,, \\ Q_4^\pm &\to i\mathcal{Q}_4^\pm\,, \\ Q_5^\pm &\to i\mathcal{Q}_5^\pm\,. \end{aligned} \tag{B.0.5}$$

In the case of operators 1,4,5 the rotation is essentially trivial, in that it preserves Fierz ($2 \leftrightarrow 4$ exchange) eigenstates. However, in the rotation of operators 2,3 the Fierz eigenvalue is exchanged. One thus has, at the level of renormalised matrix elements,

$$\langle f|\bar{\mathbf{Q}}^+(\mu)|i\rangle_{(\psi,\bar\psi)} = R\langle f|\bar{\boldsymbol{\mathcal{Q}}}^-(\mu)|i\rangle_{(\psi',\bar\psi')}\,, \tag{B.0.6}$$

where $\mathbf{Q}^+ = (Q_2^+, Q_3^+)^T$, $\boldsymbol{\mathcal{Q}}^- = (\mathcal{Q}_2^-, \mathcal{Q}_3^-)^T$, and $R = -i\tau^3$. In this latter expression we have written explicitly the renormalisation scale μ. If we now use the RG evolution operators discussed in Section **??** to run Eq. (B.0.6) to another scale μ', one then has (recall that the continuum anomalous dimensions of Q_k^+ and $\mathcal{Q}_k^+$ — respectively, Q_k^- and $\mathcal{Q}_k^-$ — are the same)

$$\begin{aligned} \langle f|\bar{\mathbf{Q}}^+(\mu')|i\rangle_{(\psi,\bar\psi)} &= U^+(\mu',\mu)\langle f|\bar{\mathbf{Q}}^+(\mu)|i\rangle_{(\psi,\bar\psi)} \\ &= U^+(\mu',\mu)R\langle f|\bar{\boldsymbol{\mathcal{Q}}}^-(\mu)|i\rangle_{(\psi',\bar\psi')} \\ &= U^+(\mu',\mu)R[U^-(\mu',\mu)]^{-1}\langle f|\bar{\boldsymbol{\mathcal{Q}}}^-(\mu')|i\rangle_{(\psi',\bar\psi')} \\ &= U^+(\mu',\mu)R[U^-(\mu',\mu)]^{-1}R^{-1}\langle f|\bar{\mathbf{Q}}^+(\mu')|i\rangle_{(\psi,\bar\psi)}\,, \end{aligned} \tag{B.0.7}$$

which implies

$$U^+(\mu',\mu) = RU^-(\mu',\mu)R^{-1} \quad \forall\mu,\mu'\,. \tag{B.0.8}$$

It is then immediate that the anomalous dimension matrices entering $U^\pm$ are related as

$$\gamma^+ = \begin{pmatrix} \gamma^+_{22} & \gamma^+_{23} \\ \gamma^+_{32} & \gamma^+_{33} \end{pmatrix} = \tau^3\gamma^-\tau^3 = \begin{pmatrix} \gamma^-_{22} & -\gamma^-_{23} \\ -\gamma^-_{32} & \gamma^-_{33} \end{pmatrix}. \tag{B.0.9}$$

The correct interpretation of this identity is that, given an anomalous dimension matrix for, say, $Q^+_{2,3}$ and $\mathcal{Q}^+_{2,3}$, one can use Eq. (B.0.9) to construct a correct anomalous dimension matrix for $Q^-_{2,3}$ and $\mathcal{Q}^-_{2,3}$, and vice versa. However, it does *not* guarantee that, given two different renormalisation conditions for each fierzing, the resulting matrices of anomalous dimensions will satisfy Eq. (B.0.9). This will only be the case if the renormalisation conditions can be related to each other by the rotation in Eq. (B.0.4); otherwise, the result of applying Eq. (B.0.9) to the γ^- that follows from the condition imposed on Fierz - operators will lead to value of γ^+ in a different renormalisation scheme than the one defined by the renormalisation condition imposed directly on Fierz + operators.

The RI-MOM conditions of [122], as well as typical $\overline{\text{MS}}$ renormalisation conditions,

result in schemes that satisfy the identity directly, since the quantities involved respect the underlying chiral symmetry — e.g. the amputated correlation functions used in RI-MOM rotate in a similar way to the three-point functions discussed above. Indeed, the known NLO anomalous dimensions in RI-MOM and $\overline{\mathrm{MS}}$ given in Appendix C, as well as (within uncertainties) the non-perturbative values of RI-MOM renormalisation constants, fulfill Eq. (B.0.9). Our SF renormalisation conditions, on the other hand, are not related among them via rotations with R, due to the chiral symmetry-breaking effects induced by the non-trivial boundary conditions imposed on the fields. As a consequence, the finite parts of the matrices of SF renormalisation constants, and hence γ_2^{SF}, do not satisfy the identity. It has to be stressed that, as a consequence of the existence of schemes where Eq. (B.0.9) is respected, the identity is satisfied by the universal matrices $\gamma_0^{\pm}$, as can be readily checked in Eq. (8.1.10); therefore, the violation of the identity in e.g. SF schemes appears only at $\mathcal{O}(g_0^4)$ in perturbation theory.

C NLO anomalous dimensions in continuum schemes

The two-loop anomalous dimension matrices in the RI-MOM scheme (in Landau gauge) [25, 24] and $\overline{\text{MS}}$ scheme [24] are given by (the factor $(4\pi)^{-4}$ has been omitted below to simplify the notation):

$$
\begin{aligned}
\gamma_{22}^{+,(1);\text{RI}} &= \frac{(297+16\log(2))N^2+45}{6N^2} - N_f\frac{2(15+4\log(2))}{3N}\,,\\
\gamma_{23}^{+,(1);\text{RI}} &= \frac{2\left(4N^2(45+2\log(2))-9\right)}{3N} - N_f\frac{4}{3}(15+4\log(2))\,,\\
\gamma_{32}^{+,(1);\text{RI}} &= \frac{(53+160\log(2))N^2+108}{12N} - N_f\frac{2}{3}(1+2\log(2))\,,\\
\gamma_{33}^{+,(1);\text{RI}} &= \frac{-379N^4+5(99+32\log(2))N^2+45}{6N^2} + N_f\frac{2\left(13N^2-4\log(2)-15\right)}{3N}\,,\\
\gamma_{44}^{+,(1);\text{RI}} &= \frac{-379N^4+2(261-88\log(2))N^3+140(3+2\log(2))N^2-4(-6+60\log(2))N-81}{6N^2}+\\
&+ N_f\frac{2\left(13N^2+(-15+8\log(2))N-4\log(2)-15\right)}{3N}\,,\\
\gamma_{45}^{+,(1);\text{RI}} &= \frac{(157-368\log(2))N^3+(-494+556\log(2))N^2-4(-39+30\log(2))N-72}{36N^2}+\\
&+ N_f\frac{((-11+16\log(2))N-20\log(2)+28)}{18N}\,,\\
\gamma_{54}^{+,(1);\text{RI}} &= \frac{4\left((-165+16\log(2))N^3+(-230+76\log(2))N^2-4(-39+30\log(2))N-72\right)}{3N^2}+\\
&+ N_f\frac{8((15+16\log(2))N-20\log(2)+28)}{3N}\,,\\
\gamma_{55}^{+,(1);\text{RI}} &= \frac{343N^4-2(-343+616\log(2))N^3+4(-95+142\log(2))N^2+(504+720\log(2))N-531}{18N^2}+\\
&- N_f\frac{2\left(13N^2+(41-56\log(2))N+52\log(2)-11\right)}{9N}\,.
\end{aligned}
$$

$$
\begin{aligned}
\gamma_{22}^{-,(1);\mathrm{RI}} &= \frac{15}{2N^2} + \frac{8\log(2)}{3} + \frac{99}{2} - N_f\frac{2(15+4\log(2))}{3N}\,,\\
\gamma_{23}^{-,(1);\mathrm{RI}} &= -\frac{8}{3}(45+2\log(2))N + \frac{6}{N} + N_f\frac{4}{3}(15+4\log(2))\,,\\
\gamma_{32}^{-,(1);\mathrm{RI}} &= -\frac{1}{12}(53+160\log(2))N - \frac{9}{N} + N_f\frac{2}{3}(1+2\log(2))\,,\\
\gamma_{33}^{-,(1);\mathrm{RI}} &= \frac{-379N^4+5(99+32\log(2))N^2+45}{6N^2} + N_f\frac{2\left(13N^2-4\log(2)-15\right)}{3N}\,,\\
\gamma_{44}^{-,(1);\mathrm{RI}} &= \frac{-379N^4+2(-261+88\log(2))N^3+140(3+2\log(2))N^2+24(-1+10\log(2))N-81}{6N^2}+\\
&+\ N_f\frac{2\left(13N^2-(-15+8\log(2))N-4\log(2)-15\right)}{3N}\,,\\
\gamma_{45}^{-,(1);\mathrm{RI}} &= \frac{(-157+368\log(2))N^3+(-494+556\log(2))N^2+12(-13+10\log(2))N-72}{36N^2}+\\
&-\ N_f\frac{((-11+16\log(2))N+20\log(2)-28)}{18N}\,,\\
\gamma_{54}^{-,(1);\mathrm{RI}} &= -\frac{4\left((-165+16\log(2))N^3+(230-76\log(2))N^2+(156-120\log(2))N+72\right)}{3N^2}+\\
&-\ N_f\frac{8((15+16\log(2))N+4(-7+5\log(2)))}{3N}\,,\\
\gamma_{55}^{-,(1);\mathrm{RI}} &= \frac{343N^4+14(-49+88\log(2))N^3+4(-95+142\log(2))N^2-72(7+10\log(2))N-531}{18N^2}+\\
&-\ N_f\frac{2\left(13N^2+(-41+56\log(2))N+52\log(2)-11\right)}{9N}\,.
\end{aligned}
$$

$$
\begin{aligned}
\gamma_{22}^{+,(1);\overline{\mathrm{MS}}} &= \frac{15}{2N^2} + \frac{137}{6} - N_f\frac{22}{3N}\,,\\
\gamma_{23}^{+,(1);\overline{\mathrm{MS}}} &= \frac{200N}{3} - \frac{6}{N} - N_f\frac{44}{3}\,,\\
\gamma_{32}^{+,(1);\overline{\mathrm{MS}}} &= \frac{71N}{4} + \frac{9}{N} - N_f 2\,,\\
\gamma_{33}^{+,(1);\overline{\mathrm{MS}}} &= -\frac{203N^2}{6} + \frac{479}{6} + \frac{15}{2N^2} + N_f\left(\frac{10N}{3} - \frac{22}{3N}\right)\,,\\
\gamma_{44}^{+,(1);\overline{\mathrm{MS}}} &= -\frac{203N^2}{6} + \frac{107N}{3} + \frac{136}{3} - \frac{12}{N} - \frac{107}{2N^2} + N_f\left(\frac{10N}{3} - \frac{2}{3} - \frac{10}{3N}\right)\,,\\
\gamma_{45}^{+,(1);\overline{\mathrm{MS}}} &= -\frac{N}{36} - \frac{31}{9} + \frac{9}{N} - \frac{4}{N^2} + N_f\left(\frac{1}{9N} - \frac{1}{18}\right)\,,\\
\gamma_{54}^{+,(1);\overline{\mathrm{MS}}} &= -\frac{364N}{3} - \frac{704}{3} - \frac{208}{N} - \frac{320}{N^2} + N_f\left(\frac{136}{3} + \frac{176}{3N}\right)\,,\\
\gamma_{55}^{+,(1);\overline{\mathrm{MS}}} &= \frac{343N^2}{18} + 21N - \frac{188}{9} + \frac{44}{N} + \frac{21}{2N^2} + N_f\left(-\frac{26N}{9} - 6 + \frac{2}{9N}\right)\,.
\end{aligned}
$$

$$
\begin{aligned}
\gamma_{22}^{-,(1);\overline{\rm MS}} &= \frac{15}{2N^2} + \frac{137}{6} - N_f \frac{22}{3N}\,, \\
\gamma_{23}^{-,(1);\overline{\rm MS}} &= -\frac{200N}{3} + \frac{6}{N} + N_f \frac{44}{3}\,, \\
\gamma_{32}^{-,(1);\overline{\rm MS}} &= -\frac{71N}{4} - \frac{9}{N} + N_f 2\,, \\
\gamma_{33}^{-,(1);\overline{\rm MS}} &= -\frac{203N^2}{6} + \frac{479}{6} + \frac{15}{2N^2} + N_f \left(\frac{10N}{3} - \frac{22}{3N} \right)\,, \\
\gamma_{44}^{-,(1);\overline{\rm MS}} &= -\frac{203N^2}{6} - \frac{107N}{3} + \frac{136}{3} + \frac{12}{N} - \frac{107}{2N^2} + N_f \left(\frac{10N}{3} + \frac{2}{3} - \frac{10}{3N} \right)\,, \\
\gamma_{45}^{-,(1);\overline{\rm MS}} &= \frac{N}{36} - \frac{31}{9} - \frac{9}{N} - \frac{4}{N^2} + N_f \left(\frac{1}{18} + \frac{1}{9N} \right)\,, \\
\gamma_{54}^{-,(1);\overline{\rm MS}} &= \frac{364N}{3} - \frac{704}{3} + \frac{208}{N} - \frac{320}{N^2} + N_f \left(\frac{176}{3N} - \frac{136}{3} \right)\,, \\
\gamma_{55}^{-,(1);\overline{\rm MS}} &= \frac{343N^2}{18} - 21N - \frac{188}{9} - \frac{44}{N} + \frac{21}{2N^2} + N_f \left(-\frac{26N}{9} + 6 + \frac{2}{9N} \right)\,.
\end{aligned}
$$

D Perturbative expansion of RG evolution for $N_{\rm f} = 3$

It is well-known that the condition in Eq. (8.1.12) that determines the leading non-trivial coefficient in the NLO perturbative expansion of the RG evolution operator, Eq. (8.1.11), is ill-behaved for the operators $Q^{\pm}_{2,3}$ for $N_{\rm f} = 30$ and, more relevantly, for $N_{\rm f} = 3$ [146, 147]. The reason is that, when Eq. (8.1.12) is written as a linear system, the 4×4 matrix that multiplies the vector of elements of J_1 has zero determinant, rendering the system indeterminate.

A simple way to understand the anatomy of this problem in greater detail proceeds by writing the explicit solution to Eq. (8.1.12) as a function of the parameter $\epsilon = 3 - N_{\rm f}$; if the NLO anomalous dimension matrix in the scheme under consideration is written as

$$\gamma_1^{\pm} = \frac{1}{(4\pi)^4} \begin{pmatrix} g_{22}^{\pm} & g_{23}^{\pm} \\ g_{32}^{\pm} & g_{33}^{\pm} \end{pmatrix} \tag{D.0.1}$$

then one finds

$$J_1^{\pm} = \frac{1}{\epsilon} J_{1,-1}^{\pm} + J_{1,0}^{\pm} + \epsilon J_{1,1}^{\pm} + \mathcal{O}(\epsilon^2)\,, \tag{D.0.2}$$

with

$$J_{1,-1}^{\pm} = \frac{1}{(4\pi)^2} \begin{pmatrix} 0 & \pm\frac{1}{2}(g_{22}^{\pm} - g_{33}^{\pm}) - \frac{3}{4} g_{23}^{\pm} + \frac{1}{3} g_{32}^{\pm} \\ 0 & 0 \end{pmatrix}, \tag{D.0.3}$$

$$J_{1,0}^{\pm} = \frac{1}{(4\pi)^2} \begin{pmatrix} \frac{1}{162}(128 - 9 g_{22}^{\pm} \mp 3 g_{32}^{\pm}) & \frac{1}{27}(\pm 128 \mp g_{22}^{\pm} - g_{32}^{\pm} \pm g_{33}^{\pm}) \\ -\frac{1}{36} g_{32}^{\pm} & \frac{1}{162}(-1024 \pm 3 g_{32}^{\pm} - 9 g_{33}^{\pm}) \end{pmatrix}, \tag{D.0.4}$$

$$J_{1,1}^{\pm} = \frac{1}{(4\pi)^2} \begin{pmatrix} \frac{1}{4374}(172 + 18 g_{22}^{\pm} \pm 9 g_{32}^{\pm}) & \pm\frac{1}{2187}(516 + 6 g_{22}^{\pm} \pm 7 g_{32}^{\pm} - 6 g_{33}^{\pm}) \\ \frac{1}{972} g_{32}^{\pm} & \frac{1}{4374}(-1376 \mp 9 g_{32}^{\pm} + 18 g_{33}^{\pm}) \end{pmatrix}. \tag{D.0.5}$$

In the limit $\epsilon \to 0$ the element 23 of $J_1^{\pm}$ diverges; it is easy to check that the aforementioned 4×4 matrix, consistently, has determinant $\propto \epsilon$. A similar expansion of the matrices $\tilde{U}^{\pm}_{\rm LO}(\mu) \equiv [\alpha_{\rm s}(\mu)]^{-\frac{\gamma_0^{\pm}}{2b_0}}$ yields

$$\tilde{U}^{\pm}_{\rm LO}(\mu) = \tilde{U}^{\pm}_{\rm LO,0}(\mu) + \epsilon \tilde{U}^{\pm}_{\rm LO,1}(\mu) + \mathcal{O}(\epsilon^2)\,, \tag{D.0.6}$$

with

$$\tilde{U}^{\pm}_{\rm LO,0}(\mu) = \begin{pmatrix} \alpha_{\rm s}^{-1/9}(\mu) & \mp\frac{2}{3}[\alpha_{\rm s}^{8/9}(\mu) - \alpha_{\rm s}^{-1/9}(\mu)] \\ 0 & \alpha_{\rm s}^{8/9}(\mu) \end{pmatrix}, \tag{D.0.7}$$

$$\tilde{U}^{\pm}_{\rm LO,1}(\mu) = \begin{pmatrix} \frac{2}{243}\alpha_{\rm s}^{-1/9}(\mu) & \pm\frac{4}{729}[8\alpha_{\rm s}^{8/9}(\mu) + \alpha_{\rm s}^{-1/9}(\mu)] \\ 0 & -\frac{16}{243}\alpha_{\rm s}^{8/9}(\mu) \end{pmatrix} \log[\alpha_{\rm s}(\mu)]\,. \tag{D.0.8}$$

When these expressions are plugged in Eq. (2.1.14), and the perturbative expansion Eq. (8.1.11) is used, one gets

$$\tilde{U}^{\pm}(\mu) = \tilde{U}^{\pm}_{\mathrm{LO},0}(\mu) + \bar{g}^2(\mu)\left[\frac{1}{\epsilon}\tilde{U}^{\pm}_{\mathrm{LO},0}(\mu)J^{\pm}_{1,-1} + \tilde{U}^{\pm}_{\mathrm{LO},0}(\mu)J^{\pm}_{1,0} + \tilde{U}^{\pm}_{\mathrm{LO},1}(\mu)J^{\pm}_{1,-1} + \mathcal{O}(\epsilon)\right] + \mathcal{O}(\bar{g}^4(\mu))\,, \tag{D.0.9}$$

which is still divergent as $\epsilon \to 0$. This implies, in particular, that RGI operators cannot be defined consistently using the above form of the perturbative expansion for W. The RG evolution operator $U(\mu_2, \mu_1) = [\tilde{U}(\mu_2)]^{-1}\tilde{U}(\mu_1)$, on the other hand, is finite: the divergent part has the form

$$\frac{1}{\epsilon}\left\{\bar{g}^2(\mu_1)U^{\pm}_{\mathrm{LO}}(\mu_2,\mu_1)J^{\pm}_{1,-1} - \bar{g}^2(\mu_2)J^{\pm}_{1,-1}U^{\pm}_{\mathrm{LO}}(\mu_2,\mu_1)\right\} = \frac{\pm\frac{1}{2}(g^{\pm}_{22} - g^{\pm}_{33}) - \frac{3}{4}g^{\pm}_{23} + \frac{1}{3}g^{\pm}_{32}}{4\pi\epsilon}\,M\,, \tag{D.0.10}$$

with

$$M = U^{\pm}_{\mathrm{LO}}(\mu_2,\mu_1)\begin{pmatrix} 0 & \alpha_s(\mu_2) \\ 0 & 0 \end{pmatrix} - \begin{pmatrix} 0 & \alpha_s(\mu_1) \\ 0 & 0 \end{pmatrix} U^{\pm}_{\mathrm{LO}}(\mu_2,\mu_1)\,, \tag{D.0.11}$$

and it is easy to check, using the explicit expression for $\tilde{U}^{\pm}_{\mathrm{LO},0}(\mu)$ and the identity $U^{\pm}_{\mathrm{LO}}(\mu_2,\mu_1) = [U^{\pm}_{\mathrm{LO},0}(\mu_2)]^{-1}U^{\pm}_{\mathrm{LO},0}(\mu_1)$, that $M = 0$.[1] The full expression for $U(\mu_2,\mu_1)$ in the $\epsilon \to 0$ limit still receives contributions from $J_{1,-1}$, via the products with the $\mathcal{O}(\epsilon)$ terms in the expansion of $\tilde{U}_{\mathrm{LO}}$, which actually give rise to the only dependence of the expanded $U(\mu_2,\mu_1)$ on $\gamma_1^{\pm}$.

A number of solutions to this problem have been proposed in the literature [146, 147, 149, 148], consisting of various regularisation schemes to treat the singular terms in $3-N_f$. Here we note that the problem can be entirely bypassed by using the numerical integration of the RG equation in Eq. (2.1.16), as done in this paper to explore the case $N_f = 2$ in detail. Indeed, applying exactly the same procedure for $N_f = 3$ — i.e., solving Eq. (2.1.16) after having substituted the perturbative expressions for γ and β to any prescribed order — is well-behaved numerically, which in turn allows to construct both the RG evolution matrix and RGI operators without trouble. The only point in the procedure where the expansion coefficient J_1 may enter explicitly is the initial condition in Eq. (8.4.2), where for the $N_f = 2$ case we have employed $W(\mu_0) = \mathbf{1} + \bar{g}^2(\mu_0)J_1$ at some very high energy scale μ_0. However, this can be replaced by the initial condition $W(\mu_0) = \mathbf{1}$ at an even higher scale, thus again avoiding the appearance of any singularity; it turns out that the required value of $\bar{g}^2(\mu)$ has to be extremely small, such that the systematics associated to the choice of coupling for the initial condition is negligible at the level of the result run down to $\bar{g}^2(\mu) \sim 2$. This in turn requires using an expensive numerical integrator to work across several orders of magnitude, which is easy e.g. using standard Mathematica functions, provided proper care is taken to chose a stable integrator.

As a crosscheck of the robustness of our numerical approach we have computed explicitly the function $W(\mu)$ for $N_f = 3$, using our numerical integration and $W = \mathbf{1}$ as an initial condition, set at an extremely small value of the coupling. Our result for W, displayed in Fig. D.1, can then be fitted to an ansatz where J is taken to have a polynomial dependence in $\bar{g}^2$, to check whether the first coefficient J_1 is compatible within systematic fit errors (obtained by trying different polynomial orders up to $\mathcal{O}(\bar{g}^8)$ and coupling values for the initial condition) with the one quoted in Eq.(2.30) of [148]. Note that in order to have a direct comparison it has to be taken into account that we are using a different

[1] This is completely analogous e.g. to the discussion leading to Eq. (53) in [148].

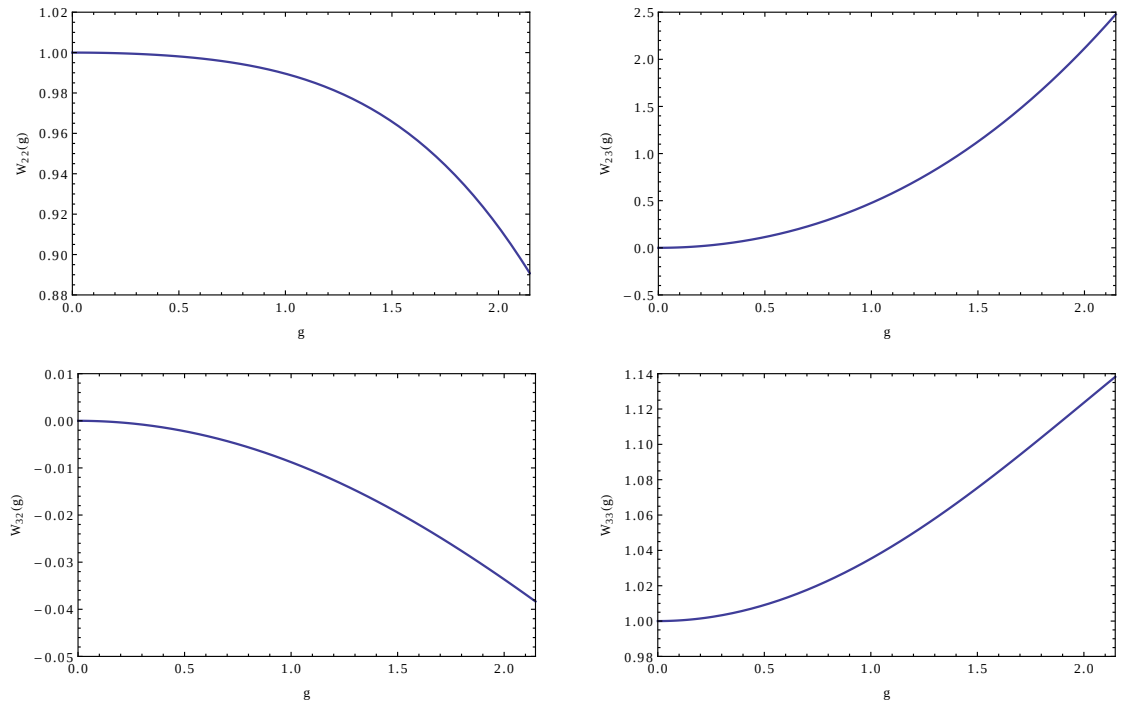

FIGURE D.1: W as a function of the coupling constant, with $N_f = 3$ for operators O_2, O_3 fierz "+", in the $\overline{\text{MS}}$ scheme.

relative normalization between operators O_2, O_3 than the one in [148] which translates into a factor -2 and $-1/2$ respectively for $[J_1^{\text{fit}}]_{23}$, $[J_1^{\text{fit}}]_{32}$ and that, since we are working with the renormalization constants instead of the Wilson coefficients, the convention used for the J is this work corresponds to J^T in [148] . What we obtain is

$$J_1^{\text{fit}} = \frac{1}{(4\pi)^2} \begin{pmatrix} -1.0470(8) & 70.13(38) \\ -1.39583(1) & 5.78550(8) \end{pmatrix} \tag{D.0.12}$$

which is indeed well-compatible with the above-mentioned result. Note that the coefficient 23 contains a precise numerical value of the parameter t employed in [148] to regularise the divergence of J in $3 - N_f$.

As a further crosscheck, we have also compared the result of computing the $N_f = 2$ evolution with the two possible initial conditions. The outcome is that, if the value of the coupling at which $W = \mathbf{1}$ is sufficiently small, the two results are equal up to several significant figures down to values of the coupling $\bar{g}^2 \gtrsim 2$, where the hadronic regimes is entered.

E Finite parts of RI-MOM renormalisation constants in Landau gauge

In this appendix we gather the results for the finite part of the one-loop matching coefficients $[\mathcal{X}_O^{(1)}]_{\mathrm{RI;lat}}$ between the lattice and the RI-MOM scheme in Landau gauge. They can be extracted from [127] and are given by

$$
\begin{aligned}
[\mathcal{X}_{22}^{+,(1)}]_{\mathrm{RI;lat}} &= 0.0272369\, c_{\mathrm{sw}}^2 + 0.0485167\, c_{\mathrm{sw}} - 0.294894\,, \\
[\mathcal{X}_{23}^{+,(1)}]_{\mathrm{RI;lat}} &= 0.0218485\, c_{\mathrm{sw}}^2 + 0.0632421\, c_{\mathrm{sw}} + 0.0753979\,, \\
[\mathcal{X}_{32}^{+,(1)}]_{\mathrm{RI;lat}} &= 0.00755569\,, \\
[\mathcal{X}_{33}^{+,(1)}]_{\mathrm{RI;lat}} &= -0.00553581\, c_{\mathrm{sw}}^2 - 0.0463464\, c_{\mathrm{sw}} - 0.362656\,, \\
[\mathcal{X}_{44}^{+,(1)}]_{\mathrm{RI;lat}} &= 0.00538842\, c_{\mathrm{sw}}^2 - 0.0147254\, c_{\mathrm{sw}} - 0.351294\,, \\
[\mathcal{X}_{45}^{+,(1)}]_{\mathrm{RI;lat}} &= 0.000303451\, c_{\mathrm{sw}}^2 + 0.000878362\, c_{\mathrm{sw}} - 0.00178318\,, \\
[\mathcal{X}_{54}^{+,(1)}]_{\mathrm{RI;lat}} &= -0.0728282\, c_{\mathrm{sw}}^2 - 0.210807\, c_{\mathrm{sw}} - 0.266293\,, \\
[\mathcal{X}_{55}^{+,(1)}]_{\mathrm{RI;lat}} &= 0.0442301\, c_{\mathrm{sw}}^2 + 0.0977049\, c_{\mathrm{sw}} - 0.290267\,.
\end{aligned}
\tag{E.0.1}
$$

$$
\begin{aligned}
[\mathcal{X}_{22}^{-,(1)}]_{\mathrm{RI;lat}} &= 0.0272369\, c_{\mathrm{sw}}^2 + 0.0485167\, c_{\mathrm{sw}} - 0.294894\,, \\
[\mathcal{X}_{23}^{-,(1)}]_{\mathrm{RI;lat}} &= -0.0218485\, c_{\mathrm{sw}}^2 - 0.0632421\, c_{\mathrm{sw}} - 0.0753979\,, \\
[\mathcal{X}_{32}^{-,(1)}]_{\mathrm{RI;lat}} &= -0.00755569\,, \\
[\mathcal{X}_{33}^{-,(1)}]_{\mathrm{RI;lat}} &= -0.00553581\, c_{\mathrm{sw}}^2 - 0.0463464\, c_{\mathrm{sw}} - 0.362656\,, \\
[\mathcal{X}_{44}^{-,(1)}]_{\mathrm{RI;lat}} &= -0.01646\, c_{\mathrm{sw}}^2 - 0.0779674\, c_{\mathrm{sw}} - 0.374019\,, \\
[\mathcal{X}_{45}^{-,(1)}]_{\mathrm{RI;lat}} &= -0.00151725\, c_{\mathrm{sw}}^2 - 0.00439181\, c_{\mathrm{sw}} + 0.0013602\,, \\
[\mathcal{X}_{54}^{-,(1)}]_{\mathrm{RI;lat}} &= 0.0145656\, c_{\mathrm{sw}}^2 + 0.0421614\, c_{\mathrm{sw}} + 0.24599\,, \\
[\mathcal{X}_{55}^{-,(1)}]_{\mathrm{RI;lat}} &= 0.0223817\, c_{\mathrm{sw}}^2 + 0.0344629\, c_{\mathrm{sw}} - 0.257729\,.
\end{aligned}
\tag{E.0.2}
$$

F Finite parts of SF renormalisation constants

In this appendix we discuss how to determine the dependence on a/L of the one-loop renormalization constants $Z^{(1)}$ defined in chapters 6, 8. The approach is essentially an application of the present context to the techniques discussed in Appendix D of [37]. Defining $\ell = L/a$ we will hence consider $F(\ell) = Z^{(1)}$ as a pure function of $\ell = \{\ell_1, \ldots, \ell_N\}$. We will also assume that all divergences have been removed from $F(\ell)$, which in general means linear divergences related to the additive renormalisation of quark masses and proportional to the one-loop value of the critical mass $m_{cr}^{(1)}$, and logarithmic divergences proportional to a LO anomalous dimension. To ensure the robustness of our method we performed separate fits, and we checked, for each ansatz, the fitted value of $\gamma^{(0)}$ was the correct one within the available precision. First of all a roundoff error has to be assigned to $F(\ell)$, which takes into account the uncertainties coming from the numerical computation itself. Following [37], we choose as an estimate for this error, in the case that the computation has been carried out in double precision,

$$\delta F(\ell) \equiv \epsilon(\ell)|F(\ell)|\,, \tag{F.0.1}$$

$$\epsilon(\ell) = \left(\frac{\ell}{2}\right)^3 \times 10^{-14}. \tag{F.0.2}$$

As showed in Section 7.3 the expected behaviour of $F(\ell)$ leads to the consideration of an asymptotic expansion of the form

$$F(\ell) = \alpha_0 + \sum_{k=1}^{n} \frac{1}{\ell^k}(\alpha_k + \beta_k \log \ell) + R_n(\ell)\,, \tag{F.0.3}$$

where the residue $R_n(\ell)$ is expected to decrease faster as $\ell \to \infty$ than any of the terms in the sum. To determine the coefficients (α_k, β_k) we minimise a quadratic form in the residues

$$\chi^2 = (F - f\xi)^T (F - f\xi)\,, \tag{F.0.4}$$

where F and ξ are the $N-$ and $(2n+1)-$column vectors $(F(\ell_1), \ldots, F(\ell))^T$ and $(\alpha_0, \alpha_1, \ldots, \alpha_n, \beta_1, \ldots, \beta_n)^T$, respectively, and f is the $N \times (2n+1)$ matrix

$$f = \begin{pmatrix} 1 & \ell_1^{-1} & \cdots & \ell_1^{-n} & \ell_1^{-1}\log\ell_1 & \cdots & \ell_1^{-n}\log\ell_1 \\ 1 & \ell_2^{-1} & \cdots & \ell_2^{-n} & \ell_2^{-1}\log\ell_2 & \cdots & \ell_2^{-n}\log\ell_2 \\ \vdots & \vdots & \vdots & \vdots & \vdots & \vdots & \vdots \\ 1 & \ell_N^{-1} & \cdots & \ell_N^{-n} & \ell_N^{-1}\log\ell_N & \cdots & \ell_N^{-n}\log\ell_N \end{pmatrix} \tag{F.0.5}$$

Again following [37], we have not introduced a matrix of weights in the definition of χ^2. A necessary condition to minimise χ^2 is

$$f\xi = PF \tag{F.0.6}$$

where we have assumed that the columns of f are linearly independent vectors (assuming $2n+1 \ll N$), and P is the projector onto the subspace of $\mathbb{R}^N$ generated by them. Eq. (F.0.6) can be solved using the singular value decomposition of f, which has the form of

$$f = USV^T \tag{F.0.7}$$

where U is an $N \times (2n+1)$ matrix such that

$$U^TU = \mathbf{1} \quad , \quad UU^T = P \tag{F.0.8}$$

S is diagonal, and $(2n+1) \times (2n+1)$ matrix V is orthonormal. With this decomposition one has

$$\xi = VS^{-1}U^TF\,. \tag{F.0.9}$$

Finally, the uncertainty in the result for ξ_k can be modelled using error propagation as

$$\delta\xi_k^2 = \sum_{l=1}^{N} (VS^{-1}U^T)_{kl}^2 (\delta F)_l^2\,, \tag{F.0.10}$$

where $(\delta F)_k \equiv \delta F(\ell_k)$.
As a remark on the above method regarding practical applications, it has to be pointed out that the choice of Eq. (F.0.4) for the quadratic form χ^2 implies, in particular, that small values of ℓ might be given excessive weight. This problem has been dealt with by considering a range $[\ell_{min}, \ell_{max}]$ with changing ℓ_{min}. For this work the better convergence in results for (α_k, β_k) was given by $\ell_{min} = 16$ and $\ell_{max} = 46$. The estimation of systematic uncertainty of the fitting procedure has be performed using the proposal by the authors of [37]. We considered two independent fits at order n and $n+1$, i.e. extending the Ansatz in Eq. (F.0.3) by terms $1/\ell^{n+1}$ and $\log \ell/\ell^{n+1}$ with coefficients α_{n+1} and β_{n+1} respectively. The systematic uncertainty of the finite part $r_0 = \alpha_0$ is defined as the difference of the value of the parameter α_0 extracted by the two different fits. In the present work we have used $n = 2$ in the fit Ansatz for the $\mathcal{O}$(a)-improved data, and $n = 3$ for unimproved ones.

α	s	$(r_0)^+_{23}(c_{sw}=0)$	$(r_0)^-_{23}(c_{sw}=0)$
0	1	$\begin{pmatrix} -0.2973(1) & 0.12889(6) \\ 0.02613(1) & -0.20350(10) \end{pmatrix}$	$\begin{pmatrix} -0.3055(1) & 0.008223(4) \\ -0.02778(1) & -0.19359(9) \end{pmatrix}$
	2	$\begin{pmatrix} -0.3027(1) & 0.13105(6) \\ 0.02322(1) & -0.20234(9) \end{pmatrix}$	$\begin{pmatrix} -0.3212(2) & 0.03063(1) \\ -0.03590(2) & -0.18199(8) \end{pmatrix}$
	3	$\begin{pmatrix} -0.3172(1) & 0.13685(7) \\ 0.03615(2) & -0.20751(10) \end{pmatrix}$	$\begin{pmatrix} -0.3252(2) & 0.03643(2) \\ -0.02962(1) & -0.19096(9) \end{pmatrix}$
	4	$\begin{pmatrix} -0.2991(1) & 0.11812(6) \\ 0.03093(1) & -0.17471(8) \end{pmatrix}$	$\begin{pmatrix} -0.3104(1) & 0.03794(2) \\ -0.03310(2) & -0.16164(8) \end{pmatrix}$
	5	$\begin{pmatrix} -0.3045(1) & 0.12028(6) \\ 0.02802(1) & -0.17355(8) \end{pmatrix}$	$\begin{pmatrix} -0.3261(2) & 0.06035(3) \\ -0.04123(2) & -0.15004(7) \end{pmatrix}$
	6	$\begin{pmatrix} -0.3190(2) & 0.12608(6) \\ 0.04095(2) & -0.17872(8) \end{pmatrix}$	$\begin{pmatrix} -0.3302(2) & 0.06615(3) \\ -0.03494(2) & -0.15901(7) \end{pmatrix}$
3/2	1	$\begin{pmatrix} -0.3100(1) & 0.12889(6) \\ 0.02613(1) & -0.2161(1) \end{pmatrix}$	$\begin{pmatrix} -0.3181(2) & 0.008223(4) \\ -0.02778(1) & -0.20623(10) \end{pmatrix}$
	2	$\begin{pmatrix} -0.3154(1) & 0.13105(6) \\ 0.02322(1) & -0.2150(1) \end{pmatrix}$	$\begin{pmatrix} -0.3338(2) & 0.03063(1) \\ -0.03590(2) & -0.19462(9) \end{pmatrix}$
	3	$\begin{pmatrix} -0.3299(2) & 0.13685(7) \\ 0.03615(2) & -0.2201(1) \end{pmatrix}$	$\begin{pmatrix} -0.3379(2) & 0.03643(2) \\ -0.02962(1) & -0.20360(9) \end{pmatrix}$
	4	$\begin{pmatrix} -0.3118(1) & 0.11812(6) \\ 0.03093(1) & -0.18734(9) \end{pmatrix}$	$\begin{pmatrix} -0.3231(2) & 0.03794(2) \\ -0.03310(2) & -0.17428(8) \end{pmatrix}$
	5	$\begin{pmatrix} -0.3172(1) & 0.12028(6) \\ 0.02802(1) & -0.18618(9) \end{pmatrix}$	$\begin{pmatrix} -0.3387(2) & 0.06035(3) \\ -0.04123(2) & -0.16267(8) \end{pmatrix}$
	6	$\begin{pmatrix} -0.3317(2) & 0.12608(6) \\ 0.04095(2) & -0.19135(9) \end{pmatrix}$	$\begin{pmatrix} -0.3428(2) & 0.06615(3) \\ -0.03494(2) & -0.17165(8) \end{pmatrix}$
1	1	$\begin{pmatrix} -0.3057(1) & 0.12889(6) \\ 0.02613(1) & -0.21192(10) \end{pmatrix}$	$\begin{pmatrix} -0.3139(1) & 0.008223(4) \\ -0.02778(1) & -0.20202(9) \end{pmatrix}$
	2	$\begin{pmatrix} -0.3111(1) & 0.13105(6) \\ 0.02322(1) & -0.21076(10) \end{pmatrix}$	$\begin{pmatrix} -0.3296(2) & 0.03063(1) \\ -0.03590(2) & -0.19041(9) \end{pmatrix}$
	3	$\begin{pmatrix} -0.3257(2) & 0.13685(7) \\ 0.03615(2) & -0.2159(1) \end{pmatrix}$	$\begin{pmatrix} -0.3336(2) & 0.03643(2) \\ -0.02962(1) & -0.19938(9) \end{pmatrix}$
	4	$\begin{pmatrix} -0.3075(1) & 0.11812(6) \\ 0.03093(1) & -0.18313(9) \end{pmatrix}$	$\begin{pmatrix} -0.3188(2) & 0.03794(2) \\ -0.03310(2) & -0.17007(8) \end{pmatrix}$
	5	$\begin{pmatrix} -0.3129(1) & 0.12028(6) \\ 0.02802(1) & -0.18197(9) \end{pmatrix}$	$\begin{pmatrix} -0.3345(2) & 0.06035(3) \\ -0.04123(2) & -0.15846(7) \end{pmatrix}$
	6	$\begin{pmatrix} -0.3275(2) & 0.12608(6) \\ 0.04095(2) & -0.18714(9) \end{pmatrix}$	$\begin{pmatrix} -0.3386(2) & 0.06615(3) \\ -0.03494(2) & -0.16744(8) \end{pmatrix}$

TABLE F.1: Numerical results of the 1-loop finite parts for operators VA-AV,PS-SP in the 18 SF renormalisation schemes under investigation defined by the source s and the parameter α as in Eq. (8.3.23).

α	s	$(r_0)^{+}_{23}(c_{sw}=1)$	$(r_0)^{-}_{23}(c_{sw}=1)$
0	1	$\begin{pmatrix} -0.22165(6) & 0.21392(6) \\ 0.026133(6) & -0.25536(2) \end{pmatrix}$	$\begin{pmatrix} -0.22981(8) & -0.0767(1) \\ -0.027786(8) & -0.24544(3) \end{pmatrix}$
	2	$\begin{pmatrix} -0.22703(5) & 0.21608(6) \\ 0.02324(1) & -0.25420(2) \end{pmatrix}$	$\begin{pmatrix} -0.24545(4) & -0.05439(7) \\ -0.035896(8) & -0.233856(10) \end{pmatrix}$
	3	$\begin{pmatrix} -0.24151(2) & 0.22187(7) \\ 0.03613(2) & -0.25936(3) \end{pmatrix}$	$\begin{pmatrix} -0.24950(3) & -0.04859(6) \\ -0.029622(1) & -0.24282(2) \end{pmatrix}$
	4	$\begin{pmatrix} -0.22344(6) & 0.20317(4) \\ 0.030919(6) & -0.22664(5) \end{pmatrix}$	$\begin{pmatrix} -0.23475(7) & -0.04710(4) \\ -0.033097(6) & -0.21357(5) \end{pmatrix}$
	5	$\begin{pmatrix} -0.22882(4) & 0.20532(5) \\ 0.0280232(1) & -0.22548(5) \end{pmatrix}$	$\begin{pmatrix} -0.25039(3) & -0.02475(2) \\ -0.04121(2) & -0.20199(7) \end{pmatrix}$
	6	$\begin{pmatrix} -0.24330(1) & 0.21111(6) \\ 0.04092(3) & -0.23064(4) \end{pmatrix}$	$\begin{pmatrix} -0.25444(2) & -0.01896(3) \\ -0.03493(1) & -0.21095(6) \end{pmatrix}$
3/2	1	$\begin{pmatrix} -0.23423(2) & 0.21392(6) \\ 0.026133(6) & -0.26795(7) \end{pmatrix}$	$\begin{pmatrix} -0.24239(3) & -0.0767(1) \\ -0.027786(8) & -0.25803(8) \end{pmatrix}$
	2	$\begin{pmatrix} -0.239614(2) & 0.21608(6) \\ 0.02324(1) & -0.26679(7) \end{pmatrix}$	$\begin{pmatrix} -0.258036(7) & -0.05439(7) \\ -0.035896(8) & -0.24644(6) \end{pmatrix}$
	3	$\begin{pmatrix} -0.25409(3) & 0.22187(7) \\ 0.03613(2) & -0.27195(8) \end{pmatrix}$	$\begin{pmatrix} -0.26209(1) & -0.04859(6) \\ -0.029622(1) & -0.25541(7) \end{pmatrix}$
	4	$\begin{pmatrix} -0.23602(1) & 0.20317(4) \\ 0.030919(6) & -0.239229(3) \end{pmatrix}$	$\begin{pmatrix} -0.24733(2) & -0.04710(4) \\ -0.033097(6) & -0.226161(3) \end{pmatrix}$
	5	$\begin{pmatrix} -0.241406(4) & 0.20532(5) \\ 0.0280232(1) & -0.238070(6) \end{pmatrix}$	$\begin{pmatrix} -0.26298(2) & -0.02475(2) \\ -0.04121(2) & -0.21458(3) \end{pmatrix}$
	6	$\begin{pmatrix} -0.25589(3) & 0.21111(6) \\ 0.04092(3) & -0.243229(6) \end{pmatrix}$	$\begin{pmatrix} -0.26703(3) & -0.01896(3) \\ -0.03493(1) & -0.22354(1) \end{pmatrix}$
1	1	$\begin{pmatrix} -0.23004(3) & 0.21392(6) \\ 0.026133(6) & -0.26375(5) \end{pmatrix}$	$\begin{pmatrix} -0.23820(5) & -0.0767(1) \\ -0.027786(8) & -0.25383(6) \end{pmatrix}$
	2	$\begin{pmatrix} -0.23542(1) & 0.21608(6) \\ 0.02324(1) & -0.26259(5) \end{pmatrix}$	$\begin{pmatrix} -0.253840(9) & -0.05439(7) \\ -0.035896(8) & -0.24225(4) \end{pmatrix}$
	3	$\begin{pmatrix} -0.24990(2) & 0.22187(7) \\ 0.03613(2) & -0.26775(6) \end{pmatrix}$	$\begin{pmatrix} -0.2578952(9) & -0.04859(6) \\ -0.029622(1) & -0.25121(6) \end{pmatrix}$
	4	$\begin{pmatrix} -0.23183(3) & 0.20317(4) \\ 0.030919(6) & -0.23503(2) \end{pmatrix}$	$\begin{pmatrix} -0.24314(4) & -0.04710(4) \\ -0.033097(6) & -0.22197(2) \end{pmatrix}$
	5	$\begin{pmatrix} -0.23721(1) & 0.20532(5) \\ 0.0280232(1) & -0.23387(2) \end{pmatrix}$	$\begin{pmatrix} -0.258780(6) & -0.02475(2) \\ -0.04121(2) & -0.21038(4) \end{pmatrix}$
	6	$\begin{pmatrix} -0.25169(2) & 0.21111(6) \\ 0.04092(3) & -0.23903(1) \end{pmatrix}$	$\begin{pmatrix} -0.26283(1) & -0.01896(3) \\ -0.03493(1) & -0.21934(3) \end{pmatrix}$

TABLE F.2: Numerical results of the 1-loop finite parts for operators VA-AV,PS-SP in the 18 SF renormalisation schemes under investigation defined by the source s and the parameter α as in Eq. (8.3.23). These results have been computed including the clover term in the fermonic action.

α	s	$(r_0)^+_{45}(c_{sw}=0)$	$(r_0)^-_{45}(c_{sw}=0)$
0	1	$\begin{pmatrix} -0.20786(10) & -0.008176(4) \\ -0.16835(8) & -0.3844(2) \end{pmatrix}$	$\begin{pmatrix} -0.18729(9) & 0.012475(6) \\ 0.3886(2) & -0.2278(1) \end{pmatrix}$
	2	$\begin{pmatrix} -0.20612(10) & -0.008902(4) \\ -0.15539(8) & -0.3898(2) \end{pmatrix}$	$\begin{pmatrix} -0.19077(9) & 0.010444(5) \\ 0.3826(2) & -0.2313(1) \end{pmatrix}$
	3	$\begin{pmatrix} -0.20882(10) & -0.007780(4) \\ -0.15920(8) & -0.3882(2) \end{pmatrix}$	$\begin{pmatrix} -0.18302(9) & 0.014967(7) \\ 0.3788(2) & -0.2335(1) \end{pmatrix}$
	4	$\begin{pmatrix} -0.18240(8) & -0.009086(4) \\ -0.11374(6) & -0.3863(2) \end{pmatrix}$	$\begin{pmatrix} -0.15486(7) & 0.014097(7) \\ 0.3496(2) & -0.2298(1) \end{pmatrix}$
	5	$\begin{pmatrix} -0.18066(8) & -0.009811(5) \\ -0.10078(5) & -0.3917(2) \end{pmatrix}$	$\begin{pmatrix} -0.15835(7) & 0.012065(6) \\ 0.3436(2) & -0.2333(1) \end{pmatrix}$
	6	$\begin{pmatrix} -0.18335(9) & -0.008689(4) \\ -0.10459(5) & -0.3901(2) \end{pmatrix}$	$\begin{pmatrix} -0.15059(7) & 0.016589(8) \\ 0.3398(2) & -0.2355(1) \end{pmatrix}$
3/2	1	$\begin{pmatrix} -0.2205(1) & -0.008176(4) \\ -0.16835(8) & -0.3970(2) \end{pmatrix}$	$\begin{pmatrix} -0.19992(9) & 0.012475(6) \\ 0.3886(2) & -0.2404(1) \end{pmatrix}$
	2	$\begin{pmatrix} -0.2188(1) & -0.008902(4) \\ -0.15539(8) & -0.4024(2) \end{pmatrix}$	$\begin{pmatrix} -0.20341(10) & 0.010444(5) \\ 0.3826(2) & -0.2439(1) \end{pmatrix}$
	3	$\begin{pmatrix} -0.2214(1) & -0.007780(4) \\ -0.15920(8) & -0.4008(2) \end{pmatrix}$	$\begin{pmatrix} -0.19565(9) & 0.014967(7) \\ 0.3788(2) & -0.2462(1) \end{pmatrix}$
	4	$\begin{pmatrix} -0.19503(9) & -0.009086(4) \\ -0.11374(6) & -0.3989(2) \end{pmatrix}$	$\begin{pmatrix} -0.16750(8) & 0.014097(7) \\ 0.3496(2) & -0.2424(1) \end{pmatrix}$
	5	$\begin{pmatrix} -0.19329(9) & -0.009811(5) \\ -0.10078(5) & -0.4043(2) \end{pmatrix}$	$\begin{pmatrix} -0.17098(8) & 0.012065(6) \\ 0.3436(2) & -0.2459(1) \end{pmatrix}$
	6	$\begin{pmatrix} -0.19599(9) & -0.008689(4) \\ -0.10459(5) & -0.4028(2) \end{pmatrix}$	$\begin{pmatrix} -0.16322(8) & 0.016589(8) \\ 0.3398(2) & -0.2481(1) \end{pmatrix}$
1	1	$\begin{pmatrix} -0.2163(1) & -0.008176(4) \\ -0.16835(8) & -0.3928(2) \end{pmatrix}$	$\begin{pmatrix} -0.19571(9) & 0.012475(6) \\ 0.3886(2) & -0.2362(1) \end{pmatrix}$
	2	$\begin{pmatrix} -0.2145(1) & -0.008902(4) \\ -0.15539(8) & -0.3982(2) \end{pmatrix}$	$\begin{pmatrix} -0.19920(9) & 0.010444(5) \\ 0.3826(2) & -0.2397(1) \end{pmatrix}$
	3	$\begin{pmatrix} -0.2172(1) & -0.007780(4) \\ -0.15920(8) & -0.3966(2) \end{pmatrix}$	$\begin{pmatrix} -0.19144(9) & 0.014967(7) \\ 0.3788(2) & -0.2419(1) \end{pmatrix}$
	4	$\begin{pmatrix} -0.19082(9) & -0.009086(4) \\ -0.11374(6) & -0.3947(2) \end{pmatrix}$	$\begin{pmatrix} -0.16329(8) & 0.014097(7) \\ 0.3496(2) & -0.2382(1) \end{pmatrix}$
	5	$\begin{pmatrix} -0.18908(9) & -0.009811(5) \\ -0.10078(5) & -0.4001(2) \end{pmatrix}$	$\begin{pmatrix} -0.16677(8) & 0.012065(6) \\ 0.3436(2) & -0.2417(1) \end{pmatrix}$
	6	$\begin{pmatrix} -0.19177(9) & -0.008689(4) \\ -0.10459(5) & -0.3985(2) \end{pmatrix}$	$\begin{pmatrix} -0.15901(7) & 0.016589(8) \\ 0.3398(2) & -0.2439(1) \end{pmatrix}$

TABLE F.3: Numerical results of the 1-loop finite parts for operators PS+SP,T$\tilde{\text{T}}$ in the 18 SF renormalisation schemes under investigation defined by the source s and the parameter α as in Eq. (8.3.23).

α	s	$(r_0)^+_{45}(c_{sw}=1)$	$(r_0)^-_{45}(c_{sw}=1)$
0	1	$\begin{pmatrix} -0.21719(1) & -0.0069948(4) \\ -0.4517(3) & -0.24249(6) \end{pmatrix}$	$\begin{pmatrix} -0.28168(3) & 0.006568(2) \\ 0.4451(2) & -0.17105(8) \end{pmatrix}$
	2	$\begin{pmatrix} -0.215453(7) & -0.007719(1) \\ -0.4388(2) & -0.24787(4) \end{pmatrix}$	$\begin{pmatrix} -0.28516(4) & 0.004541(6) \\ 0.4392(2) & -0.17453(6) \end{pmatrix}$
	3	$\begin{pmatrix} -0.21814(1) & -0.0065985(6) \\ -0.4426(2) & -0.24629(4) \end{pmatrix}$	$\begin{pmatrix} -0.27742(2) & 0.009054(4) \\ 0.4354(2) & -0.17674(6) \end{pmatrix}$
	4	$\begin{pmatrix} -0.19179(6) & -0.007902(2) \\ -0.3972(1) & -0.24444(5) \end{pmatrix}$	$\begin{pmatrix} -0.24934(5) & 0.008185(2) \\ 0.4062(1) & -0.17299(7) \end{pmatrix}$
	5	$\begin{pmatrix} -0.19006(6) & -0.008626(4) \\ -0.38433(7) & -0.24982(3) \end{pmatrix}$	$\begin{pmatrix} -0.25281(4) & 0.006158(2) \\ 0.40026(9) & -0.17647(6) \end{pmatrix}$
	6	$\begin{pmatrix} -0.19275(6) & -0.007506(2) \\ -0.38813(7) & -0.24823(3) \end{pmatrix}$	$\begin{pmatrix} -0.24507(6) & 0.010672(8) \\ 0.39646(9) & -0.17869(6) \end{pmatrix}$
3/2	1	$\begin{pmatrix} -0.22978(6) & -0.0069948(4) \\ -0.4517(3) & -0.255079(8) \end{pmatrix}$	$\begin{pmatrix} -0.29427(8) & 0.006568(2) \\ 0.4451(2) & -0.18363(3) \end{pmatrix}$
	2	$\begin{pmatrix} -0.22804(6) & -0.007719(1) \\ -0.4388(2) & -0.260460(9) \end{pmatrix}$	$\begin{pmatrix} -0.29775(9) & 0.004541(6) \\ 0.4392(2) & -0.18711(1) \end{pmatrix}$
	3	$\begin{pmatrix} -0.23073(6) & -0.0065985(6) \\ -0.4426(2) & -0.258875(8) \end{pmatrix}$	$\begin{pmatrix} -0.29001(7) & 0.009054(4) \\ 0.4354(2) & -0.18933(1) \end{pmatrix}$
	4	$\begin{pmatrix} -0.204380(9) & -0.007902(2) \\ -0.3972(1) & -0.257024(3) \end{pmatrix}$	$\begin{pmatrix} -0.2619224(2) & 0.008185(2) \\ 0.4062(1) & -0.18558(3) \end{pmatrix}$
	5	$\begin{pmatrix} -0.20264(1) & -0.008626(4) \\ -0.38433(7) & -0.26241(1) \end{pmatrix}$	$\begin{pmatrix} -0.265398(7) & 0.006158(2) \\ 0.40026(9) & -0.189057(9) \end{pmatrix}$
	6	$\begin{pmatrix} -0.205331(9) & -0.007506(2) \\ -0.38813(7) & -0.26082(1) \end{pmatrix}$	$\begin{pmatrix} -0.257660(10) & 0.010672(8) \\ 0.39646(9) & -0.191276(8) \end{pmatrix}$
1	1	$\begin{pmatrix} -0.22558(4) & -0.0069948(4) \\ -0.4517(3) & -0.25088(2) \end{pmatrix}$	$\begin{pmatrix} -0.29007(7) & 0.006568(2) \\ 0.4451(2) & -0.17944(5) \end{pmatrix}$
	2	$\begin{pmatrix} -0.22384(4) & -0.007719(1) \\ -0.4388(2) & -0.256264(6) \end{pmatrix}$	$\begin{pmatrix} -0.29355(7) & 0.004541(6) \\ 0.4392(2) & -0.18292(3) \end{pmatrix}$
	3	$\begin{pmatrix} -0.22653(4) & -0.0065985(6) \\ -0.4426(2) & -0.254679(7) \end{pmatrix}$	$\begin{pmatrix} -0.28581(6) & 0.009054(4) \\ 0.4354(2) & -0.18514(3) \end{pmatrix}$
	4	$\begin{pmatrix} -0.20018(2) & -0.007902(2) \\ -0.3972(1) & -0.25283(2) \end{pmatrix}$	$\begin{pmatrix} -0.25773(2) & 0.008185(2) \\ 0.4062(1) & -0.18138(4) \end{pmatrix}$
	5	$\begin{pmatrix} -0.19845(3) & -0.008626(4) \\ -0.38433(7) & -0.258210(1) \end{pmatrix}$	$\begin{pmatrix} -0.261202(9) & 0.006158(2) \\ 0.40026(9) & -0.18486(2) \end{pmatrix}$
	6	$\begin{pmatrix} -0.20114(2) & -0.007506(2) \\ -0.38813(7) & -0.256624(2) \end{pmatrix}$	$\begin{pmatrix} -0.25346(3) & 0.010672(8) \\ 0.39646(9) & -0.18708(2) \end{pmatrix}$

TABLE F.4: Numerical results of the 1-loop finite parts for operators PS+SP,TT̃ in the 18 SF renormalisation schemes under investigation defined by the source s and the parameter α as in Eq. (8.3.23). These results have been computed including the clover term in the fermonic action.

G NLO anomalous dimension matrices in SF schemes

α	s	$\gamma^{(1)+}_{23}$
0	1	$\begin{pmatrix} 0.001519(10) + N_f[-0.000057850(2)] & 0.00983(2) + N_f[-0.00034710(1)] \\ 0.006188(1) + N_f[-0.000080203] & -0.006776(8) + N_f[-0.00001842(2)] \end{pmatrix}$
	2	$\begin{pmatrix} 0.001080(8) + N_f[-0.000057850(2)] & 0.00936(2) + N_f[-0.00034710(1)] \\ 0.005504(3) + N_f[-0.000080203] & -0.006855(7) + N_f[-0.00001842(2)] \end{pmatrix}$
	3	$\begin{pmatrix} -0.001673(4) + N_f[-0.000057850(2)] & 0.00870(2) + N_f[-0.00034710(1)] \\ 0.008552(4) + N_f[-0.000080203] & -0.00651(1) + N_f[-0.00001842(2)] \end{pmatrix}$
	4	$\begin{pmatrix} 0.000936(10) + N_f[-0.000057850(2)] & 0.00743(2) + N_f[-0.00034710(1)] \\ 0.007320(1) + N_f[-0.000080203] & -0.00290(2) + N_f[-0.00001842(2)] \end{pmatrix}$
	5	$\begin{pmatrix} 0.000497(6) + N_f[-0.000057850(2)] & 0.00695(2) + N_f[-0.00034710(1)] \\ 0.0066351(1) + N_f[-0.000080203] & -0.00297(2) + N_f[-0.00001842(2)] \end{pmatrix}$
	6	$\begin{pmatrix} -0.002256(4) + N_f[-0.000057850(2)] & 0.00629(2) + N_f[-0.00034710(1)] \\ 0.009684(7) + N_f[-0.000080203] & -0.00263(2) + N_f[-0.00001842(2)] \end{pmatrix}$
3/2	1	$\begin{pmatrix} -0.000022(3) + N_f[-0.000057850(2)] & 0.00983(2) + N_f[-0.00034710(1)] \\ 0.006188(1) + N_f[-0.000080203] & -0.00832(2) + N_f[-0.00001842(2)] \end{pmatrix}$
	2	$\begin{pmatrix} -0.000461(1) + N_f[-0.000057850(2)] & 0.00936(2) + N_f[-0.00034710(1)] \\ 0.005504(3) + N_f[-0.000080203] & -0.00840(2) + N_f[-0.00001842(2)] \end{pmatrix}$
	3	$\begin{pmatrix} -0.003214(6) + N_f[-0.000057850(2)] & 0.00870(3) + N_f[-0.00034710(1)] \\ 0.008552(4) + N_f[-0.000080203] & -0.00805(3) + N_f[-0.00001842(2)] \end{pmatrix}$
	4	$\begin{pmatrix} -0.000605(3) + N_f[-0.000057850(2)] & 0.00743(1) + N_f[-0.00034710(1)] \\ 0.007320(1) + N_f[-0.000080203] & -0.004438(2) + N_f[-0.00001842(2)] \end{pmatrix}$
	5	$\begin{pmatrix} -0.0010440(6) + N_f[-0.000057850(2)] & 0.00695(1) + N_f[-0.00034710(1)] \\ 0.0066351(1) + N_f[-0.000080203] & -0.004516(2) + N_f[-0.00001842(2)] \end{pmatrix}$
	6	$\begin{pmatrix} -0.003797(7) + N_f[-0.000057850(2)] & 0.00629(2) + N_f[-0.00034710(1)] \\ 0.009684(7) + N_f[-0.000080203] & -0.004167(4) + N_f[-0.00001842(2)] \end{pmatrix}$
1	1	$\begin{pmatrix} 0.000492(5) + N_f[-0.000057850(2)] & 0.00983(2) + N_f[-0.00034710(1)] \\ 0.006188(1) + N_f[-0.000080203] & -0.00780(2) + N_f[-0.00001842(2)] \end{pmatrix}$
	2	$\begin{pmatrix} 0.000053(3) + N_f[-0.000057850(2)] & 0.00936(2) + N_f[-0.00034710(1)] \\ 0.005504(3) + N_f[-0.000080203] & -0.00788(2) + N_f[-0.00001842(2)] \end{pmatrix}$
	3	$\begin{pmatrix} -0.002700(4) + N_f[-0.000057850(2)] & 0.00870(2) + N_f[-0.00034710(1)] \\ 0.008552(4) + N_f[-0.000080203] & -0.00753(2) + N_f[-0.00001842(2)] \end{pmatrix}$
	4	$\begin{pmatrix} -0.000092(5) + N_f[-0.000057850(2)] & 0.00743(1) + N_f[-0.00034710(1)] \\ 0.007320(1) + N_f[-0.000080203] & -0.003924(7) + N_f[-0.00001842(2)] \end{pmatrix}$
	5	$\begin{pmatrix} -0.000530(2) + N_f[-0.000057850(2)] & 0.00695(1) + N_f[-0.00034710(1)] \\ 0.0066351(1) + N_f[-0.000080203] & -0.004002(7) + N_f[-0.00001842(2)] \end{pmatrix}$
	6	$\begin{pmatrix} -0.003283(5) + N_f[-0.000057850(2)] & 0.00629(2) + N_f[-0.00034710(1)] \\ 0.009684(7) + N_f[-0.000080203] & -0.003654(6) + N_f[-0.00001842(2)] \end{pmatrix}$

α	s	$\gamma^{(1)}{}^{-}_{23}$
0	1	$\begin{pmatrix} 0.00051(1)+N_f[-0.000118203(2)] & -0.00803(4)+N_f[0.00070922(1)] \\ -0.006546(2)+N_f[0.000063796] & -0.00660(1)+N_f[0.00056285(2)] \end{pmatrix}$
	2	$\begin{pmatrix} -0.002017(7)+N_f[-0.000118203(2)] & -0.00577(2)+N_f[0.00070922(1)] \\ -0.008464(2)+N_f[0.000063796] & -0.004564(4)+N_f[0.00056285(2)] \end{pmatrix}$
	3	$\begin{pmatrix} -0.002036(5)+N_f[-0.000118203(2)] & -0.00609(2)+N_f[0.00070922(1)] \\ -0.0069803(3)+N_f[0.000063796] & -0.006138(8)+N_f[0.00056285(2)] \end{pmatrix}$
	4	$\begin{pmatrix} -0.00049(1)+N_f[-0.000118203(2)] & -0.00498(2)+N_f[0.00070922(1)] \\ -0.007802(1)+N_f[0.000063796] & -0.00229(2)+N_f[0.00056285(2)] \end{pmatrix}$
	5	$\begin{pmatrix} -0.003025(6)+N_f[-0.000118203(2)] & -0.00272(1)+N_f[0.00070922(1)] \\ -0.009719(5)+N_f[0.000063796] & -0.00026(3)+N_f[0.00056285(2)] \end{pmatrix}$
	6	$\begin{pmatrix} -0.003045(4)+N_f[-0.000118203(2)] & -0.00305(1)+N_f[0.00070922(1)] \\ -0.008236(3)+N_f[0.000063796] & -0.00183(2)+N_f[0.00056285(2)] \end{pmatrix}$
3/2	1	$\begin{pmatrix} -0.001026(6)+N_f[-0.000118203(2)] & -0.00803(4)+N_f[0.00070922(1)] \\ -0.006546(2)+N_f[0.000063796] & -0.00814(3)+N_f[0.00056285(2)] \end{pmatrix}$
	2	$\begin{pmatrix} -0.003558(2)+N_f[-0.000118203(2)] & -0.00577(2)+N_f[0.00070922(1)] \\ -0.008464(2)+N_f[0.000063796] & -0.00611(2)+N_f[0.00056285(2)] \end{pmatrix}$
	3	$\begin{pmatrix} -0.003577(2)+N_f[-0.000118203(2)] & -0.00609(2)+N_f[0.00070922(1)] \\ -0.0069803(3)+N_f[0.000063796] & -0.00768(2)+N_f[0.00056285(2)] \end{pmatrix}$
	4	$\begin{pmatrix} -0.002034(3)+N_f[-0.000118203(2)] & -0.00498(1)+N_f[0.00070922(1)] \\ -0.007802(1)+N_f[0.000063796] & -0.003835(2)+N_f[0.00056285(2)] \end{pmatrix}$
	5	$\begin{pmatrix} -0.004566(5)+N_f[-0.000118203(2)] & -0.002722(8)+N_f[0.00070922(1)] \\ -0.009719(5)+N_f[0.000063796] & -0.00180(1)+N_f[0.00056285(2)] \end{pmatrix}$
	6	$\begin{pmatrix} -0.004586(5)+N_f[-0.000118203(2)] & -0.00305(1)+N_f[0.00070922(1)] \\ -0.008236(3)+N_f[0.000063796] & -0.003374(6)+N_f[0.00056285(2)] \end{pmatrix}$
1	1	$\begin{pmatrix} -0.000512(8)+N_f[-0.000118203(2)] & -0.00803(4)+N_f[0.00070922(1)] \\ -0.006546(2)+N_f[0.000063796] & -0.00763(2)+N_f[0.00056285(2)] \end{pmatrix}$
	2	$\begin{pmatrix} -0.003044(2)+N_f[-0.000118203(2)] & -0.00577(2)+N_f[0.00070922(1)] \\ -0.008464(2)+N_f[0.000063796] & -0.00559(1)+N_f[0.00056285(2)] \end{pmatrix}$
	3	$\begin{pmatrix} -0.0030635(3)+N_f[-0.000118203(2)] & -0.00609(2)+N_f[0.00070922(1)] \\ -0.0069803(3)+N_f[0.000063796] & -0.00717(2)+N_f[0.00056285(2)] \end{pmatrix}$
	4	$\begin{pmatrix} -0.001521(6)+N_f[-0.000118203(2)] & -0.00498(1)+N_f[0.00070922(1)] \\ -0.007802(1)+N_f[0.000063796] & -0.003321(7)+N_f[0.00056285(2)] \end{pmatrix}$
	5	$\begin{pmatrix} -0.004052(3)+N_f[-0.000118203(2)] & -0.002722(8)+N_f[0.00070922(1)] \\ -0.009719(5)+N_f[0.000063796] & -0.00129(2)+N_f[0.00056285(2)] \end{pmatrix}$
	6	$\begin{pmatrix} -0.004072(3)+N_f[-0.000118203(2)] & -0.00305(1)+N_f[0.00070922(1)] \\ -0.008236(3)+N_f[0.000063796] & -0.00286(1)+N_f[0.00056285(2)] \end{pmatrix}$

α	s	$\gamma^{(1)^+}_{45}$
0	1	$\begin{pmatrix} 0.002303(3) + N_f[0.00012884(1)] & -0.00169802(7) + N_f[0.0000026054(2)] \\ 0.00172(8) + N_f[0.00179861(4)] & 0.00081(2) + N_f[-0.00035752(1)] \end{pmatrix}$
	2	$\begin{pmatrix} 0.002685(2) + N_f[0.00012884(1)] & -0.0018770(3) + N_f[0.0000026054(2)] \\ 0.00336(7) + N_f[0.00179861(4)] & -0.00001(1) + N_f[-0.00035752(1)] \end{pmatrix}$
	3	$\begin{pmatrix} 0.002077(4) + N_f[0.00012884(1)] & -0.0015930(3) + N_f[0.0000026054(2)] \\ 0.00232(7) + N_f[0.00179861(4)] & 0.00046(1) + N_f[-0.00035752(1)] \end{pmatrix}$
	4	$\begin{pmatrix} 0.00558(2) + N_f[0.00012884(1)] & -0.0019027(6) + N_f[0.0000026054(2)] \\ 0.00795(6) + N_f[0.00179861(4)] & 0.00040(1) + N_f[-0.00035752(1)] \end{pmatrix}$
	5	$\begin{pmatrix} 0.00597(2) + N_f[0.00012884(1)] & -0.002082(1) + N_f[0.0000026054(2)] \\ 0.00959(4) + N_f[0.00179861(4)] & -0.00043(1) + N_f[-0.00035752(1)] \end{pmatrix}$
	6	$\begin{pmatrix} 0.00536(1) + N_f[0.00012884(1)] & -0.0017978(6) + N_f[0.0000026054(2)] \\ 0.00856(4) + N_f[0.00179861(4)] & 0.000048(10) + N_f[-0.00035752(1)] \end{pmatrix}$
3/2	1	$\begin{pmatrix} 0.00076(2) + N_f[0.00012884(1)] & -0.00169802(7) + N_f[0.0000026054(2)] \\ 0.00172(8) + N_f[0.00179861(4)] & -0.000727(3) + N_f[-0.00035752(1)] \end{pmatrix}$
	2	$\begin{pmatrix} 0.00114(1) + N_f[0.00012884(1)] & -0.0018770(3) + N_f[0.0000026054(2)] \\ 0.00336(7) + N_f[0.00179861(4)] & -0.001556(3) + N_f[-0.00035752(1)] \end{pmatrix}$
	3	$\begin{pmatrix} 0.00054(2) + N_f[0.00012884(1)] & -0.0015930(3) + N_f[0.0000026054(2)] \\ 0.00232(7) + N_f[0.00179861(4)] & -0.001082(3) + N_f[-0.00035752(1)] \end{pmatrix}$
	4	$\begin{pmatrix} 0.004044(3) + N_f[0.00012884(1)] & -0.0019027(5) + N_f[0.0000026054(2)] \\ 0.00795(3) + N_f[0.00179861(4)] & -0.001138(2) + N_f[-0.00035752(1)] \end{pmatrix}$
	5	$\begin{pmatrix} 0.004426(5) + N_f[0.00012884(1)] & -0.002082(1) + N_f[0.0000026054(2)] \\ 0.00959(2) + N_f[0.00179861(4)] & -0.001966(5) + N_f[-0.00035752(1)] \end{pmatrix}$
	6	$\begin{pmatrix} 0.003817(3) + N_f[0.00012884(1)] & -0.0017978(5) + N_f[0.0000026054(2)] \\ 0.00856(2) + N_f[0.00179861(4)] & -0.001492(5) + N_f[-0.00035752(1)] \end{pmatrix}$
1	1	$\begin{pmatrix} 0.00128(1) + N_f[0.00012884(1)] & -0.00169802(7) + N_f[0.0000026054(2)] \\ 0.00172(8) + N_f[0.00179861(4)] & -0.000214(7) + N_f[-0.00035752(1)] \end{pmatrix}$
	2	$\begin{pmatrix} 0.00166(1) + N_f[0.00012884(1)] & -0.0018770(3) + N_f[0.0000026054(2)] \\ 0.00336(7) + N_f[0.00179861(4)] & -0.001042(3) + N_f[-0.00035752(1)] \end{pmatrix}$
	3	$\begin{pmatrix} 0.00105(1) + N_f[0.00012884(1)] & -0.0015930(3) + N_f[0.0000026054(2)] \\ 0.00232(7) + N_f[0.00179861(4)] & -0.000568(3) + N_f[-0.00035752(1)] \end{pmatrix}$
	4	$\begin{pmatrix} 0.004557(7) + N_f[0.00012884(1)] & -0.0019027(6) + N_f[0.0000026054(2)] \\ 0.00795(4) + N_f[0.00179861(4)] & -0.000624(6) + N_f[-0.00035752(1)] \end{pmatrix}$
	5	$\begin{pmatrix} 0.004940(9) + N_f[0.00012884(1)] & -0.002082(1) + N_f[0.0000026054(2)] \\ 0.00959(3) + N_f[0.00179861(4)] & -0.001453(2) + N_f[-0.00035752(1)] \end{pmatrix}$
	6	$\begin{pmatrix} 0.004331(7) + N_f[0.00012884(1)] & -0.0017978(5) + N_f[0.0000026054(2)] \\ 0.00856(2) + N_f[0.00179861(4)] & -0.000979(1) + N_f[-0.00035752(1)] \end{pmatrix}$

α	s	$\gamma^{(1)}{}^{-}_{45}$
0	1	$\begin{pmatrix} -0.01620(2)+N_f[0.00069509(2)] & 0.001678(1)+N_f[-0.0000064430(8)] \\ 0.00879(7)+N_f[-0.002125401(8)] & 0.00907(1)+N_f[-0.0004158697(7)] \end{pmatrix}$
	2	$\begin{pmatrix} -0.01676(2)+N_f[0.00069509(2)] & 0.001156(2)+N_f[-0.0000064430(8)] \\ 0.00887(6)+N_f[-0.002125401(8)] & 0.008779(9)+N_f[-0.0004158697(7)] \end{pmatrix}$
	3	$\begin{pmatrix} -0.01560(1)+N_f[0.00069509(2)] & 0.002266(2)+N_f[-0.0000064430(8)] \\ 0.00841(6)+N_f[-0.002125401(8)] & 0.008299(9)+N_f[-0.0004158697(7)] \end{pmatrix}$
	4	$\begin{pmatrix} -0.01236(2)+N_f[0.00069509(2)] & 0.001914(1)+N_f[-0.0000064430(8)] \\ 0.00755(4)+N_f[-0.002125401(8)] & 0.00896(1)+N_f[-0.0004158697(7)] \end{pmatrix}$
	5	$\begin{pmatrix} -0.01292(2)+N_f[0.00069509(2)] & 0.0013917(10)+N_f[-0.0000064430(8)] \\ 0.00762(3)+N_f[-0.002125401(8)] & 0.008664(8)+N_f[-0.0004158697(7)] \end{pmatrix}$
	6	$\begin{pmatrix} -0.01176(2)+N_f[0.00069509(2)] & 0.002502(3)+N_f[-0.0000064430(8)] \\ 0.00716(3)+N_f[-0.002125401(8)] & 0.008184(8)+N_f[-0.0004158697(7)] \end{pmatrix}$
3/2	1	$\begin{pmatrix} -0.01774(3)+N_f[0.00069509(2)] & 0.001678(1)+N_f[-0.0000064430(8)] \\ 0.00879(7)+N_f[-0.002125401(8)] & 0.007530(5)+N_f[-0.0004158697(7)] \end{pmatrix}$
	2	$\begin{pmatrix} -0.01830(4)+N_f[0.00069509(2)] & 0.001156(2)+N_f[-0.0000064430(8)] \\ 0.00887(6)+N_f[-0.002125401(8)] & 0.007238(3)+N_f[-0.0004158697(7)] \end{pmatrix}$
	3	$\begin{pmatrix} -0.01714(3)+N_f[0.00069509(2)] & 0.002266(2)+N_f[-0.0000064430(8)] \\ 0.00841(6)+N_f[-0.002125401(8)] & 0.006758(3)+N_f[-0.0004158697(7)] \end{pmatrix}$
	4	$\begin{pmatrix} -0.013901(2)+N_f[0.00069509(2)] & 0.0019137(8)+N_f[-0.0000064430(8)] \\ 0.00755(3)+N_f[-0.002125401(8)] & 0.007415(4)+N_f[-0.0004158697(7)] \end{pmatrix}$
	5	$\begin{pmatrix} -0.014461(4)+N_f[0.00069509(2)] & 0.0013917(6)+N_f[-0.0000064430(8)] \\ 0.00762(2)+N_f[-0.002125401(8)] & 0.007123(2)+N_f[-0.0004158697(7)] \end{pmatrix}$
	6	$\begin{pmatrix} -0.013305(5)+N_f[0.00069509(2)] & 0.002502(2)+N_f[-0.0000064430(8)] \\ 0.00716(2)+N_f[-0.002125401(8)] & 0.006643(2)+N_f[-0.0004158697(7)] \end{pmatrix}$
1	1	$\begin{pmatrix} -0.01722(3)+N_f[0.00069509(2)] & 0.001678(1)+N_f[-0.0000064430(8)] \\ 0.00879(7)+N_f[-0.002125401(8)] & 0.008043(7)+N_f[-0.0004158697(7)] \end{pmatrix}$
	2	$\begin{pmatrix} -0.01778(3)+N_f[0.00069509(2)] & 0.001156(2)+N_f[-0.0000064430(8)] \\ 0.00887(6)+N_f[-0.002125401(8)] & 0.007751(5)+N_f[-0.0004158697(7)] \end{pmatrix}$
	3	$\begin{pmatrix} -0.01663(2)+N_f[0.00069509(2)] & 0.002266(2)+N_f[-0.0000064430(8)] \\ 0.00841(6)+N_f[-0.002125401(8)] & 0.007271(5)+N_f[-0.0004158697(7)] \end{pmatrix}$
	4	$\begin{pmatrix} -0.013388(7)+N_f[0.00069509(2)] & 0.0019137(10)+N_f[-0.0000064430(8)] \\ 0.00755(3)+N_f[-0.002125401(8)] & 0.007928(6)+N_f[-0.0004158697(7)] \end{pmatrix}$
	5	$\begin{pmatrix} -0.013947(4)+N_f[0.00069509(2)] & 0.0013917(6)+N_f[-0.0000064430(8)] \\ 0.00762(3)+N_f[-0.002125401(8)] & 0.007637(4)+N_f[-0.0004158697(7)] \end{pmatrix}$
	6	$\begin{pmatrix} -0.01279(1)+N_f[0.00069509(2)] & 0.002502(2)+N_f[-0.0000064430(8)] \\ 0.00716(3)+N_f[-0.002125401(8)] & 0.007156(4)+N_f[-0.0004158697(7)] \end{pmatrix}$

H Error Propagarion in the SSF recursion

We summarise here the analytical error propagation along the coupling and (non-mixing) operators SSFs. In the actual calculation (in particular the running mass) this procedure has been crosschecked with bootstrap analysis. In the final analysis we opted anyway for the latter since it allow more flexibility, but the following is still valid. The general procedure is the following:

(i) Define L by fixing the value of the renormalised coupling to some number, $u_0 = \bar{g}^2(L)$. Then construct a recursive sequence of couplings such that $u_{k-1} = \sigma(u_k)$ — explicitly

$$\begin{aligned} u_0 &= \bar{g}^2(L)\,, \\ \sigma^{-1}(u_0) &= u_1 = \bar{g}^2(L/2)\,, \\ \sigma^{-1}(u_1) &= u_2 = \bar{g}^2(L/4)\,, \\ &\vdots \\ \sigma^{-1}(u_{n-1}) &= u_n = \bar{g}^2(L/2^n)\,. \end{aligned} \tag{H.0.1}$$

(ii) Construct the sequence $v_k = \sigma_{\rm P}(u_k)v_{k-1}$, with $v_0 = 1$ — explicitly [1]

$$\begin{aligned} v_0 &= 1\,, \\ v_1 &= \sigma_{\rm P}(u_1)\,, \\ v_2 &= \sigma_{\rm P}(u_2)\sigma_{\rm P}(u_1)\,, \\ &\vdots \\ v_n &= \sigma_{\rm P}(u_n)\cdots\sigma_{\rm P}(u_2)\sigma_{\rm P}(u_1)\,. \end{aligned} \tag{H.0.2}$$

(iii) Use the identity

$$\frac{M}{\overline{m}(L)} = \hat{c}(u_n)\, v_n\,, \tag{H.0.3}$$

computing $\hat{c}(u_n)$ in perturbation theory. To that purpose, u_n has to be small enough so that the perturbative expansion employed for τ and β can be trusted within some reasonable precision.

The main application of this strategy would be to a case where $L = L_{\rm had}$, such that $L_{\rm had}$ is a convenient scale to match to bare quark masses obtained from large-volume computations.
We now assume that σ and $\sigma_{\rm P}$ have been computed and are given, within some range of

[1] This is not what have been done for the running mass. Since in that case $v_0 = \sigma_{\rm P}(u_0)$. However we present this in this way since this is the kind of recursion used for the $N_{\rm f} = 2$ composite operators running.

values of u, by polynomials of the form

$$\sigma(u) = u(1 + s_1 u + s_2 u^2 + \ldots + s_m u^m)\,, \tag{H.0.4}$$

$$\sigma_{\rm P}(u) = 1 + p_1 u + p_2 u^2 + \ldots + p_n u^n\,, \tag{H.0.5}$$

with covariance matrices C_u and $C_{\rm P}$ for the fitted coefficients, respectively. We will assume in the following that the two sets of coefficients are uncorrelated.[2]

H.0.1 Coupling

To derive an error propagation formula for the sequence $\{u_k\}$, we start by considering the change $\delta_i u_{k-1}$ of the element u_{k-1} in the sequence due to a variation δs_i of the fit parameter s_i, viz.

$$\delta_i u_{k-1} = \delta_i[\sigma(u_k)] = \left.\frac{\partial\sigma}{\partial s_i}\right|_{u_k} \delta s_i + \left.\frac{\partial\sigma}{\partial u}\right|_{u_k} \delta_i u_k\,. \tag{H.0.6}$$

Since u_0 is errorless by construction, for the first step one has

$$\delta_i u_0 = 0 = \left.\frac{\partial\sigma}{\partial s_i}\right|_{u_1} \delta s_i + \left.\frac{\partial\sigma}{\partial u}\right|_{u_1} \delta_i u_1 \tag{H.0.7}$$

$$\Downarrow$$

$$\delta_i u_1 = -\left[\left.\frac{\partial\sigma}{\partial u}\right|_{u_1}\right]^{-1} \left.\frac{\partial\sigma}{\partial s_i}\right|_{u_1} \delta s_i. \tag{H.0.8}$$

The squared error of the coupling value u_1 can then be computed as

$$(\Delta u_1)^2 = {C_u}^{ij} \delta u_1^{(i)} \delta u_1^{(j)}\,, \tag{H.0.9}$$

where

$$\delta u_1^{(i)} = -\left[\left.\frac{\partial\sigma}{\partial u}\right|_{u_1}\right]^{-1} \left.\frac{\partial\sigma}{\partial s_i}\right|_{u_1}\,. \tag{H.0.10}$$

It is then trivial to iterate the procedure for the rest of the sequence applying Eq. (H.0.6), with the result

$$(\Delta u_k)^2 = {C_u}^{ij} \delta u_k^{(i)} \delta u_k^{(j)}\,, \tag{H.0.11}$$

where

$$\begin{aligned} \delta u_k^{(i)} &= \left[\left.\frac{\partial\sigma}{\partial u}\right|_{u_k}\right]^{-1} \left(\delta u_{k-1}^{(i)} - \left.\frac{\partial\sigma}{\partial s_i}\right|_{u_k}\right)\,, \\ \delta u_0^{(i)} &= 0\,. \end{aligned} \tag{H.0.12}$$

[2] This is the case in the Alpha computation of the running mass for $N_{\rm f} = 0, 2$, under the assumption that in the fit for $\sigma_{\rm P}$ it is fair to neglect the uncertainty on the values of u that fix the constant physics lines are negligible. For $N_{\rm f} = 3$ it is again true for the part of the running performed using the SF coupling, but not on the GF side.

These quantities can be easily evaluated using

$$\left.\frac{\partial\sigma}{\partial s_i}\right|_{u_k} = (i+1)u_k^i\,. \tag{H.0.13}$$

H.0.2 Pseudoscalar

We chose the pseudoscalar as an example, but the procedure is rather general. In this case there are two sources of uncertainty: the errors on the fit coefficients p_i, and the uncertainties born by the values u_k of the coupling at which $\sigma_{\rm P}$ is evaluated.

Let us first neglect the uncertainty coming from the coupling. In that case the error on v_k can be written as

$$(\Delta v_k)^2 = {C_{\rm P}}^{ij}\frac{\partial v_k}{\partial p_i}\frac{\partial v_k}{\partial p_j}\,. \tag{H.0.14}$$

By inserting the explicit form of v_k one gets

$$\begin{aligned}
(\Delta v_1)^2 &= {C_{\rm P}}^{ij}\left.\frac{\partial\sigma_{\rm P}}{\partial p_i}\right|_{u_1}\left.\frac{\partial\sigma_{\rm P}}{\partial p_j}\right|_{u_1}\,,\\
(\Delta v_2)^2 &= {C_{\rm P}}^{ij}\left[\sigma_{\rm P}(u_2)\left.\frac{\partial\sigma_{\rm P}}{\partial p_i}\right|_{u_1} + \left.\frac{\partial\sigma_{\rm P}}{\partial p_i}\right|_{u_2}\sigma_{\rm P}(u_1)\right]\times\\
&\qquad\times\left[\sigma_{\rm P}(u_2)\left(\frac{\partial\sigma_{\rm P}}{\partial p_j}\right)_{u_1} + \left.\frac{\partial\sigma_{\rm P}}{\partial p_j}\right|_{u_2}\sigma_{\rm P}(u_1)\right]\,,\\
&\cdots\cdots
\end{aligned} \tag{H.0.15}$$

and it is easy to check by induction that

$$\begin{aligned}
(\Delta v_k)^2 &= v_k^2\,{C_{\rm P}}^{ij}\delta v_k^{(i)}\delta v_k^{(j)}\,,\\
\delta v_k^{(i)} &= \delta v_{k-1}^{(i)} + \frac{1}{\sigma_{\rm P}(u_k)}\left.\frac{\partial\sigma_{\rm P}}{\partial p_i}\right|_{u_k}\,,\quad \delta v_0^{(i)} = 0\,,
\end{aligned} \tag{H.0.16}$$

which again can be easily evaluated using

$$\left.\frac{\partial\sigma_{\rm P}}{\partial p_i}\right|_{u_k} = iu_k^{i-1}\,. \tag{H.0.17}$$

Let us now incorporate the uncertainty coming from the coupling. To that purpose we have to compute the change $\delta_i\sigma_{\rm P}(u_k)$ in $\sigma_{\rm P}(u_k)$ due to a variation δs_i of the fit parameter s_i. Using the notation introduced above for the uncertainties in u_k, one finds

$$\delta_i[\sigma_{\rm P}(u_k)] = \left.\frac{\partial\sigma_{\rm P}}{\partial s_i}\right|_{u_k}\delta s_i + \left.\frac{\partial\sigma_{\rm P}}{\partial u}\right|_{u_k}\delta u_k^{(i)}\,, \tag{H.0.18}$$

where the first term on the rhs vanishes (under the hypotesis of no-correlation between $\sigma_{\rm P}$ and σ) . After some easy algebra one then obtains for $(\Delta v_k)^2$ the final formula

$$(\Delta v_k)^2 = v_k^2\left[{C_{\rm P}}^{ij}\delta v_k^{(i)}\delta v_k^{(j)} + {C_u}^{ij}\delta\tilde{u}_k^{(i)}\delta\tilde{u}_k^{(j)}\right]\,, \tag{H.0.19}$$

where $\delta\tilde{u}_k^{(i)}$ can be obtained from the recursion

$$\delta\tilde{u}_k^{(i)} = \delta\tilde{u}_{k-1}^{(i)} + \frac{1}{\sigma_{\rm P}(u_k)} \left.\frac{\partial\sigma_{\rm P}}{\partial u}\right|_{u_k} \delta u_k^{(i)} \,, \quad \delta\tilde{u}_0^{(i)} = 0 \,. \tag{H.0.20}$$

H.0.3 Matching to perturbation theory

Finally, we come back to Eq. (H.0.3) and compute the final uncertainty on $M/\overline{m}(L)$. There are four different sources for the latter:

(i) The uncertainty Δv_n on the nonperturbative evolution.

(ii) The error on the matching factor $\hat{c}(u_n)$ induced by the uncertainty Δu_n on u_n.

(iii) The uncertainty coming from the errors on the perturbative coefficients b_n, d_n (which are known to finite precision in SF schemes, due to the need of numerical integrations in their computation).

(iv) The uncertainty coming from the perturbative truncation in $\hat{c}(u_n)$.

The last two sources of uncertainty can be estimated separately, since they are completely decorrelated from Δv_n and Δu_n. The uncertainty coming from Δu_n and Δv_n can be written as

$$\begin{aligned}\left[\Delta\left(\frac{M}{\overline{m}(L)}\right)\right]^2_{u_n,v_n} =& \hat{c}(u_n)^2(\Delta v_n)^2 + \left(\left.\frac{\partial\hat{c}(u_n)}{\partial u}\right|_{u_n}\right)^2 v_n^2(\Delta u_n)^2 + \\ &+ \frac{\partial(M/\overline{m}(L))}{\partial u_n}\frac{\partial(M/\overline{m}(L))}{\partial v_n}\left[C_u^{ij}\delta u_n^{(i)} v_n \delta\tilde{u}_n^{(j)}\right] \,,\end{aligned} \tag{H.0.21}$$

where the last term takes into account the correlation between u_n and v_n,and one can use

$$\left.\frac{\partial\hat{c}(u_n)}{\partial u}\right|_{u_n} = -\frac{1}{2g_{\rm m}}\frac{\tau(g_{\rm m})}{\beta(g_{\rm m})}\,\hat{c}(u_n) \,, \tag{H.0.22}$$

$$g_{\rm m}^2 \equiv u_n \,. \tag{H.0.23}$$

(Recall that $v_k\delta\tilde{u}_k^{(j)}$ is the fluctuation of v_k due to a change in u_k related to the uncertainty on s_j.) Thus one finally has the result[3]

$$\begin{aligned}\left[\Delta\left(\frac{M}{\overline{m}(L)}\right)\right]^2_{u_n,v_n} &= \left(\frac{M}{\overline{m}(L)}\right)^2 \times \\ \times\left[\left(\frac{\Delta v_n}{v_n}\right)^2 + \left(\left.\frac{\partial\hat{c}(u)}{\partial u}\right|_{u_n}\frac{1}{\hat{c}(u_n)}\right)^2(\Delta u_n)^2 + \left.\frac{\partial\hat{c}(u)}{\partial u}\right|_{u_n}\frac{1}{\hat{c}(u_n)}\left[C_u^{ij}\delta u_n^{(i)}\delta\tilde{u}_n^{(j)}\right]\right] \,.\end{aligned} \tag{H.0.24}$$

Typically, the total relative error will be dominated by the relative error $\Delta v_n/v_n$ of the $\sigma_{\rm P}$ recursion, but the contribution from the coupling coming with Δu_n will not be negligible.

[3] This formula is the one that can be found in the old quenched analysis codes from the Capitani et al. paper, *but* for the factor of $1/g_{\rm m}$ in Eq. (H.0.22) — which results in a very small effect anyway, since $g_{\rm m}^2 \sim 1$ and this term appears in the smallest contribution to the error.

I Correlated random samples

Bootstrap resampling methods are vastly discussed in literature (among others [150]) and have a large application when dealing with the autocorrelation of data coming from a stocastic process, like a Markov Chain Monte Carlo (MCMC). In order to apply such a resampling, the starting point is to have a sample. We report here a general method to take advantage of bootstrap from parameters with a given covariance, instead of a bunch of data.
Suppose we have a vector of N parameters $\mathbf{x} = (x_1, \dots, x_N)$ with an $N \times N$ semi-positive definite covariance matrix C. What we need in order to use a resampling methods is to build the "original" samples starting from $\mathbf{x}$ and C. We built a gaussian random distribution $\tilde{x}_i$ with $i = 1, \dots, N$ so that

$$\langle \tilde{x}_i \rangle = 1 \,, \quad \sigma^2_{\tilde{x}_i} = 1 \,. \tag{I.0.1}$$

Given the properties of C it is possible to apply the *Cholesky decomposition* and write it as $C = LL^T$ with L an upper triangular matrix. The correct mean value and correlation for our gaussian samples are given by

$$\tilde{x}'_j = \tilde{x}_i L_{ij} + x_i \otimes 1_{N \times N} \,, \tag{I.0.2}$$

where the sum is intended for every random component of the sample $\tilde{x}_i$. Finally we have

$$\langle \tilde{x}'_i \rangle = x_i \quad COV(\tilde{x}'_i, \tilde{x}'_j) = C_{ij} \,. \tag{I.0.3}$$

Once the "original" samples are obtained it is straightforward to proceed with the standard bootstrap and propagate the error to any interesting derived observable. While this seems a useless exercise, it offer a very flexible tool to crosscheck or eventually avoid cumbersome error propagation (like the one in Appendix H). Moreover it finds a natural application in non-linear fitting procedures.
Suppose we want to fit some data $Y_i^{\exp}$ with uncertainty $dY_i^{\exp}$ for $i = 1, \dots, M$ to a model $F(k_1, \dots, k_n, p_1, \dots, p_m; X)$ with parameters $k_1, \dots, k_n, p_1, \dots, p_m$. We denote by $k_1, \dots, k_n$ some theoretically-fixed parameters (i.e. coming from a previous analysis) with a covariance K and $p_1, \dots, p_m$ free fitting parameter. Choosing the χ^2 as the likelyhood function which can test the goodness of our data model we can write is as the sum over normalized residues R as

$$\chi^2 = \sum_i^{\text{data}} \frac{(R_i)^2}{(\delta R_i)^2} \quad \text{with} \quad R_i = (Y_i^{\exp} - F(k_1, \dots, k_n, p_1, \dots, p_m; X_i)) \,. \tag{I.0.4}$$

In general, δR_i can be very difficult to calculate, and can contain fit parameters p_i making the regression non-linear and thus the minimization of the χ^2 computationally and theoretically challenging[1]. One way to proceed can be to first create correlated bootstrap samples of the parameters k_i and then linearise (in terms of parameters) the χ^2 with the

[1] because of the possible presence of relative minima

following factorisation

$$\chi^2_l = \sum_i^{\text{data}} \frac{(Y_i^{\text{exp}} - F(\bar{k}_1^l, \ldots, \bar{k}_n^l, p_1^l, \ldots, p_m^l; X_i))^2}{(dY_i^{\text{exp}})^2} + \sum_j^n \frac{(\bar{k}_j^l - k_j^l)^2}{K_{jj}} \tag{I.0.5}$$

where l is the bootstrap index and $\bar{k}$ are some "additional" fit parameters which does not count as degrees of freedom. The χ^2_l is than minimized for all l and errors on fitting parameters is simply given by the covariance computed over the samples. This procedure have been crosschecked all the times with both an analitical and numerical error propagation.

Bibliography

[1] P. A. M. Dirac, *The Quantum Theory of the Emission and Absorption of Radiation*. Springer, Netherlands, Drodrecht, 1988.

[2] D. J. Gross and F. Wilczek, *Asymptotically Free Gauge Theories. 1*, *Phys. Rev.* **D8** (1973) 3633–3652.

[3] M. Zimmermann, *Local operator products and renormalization in quantum field theory*, .

[4] M. Artuso *et. al.*, *B, D and K decays*, *Eur. Phys. J.* **C57** (2008) 309–492, [arXiv:0801.1833].

[5] M. Antonelli *et. al.*, *Flavor Physics in the Quark Sector*, *Phys. Rept.* **494** (2010) 197–414, [arXiv:0907.5386].

[6] T. Blake, G. Lanfranchi, and D. M. Straub, *Rare B Decays as Tests of the Standard Model*, *Prog. Part. Nucl. Phys.* **92** (2017) 50–91, [arXiv:1606.0091].

[7] T. Bhattacharya, V. Cirigliano, R. Gupta, H.-W. Lin, and B. Yoon, *Neutron Electric Dipole Moment and Tensor Charges from Lattice QCD*, *Phys. Rev. Lett.* **115** (2015), no. 21 212002, [arXiv:1506.0419].

[8] T. Bhattacharya, V. Cirigliano, S. Cohen, R. Gupta, H.-W. Lin, and B. Yoon, *Axial, Scalar and Tensor Charges of the Nucleon from 2+1+1-flavor Lattice QCD*, *Phys. Rev.* **D94** (2016), no. 5 054508, [arXiv:1606.0704].

[9] M. Abramczyk, S. Aoki, T. Blum, T. Izubuchi, H. Ohki, and S. Syritsyn, *On Lattice Calculation of Electric Dipole Moments and Form Factors of the Nucleon*, arXiv:1701.0779.

[10] **ALPHA** Collaboration, M. Dalla Brida, P. Fritzsch, T. Korzec, A. Ramos, S. Sint, and R. Sommer, *Slow running of the Gradient Flow coupling from 200 MeV to 4 GeV in $N_{\rm f} = 3$ QCD*, arXiv:1607.0642.

[11] P. Fritzsch and A. Ramos, *The gradient flow coupling in the Schrödinger Functional*, *JHEP* **10** (2013) 008, [arXiv:1301.4388].

[12] J. Cardy, *Scaling and Renormalization in Statistical Physics*. Cambridge University Press, 1996.

[13] K. G. Wilson, *The Renormalization Group and Strong Interactions*, *Phys. Rev.* **D3** (1971) 1818.

[14] K. G. Wilson, *The Renormalization Group and Critical Phenomena. 1. Renormalization Group and the Kadanoff Scaling Picture*, .

[15] K. G. Wilson and J. B. Kogut, *The Renormalization group and the epsilon expansion*, *Phys. Rept.* **12** (1974) 75–200.

[16] D. Skinner, *Lecture notes on Quantum Field Theory II*, Oxford University, 2017.

[17] M. Lüscher, R. Narayanan, P. Weisz, and U. Wolff, *The Schrödinger functional: A Renormalizable probe for nonAbelian gauge theories*, *Nucl. Phys.* **B384** (1992) 168–228, [hep-lat/9207009].

[18] D. J. Gross and F. Wilczek, *Ultraviolet Behavior of Nonabelian Gauge Theories*, *Phys. Rev. Lett.* **30** (1973) 1343–1346.

[19] S. Catterall and F. Sannino, *Minimal walking on the lattice*, *Phys. Rev.* **D76** (2007) 034504, [arXiv:0705.1664].

[20] T. J. Hollowood, *6 Lectures on QFT, RG and SUSY*, in *39th British Universities Summer School in Theoretical Elementary Particle Physics (BUSSTEPP 2009) Liverpool, United Kingdom, August 24-September 4, 2009*, 2009. arXiv:0909.0859.

[21] J. Gasser and H. Leutwyler, *Quark Masses*, *Phys. Rept.* **87** (1982) 77–169.

[22] J. Gasser and H. Leutwyler, *Chiral Perturbation Theory to One Loop*, *Annals Phys.* **158** (1984) 142.

[23] J. Gasser and H. Leutwyler, *Chiral Perturbation Theory: Expansions in the Mass of the Strange Quark*, *Nucl.Phys.* **B250** (1985) 465.

[24] A. Buras, M. Misiak, and J. Urban, *Two loop QCD anomalous dimensions of flavor changing four quark operators within and beyond the standard model*, *Nucl.Phys.* **B586** (2000) 397–426, [hep-ph/0005183].

[25] M. Ciuchini, E. Franco, V. Lubicz, G. Martinelli, I. Scimemi, *et. al.*, *Next-to-leading order QCD corrections to $\Delta F = 2$ effective Hamiltonians*, *Nucl.Phys.* **B523** (1998) 501–525, [hep-ph/9711402].

[26] K. G. Wilson, *Confinement of Quarks*, *Phys. Rev.* **D10** (1974) 2445–2459. [,45(1974)].

[27] R. Setoodeh, C. T. H. Davies, and I. M. Barbour, *Wilson Fermions on the Lattice: A Study of the Eigenvalue Spectrum*, *Phys. Lett.* **B213** (1988) 195–202.

[28] L. H. Karsten and J. Smit, *Lattice Fermions: Species Doubling, Chiral Invariance, and the Triangle Anomaly*, *Nucl. Phys.* **B183** (1981) 103. [,495(1980)].

[29] A. Vladikas, *Three Topics in Renormalization and Improvement*, in *Modern perspectives in lattice QCD: Quantum field theory and high performance computing. Proceedings, International School, 93rd Session, Les Houches, France, August 3-28, 2009*, pp. 161–222, 2011. arXiv:1103.1323.

[30] M. Bochicchio, L. Maiani, G. Martinelli, G. C. Rossi, and M. Testa, *Chiral Symmetry on the Lattice with Wilson Fermions*, *Nucl. Phys.* **B262** (1985) 331.

[31] G. Martinelli, C. Pittori, C. T. Sachrajda, M. Testa, and A. Vladikas, *A General method for nonperturbative renormalization of lattice operators*, *Nucl. Phys.* **B445** (1995) 81–108, [hep-lat/9411010].

[32] L. Giusti and A. Vladikas, *RI / MOM renormalization window and Goldstone pole contamination*, *Phys. Lett.* **B488** (2000) 303–312, [hep-lat/0005026].

[33] K. Symanzik, *Some topics in quantum field theory*, vol. 153. Lecture Notes in Physics. Springer Berlin Heidelberg, 1982.

[34] M. Luscher, *The Schrodinger functional in lattice QCD with exact chiral symmetry*, *JHEP* **05** (2006) 042, [hep-lat/0603029].

[35] S. Sint, *On the Schrodinger functional in QCD*, *Nucl. Phys.* **B421** (1994) 135–158, [hep-lat/9312079].

[36] A. A. Belavin, A. M. Polyakov, A. S. Schwartz, and Yu. S. Tyupkin, *Pseudoparticle Solutions of the Yang-Mills Equations*, *Phys. Lett.* **59B** (1975) 85–87.

[37] **ALPHA** Collaboration, A. Bode, P. Weisz, and U. Wolff, *Two loop computation of the Schrodinger functional in lattice QCD*, *Nucl. Phys.* **B576** (2000) 517–539, [hep-lat/9911018]. [Erratum: Nucl. Phys.B600,453(2001)].

[38] Y. Taniguchi, *Schroedinger functional formalism with Ginsparg-Wilson fermion*, *JHEP* **12** (2005) 037, [hep-lat/0412024].

[39] M. Lüscher, R. Sommer, P. Weisz, and U. Wolff, *A Precise determination of the running coupling in the SU(3) Yang-Mills theory*, *Nucl. Phys.* **B413** (1994) 481–502, [hep-lat/9309005].

[40] A. Hietanen, T. Karavirta, and P. Vilaseca, *Schrödinger functional boundary conditions and improvement for N ¿ 3*, *JHEP* **11** (2014) 074, [arXiv:1408.7047].

[41] S. Sint and P. Vilaseca, *Lattice artefacts in the Schródinger Functional coupling for strongly interacting theories*, *PoS* **LATTICE2012** (2012) 031, [arXiv:1211.0411].

[42] S. Sint, *The Schrodinger functional in QCD*, *Nucl. Phys. Proc. Suppl.* **42** (1995) 835–837, [hep-lat/9411063].

[43] **ALPHA** Collaboration, M. Della Morte, R. Hoffmann, F. Knechtli, J. Rolf, R. Sommer, I. Wetzorke, and U. Wolff, *Non-perturbative quark mass renormalization in two-flavor QCD*, *Nucl. Phys.* **B729** (2005) 117–134, [hep-lat/0507035].

[44] M. Luscher, S. Sint, R. Sommer, P. Weisz, and U. Wolff, *Nonperturbative O(a) improvement of lattice QCD*, *Nucl. Phys.* **B491** (1997) 323–343, [hep-lat/9609035].

[45] M. Luscher, *Trivializing maps, the Wilson flow and the HMC algorithm*, *Commun. Math. Phys.* **293** (2010) 899–919, [arXiv:0907.5491].

[46] M. Luscher, *Chiral symmetry and the Yang–Mills gradient flow*, *JHEP* **04** (2013) 123, [arXiv:1302.5246].

[47] M. Luscher and P. Weisz, *Perturbative analysis of the gradient flow in non-abelian gauge theories*, *JHEP* **02** (2011) 051, [arXiv:1101.0963].

[48] M. Lüscher, *Properties and uses of the Wilson flow in lattice QCD*, *JHEP* **08** (2010) 071, [arXiv:1006.4518]. [Erratum: JHEP03,092(2014)].

[49] M. Lüscher, *Step scaling and the Yang-Mills gradient flow*, *JHEP* **06** (2014) 105, [arXiv:1404.5930].

[50] Z. Fodor, K. Holland, J. Kuti, D. Nogradi, and C. H. Wong, *The gradient flow running coupling scheme*, *PoS* **LATTICE2012** (2012) 050, [arXiv:1211.3247].

[51] Z. Fodor, K. Holland, J. Kuti, D. Nogradi, and C. H. Wong, *The Yang-Mills gradient flow in finite volume*, *JHEP* **11** (2012) 007, [arXiv:1208.1051].

[52] A. Ramos and S. Sint, *Symanzik improvement of the gradient flow in lattice gauge theories*, *Eur. Phys. J.* **C76** (2016), no. 1 15, [arXiv:1508.0555].

[53] R. Sommer and U. Wolff, *Non-perturbative computation of the strong coupling constant on the lattice*, *Nucl. Part. Phys. Proc.* **261-262** (2015) 155–184, [arXiv:1501.0186].

[54] S. Sint and R. Sommer, *The Running coupling from the QCD Schrodinger functional: A One loop analysis*, *Nucl. Phys.* **B465** (1996) 71–98, [hep-lat/9508012].

[55] R. Sommer, *A New way to set the energy scale in lattice gauge theories and its applications to the static force and alpha-s in SU(2) Yang-Mills theory*, *Nucl. Phys.* **B411** (1994) 839–854, [hep-lat/9310022].

[56] M. Bruno, T. Korzec, and S. Schaefer, *Setting the scale for the CLS* $2+1$ *flavor ensembles*, *Phys. Rev.* **D95** (2017), no. 7 074504, [arXiv:1608.0890].

[57] S. Capitani, M. Della Morte, G. von Hippel, B. Knippschild, and H. Wittig, *Scale setting via the* Ω *baryon mass*, *PoS* **LATTICE2011** (2011) 145, [arXiv:1110.6365].

[58] **ALPHA** Collaboration, M. Della Morte, R. Frezzotti, J. Heitger, J. Rolf, R. Sommer, and U. Wolff, *Computation of the strong coupling in QCD with two dynamical flavors*, *Nucl. Phys.* **B713** (2005) 378–406, [hep-lat/0411025].

[59] **ALPHA** Collaboration, F. Tekin, R. Sommer, and U. Wolff, *The Running coupling of QCD with four flavors*, *Nucl. Phys.* **B840** (2010) 114–128, [arXiv:1006.0672].

[60] M. Lüscher, R. Sommer, U. Wolff, and P. Weisz, *Computation of the running coupling in the SU(2) Yang-Mills theory*, *Nucl. Phys.* **B389** (1993) 247–264, [hep-lat/9207010].

[61] M. Dalla Brida and M. Lüscher, *The gradient flow coupling from numerical stochastic perturbation theory*, *PoS* **LATTICE2016** (2016) 332, [arXiv:1612.0495].

[62] M. Bruno *et. al.*, *Simulation of QCD with* $N_f = 2 + 1$ *flavors of non-perturbatively improved Wilson fermions*, *JHEP* **02** (2015) 043, [arXiv:1411.3982].

[63] M. Bruno, M. Dalla Brida, P. Fritzsch, T. Korzec, A. Ramos, S. Schaefer, H. Simma, S. Sint, and R. Sommer, *The* Λ*-parameter in 3-flavour QCD and* $\alpha_s(m_Z)$ *by the ALPHA collaboration*, *PoS* **LATTICE2016** (2016) 197, [arXiv:1701.0307].

[64] K. Symanzik, *Some Topics in Quantum Field Theory*, in *Mathematical Problems in theoretical Physics. Proceedings, 6th International Conference on Mathematical Physics, West Berlin, Germany, August 11-20, 1981*, pp. 47–58, 1981.

[65] K. Symanzik, *Continuum Limit and Improved Action in Lattice Theories. 1. Principles and phi**4 Theory*, *Nucl. Phys.* **B226** (1983) 187–204.

[66] K. Symanzik, *Continuum Limit and Improved Action in Lattice Theories. 2. O(N) Nonlinear Sigma Model in Perturbation Theory*, *Nucl. Phys.* **B226** (1983) 205–227.

[67] B. Sheikholeslami and R. Wohlert, *Improved Continuum Limit Lattice Action for QCD with Wilson Fermions*, *Nucl. Phys.* **B259** (1985) 572.

[68] P. Weisz, *Renormalization and lattice artifacts*, in *Modern perspectives in lattice QCD: Quantum field theory and high performance computing. Proceedings, International School, 93rd Session, Les Houches, France, August 3-28, 2009*, pp. 93–160, 2010. arXiv:1004.3462.

[69] M. Luscher and P. Weisz, *On-Shell Improved Lattice Gauge Theories*, *Commun. Math. Phys.* **97** (1985) 59. [Erratum: Commun. Math. Phys.98,433(1985)].

[70] S. Sint and P. Weisz, *Further one loop results in* $O(a)$ *improved lattice QCD*, *Nucl. Phys. Proc. Suppl.* **63** (1998) 856–858, [hep-lat/9709096].

[71] A. Ramos, *The gradient flow running coupling with twisted boundary conditions*, *JHEP* **11** (2014) 101, [arXiv:1409.1445].

[72] S. Capitani, M. Lüscher, R. Sommer, and H. Wittig, *Non-perturbative quark mass renormalization in quenched lattice QCD*, *Nucl. Phys.* **B544** (1999) 669–698, [hep-lat/9810063]. [Erratum: Nucl. Phys.B582,762(2000)].

[73] I. Campos, P. Fritzsch, C. Pena, D. Preti, A. Ramos, and A. Vladikas, *Non-perturbative running of quark masses in three-flavour QCD*, *PoS* **LATTICE2016** (2016) 201, [arXiv:1611.0971].

[74] I. Campos, P. Fritzsch, C. Pena, D. Preti, A. Ramos, and A. Vladikas, *Controlling quark mass determinations non-perturbatively in three-flavour QCD*, *EPJ Web Conf.* **137** (2017) 08006, [arXiv:1611.0610].

[75] J. A. Gracey, *Three loop MS-bar tensor current anomalous dimension in QCD*, *Phys. Lett.* **B488** (2000) 175–181, [hep-ph/0007171].

[76] L. G. Almeida and C. Sturm, *Two-loop matching factors for light quark masses and three-loop mass anomalous dimensions in the RI/SMOM schemes*, *Phys. Rev.* **D82** (2010) 054017, [arXiv:1004.4613].

[77] A. Skouroupathis and H. Panagopoulos, *Two-loop renormalization of vector, axial-vector and tensor fermion bilinears on the lattice*, *Phys. Rev.* **D79** (2009) 094508, [arXiv:0811.4264].

[78] M. Gockeler, R. Horsley, H. Oelrich, H. Perlt, D. Petters, P. E. L. Rakow, A. Schafer, G. Schierholz, and A. Schiller, *Nonperturbative renormalization of composite operators in lattice QCD*, *Nucl. Phys.* **B544** (1999) 699–733, [hep-lat/9807044].

[79] D. Becirevic, V. Gimenez, V. Lubicz, G. Martinelli, M. Papinutto, and J. Reyes, *Renormalization constants of quark operators for the nonperturbatively improved Wilson action*, *JHEP* **08** (2004) 022, [hep-lat/0401033].

[80] Y. Aoki *et. al.*, *Non-perturbative renormalization of quark bilinear operators and B(K) using domain wall fermions*, *Phys. Rev.* **D78** (2008) 054510, [arXiv:0712.1061].

[81] C. Sturm, Y. Aoki, N. H. Christ, T. Izubuchi, C. T. C. Sachrajda, and A. Soni, *Renormalization of quark bilinear operators in a momentum-subtraction scheme with a nonexceptional subtraction point*, *Phys. Rev.* **D80** (2009) 014501, [arXiv:0901.2599].

[82] **ETM** Collaboration, M. Constantinou *et. al.*, *Non-perturbative renormalization of quark bilinear operators with $N_f = 2$ (tmQCD) Wilson fermions and the tree-level improved gauge action*, *JHEP* **08** (2010) 068, [arXiv:1004.1115].

[83] C. Alexandrou, M. Constantinou, T. Korzec, H. Panagopoulos, and F. Stylianou, *Renormalization constants of local operators for Wilson type improved fermions*, *Phys. Rev.* **D86** (2012) 014505, [arXiv:1201.5025].

[84] M. Constantinou, R. Horsley, H. Panagopoulos, H. Perlt, P. E. L. Rakow, G. Schierholz, A. Schiller, and J. M. Zanotti, *Renormalization of local quark-bilinear operators for N_f=3 flavors of stout link nonperturbative clover fermions*, *Phys. Rev.* **D91** (2015), no. 1 014502, [arXiv:1408.6047].

[85] I. Campos, P. Fritzsch, C. Pena, D. Preti, A. Ramos, and A. Vladikas, "Non perturbative renormalization and running of quark masses in $n_f = 3$ qcd." to appear.

[86] B. Blossier, M. della Morte, N. Garron, and R. Sommer, *HQET at order $1/m$: I. Non-perturbative parameters in the quenched approximation*, *JHEP* **06** (2010) 002, [arXiv:1001.4783].

[87] **ALPHA** Collaboration, F. Bernardoni *et. al.*, *Decay constants of B-mesons from non-perturbative HQET with two light dynamical quarks*, *Phys. Lett.* **B735** (2014) 349–356, [arXiv:1404.3590].

[88] **ALPHA** Collaboration, M. Guagnelli, J. Heitger, C. Pena, S. Sint, and A. Vladikas, *Non-perturbative renormalization of left-left four-fermion operators in quenched lattice QCD*, *JHEP* **03** (2006) 088, [hep-lat/0505002].

[89] F. Palombi, C. Pena, and S. Sint, *A Perturbative study of two four-quark operators in finite volume renormalization schemes*, *JHEP* **03** (2006) 089, [hep-lat/0505003].

[90] P. Dimopoulos, L. Giusti, P. Hernández, F. Palombi, C. Pena, *et. al.*, *Non-perturbative renormalisation of left-left four-fermion operators with Neuberger fermions*, *Phys.Lett.* **B641** (2006) 118–124, [hep-lat/0607028].

[91] **ALPHA Collaboration** Collaboration, P. Dimopoulos *et. al.*, *Non-perturbative renormalisation of Delta F=2 four-fermion operators in two-flavour QCD*, *JHEP* **0805** (2008) 065, [arXiv:0712.2429].

[92] F. Palombi, M. Papinutto, C. Pena, and H. Wittig, *Non-perturbative renormalization of static-light four-fermion operators in quenched lattice QCD*, *JHEP* **09** (2007) 062, [arXiv:0706.4153].

[93] M. Papinutto, C. Pena, and D. Preti, *Non-perturbative renormalization and running of $\Delta F = 2$ four-fermion operators in the SF scheme*, *PoS* **LATTICE2014** (2014) 281, [arXiv:1412.1742].

[94] M. Papinutto, C. Pena, and D. Preti, *On the perturbative renormalisation of four-quark operators for new physics*, arXiv:1612.0646.

[95] P. Fritzsch, C. Pena, and D. Preti, *Non-perturbative renormalization of tensor bilinears in Schrödinger Functional schemes*, *PoS* **LATTICE2015** (2016) 250, [arXiv:1511.0502].

[96] M. Dalla Brida, S. Sint, and P. Vilaseca, *The chirally rotated Schrödinger functional: theoretical expectations and perturbative tests*, *JHEP* **08** (2016) 102, [arXiv:1603.0004].

[97] **ALPHA** Collaboration, M. Dalla Brida, P. Fritzsch, T. Korzec, A. Ramos, S. Sint, and R. Sommer, *Determination of the QCD Λ-parameter and the accuracy of perturbation theory at high energies*, *Phys. Rev. Lett.* **117** (2016), no. 18 182001, [arXiv:1604.0619].

[98] M. Bruno, M. Dalla Brida, P. Fritzsch, T. Korzec, A. Ramos, S. Schaefer, H. Simma, S. Sint, and R. Sommer, *The strong coupling from a nonperturbative determination of the Λ parameter in three-flavor QCD*, arXiv:1706.0382.

[99] I. Campos, P. Fritzsch, C. Pena, D. Preti, A. Ramos, and A. Vladikas, "Non perturbative renormalization and running of tensor currents in $n_f = 3$ qcd." to appear.

[100] S. Capitani, M. Guagnelli, M. Lüscher, S. Sint, R. Sommer, P. Weisz, and H. Wittig, *Nonperturbative quark mass renormalization*, *Nucl. Phys. Proc. Suppl.* **63** (1998) 153–158, [hep-lat/9709125].

[101] **ALPHA** Collaboration, S. Sint and P. Weisz, *The Running quark mass in the SF scheme and its two loop anomalous dimension*, *Nucl. Phys.* **B545** (1999) 529–542, [hep-lat/9808013].

[102] I. Campos, P. Fritzsch, C. Pena, D. Preti, A. Ramos, and A. Vladikas, *Prospects and status of quark mass renormalization in three-flavour QCD*, *PoS* **LATTICE2015** (2016) 249, [arXiv:1508.0693].

[103] M. Guagnelli, K. Jansen, and R. Petronzio, *Nonperturbative running of the average momentum of nonsinglet parton densities*, *Nucl. Phys.* **B542** (1999) 395–409, [hep-lat/9809009].

[104] M. Guagnelli, K. Jansen, and R. Petronzio, *Renormalization group invariant average momentum of nonsinglet parton densities*, *Phys. Lett.* **B459** (1999) 594–598, [hep-lat/9903012].

[105] **ZeRo** Collaboration, A. Shindler, M. Guagnelli, K. Jansen, F. Palombi, R. Petronzio, and I. Wetzorke, *Nonperturbative renormalization of moments of parton distribution functions*, *Nucl. Phys. Proc. Suppl.* **129** (2004) 278–280, [hep-lat/0309181]. [,278(2003)].

[106] C. Pica, *Beyond the Standard Model: Charting Fundamental Interactions via Lattice Simulations*, *PoS* **LATTICE2016** (2016) 015, [arXiv:1701.0778].

[107] M. Lüscher, S. Sint, R. Sommer, and P. Weisz, *Chiral symmetry and $O(a)$ improvement in lattice QCD*, *Nucl. Phys.* **B478** (1996) 365–400, [hep-lat/9605038].

[108] S. Capitani, M. Göckeler, R. Horsley, H. Perlt, P. E. L. Rakow, G. Schierholz, and A. Schiller, *Renormalization and off-shell improvement in lattice perturbation theory*, *Nucl. Phys.* **B593** (2001) 183–228, [hep-lat/0007004].

[109] J. A. Gracey, *Three loop anomalous dimension of the second moment of the transversity operator in the MS-bar and RI-prime schemes*, *Nucl. Phys.* **B667** (2003) 242–260, [hep-ph/0306163].

[110] S. Sint and P. Weisz, *Further results on $O(a)$ improved lattice QCD to one loop order of perturbation theory*, *Nucl. Phys.* **B502** (1997) 251–268, [hep-lat/9704001].

[111] **ALPHA** Collaboration, K. Jansen and R. Sommer, *$O(\alpha)$ improvement of lattice QCD with two flavors of Wilson quarks*, *Nucl. Phys.* **B530** (1998) 185–203, [hep-lat/9803017]. [Erratum: Nucl. Phys.B643,517(2002)].

[112] **ALPHA** Collaboration, U. Wolff, *Monte Carlo errors with less errors*, *Comput. Phys. Commun.* **156** (2004) 143–153, [hep-lat/0306017]. [Erratum: Comput. Phys. Commun.176,383(2007)].

[113] C. Pena and D. Preti, *Non-perturbative renormalization of tensor currents: strategy and results for $N_f = 0$ and $N_f = 2$ QCD*, arXiv:1706.0667.

[114] S. Weinberg, *Nonlinear realizations of chiral symmetry*, *Phys. Rev.* **166** (1968) 1568–1577.

[115] S. Weinberg, *Phenomenological Lagrangians*, *Physica* **A96** (1979) 327–340.

[116] S. Scherer and M. R. Schindler, *A Chiral perturbation theory primer*, hep-ph/0505265.

[117] P. Fritzsch, A. Ramos, and F. Stollenwerk, *Critical slowing down and the gradient flow coupling in the Schrödinger functional*, *PoS* **Lattice2013** (2014) 461, [arXiv:1311.7304].

[118] J. Bulava, M. Della Morte, J. Heitger, and C. Wittemeier, *Nonperturbative renormalization of the axial current in $N_f = 3$ lattice QCD with Wilson fermions and a tree-level improved gauge action*, *Phys. Rev.* **D93** (2016), no. 11 114513, [arXiv:1604.0582].

[119] S. Sint and M. Della Brida. private communication.

[120] R. Frezzotti and G. C. Rossi, *Twisted mass lattice QCD with mass nondegenerate quarks*, *Nucl. Phys. Proc. Suppl.* **128** (2004) 193–202, [hep-lat/0311008]. [,193(2003)].

[121] **Alpha** Collaboration, R. Frezzotti, P. A. Grassi, S. Sint, and P. Weisz, *Lattice QCD with a chirally twisted mass term*, *JHEP* **08** (2001) 058, [hep-lat/0101001].

[122] A. Donini, V. Giménez, G. Martinelli, M. Talevi, and A. Vladikas, *Nonperturbative renormalization of lattice four fermion operators without power subtractions*, *Eur. Phys. J.* **C10** (1999) 121–142, [hep-lat/9902030].

[123] J. A. Bagger, K. T. Matchev, and R.-J. Zhang, *QCD corrections to flavor changing neutral currents in the supersymmetric standard model*, *Phys. Lett.* **B412** (1997) 77–85, [hep-ph/9707225].

[124] S. Narison and R. Tarrach, *Higher Dimensional Renormalization Group Invariant Vacuum Condensates in Quantum Chromodynamics*, *Phys. Lett.* **B125** (1983) 217–222.

[125] A. J. Buras, M. Jamin, M. E. Lautenbacher, and P. H. Weisz, *Effective Hamiltonians for $\Delta S = 1$ and $\Delta B = 1$ nonleptonic decays beyond the leading logarithmic approximation*, *Nucl. Phys.* **B370** (1992) 69–104. [Addendum: Nucl. Phys.B375,501(1992)].

[126] A. J. Buras, M. Jamin, M. E. Lautenbacher, and P. H. Weisz, *Two loop anomalous dimension matrix for $\Delta S = 1$ weak nonleptonic decays I: $\mathcal{O}(\alpha_s^2)$*, *Nucl. Phys.* **B400** (1993) 37–74, [hep-ph/9211304].

[127] M. Constantinou, P. Dimopoulos, R. Frezzotti, V. Lubicz, H. Panagopoulos, A. Skouroupathis, and F. Stylianou, *Perturbative renormalization factors and $O(a^2)$ corrections for lattice 4-fermion operators with improved fermion/gluon actions*, *Phys. Rev.* **D83** (2011) 074503, [arXiv:1011.6059].

[128] R. Gupta, T. Bhattacharya, and S. R. Sharpe, *Matrix elements of four fermion operators with quenched Wilson fermions*, *Phys. Rev.* **D55** (1997) 4036–4054, [hep-lat/9611023].

[129] **SWME** Collaboration, J. Kim, W. Lee, J. Leem, S. R. Sharpe, and B. Yoon, *Toolkit for staggered $\Delta S = 2$ matrix elements*, *Phys. Rev.* **D90** (2014), no. 1 014504, [arXiv:1404.2368].

[130] S. Sint. unpublished notes, 2001.

[131] H. Panagopoulos and Y. Proestos, *The Critical hopping parameter in O(a) improved lattice QCD*, *Phys. Rev.* **D65** (2002) 014511, [hep-lat/0108021].

[132] P. Fritzsch, F. Knechtli, B. Leder, M. Marinkovic, S. Schaefer, R. Sommer, and F. Virotta, *The strange quark mass and Lambda parameter of two flavor QCD*, *Nucl. Phys.* **B865** (2012) 397–429, [arXiv:1205.5380].

[133] M. Papinutto, G. Herdoiza, C. Pena, and A. Vladikas, *Renormalization of HQET $\Delta B = 2$ operators: O(a) improvement and $1/m$ matching with QCD*, *PoS* **LATTICE2013** (2014) 317, [arXiv:1311.5177].

[134] C. Pena. private communication.

[135] S. Sint, *The Chirally rotated Schródinger functional with Wilson fermions and automatic O(a) improvement*, *Nucl. Phys.* **B847** (2011) 491–531, [arXiv:1008.4857].

[136] M. Dalla Brida, M. Papinutto, and P. Vilaseca, *Perturbative renormalization of $\Delta F = 2$ four-fermion operators with the chirally rotated Schrödinger functional*, arXiv:1605.0905.

[137] M. Papinutto, C. Pena, and D. Preti, "Non-perturbative renormalization of $\Delta F = 2$ four-fermion operators for new physics in $N_f = 2$ QCD." to appear.

[138] **RBC, UKQCD** Collaboration, R. Arthur, P. A. Boyle, N. Garron, C. Kelly, and A. T. Lytle, *Opening the Rome-Southampton window for operator mixing matrices*, *Phys. Rev.* **D85** (2012) 014501, [arXiv:1109.1223].

[139] **RBC, UKQCD** Collaboration, P. A. Boyle, N. Garron, and R. J. Hudspith, *Neutral kaon mixing beyond the standard model with $n_f = 2 + 1$ chiral fermions*, *Phys. Rev.* **D86** (2012) 054028, [arXiv:1206.5737].

[140] **ETM** Collaboration, V. Bertone *et. al.*, *Kaon Mixing Beyond the SM from N_f=2 tmQCD and model independent constraints from the UTA*, *JHEP* **03** (2013) 089, [arXiv:1207.1287]. [Erratum: JHEP07,143(2013)].

[141] **ETM** Collaboration, N. Carrasco, P. Dimopoulos, R. Frezzotti, V. Lubicz, G. C. Rossi, S. Simula, and C. Tarantino, *$\Delta S = 2$ and $\Delta C = 2$ bag parameters in the standard model and beyond from N_f=2+1+1 twisted-mass lattice QCD*, *Phys. Rev.* **D92** (2015), no. 3 034516, [arXiv:1505.0663].

[142] **SWME** Collaboration, B. J. Choi *et. al.*, *Kaon BSM B-parameters using improved staggered fermions from $N_f = 2 + 1$ unquenched QCD*, *Phys. Rev.* **D93** (2016), no. 1 014511, [arXiv:1509.0059].

[143] **RBC/UKQCD** Collaboration, N. Garron, R. J. Hudspith, and A. T. Lytle, *Neutral Kaon Mixing Beyond the Standard Model with $n_f = 2 + 1$ Chiral Fermions Part 1: Bare Matrix Elements and Physical Results*, *JHEP* **11** (2016) 001, [arXiv:1609.0333].

[144] C. Pena, S. Sint, and A. Vladikas, *Twisted mass QCD and lattice approaches to the $\Delta I = 1/2$ rule*, *JHEP* **0409** (2004) 069, [hep-lat/0405028].

[145] R. Frezzotti and G. Rossi, *Chirally improving Wilson fermions. II. Four-quark operators*, *JHEP* **0410** (2004) 070, [hep-lat/0407002].

[146] M. Ciuchini, E. Franco, G. Martinelli, and L. Reina, *The Delta S = 1 effective Hamiltonian including next-to-leading order QCD and QED corrections*, *Nucl. Phys.* **B415** (1994) 403–462, [hep-ph/9304257].

[147] M. Ciuchini, E. Franco, G. Martinelli, and L. Reina, *ϵ'/ϵ at the Next-to-leading order in QCD and QED*, *Phys. Lett.* **B301** (1993) 263–271, [hep-ph/9212203].

[148] T. Kitahara, U. Nierste, and P. Tremper, *Singularity-free next-to-leading order $\Delta S = 1$ renormalization group evolution and ϵ'_K/ϵ_K in the Standard Model and beyond*, *JHEP* **12** (2016) 078, [arXiv:1607.0672].

[149] T. Huber, E. Lunghi, M. Misiak, and D. Wyler, *Electromagnetic logarithms in* $\bar{B} \to X_s l^+ l^-$, *Nucl. Phys.* **B740** (2006) 105–137, [hep-ph/0512066].

[150] R. Tibshirani and B. Efron, *An Introduction to the Bootstrap*. Chapman And Hall, 1993.